Universidade de Aveiro Departamento de Geociências
2009

Clara Araújo Sena da Silva

Modelação numérica da migração de radionuclídeos em sistemas subsuperficiais

Numerical modelling of radionuclide migration in near-surface systems

Universidade de Aveiro Departamento de Geociências
2009

Clara Araújo Sena da Silva

Modelação numérica da migração de radionuclídeos em sistemas subsuperficiais

Numerical modelling of radionuclide migration in near-surface systems

Dissertação apresentada à Universidade de Aveiro para cumprimento dos requisitos necessários à obtenção do grau de Doutor em Geociências, realizada sob a orientação científica da Doutora Maria Teresa Condesso de Melo, Professora Auxiliar Convidada do Departamento de Geociências da Universidade de Aveiro e do Doutor David Arcos, Director do grupo Site and Engineered Barrier Assessment na empresa Amphos 21

Apoio financeiro do POCI 2010, BD/16647/2004 no âmbito do III Quadro Comunitário de Apoio.

Apoio financeiro da FCT e do FSE no âmbito do III Quadro Comunitário de Apoio.

to Ilidio

o júri

presidente — Reitora de Universidade de Aveiro

Doutor Manuel Augusto Marques da Silva
Professor Catedrático da Universidade de Aveiro

Doutor Jorge Molinero
Professor Associado da Universidade Politécnica da Catalunha, Barcelona, Espanha

Doutor Mário Abel Carreira Gonçalves
Professor Auxiliar da Faculdade de Ciências da Universidade de Lisboa

Doutora Maria Teresa Condesso de Melo (Orientadora)
Investigadora Auxiliar do Instituto Superior Técnico da Universidade Técnica de Lisboa

Doutor David Arcos (Co-orientador)
Director do grupo Site and Engineered Barrier Assessment na AMPHOS 21 Consulting, Espanha

Doutor Sten Berglund
PhD Water Resources Engineering, Swedish Nuclear Fuel and Waste Management Company (SKB), Suécia

agradecimentos

I am eternally grateful to Teresa Melo who encouraged me towards hydrogeology research, and has always supported my decisions with her valuable advises. I especially thank Lara Duro for believing on my skills and giving me the opportunity to work and learn countless things related to spent nuclear fuel and numerical modelling, with the wonderful team of Amphos 21. Sincere thanks are given to Jordi Bruno who gave me the opportunity to work at Amphos 21. I especially thank his energetic cafeeeeee's in the morning and wonderful drum sessions in the garden of Amphos 21 office.

Without the contracts made between Amphos 21 and the Japan Atomic Energy Agency (JAEA), and the Swedish Nuclear Fuel and Waste Management Company (SKB) I would not be able to access the data owned by these two national agencies for nuclear waste management. These valuable data provided the motivation and inputs for all the work presented in this thesis. I acknowledge the two national agencies: JAEA and SKB.

I thank all the people of Amphos 21 for their contagious dedication to the scientific work coupled with environmental consulting. I will never forget the warm smiles I received in Amphos 21 office. I thank Xavi for his friendship. I especially thank Ana for performing the last numerical calculations of this thesis with the distance between Barcelona and Coimbra.

I am grateful to David Arcos, who advised me throughout the different stages of this thesis with lightening discussions and with his rigour. I sincerely acknowledge Fidel Grandia for his clarifying lessons on geochemical modelling, and especially on the interesting subject of solid solutions. Eternal thanks are given to Jorge Molinero, a wonderful hydrogeologist who guided me through the amazing world of hydrogeological modelling, and inspired me with delightful discussions.

I thank Pascale her everlasting friendship and good neighbourhood. Special thanks are also given to Carles Ibañez, and his beautiful dancers, for the wonderful ballet classes that were able to drive me away from numbers and equations, leaving me with the pleasure of dance.

I thank all my family who supported me, made me so strong and gave me the warmth of home whenever I needed.

Finally, I thank Ilidio who faithfully awaited my return, listened to my fears, gave me valuable advices, and cooked so many delicious meals with the smell of Portugal and the Atlantic.

palavras-chave

Modelação numérica, hidrogeoquímica, biogeoquímica, resíduos nucleares de elevada actividade, radioinuclídeos, repositório geológico profundo.

resumo

Em todo o mundo são usados, hoje em dia, modelos numéricos hidrogeoquímicos para simular fenómenos naturais e fenómenos decorrentes de actividades antrópicas. Estes modelos ajudam-nos a compreender o ambiente envolvente, a sua variabilidade espacial e evolução temporal.
No presente trabalho apresenta-se o desenvolvimento de modelos numéricos hidrogeoquímicos aplicados no contexto do repositório geológico profundo para resíduos nucleares de elevada actividade.
A avaliação da performance de um repositório geológico profundo inclui o estudo da evolução geoquímica do repositório, bem como a análise dos cenários de mau funcionamento do repositório, e respectivas consequências ambientais.
Se se escaparem acidentalmente radionuclídeos de um repositório, estes poderão atravessar as barreiras de engenharia e barreiras naturais que constituem o repositório, atingindo eventualmente, os ecosistemas superficiais. Neste caso, os sedimentos subsuperficiais constituem a última barreira natural antes dos ecosistemas superficiais.
No presente trabalho foram desenvolvidos modelos numéricos que integram processos biogeoquímicos, geoquímicos, hidrodinâmicos e de transporte de solutos, para entender e quantificar a influência destes processos na mobilidade de radionuclídeos em sistemas subsuperficiais.
Os resultados alcançados reflectem a robustez dos instrumentos numéricos utilizados para desenvolver simulações descritivas e predictivas de processos hidrogeoquímicos que influenciam a mobilidade de radionuclídeos.
A simulação (descritiva) de uma experiência laboratorial revela que a actividade microbiana induz a diminuição do potencial redox da água subterrânea que, por sua vez, favorece a retenção de radionuclídeos sensíveis ao potencial redox, como o urânio.
As simulações predictivas indicam que processos de co-precipitação com minerais de elementos maioritários, precipitação de fases puras, intercâmbio catiónico e adsorção à superfície de minerais favorecem a retenção de U, Cs, Sr e Ra na fase sólida de uma argila glaciar e uma moreia rica em calcite.
A etiquetagem dos radionuclídeos nas simulações numéricas permitiu concluir que a diluição isotópica joga um papel importante no potencial impacte dos radionuclídeos nos sistemas subsuperficiais.
A partir dos resultados das simulações numéricas é possivel calcular coeficientes de distribuição efectivos. Esta metodologia proporciona a simulação de ensaios de traçadores de longa duração que não seriam exequíveis à escala da vida humana. A partir destas simulações podem ser obtidos coeficientes de retardamento que são úteis no contexto da avaliação da performance de repositórios geológicos profundos.

keywords

Numerical modelling, hydrogeochemistry, biogeochemistry, high level nuclear waste, radionuclides, deep geological repository.

abstract

Hydrogeochemical numerical modelling is worldwide used to simulate natural and anthropogenically induced phenomena. These simulations help us to understand the surrounding environment; its spatial variability and temporal evolution.

In the present work, hydrogeochemical numerical models are developed in the context of the deep geological repository for high level nuclear waste (HLNW). Performance assessment of a deep geological repository includes the study of its geochemical evolution, as well as the analysis of failure scenarios of the repository and their environmental consequences.

If a repository release takes place, radionuclides from the HLNW could migrate through the surrounding engineered and natural barriers and eventually reach the surface ecosystems. In this case, near-surface sediments constitute the last natural barrier between the repository and the surface ecosystems.

In this study biogeochemical, geochemical, hydrodynamic and solute transport processes are coupled in different numerical models to understand and quantify the influence of these processes on radionuclide mobility in near-surface systems.

The results attained here prove the robustness of such numerical tools to develop both descriptive and predictive simulations of hydrogeochemical processes that affect radionuclide mobility.

The (descriptive) simulation of a jar-fermentor experiment reveals that microbial activity tends to decrease the redox state of groundwater which favours the retention of redox sensitive radionuclides such as uranium.

Predictive simulations reveal that co-precipitation with major element phases, precipitation of pure phases, cation exchange and adsorption on charged mineral surfaces provide the retention of uranium, caesium, strontium and radium in the solid phase of a glacial clay and a calcite-rich till deposit.

Labelling of radionuclides in the numerical simulations shows that isotopic dilution also plays an important role in the potential impact of radionuclides in the near-surface systems.

Finally, effective distribution coefficients can be calculated from the outputs of previous reactive solute transport simulations. This methodology provides the simulation of synthetic tracer tests with long time spans that would not be feasible at the human life scale. The outputs of these synthetic tracer tests provide the estimation of effective retardation factors that may be useful for performance assessment of deep geological repositories.

Index

1. Introduction 1
1.1 Motivation 1
1.2 Scope 3
1.3 Methodology 8
1.4 State-of-the-art 13
1.4.1 Kd-based models versus reactive transport models 13
1.4.2 Hydrogeochemical models in the context of the HLNW management 17
1.4.3 Modelling microbially mediated redox reactions in the context of the deep geological repository 19
1.5 Objectives 21
1.6 References 23
2. Modelling microbially mediated redox processes in lake sediments 31
2.1 Introduction 32
2.2 Experimental set up 33
2.3 Conceptual model 35
2.3.1 Evidences from experimental results 35
2.3.2 Microbially mediated reactions and abiotic processes 36
2.4 Numerical model 40
2.4.1 Mathematical model 40
2.4.2 Initial conditions 46
2.4.3 Parameterization 50
2.5 Discussion 53
2.5.1 Processes 53
2.5.2 Uncertainties on Monod parameters 63
2.6 Conclusions 65
2.7 References 68
3. Quantitative assessment of radionuclide retention in glacial clays related to groundwater discharge areas 71
3.1 Introduction 72
3.2 Scope 73
3.3 Near-surface hydrogeology at Forsmark 74
3.4 Natural occurrence of uranium, strontium, caesium and radium at Forsmark 75

3.4.1 Uranium 75
3.4.2 Strontium 76
3.4.3 Caesium 77
3.4.4 Radium 77
3.5 Reactive solute transport modelling 77
3.5.1 Hydrodynamic processes and parameters 78
3.5.2 Geochemical processes and parameters 79
3.5.3 Initial and boundary conditions 82
3.5.4 Spatial and time discretisation 87
3.6 Results 88
3.6.1 Transport of conservative and reactive solutes 88
3.6.2 Present-day hydrogeochemical conditions 88
3.6.3 Retention of repository-derived radionuclides 91
3.7 Conclusions 96
3.8 References 98
4. Quantitative assessment of radionuclide retention in the Quaternary sediments/granite interface of the Fennoscandian shield (Sweden) 103
4.1 Introduction 104
4.1.1 Scope 105
4.2 Near-surface hydrogeology at Forsmark 106
4.3 Model development 106
4.3.1 Natural isotopes of the studied radionuclides at Forsmark 107
4.3.2 Hydrodynamic processes and parameters 109
4.3.3 Geochemical processes and parameters 110
4.3.4 Initial and boundary conditions 112
4.3.5 Spatial and time discretisation 116
4.4 Numerical results 116
4.4.1 Present-day hydrogeochemical conditions 116
4.4.2 Retention of repository-derived radionuclides 118
4.5 Conclusions 124
4.6 References 125
5. Estimating effective distribution coefficients of selected radionuclides from reactive transport numerical models 129
5.1 Introduction 130
5.2 Scope 131

5.3 Reactive solute transport model....132
5.3.1 Hydrodynamic and geochemical processes....133
5.3.2 Initial and boundary conditions....136
5.3.3 Spatial and time discretisation....138
5.4 Results from the reactive solute transport model....139
5.4.1 Transport of a conservative solute....139
5.4.2 Distribution coefficient (Kd) of radionuclides and their natural isotopes....140
5.4.3 Retention and breakthrough curves of repository-derived radionuclides....146
5.5 Retardation factor (R) of repository-derived radionuclides....147
5.6 Conclusions....153
5.7 References....155
6. Summary, conclusions and discussion....159
6.1 Summary and Conclusions....159
6.2 Discussion....161
6.2.1 Chapter 2: lactate fermentation and the inorganic carbon system....162
6.2.2 Chapter 3: geochemical behaviour of radium in the glacial clay....163
6.2.3 Chapters 3 and 4: coupling of wider and more complex geological settings 163
6.2.4 Chapters 3 and 4: reliability of the numerical predictions....164
6.2.5 Chapter 5: uncertainties on the parameterization of solute transport....165
6.3 References....166
Appendix 1....167
A1. References....170

List of Figures

Figure 1.1 – Sketch of the near-surface systems overlying a deep geological repository (modified with permission from SKB image archive; www.skb.se). 2

Figure 1.2 – Sketch of a hydro-bio-geochemical system where the main heterogeneous and homogeneous reactions are illustrated. The yellow arrows illustrate the possible fluxes of chemical species between the different phases: gas, aqueous, solid, and biomass (green symbol). 4

Figure 1.3 – Representative elemental volume (REV) showing the mass fluxes that cross its boundaries. The conservation of mass within the REV is described by the following equation: $(J_x + J_y + J_z) – (J_{x+\Delta x} + J_{y+\Delta y} + J_{z+\Delta z}) = \Delta S$..... 6

Figure 1.4 – Sketch of a deep geological repository for HLNW in a granitic host rock showing a hypothetical path for radionuclides potentially released from the repository. The near-surface systems that have been modelled in Chapters 3 and 4 (glacial clay and till) are highlighted with a red rectangle. 10

Figure 2.1 – Sketch of the jar-fermentor experiment. The step of the jar-fermentor experiment that has been modelled is highlighted with a blue rounded rectangle. 34

Figure 2.2 – Measured time evolution of pH and pe in the jar-fermentor experiment. 35

Figure 2.3 – Measured time evolution of: a) DO, Lactate, Acetate and Propionate in solution; and, b) SO_4^{2-}, Fe^{2+} in solution, and $CH_4(g)$ in the headspace gas of the jar-fermentor. 36

Figure 2.4 – Sketch of organic matter (OM) oxidation and EA reduction following the partial equilibrium approach. Gibbs free energy change increases from O_2 reduction to CO_2 reduction and the energy gained in these redox reactions increases at the opposite direction. 41

Figure 2.5 – Measured (symbols) and simulated (red line) time evolution of DO (a) and NO_3^- (b). Computed evolution of aerobes (a) and denitrifiers (b) biomass is also shown (green lines). 53

Figure 2.6 – Time evolution of measured (symbols) and simulated (red line) dissolved lactate, acetate and propionate concentrations. Computed evolution of fermentative (a) and methanogenic (c) bacteria is also shown (green line). 55

Figure 2.7 – Time evolution of measured (symbols) and simulated (red line) dissolved Fe(II) (a), and SO_4^{2-} (b) concentrations. Computed evolution of IRB's (a) and SRB's (b) is shown with green lines. Computed concentration of FeOOH(s) and the secondary

mineral phases $FeCO_3$ and FeS are shown in graphic c, and computed concentration of HS^- is plotted in graphic d. 57
Figure 2.8 – Time evolution of measured (symbols) and simulated (red line) partial pressure of $CO_2(g)$ in the headspace and pH. Computed concentration of calcite during the experiment is also shown (blue line). 58
Figure 2.9 – Time evolution of measured (symbols) and simulated (red line) partial pressure of $CH_4(g)$ in the headspace. Computed concentration of methanogens is also shown (green line). 60
Figure 2.10 – Time evolution of measured (symbols) and simulated (red line) pe. Computed evolution of biomass of all microbial groups considered in the simulation is also shown, in the lower graphic. 61
Figure 2.11 – Time evolution of measured (symbols) and simulated (red line) pe considering an alternative stoichiometry for lactate fermentation. 62
Figure 2.12 – Time evolution of measured (symbols) and simulated (red line) pH, DO, NO_3^-, lactate, acetate, propionate, Fe(II) and SO_4^{2-}. Computed evolution of calcite concentration is plotted with a blue line, and computed evolution of the biomass of each microbial group (related to each EA, and also fermenters for lactate) is plotted with green lines. 65
Figure 3.1 – Geological map of the Forsmark area with location of the candidate site (SKB, 2002, reproduced with permission). 74
Figure 3.2 – Observed correlations between strontium and calcium in shallow groundwaters of Forsmark candidate area. 76
Figure 3.3 – Near-surface hydrogeological conceptual model of Forsmark candidate site (modified from Johansson et al., 2005) showing a hypothetical path of radionuclides released from a repository. The glacial clay under study is highlighted with a red rectangle. 78
Figure 3.4 – Preliminary model developed to find the boundary conditions of the glacial clay, and modelled domain developed for the glacial clay sediment with the corresponding boundary conditions. 83
Figure 3.5 – Computed concentration of Cl(aq) in the modelled domain at the transport steady state, and computed breakthrough curve at the discharge area of the modelled domain (node X= 10 m, Y= 1 m). *[Cl] normalised stands for: $([Cl(aq)]_{predicted} - [Cl(aq)]_{initial})/ ([Cl(aq)]_{final} - [Cl(aq)]_{initial})$. 88
Figure 3.6. Computed evolution of the concentration of natural: a) U(aq); b) Sr(aq); and, c) Cs(aq) during the approach to the geochemical quasi-steady state that represents the

present-day conditions of the glacial clays at Forsmark (observation node: X= 10 m; Y= 1 m). The concentrations at 2700 years are in the range of concentrations observed nowadays which are reported in the forth section of this work. 90
Figure 3.7 – Comparison between simulated (red symbols) composition of the porewater of the glacial clay at the present-day hydrogeochemical conditions (after 2700 years of reactive transport) and measured (black symbols) composition of the shallow groundwaters at Forsmark. a) Aqueous concentration of uranium against bicarbonate; b) Aqueous concentration of strontium against calcium; c) Location of the selected points of the modelled domain (red dots) plotted in graphics a and b. 91
Figure 3.8 – Computed distribution of repository-derived uranium precipitated as amorphous uraninite, 2700 years after repository release (in $^{RD}U(s)$, s stands for concentration in the solid phase). Breakthrough curves for natural (black symbols) and repository-derived (red symbols) aqueous uranium are also shown. 92
Figure 3.9 – Computed distribution of repository-derived strontium retained in the planar sites of illite ($^{RD}SrX_2$) and calcite ($SrCO_3$), 2700 years after repository release (distinct scales are used for each phase). Breakthrough curves for natural (black symbols) and repository-derived (red symbols) Sr(aq) are also shown. 93
Figure 3.10 – Computed distribution of repository-derived caesium retained in the FES of illite ($^{RD}CsX^{FES}$), 2700 years after repository release. Breakthrough curves for natural (black symbols) and repository-derived (red symbols) Cs(aq) are also shown. 94
Figure 3.11 – Computed distribution of repository-derived radium retained in the aqueous phase of the glacial clay, 2700 years after repository release. The breakthrough curve for repository-derived (red symbols) Ra(aq) is also shown. 94
Figure 3.12 – Computed evolution of retention efficiency for ^{RD}U (dashed line), ^{RD}Sr (grey squares) and ^{RD}Cs (solid line), at the discharge area of the glacial clay (top right corner of modelled domain; node X= 10 m, Y= 1 m). 96
Figure 4.1 – Near-surface hydrogeological conceptual model of Forsmark candidate site (modified from Johansson et al., 2005) showing a hypothetical path of radionuclides released from a repository. The section of the Quaternary till under study is highlighted with a red rectangle. 107
Figure 4.2 – Observed correlations between strontium and calcium in shallow groundwaters of Forsmark candidate area. 108
Figure 4.3 – Flow boundary conditions for the numerical model of the Quaternary till. .. 113
Figure 4.4 – Comparison between simulated (red symbols) composition of the porewater of the glacial clay at the present-day hydrogeochemical conditions (after 2700 years of

reactive transport) and measured (black symbols) composition of the shallow groundwaters at Forsmark. a) Aqueous concentration of uranium against bicarbonate; b) Aqueous concentration of strontium against calcium; c) Location of the selected points of the modelled domain (grey dots) plotted in graphics a and b. 117
Figure 4.5 – a) Predicted evolution of the concentration of natural (U(aq)) and repository-derived (RDU(aq)) uranium after repository release, at the discharge area; b) Predicted concentration of RDU retained in the strong sites of ferrihydrite at the end of simulation period (2700 years after repository release). $(HFO\_sO)_2{}^{RD}UO_2CO_3^{2-}$ stands for the major species of repository-derived uranium sorbed onto ferrihydrite.....119
Figure 4.6 – a) Predicted evolution of natural (Sr(aq)) and repository-derived (RDSr(aq)) strontium after repository release, at the discharge area; b) RDSr retained in illite ($^{RD}SrX_2$); c) RDSr in $(Ca,Sr)CO_3$ solid solution, at the end of the simulation period (2700 years after repository release). RDSr is preferentially incorporated in illite (note the different scales for plots b and c.....120
Figure 4.7 – a) Predicted evolution of natural (Cs(aq)) and repository-derived (RDCs(aq)) caesium after repository release, at the discharge area; b) Predicted concentration of RDCs retained in the FES of illite ($^{RD}CsX^{FES}$) at the end of the simulation (2700 years after repository release). 121
Figure 4.8 – a) Predicted evolution of repository-derived (Ra(aq)) radium after repository release, at the discharge area; b) Predicted concentration of Radium retained in $(Ba,Ra)SO_4$ solid solution at the end of the simulation time.....122
Figure 4.9 – Computed retention efficiencies for uranium (dashed line), strontium (grey squares), caesium (solid line) and radium (black triangles), derived from repository release, at the discharge area of the Quaternary till. 123
Figure 5.1 – Near-surface hydrogeological conceptual model of Forsmark candidate site (modified from Johansson et al., 2005) showing a hypothetical path of radionuclides released by a repository. 133
Figure 5.2 – Boundary conditions for the numerical model of the till domain. 136
Figure 5.3 – Computed concentration of Cl(aq) in the modelled domain at the transport steady state, and computed breakthrough curve at the discharge area of the modelled domain (node X= 80 m, Y= 3 m). *[Cl] normalised stands for: $([Cl(aq)]_{predicted} - [Cl(aq)]_{initial})/ ([Cl(aq)]_{final} - [Cl(aq)]_{initial})$. 139
Figure 5.4 – Predicted evolution of Kd(U) along the simulation time. In the beginning of the simulation period the Kd varies with time. From 2700 years until the end of the

simulation (10,700 years), relatively small geochemical changes occur, and hence Kd does not vary much. 142
Figure 5.5 – Predicted evolution of Kd(Sr) along the simulation time. In the beginning of the simulation period the Kd varies with time. From 2700 years until the end of the simulation (10,700 years), relatively small geochemical changes occur, and hence Kd does not vary much. 143
Figure 5.6 – Predicted evolution of Kd(Cs) along the simulation time. In the beginning of the simulation period the Kd varies with time. From 2700 years until the end of the simulation (10,700 years), relatively small geochemical changes occur, and hence Kd does not vary much. 144
Figure 5.7 – Predicted distribution of Kd(Ra) at the end of the simulation time, 8000 years after repository release. 145
Figure 5.8 – Computed breakthrough curves at the discharge area of the modelled domain (node X= 80 m; Y= 3 m, see Figure 5.3) for repository-derived radionuclides, considering the geochemical reactions that affect radionuclide mobility (reactive transport, red line) and without considering any geochemical reaction (conservative transport, black line). 147
Figure 5.9 – Predicted breakthrough curves for a conservative solute in PHAST and the calibrated conservative transport model built in FEFLOW. Monitoring point X= 80 m, Y= 3 m (discharge area). 149
Figure 5.10 – Computed distribution of kinematic Kd for the selected radionuclides 8000 years after repository release. Kinematic Kd is calculated for each node of the modelled domain by applying equation 5.2, using the effective porosity (0.0789) instead of the total porosity (0.25). 151
Figure 5.11 – Computed breakthrough curves for RDSr normalised. Legend: symbols: Kd-based model computed in FEFLOW; red line: reactive transport model (computed in PHAST) solved backwards-in-time and upstream-in-space; blue line: reactive transport model (computed in PHAST) solved centred-in-time and centred-in-space. 152
Figure 5.12 – Computed breakthrough curves for RDU normalised. Legend: symbols: Kd-based model computed in FEFLOW; red line: reactive transport model (computed in PHAST) solved backwards-in-time and upstream-in-space; blue line: reactive transport model (computed in PHAST) solved centred-in-time and centred-in-space. 153

List of Tables

Table 2.1 – Summary of the biotic and abiotic reactions implemented in the numerical simulation of the jar-fermentor experiment. 38
Table 2.2 – Summary of the ED's, EA's and inhibitors implemented for each microbial group. 43
Table 2.3 – Measured data and input data for the initial composition of the aquatic system modelled. Reasoning for setting a different initial value than the one measured is also shown. 49
Table 2.4 – Summary of the calibrated values of the parameters that describe the microbially mediated reactions. 52
Table 3.1 – Values of the hydrodynamic parameters implemented in the numerical model for the glacial clay. (from Johansson et al., 2005). 79
Table 3.2 – Complexation reactions of aqueous Fe(III) carbonates and corresponding thermodynamic constants (from Grivé, 2005). 80
Table 3.3 – Complexation reactions of organic compounds and the corresponding thermodynamic constants. 81
Table 3.4 – Initial concentration of the reactive minerals considered for the reactive transport simulations. Potentially retained radionuclides and respective mechanism of retention are also shown. 82
Table 3.5 – Initial composition of glacial clay porewater and deep groundwater (Deep GW). Concentrations of RDCs, RDU, RDSr and Ra in the deep GW (after repository release) represent the increment of these elements due to repository release. 85
Table 4.1 – Values of the hydrodynamic parameters implemented in the numerical model for the Quaternary till (from Johansson et al., 2005). 109
Table 4.2 – Initial concentration of the reactive minerals considered for the reactive transport simulations. Potentially retained radionuclides and respective mechanism of retention are also shown. 112
Table 4.3 – Initial composition of till porewater and deep groundwater (Deep GW). Concentrations of RDCs, RDU, RDSr and Ra in the deep GW (after repository release) represent the increment of these elements due to repository release. 114
Table 5.1 – Values of the hydrodynamic parameters implemented in the numerical model for the Quaternary till. Values taken from Johansson et al. (2005). 134

Table 5.2 – Initial concentration of the reactive minerals implemented in the reactive transport simulations..... 135
Table 5.3 – Initial composition of till porewater and deep groundwater (Deep GW). Concentrations of RDCs, RDU, RDSr and Ra in the Deep GW (after repository release) represent the increment of these elements due to repository release. 137
Table A1.1 - Cation exchange reactions and thermodynamic constants in the illite interlayer..... 167
Table A1.2 – Dissolution/precipitation reactions of the reactive solid phases considered in the numerical simulations developed in Chapters 3 to 5. Thermodynamic equilibrium constants and corresponding references are also listed. 168
Table A1.3 – Complexation reactions on ferrihydrite surface and corresponding thermodynamic constants (from Waite et al., 1994). 169

“The time scale of development of man, and the similar time scale indicated by the decay of radionuclides in waste, appears unimportant compared with cosmic evolution. Even more striking is the perspective of universal space and the distribution of matter in it. We live in a tiny speck of a planet, and have only a narrow knowledge of a thin layer of this planet earth. But from this perspective we learn that the masses of matter within our reach are tremendous. This makes us feel humble and at the same time it inspires confidence that our waste problems can find quite natural solutions – if we are ready to make use of our talents.”

Rudolf Rometsch

In:

Cécille, 1991. Radioactive waste management and disposal.
Proceedings of the 3rd European Community Conference
on Radioactive Waste Management and Disposal.

Chapter 1

Introduction

1. Introduction

1.1 Motivation

Hydrogeochemical numerical modelling is worldwide used to simulate natural and anthropogenically induced phenomena. These simulations help us to understand the surrounding environment; its spatial variability and temporal evolution. Dealing with evolving systems requires understanding the past which, in turn, sustains predictions about the future.

During the last decades, management and disposal of high level nuclear waste (HLNW) have been motivating an increasing number of scientific research projects where hydrogeochemical numerical modelling plays an important role. The present work is in close relation to two national programmes dedicated to the final disposal of HLNW: the national programme hosted by the Japan Atomic Energy Agency (JAEA) and the national programme hosted by the Swedish Nuclear Fuel and Waste Management Company (SKB). Both programmes consider the deep geological repository as the solution for the final disposal of HLNW.

According to international agreements, the nuclear waste must not burden future generations. HLNW has to be managed responsibly to ensure public safety, protection of the environment, and security from malicious intervention now and in the future (OECD, 1999). Since HLNW is partially composed of long-lived radionuclides its final disposal must guarantee safety and isolation for at least 100,000 years after repository closure (SKB, 2006). The deep geological repository is the most widely accepted solution among countries with nuclear power plants (Brookins, 1987; Cécille, 1991).

According to the Swedish (and also Finish) concept, a deep geological repository consists of deposition holes excavated at a depth of approximately 500 m where HLNW is stored. The packages of HLNW are surrounded by several engineered barriers which may vary from country to country. Some of these engineered barriers include metal canisters, clay barriers and cement liners. The host rock and the overlying surface sediments represent the natural barriers of a deep geological repository.

The chemical and physical properties of the HLNW show some differences from country to country. In Sweden, HLNW is the spent nuclear fuel that is no longer energetically efficient to keep being used in nuclear power plants. It is a ceramic material composed of uranium dioxide that is very stable under the conditions of the repository (i.e. under the pH

and redox conditions of groundwater at repository depths). On the other hand, in Japan, HLNW is a non-profitable product of the reprocessing of spent nuclear fuel to recover uranium and plutonium. In Japan, the HLNW is vitrified in borosilicate glass to ensure its physico-chemical stability.

When dealing with the final disposal of HLNW, the potential migration of radionuclides through the engineered and natural barriers that surround the repository must be assessed. In performance assessment of deep geological repositories, failure scenarios of the repository and their environmental consequences are being analysed (e.g. SKB, 2006). In case of repository release, the surface sediments overlying the repository host rock represent the last geological barrier prior to the surface ecosystems.

In the framework of performance assessment, the geochemical long-term evolution of a deep geological repository is usually assessed by using hydrogeochemical numerical simulations which couple laboratory and field data for the long time spans needed to be considered when dealing with HLNW.

The present work is focused on the hydrodynamic and geochemical processes that prevail in the near-surface systems overlying a potential host rock which influence radionuclide mobility (Figure 1.1).

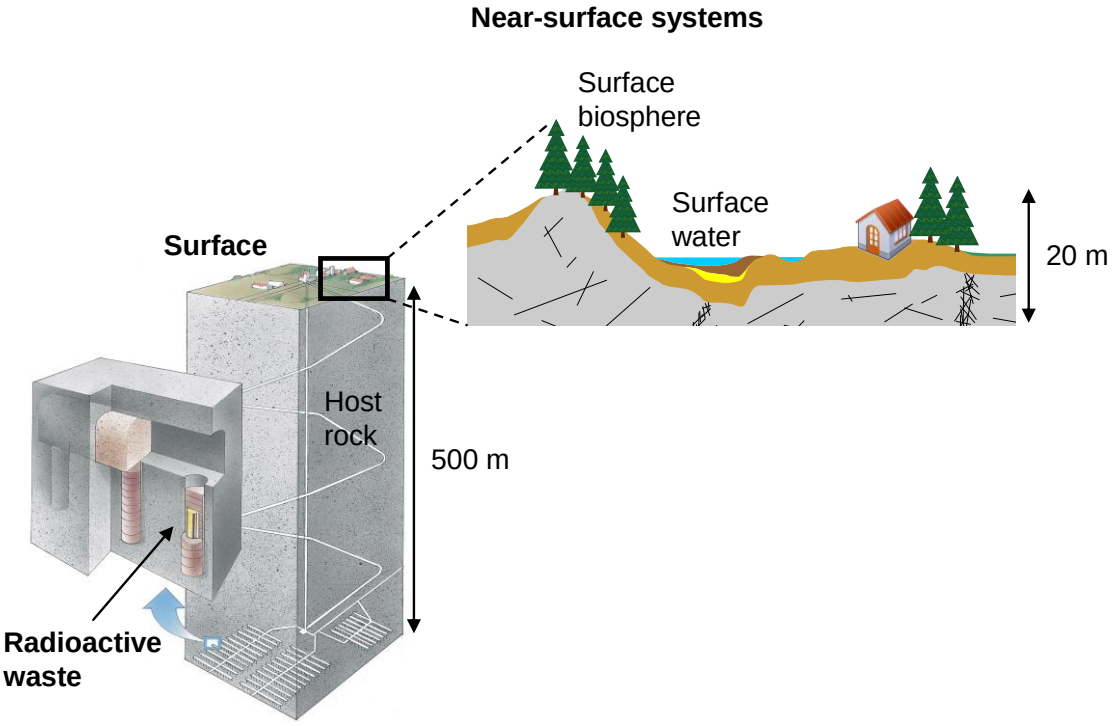

Figure 1.1 – Sketch of the near-surface systems overlying a deep geological repository (modified with permission from SKB image archive; www.skb.se).

1.2 Scope

This thesis is composed of four main chapters presenting different examples of hydrogeochemical simulations developed to assess radionuclide mobility in near-surface systems that overly a potential host rock for a deep geological repository. The numerical models developed are focused on a laboratory-scale problem (Chapter 2) and two-dimensional field-scale problems (Chapters 3 to 5). Besides the four main chapters, two other chapters provide the introduction to (Chapter 1) and the general conclusions of (Chapter 6) the whole research work.

In Chapter 1, the motivation, scope, methodology, state-of-the-art and main objectives of the research work are presented. In Chapter 2 an aquatic system with no transport of solutes is simulated. The concentration of solutes is considered to vary over time due to geochemical and biochemical reactions. In Chapters 3 to 5, two-dimensional groundwater systems where water flows and transports solutes that may react with the solid matrix of the porous media are developed.

Concerning the master variables time and space, two main types of hydrogeochemical problems may be found:

- Hydrogeochemical problems where water flow and solute transport are negligible; i.e. the concentration of chemical species does not vary in space. In this type of problems, the concentration of solutes varies over time due to heterogeneous and homogeneous chemical reactions (heterogeneous meaning those reactions that take place between aqueous, solid, and gaseous phases, while homogeneous reactions take place within a single phase; e.g. aqueous complexation). In addition, these chemical reactions can occur under local thermodynamic equilibrium or under kinetics. Chapter 2 presents the development of a numerical model of this type of problem.
- Reactive transport problems where the concentration of solutes varies over time and space due to groundwater flow which transports dissolved species that may react with solid (minerals, organic matter, etc.) and gaseous components (e.g. $O_2(g)$). Chapters 3 to 5 present examples for the development of numerical models of this type of problem.

In Figure 1.2, the main (bio)geochemical reactions that are believed to occur in an aquatic system such as the jar-fermentor experiment that was studied in Chapter 2 are illustrated. In the aqueous phase, solutes may be complexed with other species, or undergo redox and acid-base reactions. When organic matter is available, microbial respiration is able to

trigger redox reactions involving inorganic (O_2, NO_3^-, Fe^{3+}, SO_4^{2-}) and organic solutes (dissolved organic matter such as lactate, propionate and acetate). In addition, elements like carbon, hydrogen, nitrogen and oxygen can be removed from solution and incorporated into biomass cells (biomass growth), or they can be released into solution due to biomass decay. Finally, solutes may be transferred to other phases (gas and solid) due to the different heterogeneous geochemical reactions that are shown in Figure 1.2.

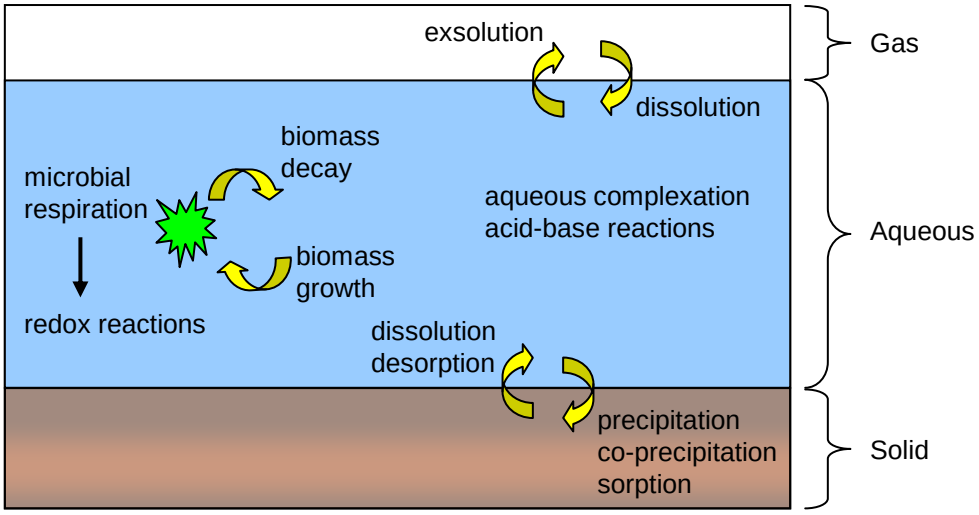

Figure 1.2 – Sketch of a hydro-bio-geochemical system where the main heterogeneous and homogeneous reactions are illustrated. The yellow arrows illustrate the possible fluxes of chemical species between the different phases: gas, aqueous, solid, and biomass (green symbol).

In a hydrogeochemical problem, such as the one developed in Chapter 2, two main equations must be solved to describe the changes in the concentration of chemical species due to local thermodynamic equilibrium reactions (equation 1.1) and kinetic reactions (equation 1.2). The general equation describing local thermodynamic equilibrium reactions is (e.g. Parkhurst and Appelo, 1999):

$$K = \frac{\prod_{products} a_p^{\upsilon_p}}{\prod_{reactants} a_r^{\upsilon_r}} \qquad \text{(equation 1.1)}$$

where K is the equilibrium constant, a is the activity, υ_r and υ_p are the stoichiometric coefficients of the reactants and products of a given chemical reaction, respectively.

Activities of the aqueous species are related to molalities through activity coefficients which may be calculated using different expressions, such as the Debye-Hückel equation. In equation 1.1 there is no integration in time for the concentration of a species, since local equilibrium reactions do not depend on the master variable time. Therefore, for the concentration of a given chemical species to vary in time, under local equilibrium, some external source/sink term must occur to induce the change in concentration. This external source/sink term can be the addition of a new substance (mineral, gas or a different solution) which is not in equilibrium with the original solution or the presence of mineral phases of which dissolution/precipitation is kinetically driven.

Besides local thermodynamic equilibrium, the kinetic chemical reactions can be described by the following general equation (e.g. Parkhurst and Appelo, 1999):

$$\frac{dm_i}{dt} = \upsilon_{i,k} R_k \qquad \text{(equation 1.2)}$$

where m_i is the molality of species i, t is time, $\upsilon_{I,k}$ is the stoichiometric coefficient of species i in the kinetic reaction for substance k, and R_k is the overall reaction rate for substance k.

The reactive transport models developed in Chapters 3 to 5 rely on the continuum hypothesis, where a real groundwater system is approximated by using partial differential equations that describe the variations of mass (of water and chemical species) over time and space. In the continuum representation of the porous medium, the physico-chemical variables describing the system, such as porosity, hydraulic conductivity, mineral concentration, etc., are averaged over a representative elemental volume (REV; Bear, 1972, Figure 1.3). In the REV, each variable assumes a single value for each time step.

If we consider the mass balance for groundwater flow in a saturated porous medium, the net flux J shown in Figure 1.3 represents Darcy's velocity, and the corresponding mass balance for a three-dimensional groundwater flow can be expressed by the following equation:

$$\frac{\partial}{\partial x}\left(k_x \frac{\partial h}{\partial x}\right) + \frac{\partial}{\partial y}\left(k_y \frac{\partial h}{\partial y}\right) + \frac{\partial}{\partial z}\left(k_z \frac{\partial h}{\partial z}\right) = S_s \frac{\partial h}{\partial t} \qquad \text{(equation 1.3)}$$

where x, y and z are the Cartesian coordinates describing space, k is the hydraulic conductivity in units of [LT^{-1}] which can be anisotropic, meaning that it assumes different values depending on the direction in space, h is the hydraulic head [L], S_s is the specific storage coefficient (dimensionless), and t is time.

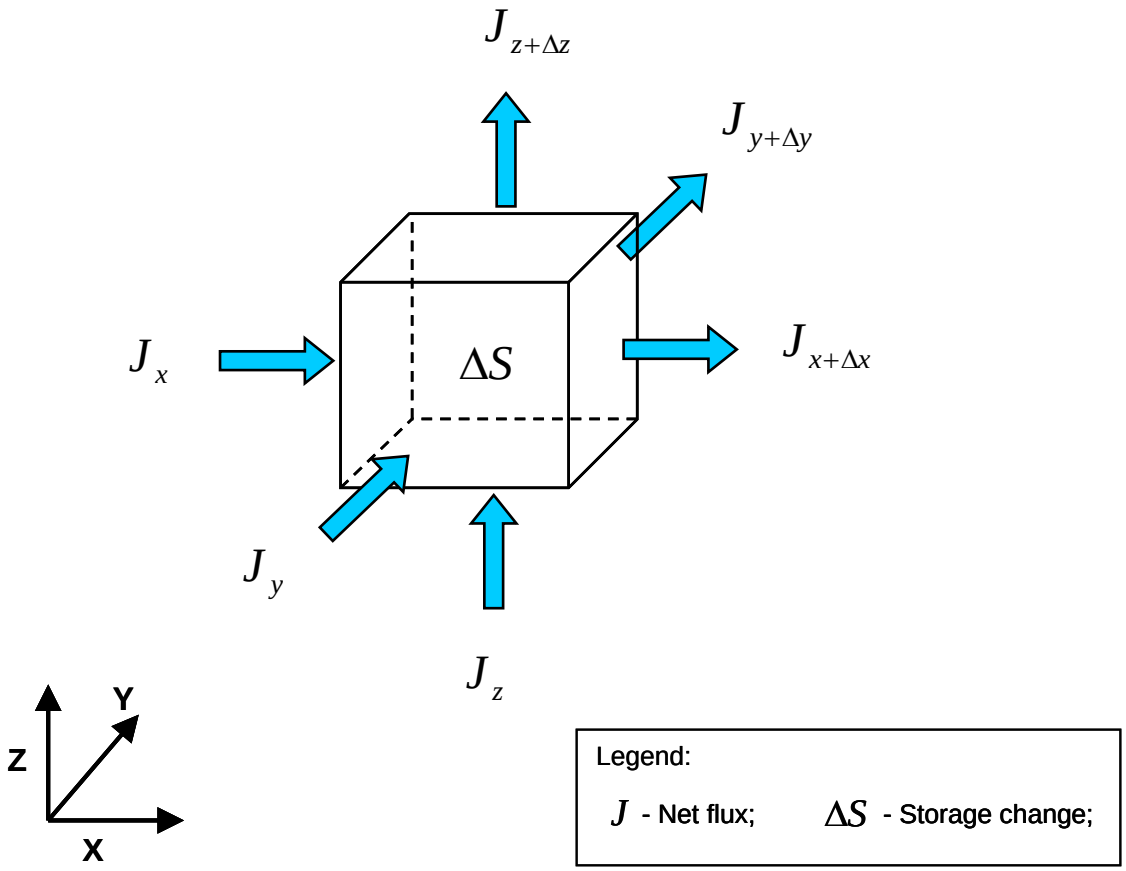

Figure 1.3 – Representative elemental volume (REV) showing the mass fluxes that cross its boundaries. The conservation of mass within the REV is described by the following equation: $(J_x + J_y + J_z) – (J_{x+\Delta x} + J_{y+\Delta y} + J_{z+\Delta z}) = \Delta S$.

If we consider the mass balance for a conservative solute in a hydrodynamic system, then, the net flux J in Figure 1.3 represents the sum of the advective, dispersive and diffusive fluxes. In addition, if we consider the mass balance for a reactive solute, we must add a source/ sink term that represents the addition or removal of the reactive solute to or from solution, due to chemical reactions between this solute and the solid matrix of the porous medium.

The overall equation describing the mass balance for a reactive solute in a saturated porous medium is:

$$-q_x \frac{\partial C}{\partial x} - q_Y \frac{\partial C}{\partial y} - q_z \frac{\partial C}{\partial z} + \phi \frac{\partial}{\partial x}\left(D_x \frac{\partial C}{\partial x} \right) + \phi \frac{\partial}{\partial y}\left(D_y \frac{\partial C}{\partial y} \right) + \phi \frac{\partial}{\partial z}\left(D_z \frac{\partial C}{\partial z} \right) + w = \phi \frac{\partial C}{\partial t}$$

(equation 1.4)

where q is Darcy's velocity [LT^{-1}], C is the concentration of a solute [ML^{-3}], ϕ is porosity (dimensionless), D is the dispersion-diffusion tensor [L^2T^{-1}], and w is the source/sink term due to chemical reactions, given in units of [ML^{-3}]. If w is null, then the corresponding solute is considered a conservative solute, which does not react with the solid matrix of the porous medium.

If the source/ sink term w is calculated using equations 1.1 and 1.2, that describe equilibrium and kinetic chemical reactions, the numerical model is considered a reactive transport model. On the other hand, if the source/ sink term w is calculated by using a distribution coefficient (Kd) which defines the ratio between the concentration of a solute in solid and aqueous phases, then the model is considered a Kd-based model.

The numerical models developed in Chapters 3 and 4 are reactive solute transport models where water flow and transport of dissolved species are coupled with geochemical reactions between solid and aqueous phases. In Chapter 3, a diffusion dominated porous media that represents a glacial clay sediment is modelled, while in Chapter 4 an advection dominated porous media, represented by a till deposit that hosts unconfined aquifers, is developed.

Chapter 5 presents a methodology for estimating effective Kd's from the outputs of the reactive transport numerical simulations developed in Chapter 4. The meaning and applicability of these Kd values estimated from reactive solute transport simulations are discussed and validated in Chapter 5.

The work presented in Chapter 2 has been developed in the framework of JAEA programme for the management of HLNW, and has been presented as a poster at the 19th V.M. Goldschmidt™ conference.

The work presented in Chapters 3 to 5 has been developed in the framework of SKB Site Characterization Programme for Sweden's deep geological repository. This work resulted in two technical reports published by SKB which are available for download at www.skb.se. The two publications are: Grandia et al. (2007) and Sena et al. (2008).

Chapter 6 summarizes the work presented in the preceding chapters, integrates the main conclusions attained in each chapter, and presents the final discussions related to some unsolved problems and future works.

1.3 Methodology

The development of any numerical model relies on the definition of a sound conceptual model which couples the data available for the system under study with information on other similar systems, as well as information gathered from laboratory experiments. The conceptual model identifies the features, events and processes that describe the system under study, and also the limits of the system. The conservation of mass and energy must, therefore, be fulfilled within the limits of the conceptual model. The conceptual model reflects the information gathered to describe the system under study and also the interpretations and assumptions which, in turn, are based on the observations and measurements of the system and on the information obtained on other similar systems.

After building a sound and reliable conceptual model, the numerical model is built based on the data, interpretations and assumptions that describe the conceptual model, but with the limitations associated to the capabilities of the codes and of process understanding and parameterization. Calibration of the numerical model represents the step where the conceptual model is validated and questioned. This procedure has been adopted in all the numerical models developed in the present work.

In Chapter 2 a numerical model that simulates microbially mediated redox processes in lake sediments is developed using PHREEQC (Parkhurst and Appelo, 1999). This numerical model simulates a jar-fermentor experiment that was conducted by JAEA to assess the role of microbial activity in aquatic subsurface systems. During this experiment lake water and sediment samples were mixed and oxidized by atmosphere bubbling during 5 days. Then, an organic electron donor substance (lactate) was added to the jar-fermentor which was kept in closed conditions for additional 13 days. During the experiment the main geochemical parameters and bacterial flora were analyzed (Nakajima et al., 2008).

In this modelling exercise, Monod kinetic equations have been implemented to simulate microbially mediated reactions. In addition, abiotic, kinetic and equilibrium, geochemical reactions have also been considered. The numerical model developed is intended to simulate the observed consumption of organic electron donors (lactate, acetate and propionate) and inorganic electron acceptors (O_2, NO_3^-, Fe^{3+} and SO_4^{2-}), as well as their effect on the master variables pH and Eh.

From all the biogeochemical parameters that were implemented in the numerical model developed in Chapter 2, the Monod kinetic parameters are subject to a relatively high degree of uncertainty. Therefore, the calibration of the numerical model developed in Chapter 2 relies on that combination of the Monod kinetic parameters which leads to the

best agreement between measured and simulated values of the different organic and inorganic geochemical variables.

Simulation of microbially mediated kinetic reactions follows the so called partial equilibrium approach in which the oxidation of organic matter is considered to be the rate limiting process, and the geochemical system is led to respond under local equilibrium by reducing the most thermodynamically favourable electron acceptor (EA). In addition, inhibition terms have been used to describe mathematically the sequential use of EA's (Barry et al., 2002, and references therein).

Chapters 3 and 4 encompass a modelling procedure using PHREEQC (Parkhurst and Appelo, 1999) and PHAST (Parkhurst et al., 2004) to predict radionuclide retention in two distinct near-surface sediments present at Forsmark (Sweden). Forsmark is the candidate site that has been selected in June 2009 for the location of a deep geological repository in Sweden. In order to assess radionuclide retention in the near-surface systems at Forsmark four radionuclides (^{235}U, ^{135}Cs, ^{226}Ra and ^{90}Sr) have been selected according to their different geochemical behaviour and potential dose relevance to surface ecosystems.

The sediment modelled in Chapter 3 is a glacial clay located between surface water bodies and the shallow unconfined aquifers hosted by till deposits, while in Chapter 4 the calcite-rich Quaternary till that overlies the granite candidate host rock is modelled. Prediction of radionuclide retention in both Quaternary sediments relies on a hypothetical scenario of repository release where deep groundwater flowing through a fracture in the granite candidate host rock is considered to transport dissolved radionuclides from the repository to the near-surface systems (Figure 1.4).

The main steps of the modelling procedure applied in Chapters 3 and 4 include:

1) the detailed analysis of SKB's hydrogeochemical database for the near-surface systems at Forsmark;
2) the development of the conceptual model of each modelled system based on data gathered in the first step and on the comparison of the systems under study with similar systems;
3) the thorough review of the thermodynamic parameters required for the simulation of geochemical processes;
4) the implementation of the conceptual model in reactive transport numerical simulations;
5) the simulation of the present-day hydrogeochemical conditions observed at Forsmark, by developing a long-term reactive transport simulation;

6) the simulation of a hypothetical repository release in the numerical model; and,
7) the quantitative assessment of radionuclide retention in the modelled systems based on the outputs of the numerical simulations.

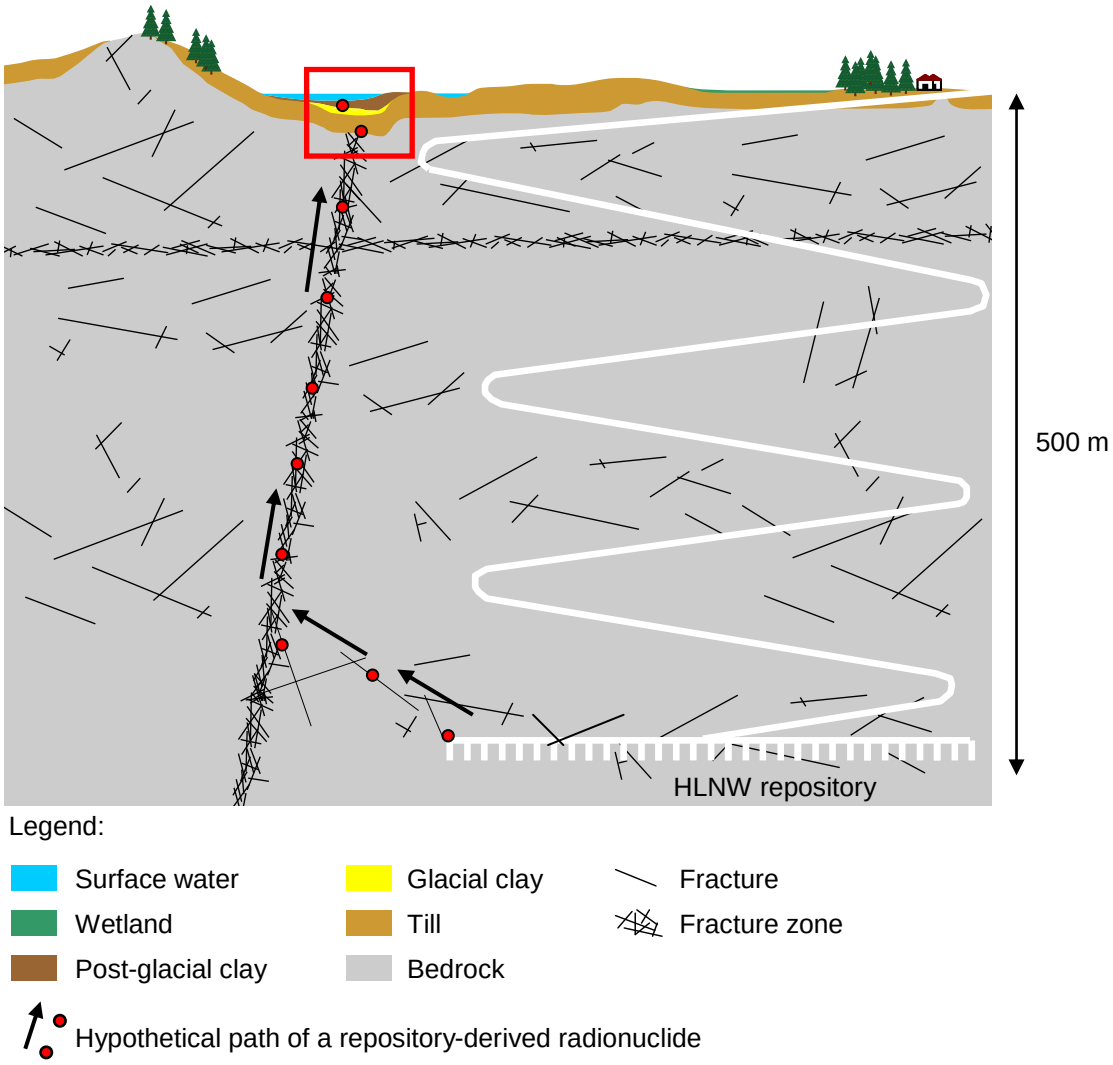

Figure 1.4 – Sketch of a deep geological repository for HLNW in a granitic host rock showing a hypothetical path for radionuclides potentially released from the repository. The near-surface systems that have been modelled in Chapters 3 and 4 (glacial clay and till) are highlighted with a red rectangle.

After analysing SKB's hydrogeochemical database for the Forsmark site, (1) the glacial-clay porewater; (2) the shallow groundwater of the till deposit; and, (3) the deep granitic groundwater have been selected as the most representative near-surface waters for the simulations. The selection of the reactive minerals considered in the numerical models of the glacial clay and till sediments relies on three main premises: (1) which are the

minerals present in the system under consideration?; (2) which are the minerals that control pH and Eh in each Quaternary sediment?; and, (3) which are the minerals that may affect the mobility of the selected radionuclides? Unfortunately, in some cases the information on the minerals present in the system is not always available or it is incomplete. In these cases, the selection of the reactive minerals must be based on the knowledge on this type of systems coupled with the analysis of the geochemical data available for the system under study.

In natural aquatic systems, the most common geochemical reactions that radionuclides may undergo are:

1) Cation exchange in clay minerals. Cation exchange is the replacement of a cation initially adsorbed in the interlayer of a clay mineral by another cation present in groundwater (Appelo and Postma, 2005; Stumm and Morgan, 1996).
2) Adsorption on charged surfaces of minerals such as oxyhydroxides or clays. Adsorption is the adherence of an ion on the charged surface of a mineral. The charge of a given mineral may vary from negatively charged to positively charged, passing through a non-charged surface which is called the point of zero charge, depending on the pH conditions of groundwater (Dzombak and Morel, 1990; Stumm and Morgan, 1996).
3) Sorption onto organic tissues. As on charged mineral phases, ions can also adsorb on the charged surfaces of organic tissues (Appelo and Postma, 2005; and references therein).
4) Co-precipitation with major element solid phases such as sulphates, sulphides, oxyhydroxides and carbonates. Co-precipitation is the formation of solid solutions between two or more solid phases. Solid solutions are, therefore, minerals with variable compositions of pure end-member minerals (Glynn and Reardon, 1990; and references therein).
5) Aqueous complexation with organic and inorganic ligands such as humic acids and aqueous carbonates. Aqueous complexation depends greatly on the pH and redox state of groundwater. In addition, by complexing with aqueous species, the precipitation of solid phases that incorporate radionuclides may be hindered.
6) Precipitation of pure phases. In some cases, and despite the relatively low concentrations of radionuclides, precipitation of pure phases such as amorphous uraninite can be relevant.

In the numerical simulations developed in Chapters 3 and 4, radionuclides potentially released by the repository were labelled to trace and distinguish them from natural occurring isotopes in the numerical simulations (RDSr, RDCs and RDU, where RD stands for Repository-Derived). Radium was not labelled since it was considered to be below detection limit in the porewater of the studied Quaternary deposits, before repository release.

Labelling of repository-derived radionuclides involved the addition of the labelled species as primary species to the thermodynamic database used in the numerical simulations. The secondary aqueous species for labelled radionuclides had to be added by duplicating the reactions for non-labelled isotopes and replacing the isotope with the labelled radionuclide. In order to consider the incorporation of both repository-derived radionuclides and naturally occurring isotopes in the same solid phase, without causing an artificial isotopic fractionation, new ideal solid solutions involving both species had also to be added to the thermodynamic database.

The numerical results attained in Chapters 3 and 4 have proven that the labelling procedure has been done correctly, and no artificial isotopic fractionation has been introduced. Actually, in Chapter 5, the Kd values calculated from the outputs of the numerical simulations developed in Chapter 4 are the same for each isotope (labelled and unlabelled species) of a given element which reflects the inexistence of an unintended fractionation process.

Radionuclide retention in the Quaternary sediments was quantitatively assessed from the outputs of the numerical simulations developed in Chapters 3 and 4. This modelling procedure has proven to be a robust methodology for such quantitative assessment.

The work presented in Chapters 2 to 4 entails numerical models that account for biochemical (Chapter 2) and geochemical (Chapters 2, 3 and 4) processes influencing solute mobility. This type of models is usually assigned to the so called “component additivity” (CA) approach, i.e. these models assume that each mineral in a complex mineral assemblage has unique thermodynamic properties, where the important linkage between solid and aqueous species is retained through the coupling of mass action equations (Davis et al. 1998, and references therein). This approach is much more complex and computational demanding than a constant Kd approach, but it is much more reliable when dealing with complex near-surface systems like the ones modelled here.

Near-surface systems are affected by changes in key geochemical parameters (pH, Eh, ionic strength) which strongly influence the Kd value. In addition, if a given mineral precipitates or dissolves, a Kd-based model is not able to account for the increase or

decrease of the solid pool that retains a reactive solute. Nevertheless, for the time being, Kd-based models are still considered to be a very useful tool to simulate groundwater systems with large dimensions and extremely complex flow conditions, as the fractured kilometric volumes of a candidate host rock for a deep geological repository. In addition, hydrogeochemical models depend on reliable site specific data and thermodynamic parameters which may be difficult to get or eventually have not been developed yet.

A Kd-based model does not depend on thermodynamic data, and site specific data may be more generic than for the component additivity type of models. In this context, Kd-based models can be used for the preliminary and more general assessments of a given problem. In this context, in Chapter 5, effective Kd values have been estimated from the outputs of the reactive transport numerical model developed in Chapter 4. The meaning and validity of these Kd values has been assessed and discussed in Chapter 5 by developing Kd-based transport models using FEFLOW (Diersch, 2005).

1.4 State-of-the-art

1.4.1 Kd-based models versus reactive transport models

When a modeller selects a code for solving groundwater flow coupled with reactive solute transport two main approaches may be found. On one hand, there are codes that solve groundwater flow coupled with a set of non-linear equations that describe the geochemical reactions between reactive solutes and the solid phase (also called the component additivity approach, Davis et al., 1998); and, on the other hand there are models based on effective distribution coefficients (Kd) or retardation factors (R) that integrate the retention provided by the overall geochemical reactions that affect the transport of a reactive solute (also called generalized composite approach, Davis et al., 1998).

In 1981, Reardon discussed the reliability of Kd-based models to describe reversible ion sorption reactions in contaminant migration. The author concluded that if the groundwater system is in a steady state chemical evolution a Kd-based model should be as reliable as a reactive transport model. At chemical steady state, the sorbing sites at any point in the flow path are in equilibrium with the way in which groundwater is evolving chemically and therefore the Kd of a given location should be constant over time. Based on these results, Glynn (2003) performed 1D geochemical transport simulations to demonstrate the effects of aqueous speciation and sorption reactions on the transport of neptunium and plutonium. The author concluded that a Kd-based model would lead to remarkably

different results from those attained in the previous geochemical transport simulations, pointing out the care that must be taken when choosing the type of model to be used in performance assessment of nuclear waste-disposal sites.

Over the past decades a considerable amount of computer codes that solve groundwater flow coupled with multicomponent reactive solute transport has emerged which reflects on one hand the increasing need for using these tools and on the other hand the fast increase of computer computational capacity. Allied to the advances on computing techniques, improved scientific understanding, experimental and site specific data, together with improved numerical models have provided representations of the potential behaviour of geological disposal systems which increase confidence on performance assessment programmes (OECD, 1999).

It is not intended to provide here a thorough review of computer codes that solve hydrogeochemical problems (the reader is referred to Brun and Engesgaard, 2002, for a review on biogeochemical modelling; MacQuarrie and Mayer, 2005, for a review on reactive transport in fractured rock; and, Gaucher and Blanc, 2006, for a review on modelling cement/clay interactions), but since some of these codes have been extensively used in the work developed in this thesis, a brief review of some of the most important codes is provided, some of which have been developed and/or often used in the context of deep geological repositories for HLNW:

1) PHREEQC (Parkhurst and Appelo, 1999) is a well known geochemical code based on an ion-association aqueous model that solves speciation and saturation-index calculations; batch-reaction and one-dimensional (1D) transport calculations involving a wide variety of reversible equilibrium and kinetic geochemical reactions, as well as inverse modelling;
2) PHAST (Parkhurst et al., 2004) is a finite-difference code that simulates multi-component, reactive solute transport in three-dimensional (3D) saturated groundwater flow systems. The geochemical code PHREEQC is embedded in PHAST.
3) RETRASO (Saaltink et al., 1997) is a finite-element code that solves two-dimensional (2D) reactive solute transport in saturated media.
4) CORE^{2D} (Samper et al., 2000) is a finite element code for solving 2D groundwater flow, heat transfer and multicomponent reactive solute transport in partially or fully saturated media.

5) TOUGHREACT (Xu et al., 2008) is a finite-element code that solves 3D non-isothermal multi-component reactive solute transport, multi-phase fluid and heat flow.
6) CrunchFlow (Steefel, 2008) is a finite volume code currently restricted to orthogonal grids.

The work presented in this thesis provides examples of hydrogeochemical models that have been developed using PHREEQC and PHAST to solve different problems concerning the processes affecting the mobility of radionuclides in the near-surface systems that overly potential host rocks for a deep geological repository.

Feflow (Diersch, 2005) was used in Chapter 5 to test the meaning of the Kd values estimated from the outputs of the reactive transport model developed in Chapter 4. Feflow is a finite difference code that simulates groundwater flow under non-isothermal and variably saturated conditions, and transport of conservative and reactive solutes. Transport of reactive solutes is simulated by using the Kd approach (Diersch, 2005).

PHREEQC version 2 is a numerical code that simulates a wide variety of low-temperature aqueous geochemical calculations. It is based on an ion-association aqueous model and has capabilities for (1) speciation and saturation-index calculations; (2) batch-reaction and 1D transport calculations involving reversible reactions, which include aqueous, mineral, gas, solid-solution, surface-complexation, and ion-exchange equilibria, and irreversible reactions such as kinetically controlled reactions, mixing of solutions, and temperature changes; and (3) inverse modelling, which finds sets of mineral and gas mole transfers that account for differences in composition between waters, within specified compositional uncertainty limits. The equations solved by PHREEQC for the chemical equilibrium and kinetic reactions are non-linear algebraic equations (NLAE's) describing equilibrium chemical reactions, and ordinary differential equations (ODE's) describing rates of kinetic chemical reactions (Parkhurst and Appelo, 1999).

PHAST is a multi-component, reactive solute transport code for up to 3D saturated groundwater flow systems, with capabilities to model a wide range of equilibrium and kinetic geochemical reactions. The flow and transport calculations are based on a modified version of HST3D (Kipp, 1987) that is restricted to constant fluid density and constant temperature. The geochemical reactions are simulated with the geochemical code PHREEQC, which is embedded in PHAST (Parkhurst et al., 2004).

The governing equations solved by PHAST are a set of (1) partial differential equations (PDE's) describing groundwater flow and solute transport for each aqueous component;

(2) NLAE's describing equilibrium chemical reactions; and, (3) ODE's describing rates of kinetic chemical reactions (Parkhurst et al., 2004).

In PHAST, an operator splitting of the (i) flow, (ii) transport, and (iii) geochemical equations is used to separate the three processes into three sequential calculations. No iterations between transport and reaction calculations are implemented. A three-dimensional Cartesian coordinate system and finite-difference techniques are used for the spatial and temporal discretization of the flow and transport PDE's. The NLAE's that describe the local equilibrium chemical reactions are solved by a Newton-Raphson method, and the kinetic reaction ODE's are solved by a Runge-Kutta or an implicit method for integrating ODE's (Parkhurst et al., 2004).

A multicomponent reactive transport code, such as PHAST, solves the following equations:

- Equations (1.1 and 1.2) for heterogeneous equilibrium and kinetic reactions;
- Flow equation (1.3) which combines the Darcy's law and the mass balance equation;
- Solute transport equation (1.4)

After establishing the hydrodynamic and geochemical initial conditions, the sequence of calculations performed by PHAST includes three steps (Parkhurst et al., 2004):

1. The flow equation is solved for the hydraulic head values, and these are used for calculating the water velocity that is used in the solute transport equation.
2. The solute transport equation is calculated for each primary aqueous species.
3. The equations for equilibrium and kinetic reactions are solved.

In 1996, Lichtner et al. mentioned the inevitable reliance of the performance assessment of a deep geological repository on reactive transport numerical models. Without these tools quantitative assessment of the long-term performance of a deep geological repository would be very difficult or even impossible due to the large amount of non-linear equations and long time spans needed to be solved when dealing with a HLNW repository. This is why today we find in the scientific literature a considerable amount of work dealing with hydrogeochemical numerical models applied in the context of the deep geological repository.

In the SKB programme that supports the decision making process for sitting the first deep geological repository in Sweden one may find a considerable amount of technical reports dealing with hydrogeochemical modelling (these reports may be downloaded from the website http://www.skb.se). From this programme, many scientific articles have also been published (the reader is referred to the special issue, volume 23, issue 7 of Applied Geochemistry, published in 2008, and the special issue volume 35, issue 8 of Ambio Journal, published in 2006).

1.4.2 Hydrogeochemical models in the context of the HLNW management

Different types of reactive transport models have been developed in the past decades in the context of the HLNW management. These include numerical models that simulate:

1. the dissolution of the spent nuclear fuel and subsequent release of radionuclides into the aqueous phase (Bruno et al., 2004; Duro et al., 2006; Haschkea and Oversby , 2002; Johnson et al., 2005; Macedo et al., 1982; Nielsen, 2007)
2. the processes occurring at the near-field of a repository, i.e. the vicinity of the copper canisters that contain the spent nuclear fuel (Arcos et al., 2008; Jolley et al., 2003; Ochs et al., 2003; Puranen et al., 2009; Samper et al., 2008; Yamaguchi et al., 2008)
3. the processes occurring at the far-field, i.e. the host rock of the repository and the more recent sediments that overly the host rock (Molinero et al., 2008; Robinson et al., 2003; Sullivan et al., 2003; Thorne et al 2000; Turner and Pabalan, 1999)

Concerning the dissolution of the spent nuclear fuel, Bruno et al. (2004) developed an overview of the conceptual models that describe radioactive waste/water interactions with special emphasis on UO_2-rich spent nuclear fuel. By combining thorough laboratory studies, comprehensive geochemical modelling and its application to natural analogue studies, these authors have provided confidence on the predictions for the repository performance. In 2006, Duro et al. evaluated the concentration limits of the radionuclides in the near field for different scenarios and calculated their solubility limits; i.e. the maximum concentration expected for the radionuclides taking into account the most favourable mineral phases that can precipitate and retain radionuclides in the solid phase. Nielsen (2007) developed mathematical models to simulate the dissolution of spent nuclear fuel after a hypothetical damage of the canister. These simulations showed that a steady-state concentration of H_2O_2 (an important oxidant resulting from water radiolysis due to

emission of alpha, beta and gamma radiation from the radioactive decay) is reached at the fuel surface in a very short time.

In 2008, Arcos et al. developed 3D numerical models to assess the long-term hydrogeochemical evolution of the near-field in evolving geochemical environments due to climate change. These numerical models gather information from underground laboratory experiments and natural analogues. The numerical results indicate that the most significant changes in the evolution of the near-field system could occur when highly diluted and alkaline ice-melting water enters into the system.

Natural analogues are natural systems with special characteristics that resemble those expected for a deep geological repository, and therefore, they have been object of many studies for the performance assessment of these repositories (Miller et al., 1994; Miller et al., 2000; Miller et al., 2006, among others). In 1990, Nordstrom et al. performed geochemical simulations of water-rock interactions at the Poços de Caldas natural analogue using groundwater compositions, mineralogical data, speciation and mass balance calculations. The models developed were able to reproduce water chemistry and mineral occurrences. The dominant hydrogeochemical processes occurring at the Poços de Caldas site were also identified. This work provided testing thermodynamic equilibrium codes and their associated databases. Afterwards, in 1991, Bruno et al. performed “blind” predictive geochemical models for the speciation and solubility limiting phases of a number of trace elements of Poços de Caldas natural analogue to test geochemical models used in repository performance assessments. One of the major findings of this study was that neglecting processes such as co-precipitation of radionuclides with major ion phases, which were not included in the models due to the lack of appropriate data, led to conservative (pessimistic) results by overestimating radionuclide concentration.

From the beginning of 1990’s until the present, new thermodynamic and kinetic data, as well as improved understanding of specific geochemical processes (e.g. biochemical processes) has been achieved which enables the construction of more sound and reliable reactive transport models.

In 2004, Salas and Ayora modelled the groundwater system at one of the natural analogues of the Oklo uranium deposit to improve the understanding of the observed site geochemistry. The methodology adopted in this work was useful to prove the reliability of the conceptual and numerical models developed to describe the complex behaviour of the natural analogue at the Okélobondo uraninite deposit.

Besides predictive models of the repository system and natural analogue models, descriptive models of the candidate sites are important tools providing confidence on the

numerical tools used, assumptions made and conceptual models defined for the candidate sites. Molinero et al. (2008) developed a coupled regional groundwater flow and reactive solute transport model of the Simpevarp area (one of the two candidate sites that were under consideration by SKB). By providing a qualitative framework for data analysis and testing of conceptual assumptions in a process-oriented approach, the results of this work have demonstrated how powerful the numerical tools are for the interpretation of hydrogeochemical data of candidate host rocks.

1.4.3 Modelling microbially mediated redox reactions in the context of the deep geological repository

Modelling microbially mediated geochemical reactions in the context of deep geological repositories is not as widespread as modelling abiotic geochemical reactions. Nevertheless, many geochemical reactions have long been identified to be mediated by microbes (e.g. Chapelle, 1993; Lovley et al., 1991). Hydrogeochemical models accounting for microbially mediated geochemical reactions are much more abundant in the field of subsurface groundwater modelling (e.g. Hunter et al., 1998), landfill plumes (e.g. Brun et al., 2002; Christensen et al., 2000) and degradation of organic contaminants such as chlorinated hydrocarbons, phenol and benzene (Mayer et al., 2001; Prommer et al., 2006; Watson et al., 2005, among others).

In 1996, Van Cappellen and Gaillard described sediment biogeochemistry with a detailed discussion on the mathematical formulation of transport fluxes and rates of biogeochemical reactions. In the same volume, Rittmann and VanBriesen (1996) developed a proper formulation for incorporating microbiological reactions into reactive transport models. As will be shown in Chapter 2 of this thesis, the formulation developed by Rittman and VanBriesen (1996) has been successfully applied to the numerical model developed.

By catalysing geochemical redox reactions, microbes often contribute to maintain the redox potential of groundwater at a low level which enhances the geochemical stability of a deep geological repository (Pedersen, 1999).

In 1996, Banwart et al. identified organic carbon oxidation induced by large-scale shallow water intrusion into a vertical fracture zone at the Äspö Hard Rock Laboratory in Sweden. These authors concluded that surface water inflow due to excavation of a tunnel in a repository host rock adds reducing capacity in the form of organic carbon, implying that

the soil cover may provide important protection against input of dissolved oxygen to fractures drained during the open phase of the repository.

In 2004, Arcos et al. developed a numerical model using PHREEQC to simulate the Pore Water Chemistry (PC) Experiment in the Opalinus Clay at Switzerland. This model accounted for diffusional flow and transport coupled to several local equilibrium and kinetic geochemical reactions and microbially driven degradation of organic matter. The model was able to describe the redox evolution of the system, indicating the adequacy of considering the role of microbially driven organic matter oxidation.

Yang et al. (2007) developed a coupled hydrobiogeochemical model, accounting for dissolved organic carbon (DOC) respiration and methane oxidation, to evaluate the geochemical and microbial consumption of dissolved oxygen (DO) in bentonite porewater after backfilling a HLNW repository. Parameters for microbial processes were derived from calibration of an *in situ* experiment carried out at the Äspo underground laboratory in Sweden. Numerical results showed that both geochemical and microbial processes are relevant for DO consumption.

Since microbial processes can directly affect repository performance Jolley et al. (2003) developed a model to predict the quantity of microbial biomass that could be generated over time as a result of emplacement of the HLNW packages at Yucca Mountain, in southern Nevada. The model uses the MING code (Ehrhorn and Jolley, 1998) which is based on environmental thresholds for limiting microbial growth in the near field of a repository.

In the context of the near-field geochemical stability, King et al. (2008) developed a reactive transport model to predict the corrosion behaviour of the copper canisters within a deep geological repository, accounting for aerobic bacteria respiration which was predicted to be the main O_2 reduction process during the preliminary stages of the repository evolution.

Besides promoting the geochemical stability of a deep geological repository by maintaining relatively reducing geochemical conditions, microbes can directly interact with radionuclides. In order to evaluate radionuclide migration in a shallow carbonate-rock aquifer, accounting for microbially-driven redox reactions, Wang and Papenguth (2001) proposed a general approach to incorporate microbial population dynamics into the biogeochemical model developed by Hunter et al. (1998). Wang and Papenguth (2001) extended this model to include radionuclide redox chemistry and its coupling with major biogeochemical processes. The results attained in this work showed that U(VI) can be reduced to insoluble U(IV) in anoxic zones triggered by microbial activity. Roden and

Scheibe (2005) reached similar conclusions by developing numerical simulations of bacterial U(VI) reduction which considered flow of anaerobic groundwater with and without acetate as an electron donor. The addition of acetate favoured the reduction of U(VI) to insoluble U(IV) (uraninite) by dissimilatory metal-reducing bacteria.

1.5 Objectives

The overall objective of this thesis is to develop hydrogeochemical conceptual models and numerical simulations that integrate laboratory experimental results, site specific data and thermodynamic databases to assess the influence of geochemical and microbially-driven processes on radionuclide migration, in near-surface systems.

The main goal of the work presented in Chapter 2 is to develop a conceptual and numerical model that is able to describe and simulate the processes observed in the jar-fermentor experiment developed by JAEA, with special focus on the microbially-driven redox sequence from O_2 reduction to methanogenesis. Besides simulation of direct parameters such as the concentration of organic electron donors and inorganic electron acceptors, the numerical model is intended to accurately simulate measured, with special emphasis on the master variables redox potential and pH. In order to develop such a sound and complete model, the partial equilibrium approach has been chosen for modelling microbially-driven geochemical reactions.

The objective of the work presented in Chapters 3 and 4 is to develop a reliable conceptual model and reactive solute transport numerical simulations to predict the migration and retention of radionuclides derived from a hypothetical repository release in the near-surface systems of the site selected for the construction of a deep geological repository in Sweden (Forsmark). In order to build such reliable numerical simulations a complete modelling procedure is developed and tested on two different scenarios: (1) the first scenario entails a glacial clay deposit that underlies surface water bodies and is related to groundwater discharge areas at Forsmark, and the (2) second scenario simulates a shallow unconfined aquifer hosted by a till deposit that discharges to surface water bodies, such as streams, lakes or the Baltic Sea.

At Forsmark the till deposit covers most of the surface of the granitic bedrock. Associated to surface water bodies, glacial clays can be found between the lake sediments and the till deposit, meaning that the glacial clays and till deposit are most likely hydraulically connected (Johansson et al., 2005). This feature has motivated us to initially conceptualize and model the two sediments in a single reactive transport numerical

model. Nevertheless some difficulties have arisen which are related to both the understanding and the numerical implementation of the hydrodynamic and geochemical processes responsible for the differentiation between both sediments. Therefore, we have decided to model the glacial clay and till deposits in two separate numerical models which are described in Chapters 3 and 4, respectively.

While Chapter 2 deals with a descriptive numerical model where the main goal is to fit simulated data to measured data and therefore improve our understanding on the geochemical processes triggered by microbial activity, and prove the reliability of the conceptual model that underlies the numerical model, Chapters 3 and 4 deal with predictive simulations that rely on the present-day knowledge of the hydrodynamic and geochemical behaviour of the near-surface systems at Forsmark. Here, the main focus is put on the predictive capacity of the simulations.

The model presented in Chapter 2 is focused in smaller scale processes, such as the evolution of pH and redox potential triggered by microbial activity, while Chapters 3 and 4 are focused on larger and hydrodynamic systems where coupling between geochemical processes, groundwater flow and solute transport play a major role.

By considering groundwater flow and transport of solutes, the models developed in Chapters 3 and 4 provide a wider perspective of radionuclide mobility in the near-surface systems. Chapter 5 provides an ultimate upscaling of all the processes responsible for radionuclide mobility in the Quaternary till, by transforming the complex and mechanistic approach that underlies the reactive transport numerical model presented in Chapter 4 into a simpler and CPU more efficient Kd-based model. In this context, the work presented in this thesis can be viewed as a progressive upscaling from hydrogeochemical retention processes to effective retardation parameters.

1.6 References

Appelo C.A.J. and Postma D. (2005) *Geochemistry, groundwater and pollution*. A.A. Balkema Publishers. Amsterdam, The Netherlands, 649 pp.

Arcos D., Gimmi T., Duro L. and Waber H.N. (2004) Modelling of tracer behaviour and dominant reactions during the pore water chemistry (PC) experiment in the Opalinus Clay, Switzerland. In: Wantry, R.B. and Seal R.R. II, eds. Water Rock-Interaction: Proceedings of the 11th International Symposium on Water-Rock Interaction – WRI-11. A.A. Balkema Publishers: 337-341.

Arcos D., Grandia F., Domènech C., Fernández A.M., Villar M.V., Muurinen A., Carlsson T., Sellin P. and Hernán P. (2008) Long-term geochemical evolution of the near field repository: insights from reactive transport modelling and experimental evidences. *Journal of Contaminant Hydrology*, 102, 196-209.

Banwart S., Tullborg E-L., Pedersen K., Gustafsson E., Laaksoharju M., Nilsson A-C., Wallin B., Wikberg P. (1996) Organic carbon oxidation induced by large-scale shallow water intrusion into a vertical fracture zone at the Äspö Hard Rock Laboratory (Sweden). *Journal of Contaminant Hydrology*, 21: 115-125.

Barry D.A., Prommer H., Miller C.T., Engesgaard P., Brun A. and Zheng C. (2002) Modelling the fate of oxidisable organic contaminants in groundwater. *Advances in Water Resources*, 25, 945-983.

Bear J. (1972). Dynamics of fluids in porous media. Elsevier, 764 pp.

Brookins D.G. (1987) *The geological disposal of high level radioactive wastes. Theophrastus*, Athens, Greece, 606 pp.

Brun A. and Engesgaard P. (2002) Modelling of transport and biogeochemical processes in pollution plumes: literature review and model development. *Journal of Hydrology*, 256(3-4): 211-227.

Brun A., Engesgaard P., Christensen T.H. and Rosbjerg D. (2002) Modelling of transport and biogeochemical processes in pollution plumes: Vejen landfill, Denmark. *Journal of Hydrology*, 256, 228-247.

Bruno J., Arcos D., Cera E., Duro L. and Grive M. (2004) Modelling near- and far-field processes in nuclear waste management In: Energy, Waste and the Environment: a geochemical perspective. Gieré, R. and Stille, P. (eds.), *Geological Society Special Publications*, 236, 515-528.;

Bruno J., Cross J.E., Eikenberg J., Mckinley I.G., Read D., Sandino A. and Sellin P. (1991) *Testing geochemical models in the Poços de Caldas analogue study.* SKB

report TR 90-20.

Cécille L. (1991) *Radioactive waste management and disposal*. Proceedings of the 3rd European Community Conference on Radioactive Waste Management and Disposal. Elsevier, Essex, United Kingdom, 718 pp.

Chapelle F.H. (1993) *Groundwater Microbiology and Geochemistry*. Wiley, New York.

Christensen T.H., Bjerg P.L., Banwart S.A., Jakobsen R., Heron G. and Albrechtsen H.J. (2000) Characterization of redox conditions in groundwater contaminant plumes. *Journal of Contaminant Hydrology* 45: 165 – 241.

Davis J.A., Coston J.A., Kent D.B. and Fuller C.C. (1998) Application of the surface complexation concept to complex mineral assemblages. *Environmental Science and Technology*, 32, 2820–2828.

Diersch H.J.G. (2005) *WASY software FEFLOW, Finite element subsurface flow and transport simulation system, user's manual*, Berlin, Germany.

Duro L., Grivé M., Cera E., Gaona X., Domènech C., Bruno J. (2006) *Determination and assessment of the concentration limits to be used in SR-Can*. SKB report TR-06-32, Swedish Nuclear Fuel and Waste Management Co., Stockholm, Sweden

Dzombak D.A. and Morel F.M.M. (1990) *Surface complexation modelling.* New York, Wiley Interscience, 431 pp.

Ehrhorn T.F. and Jolley D.M. (1998) *Computer Software Documentation and Users Manual, MING Microbial Impacts to the Near-Field Environment Geochemistry* Version 1.0 CSCI 30018 V1.0. CSCI: 30018 V1.0. DI: 30018-2003, Rev. 0. CRWMS M&O, Las Vegas, NV. 90 pp.

Gaucher E.C. and Blanc P. (2006) Cement/clay interactions – A review: Experiments, natural analogues, and modeling. *Waste Management*, 26(7) : 776-788.

Glynn P.D. (2003) Modeling Np and Pu transport with surface a complexation model and spatially variant sorption capacities: implications for reactive transport modelling and performance assessments of nuclear waste disposal sites. *Computers and Geosciences*, 29, 331-349.

Glynn P.D. and Reardon E.J. (1990) Solid-solution aqueous-solution equilibria: thermodynamic theory and representation. *American Journal of Science*, 290: 164-201.

Grandia F., Sena C., Arcos D., Molinero J., Duro L., Bruno J. (2007) *Quantitative assessment of radionuclide retention capacity of the Quaternary near-surface system at Forsmark – Conceptual and numerical development of a coupled groundwater flow and reactive transport model based on Forsmark v1.2 Site*

Descriptive Model. SKB report R-07-64. Swedish Nuclear Fuel and Waste Management Co., Stockholm, Sweden

Haschke J.M. and Oversby V. M. (2002) Plutonium chemistry: a synthesis of experimental data and a quantitative model for plutonium oxide solubility. *Journal of Nuclear Materials*, 305(2-3): 187-201.

Hunter K.S., Wang Y. and Van Cappellen P. (1998) Kinetic modeling of microbially-driven redox chemistry of subsurface environments: coupling transport, microbial metabolism and geochemistry. *Journal of Hydrology* 209, 53–80.

Johansson P.O., Werner K., Bosson E., Berglund S., Juston J. (2005) *Description of climate, surface hydrology, and near-surface hydrogeology Preliminary site description. Forsmark area – version 1.2*. SKB R-05-06, Swedish Nuclear Fuel and Waste Management Co., Stockholm, Sweden

Johnson L., Ferry C., Poinssot C. and Lovera P. (2005) Spent fuel radionuclide source-term model for assessing spent fuel performance in geological disposal. Part I: Assessment of the instant release fraction. *Journal of Nuclear Materials*, 346(1): 56-65.

Jolley D. M., Ehrhorn T.F. and Horn J. (2003) Microbial Impacts to the Near-Field Environment Geochemistry: a model for estimating microbial communities in repository drifts at Yucca Mountain. *Journal of Contaminant Hydrology*, 62-63: 553-575.

King F., Kolar M. and Maak P. (2008) Reactive-transport model for the prediction of the uniform corrosion behaviour of copper used fuel containers. *Journal of Nuclear Materials*, 379, 133-141.

Kipp K.L. (1987) *HST3D – A computer code for simulation of heat and solute transport in three-dimensional ground-water flow systems.* U.S. Geological Survey Water-Resources Investigations Report 86-4095, 517 p.

Lichtner P.C., Steefel C.I. and Oelkers E.H. (1996) Reactive transport in porous media. *Reviews in Mineralogy*, v. 34. Mineralogical Society of America.

Lovley D.R., Phillips E.J.P. and Lonergan D.J. (1991) Enzimic versus nonenzymic mechanisms for iron reduction in aquatic sediments. *Environmental Science and Technology*, 25(6), 1062-1067.

Macedo P.B., Barkatta A. and Simmonsa J.H. (1982) A flow model for the kinetics of dissolution of nuclear waste glasses. *Nuclear and Chemical Waste Management*, 3(1): 13-21.

MacQuarrie K.T.B. and Mayer U. (2005) Reactive transport modeling in fractured rock: A

state-of-the-science review. *Earth-Science Reviews*, 72(3-4): 189-227.

Mayer K.U., Benner S.G., Frind E.O., Thornton S.F. and Lerner D.N. (2001) Reactive transport modelling of processes controlling the distribution and natural attenuation of phenolic compounds in a deep sandstone aquifer. *Journal of Contaminant Hydrology* 53: 341 – 368.

Miller B., Hooker P., Smellie J., Dalton J., Degnan P., Knight L., Nosek U., Ahonen L., Laciok A., Trotignon L., Wouters L., Hernán P. and Vela A. (2006) *Network to review natural analogue studies and their applications to repository safety assessment and public Communication (NAnet).* SYNTHESIS REPORT of the EU project NANET, EUR 21919

Miller, W., Alexander, R., Chapman, N., McKinley, I., Smellie, J., 1994. *Natural analogue studies in the geological disposal of radioactive wastes*. Stud. Environ. Sci., vol. 57. Elsevier, The Netherlands, 395 pp.

Miller, W., Alexander, R., Chapman, N., McKinley, I., Smellie, J., 2000. *Geological disposal of radioactive wastes and natural analogues*. Waste Management Series, vol. 2. Pergamon, The Netherlands.

Molinero J., Raposo J.R., Galíndez J.M., Arcos D. and Guimerá (2008) Coupled hydrogeological and reactive transport modelling of the Simpevarp area (Sweden). *Applied Geochemistry*, 23, 1957 – 1981.

Nakajima S., Nagaoka T., Hirano S., Nakamura T. and Yoshida N. (2008) Microbial and geochemical processes in subsurface environments: Implication of microbially mediated redox changes during operation of nuclear waste repositories. In Proceedings of *7th International Symposium for Subsurface Microbiology, Shizuoka*, Japan, Nov 16-21, 2008 (ISSM2008), S6-P8

Nielsen F. (2007) *The steady-state approach – A model describing the dynamics of spent nuclear fuel dissolution in groundwater.* PhD thesis. Royal Institute of technology, Sweden. TRITE-CHE Report 2007:20.

Nordstrom D. K., Puigdomènech I. and McNutt R.H. (1990) *Geochemical modelling of water-rock interactions at the Osamu Utsumi mine and Morro do Ferro analogue study sites, Poços de Caldas, Brazil.* SKB report TR 90-23

Ochs M., Lothenbach B., Shibata M., Sato H. and Yui M. (2003) Sensitivity analysis of radionuclide migration in compacted bentonite: a mechanistic model approach. In: 8th Internation Conference on Chemistry and Migration Behaviour of Actinides and Fission Products in the Geosphere - Migration 01. *Journal of Contaminant Hydrology*, 61(1-4): 313-328.

OECD (1999) *Progress towards geologic disposal of radioactive waste: Where do we stand? An International Assessment.* Nuclear Energy Agency. Organization for Economic Co-operation and Development.

Parkhurst D.L. and Appelo C.A.J. (1999) *User's guide to PHREEQC (version 2) – A computer program for speciation, batch-reaction, one-dimensional transport and inverse geochemical calculations*. U.S. Geological Survey Water Resources investigations report 99-4259, 312 pp.

Parkhurst D.L., Kipp K.L., Engesgaard P. and Charlton S.R. (2004) *PHAST: A program for simulating ground-water flow, solute transport, and multicomponent geochemical reactions*. U.S. Geological Survey Techniques and Methods 6-A8, 154 pp.

Pedersen K. (1999) Subterranean microorganisms and radioactive waste disposal in Sweden. *Engineering Geology*, 52, 163–176.

Prommer H., Tuxen N. and Bjerg P. (2006) Fringe-controlled natural attenuation of phenoxy acids in a landfill plume: integration of field-scale processes by reactive transport modeling. *Environmental Science and Technology*, 40(15), 4732-4738.

Puranen A., Trummer M. and Jonsson M. (2009) Can redox sensitive radionuclides be immobilized on the surface of spent nuclear fuel? – A model study on the reduction of $Se(IV)_{aq}$ on Pd-doped UO_2 under H_2 atmosphere. *Journal of Nuclear Materials*, 392(3): 505-509.

Reardon E.J. (1981) Kd's – Can they be used to describe reversible ion sorption reactions in contaminant migration? *Ground Water*, v. 19(3), 279-286.

Rittmann B.E. and VanBriesen J.M. (1996). Microbiological processes in reactive modelling. In: Lichtner, P.C., Steefel, C.I. and Oelkers, E.H. Reactive transport in porous media. *Reviews in Mineralogy*, 34: 311 – 332.

Robinson B. A., Li C. and Ho C.K. (2003) Performance assessment model development and analysis of radionuclide transport in the unsaturated zone, Yucca Mountain, Nevada. *Journal of Contaminant Hydrology*, 62-63: 249-268.

Roden E.E. and Scheibe T.D. (2005) Conceptual and numerical model of uranium (VI) reductive immobilization in fractured subsurface sediments. *Chemosphere*, 59, 617-628.

Saaltink, M., Benet, I. y Ayora, C. (1997). *RETRASO, Fortran Code for Solving 2D Reactive Transport of Solutes*. User's Guide. Departament de Enginyeria del Terreny, Universitat Politècnica de Catalunya y Institut de Ciències de la Terra Jaume Almera, CSIC, Barcelona.

Salas J. and Ayora C. (2004) Groundwater chemistry of the Okélobondo uraninite deposit area (Oklo, Gabon): two-dimensional reactive transport modelling. *Journal of Contaminant Hydrology*, 69, 115 – 137.

Samper J., Lu C. and Montenegre L. (2008) Reactive transport model of interactions of corrosion products and bentonite. In: Clays in Natural & Engineered Barriers for Radioactive Waste Confinement. *Physics and Chemistry of the Earth*, 33(1): S306-S316.

Samper, J., Juncosa, R., Delgado, J. y Montenegro, L. (2000). *CORE^{2D}. A code for non-isothermal water flow and reactive solute transport.* User's manual version 2. Technical publication 6/2000*,* ENRESA, 132 p.

Sena C. Grandia F., Arcos D., Molinero J. and Duro L. 2008. *Quantitative assessment of radionuclide retention capacity of the near-surface system at Forsmark – Geochemical conceptual model and reactive-transport simulations based on Forsmark v1.2 Site Descriptive Model*. SKB report R-08-107. Swedish Nuclear Fuel and Waste Management Co., Stockholm, Sweden

SKB (2006) *Long-term safety for KBS-3 repositories at Forsmark and Laxemar – a first evaluation. Main Report of the SR-Can project.* SKB report TR-06-09. Swedish Nuclear Fuel and Waste Management Co., Stockholm, Sweden

Steefel C. (2008) CrunchFlow – *Software for Modeling Multicomponent Reactive Flow and Transport - USER'S MANUAL*. Lawrence Berkeley National Laboratory.

Stumm W. and Morgan J.J. (1996) *Aquatic chemistry*. 3rd ed. Wiley and Sons, New York, 1022 pp.

Sullivan E.J., Reimus P.W. and Counce D.A. (2003) Transport of a reactive tracer in saturated alluvium described using a three-component cation-exchange model. *Journal of Contaminant Hydrology*, 62-63: 675-694.

Thorne M.C., Degnan P., Ewen J. and Parkin G. (2000) Validation of a physically based catchment model for application in post-closure radiological safety assessments of deep geological repositories for solid radioactive wastes. *Journal of Radiological Protection*, 20: 403-421.

Turner D.R. and Pabalan R.T. (1999) Abstraction of mechanistic sorption model results for performance assessment calculations at Yucca Mountain, Nevada. *Waste Management*, 19(6): 375-388.

Van Cappellen P. and Gaillard J-F (1996) Biogeochemical dynamics in aquatic systems. In: Lichtner, P.C., Steefel, C.I. and Oelkers, E.H. Reactive transport in porous media. *Reviews in Mineralogy*, 34: 335 – 376.

Wang Y. and Papenguth H.W. (2001) Kinetic modeling of microbially-driven redox chemistry of radionuclides in subsurface environments: coupling transport, microbial metabolism and geochemistry. *Journal of Contaminant Hydrology*, 47, 297-309.

Watson I.A., Oswald S.E., Banwart S.A., Crouch R.S. and Thornton S.F. (2005) Modeling the dynamics of fermentation and respiratory processes in a groundwater plume of phenolic contaminants interpreted from laboratory-to field-scale. *Environmental Science and Technology*, 8829-8839.

Xu T., Sonnenthal E., Spycher N. and Pruess K. (2008) *TOUGHREACT User's Guide: A simulation program for non-isothermal multiphase reactive geochemical transport in variably saturated geologic media.* Lawrence Berkeley National Laboratory. University of California. Berkeley.

Yamaguchi T., Yamada F., Negishi K., Hoshino S., Mukai M., Tanaka T. and Nakayama S. (2008) Development and verification of a reactive transport model for long-term alteration of bentonite–cement–seawater systems. In: Clays in Natural & Engineered Barriers for Radioactive Waste Confinement. *Physics and Chemistry of the Earth*, 33(1): S285-S294.

Yang C., Samper J., Molinero J. and Bonilla M. (2007) Modelling geochemical and microbial consumption of dissolved oxygen after backfilling a high level radioactive waste repository. *Journal of Contaminant Hydrology*, 93: 130-148.

Chapter 2

Modelling microbially mediated redox processes in lake sediments

2. Modelling microbially mediated redox processes in lake sediments[1]

Abstract

Performance assessment of a deep geological repository for high level nuclear waste (HLNW) must comprise predictions for the long-term geochemical evolution of the repository. In aquatic systems, microbial respiration oxidizes organic carbon whilst reduces inorganic components such as O_2, NO_3^-, Fe^{3+}, SO_4^{2-} and C(IV) which, in turn, triggers changes in key geochemical parameters such as pH and redox potential. The inorganic carbon system is also influenced by microbial respiration and growth. In this context, a jar-fermentor experiment with lake water and sediment samples was conducted by the Japan Atomic Energy Agency (JAEA) to assess the role of microbial activity in aquatic systems. During the experiment, the main geochemical parameters were measured. A numerical model has been developed in order to simulate the jar-fermentor experiment and quantify the role of each microbial group that is believed to influence the geochemical evolution observed. Monod kinetic equations have been implemented to simulate microbially mediated reactions. Abiotic, kinetic and equilibrium, geochemical reactions have also been considered. Reduction of O_2, NO_3^-, Fe^{3+} and SO_4^{2-}, lactate fermentation, evolution of pH and Eh, and production of CO_2(g) and CH_4(g) are well reproduced by the model. There is a relatively high uncertainty related to the values of the Monod kinetic parameters; very similar numerical solutions can be attained with different combinations of the Monod parameters.

Keywords: redox reactions; microbial activity; HLNW; jar-fermentor; (bio)geochemical modelling.

---

[1] This work has been presented as a poster at the 19th Annual V.M. Goldschmidt Conference, and has been published in: "Awards Ceremony Speeches and Abstracts of the 19th Annual V.M. Goldschmidt Conference" Geochimica et Cosmochimica Acta, 73(13).

It has been developed by the following co-authors: Clara Sena[a,b], Jorge Molinero[a], Toru Nagaoka[c], Takamichi Nakamura[c], David Arcos[a], Shuji Ajima[d], Tuyoshi Itoh[e], Yoshito Sasaki[e], Takahiro Asano[e], Hideki Yoshikawa[e]

[a]Amphos XXI Consulting S.L., Spain; [b]I&D GeoBioTec, University of Aveiro, Portugal; [c]Biotechnology sector, Central Research Institute of Electric Power Industry, Japan; [d]Electric Power Development Co., Ltd., Japan; [e]Japan Atomic Energy Agency, Japan

2.1 Introduction

Microbially mediated redox reactions are known to occur in natural aquatic systems. Microbes use available organic matter to build up new biomass, and to respire. The build up of new biomass requires nutrients, such as C, H, N, and O, from available organic matter and other sources to form new organic cells. On the other hand, microbial respiration oxidizes organic carbon whilst reduces inorganic components such as O_2, SO_4^{2-}, NO_3^-, Fe^{3+}, and C(IV) (Chapelle, 1993; Lovley et al., 1991; Rittmann and VanBriesen, 1996; Van Cappellen and Gaillard, 1996; von Gunten and Zobrist, 1993). Due to the interaction with inorganic components, microbial respiration triggers changes in key geochemical parameters such as redox potential and pH.

Microbial activity involves using carbon from organic matter to build up new biomass cells and to respire. Building up new biomass leads to the transfer of carbon from the organic matter substances to the new biomass cells (Chapelle, 1993). When the microbial population decreases (i.e., the living organisms die), this carbon that was incorporated in biomass can degrade and be transformed again into an organic non-living matter, and ultimately be oxidized to inorganic carbon. Besides the build up of biomass, microbial respiration can act as a catalyser for the oxidation of carbon present in organic matter to inorganic carbon, which may divert into different physical states of inorganic carbon, such as HCO_3^-(aq), CO_2(g) or even as carbonate minerals like calcite. Methanogenesis, a type of anaerobic respiration where carbon is the terminal electron acceptor (Thauer, 1998), also induces changes on the oxidation state of carbon, from C(0) in organic matter or C(IV) in carbon dioxide, to C(-IV) in methane. Microbial activity is, therefore, able of triggering the partitioning of carbon initially present in organic matter, through the three phases (aqueous, gaseous and solid) which also involves changes on the oxidation state of carbon.

Performance assessment of deep geological repositories for HLNW must include predictions for the long-term geochemical evolution of these repositories. A deep geological repository accounts for several engineered (metallic canisters, bentonite, and cement) and natural (host rocks like granite, and surface sediments) barriers that prevent radionuclides, present in HLNW, from escaping to the surrounding natural environment and eventually interact with the surface ecosystems.

Prediction of the geochemical evolution of a deep geological repository must provide reliable estimates for the long-term geochemical integrity of the metallic canisters that prevent direct contact between groundwater and the HLNW. Puigdomènech and Taxen

(2000) concluded that dissolved oxygen (DO) and sulphide (HS^-(aq)) in groundwater are the most damaging components for copper corrosion. In addition, if a copper canister becomes damaged; leading to direct contact between groundwater and the HLNW, a predominately reducing environment will mitigate the mobility of most radionuclides, e.g. U, Th and Se (Duro et al., 2006).

Microbes may be present at repository depth (which is about 500 m), and therefore microbial activity could influence the geochemical evolution of a deep geological repository (Ajima et al., 2008; Banwart, 1999; and, Yang et al., 2007).

Microbial activity may have a two folded role on the geochemical evolution of metallic canisters. On one hand, microbial activity favours the integrity of a copper canister by reducing DO but on the other hand, by reducing sulphate to sulphide, microbial activity may contribute to the corrosive attack of a copper canister.

In the last years, JAEA has been performing laboratory experiments to assess the role of microbial activity in the geochemical evolution of aquatic systems (Nakajima et al., 2008 and Todaka et al., 2007). Here, a numerical model of a jar-fermentor experiment with lake water and sediment samples that were oxidized by atmosphere bubbling is developed. Lactate was added to the jar-fermentor which was kept in closed conditions for approximately 13 days. During the experiment the main geochemical parameters and bacterial flora were analyzed (Nakajima et al., 2008).

In the present work, the main biotic and abiotic processes that are believed to occur in the jar-fermentor experiment have been identified and implemented in a numerical model using PHREEQC (Parkhurst and Appelo, 1999). The numerical model follows the partial equilibrium approach, in which the oxidation of organic matter is considered to be the rate limiting process, and the geochemical system is led to respond under local equilibrium by reducing the most thermodynamically favourable electron acceptor (EA). In addition, inhibition terms are used to describe mathematically the sequential use of EA's (Barry et al., 2002, and references therein).

2.2 Experimental set up

The jar-fermentor experiment consists of a reactor with a capacity of 2.3 L in which 20 g of lake sediment were mixed with 2 L of lake water, at a constant temperature of 30ºC. The jar-fermentor was kept with a headspace of 5 mL. The sediment suspension was oxidized by atmosphere bubbling and stirred at 300 rpm. After 5 days, a solution of sodium lactate

(final concentration of 10 mM) was added to the reactor which was kept in closed conditions for further 8 days (Figure 2.1). During the experiment, pH, DO concentration and redox potential data were monitored automatically by a data logger. In addition, water and gas samples were collected periodically for measuring selected parameters. DNA from microbes in the sediment suspension was also collected and bacterial flora analysis was carried out by PCR-DGGE method. The system was sterilized by autoclave and treatment by sodium azide (NaN_3, final concentration of 10 mM) in order to prevent microbial contamination.

The main mineral components of the sediment sample used in the experiment have been identified by XRD analysis. These are quartz, plagioclase, K-feldspar, pyrite, calcite and clay minerals (smectite and kaolinite). Redox potential and pH of the sediment suspension were measured by ORP electrode (platinum electrode) and pH electrode (glass electrode). DO concentration was measured by DO electrode (diaphragm galvanic cell method). Dissolved anion concentrations (NO_3^-, NO_2^-, SO_4^{2-}, lactic acid ion, propionate ion, acetic acid ion, formic acid ion and pyruvate ion) were measured by ion chromatograph (DIONEX, ICS-1500 and ICS-2000). In the headspace, CO_2(g) and CH_4(g) concentrations were measured by gas chromatography (Varian, CP4900 with TCD detector).

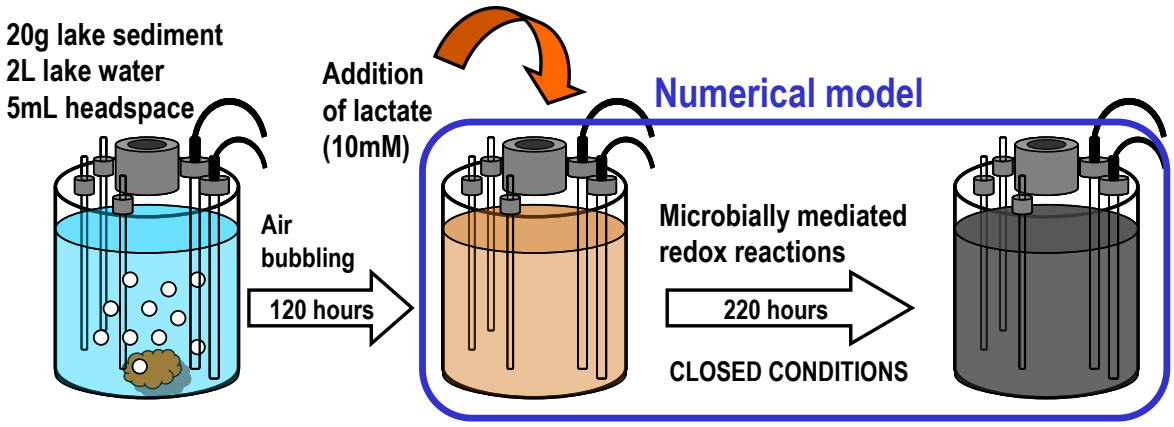

Figure 2.1 – Sketch of the jar-fermentor experiment. The step of the jar-fermentor experiment that has been modelled is highlighted with a blue rounded rectangle.

2.3 Conceptual model

2.3.1 Evidences from experimental results

The jar-fermentor experiment may be viewed as a two steps experiment: (1) the first step concerns the period when the system is being disturbed due to bubbling, and (2) the second step begins when bubbling stops and lactate is added to the system which is kept in closed conditions. The present work is focused on understanding and modelling the results attained during the second step of the experiment, and therefore the initial conditions of the numerical model refer to the time when lactate is added to the jar-fermentor (Figure 2.1).

After the addition of lactate, the overall behaviour of the jar-fermentor shows a decrease of pe[2] from approximately 8 to -4, and pH shows a small decrease during the first 70 hours towards a circum-neutral pH that is maintained until the end of the experiment (Figure 2.2).

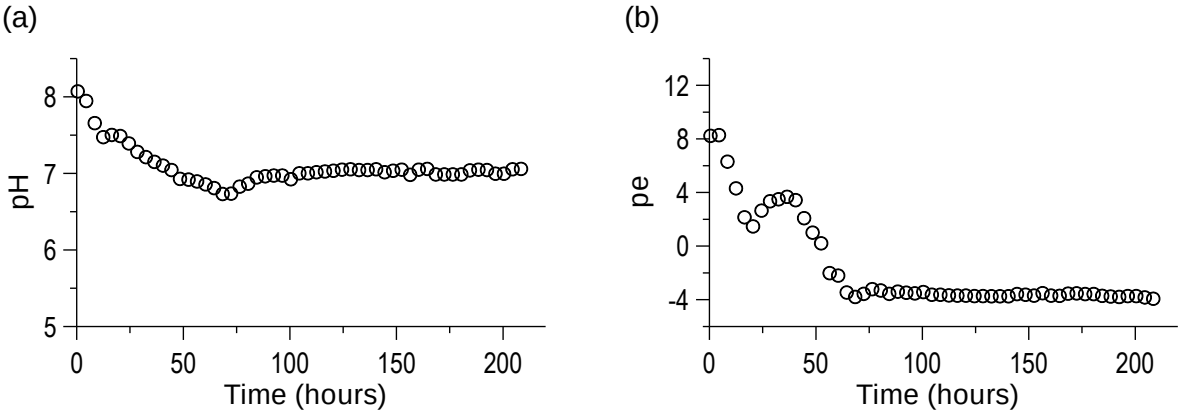

Figure 2.2 – Measured time evolution of pH and pe in the jar-fermentor experiment.

DO and nitrate are reduced within the first 10 hours (data will be shown in section 2.5). After the reduction of these species, lactate fermentation leads to the production of propionate and acetate. As lactate fermentation becomes less important, sulphate is

[2] In analogy to pH, pe= -log[e-]. pe was calculated from the Eh values measured during the experiment by, firstly correct measured Eh, relative to the platinum electrode, to Eh values that are relative to the standard hydrogen electrode (the reader is referred to p. 420 in Appelo and Postma, 2005, for further reading on this subject). Then, corrected Eh values were transformed into pe values, by using the equation 9.22 in Appelo and Postma, 2005.

progressively reduced, and ferrous iron concentration increases. Methanogenesis is evidenced by the increase of methane in the headspace gas and also by the maintenance of a pe of -4 during the last 50 hours of the experiment. Besides methane, the partial pressure of carbon dioxide also increases in the headspace gas, reflecting the accumulation of the end-products of organic matter oxidation and methanogenesis (Figure 2.3).

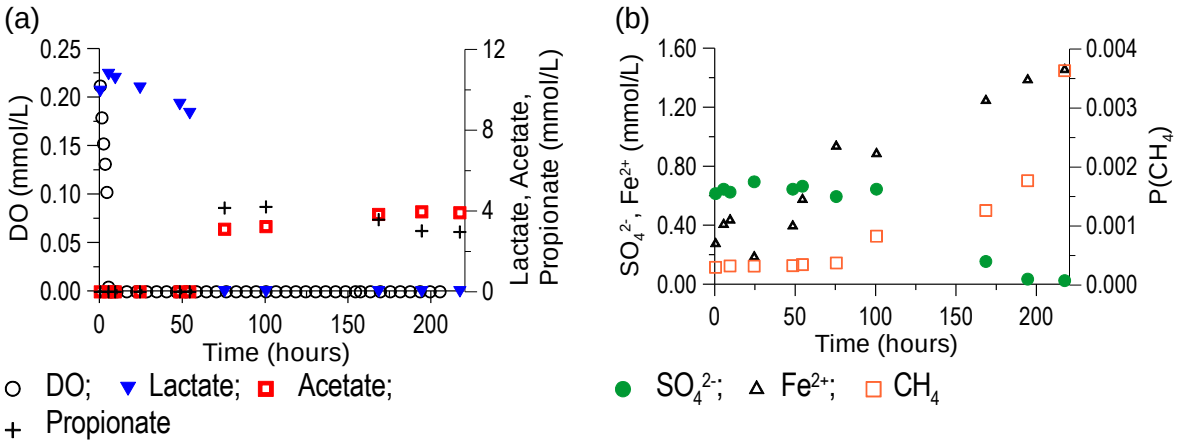

Figure 2.3 – Measured time evolution of: a) DO, Lactate, Acetate and Propionate in solution; and, b) SO_4^{2-}, Fe^{2+} in solution, and CH_4(g) in the headspace gas of the jar-fermentor.

2.3.2 Microbially mediated reactions and abiotic processes

The observed evolution of the inorganic and organic components in the aqueous and gaseous phases of the jar-fermentor reflects the occurrence of microbially mediated redox reactions that oxidize the added lactate and its fermentation products; propionate and acetate.

Microbially mediated oxidation and fermentation of lactate have been reported elsewhere (von Gunten and Zobrist, 1993, among others). According to the evolution of the parameters measured in the jar-fermentor experiment, the microbially mediated redox reactions that are believed to occur in the jar-fermentor are:

1) oxidation of lactate with reduction of DO and nitrate;
2) oxidation of propionate with reduction of sulphate and reductive dissolution of FeOOH;
3) methanogenesis.

Fermentation of lactate is also evidenced by the decrease of lactate concentration accompanied by the increment of propionate and acetate concentration. The microbial groups that are believed to mediate the redox reactions occurring in the jar-fermentor experiment are listed in Table 2.1.

Besides biotic reactions, abiotic reactions seem to occur in the jar-fermentor experiment. These abiotic reactions are evidenced by the general tendency of a relatively stable circum-neutral pH which seems to be buffered by calcite equilibrium. If calcite would not be present, the biological production of CO_2 would most probably lead the system towards more acidic conditions than the ones observed. In addition, the evolution of Fe(II) in solution reveals that not only microbial activity is influencing its concentration, but also the precipitation of Fe(II) secondary phases which tend to lower Fe(II) aqueous concentration during the final stage of the jar-fermentor experiment. The precipitation of Fe(II) secondary phases is most likely triggered by the low pe that prevails during the last stages of the experiment, and the increased concentration of bicarbonate and S(-II) which can promote the precipitation of $FeCO_3$ and FeS, respectively. It is worth mentioning that $FeCO_3$ rarely precipitates as a pure phase but it forms solid solutions with calcium carbonate (ankerite, $CaFe(CO_3)$; Dromgoole and Walter, 1990). The thermodynamics of this solid solution series are still not well known, which is why the pure phase is selected for the current model calculations.

Abiotic reductive dissolution of FeOOH (Pyzik and Sommer, 1981) is also expected due to the increment of HS^- as a consequence of microbially mediated reduction of S(VI) to S(-II). FeOOH has not been identified in the primary mineral assemblage of the lake sediment that was used for the jar-fermentor experiment. Instead, qualitative analysis of the lake sediment has identified the presence of pyrite. Nevertheless bubbling of the sediment performed during 120 hours, in the first step of the jar-fermentor experiment, may have triggered the oxidative dissolution of pyrite (Moses and Herman, 1991; Nicholson et al., 1988) and subsequent precipitation of Fe(III) phases. For this purpose, kinetic calculations using PHREEQC were performed to assess the feasibility of pyrite oxidative dissolution (using the rate expression proposed by Nicholson et al., 1988) in a solution in contact with atmospheric O_2, and letting FeOOH precipitate under local equilibrium, during 120 hours. The numerical results of these preliminary calculations have proven the possibility for the stated hypothesis of pyrite oxidation and subsequent precipitation of FeOOH, and, therefore FeOOH was considered the main Fe solid phase at the initial conditions of the numerical model.

The observed accumulation of CO_2 and CH_4 in the headspace gas of the jar-fermentor reflects the accumulation of the main end-products of the biological activity that has occurred during the experiment. The oxidation of organic matter by microbes leads to the production of CO_2 and, when a more reducing environment prevails, reduction of C(IV) and C(0) from acetate to C(-IV) can be triggered by the activity of methanogens. It should be noted that in order to apply the partial equilibrium approach to simulate methanogenesis, the local equilibrium reaction describing the reduction of CO_2 to CH_4:

$$HCO_3^-(aq) + 9H^+(aq) + 8e^- \leftrightarrow 3H_2O + CH_4(aq) \qquad \log K = 27.8493 \qquad \text{(equation 2.1)}$$

has been maintained in the thermodynamic database used for the calculations. This has implications on the accuracy of the numerical solution attained for the simulation of methanogenesis, as will be shown later in section 2.5.1.5.

Table 2.1 – Summary of the biotic and abiotic reactions implemented in the numerical simulation of the jar-fermentor experiment.

Reaction	**Biotic**	**Abiotic**
	Microbial group	**Local equilibrium or kinetics**
Lactate ($C_3H_5O_3^-$) oxidation	- Aerobes - Denitrifiers	
Lactate fermentation	- Fermenters	
Propionate ($C_3H_5O_2^-$) oxidation	- Sulphate reducing bacteria (SRB) - Iron reducing bacteria (IRB)	
Acetate ($C_2H_3O_2^-$) reduction	- Methanogens	
Reduction of O_2(aq), NO_3^-, SO_4^{2-}, Fe^{3+}, and C(IV)		Local equilibrium
Abiotic reductive dissolution of FeOOH		Kinetics
Precipitation of S(0)		Kinetics
Precipitation of $FeCO_3$		Kinetics
Precipitation of FeS		Kinetics
Precipitation/ dissolution of $CaCO_3$		Local equilibrium
Cation exchange in smectite		Local equilibrium
Reduction of CO_2(aq) to CH_4(aq)		Local equilibrium

Analytical data of the lake sediment prior to the jar-fermentor experiment show the presence of Ca and Fe, among other elements, in the solid phase. Ca is most likely linked

to calcite and smectite while Fe is most likely linked to smectite and pyrite (the later being oxidised in the first stage of the experiment as indicated above). In smectite interlayer, cations such as Na^{+}, Ca^{2+}, and Fe^{2+} may exchange (Fletcher and Sposito, 1989), and therefore, the numerical simulations account for the presence of smectite with exchangeable sites for these cations.

The amount of smectite defined in the numerical model was set according to the amount of Na reported in the lake sediment used in the experiment. Analytical data of the lake sediment show the presence of 1.37 wt% of Na in the sediment, and assuming that all Na in the solid phase is linked to smectite (with a theoretical chemical formula of $(Na,Ca)(Al,Mg)_6(Si_4O_{10})_3(OH)_6$, and molar weight of 1287 g/mol) a total of 1.2×10^{-2} mol of smectite in 20 g of sediment are obtained. Knowing that 20 g of sediment were mixed with 2 L of water, 6×10^{-3} mol of smectite per litre of water are obtained. In addition, since the jar-fermentor experiment was conducted within a circum-neutral pH, smectite dissolution has been neglected, and therefore the total amount of exchangeable sites is kept constant throughout the simulation.

From elemental analysis of the sediment, a concentration of 3.1 wt% of Ca is reported. Assuming that almost all Ca in the solid phase is linked to calcite, an initial concentration of 3×10^{-3} mol of calcite per litre of water is estimated. Calcite dissolution and precipitation have been considered to occur under local equilibrium (Table 2.1).

As already mentioned, the pe of the system at the moment of lactate addition is 8 which is far from equilibrium with pyrite (a pe of -3 would be attained if the initial solution is equilibrated with pyrite). In this context, pyrite has been discarded from the initial mineral assemblage of the simulation and, in turn, FeOOH is considered to be present when lactate is added. From elemental analysis of the sediment, a concentration of 8.4 wt% of Fe is reported, and assuming that almost all Fe in the solid phase is linked to FeOOH, we obtain an initial concentration of 1×10^{-2} mol of FeOOH per litre of water. In the numerical model, dissolution of FeOOH is considered to be kinetically controlled both by biotic and abiotic processes (Table 2.1). The biotic dissolution of FeOOH is believed to be triggered by propionate oxidation mediated by IRB's (e.g. Lovley et al., 1991, von Gunten and Zobrist, 1993), while the abiotic kinetic dissolution of FeOOH corresponds to the reductive dissolution of FeOOH triggered by the increase of HS^{-} concentration (Pyzik and Sommer, 1981).

The occurrence of black precipitates has been reported during the second step of the jar-fermentor experiment which has been interpreted as an evidence for the precipitation of Fe(II) sulphides. Pyrite precipitation is known to be preceded by the precipitation of FeS

(Rickard, 1997) which, in turn, is expected to be kinetically controlled under the prevailing conditions of the jar-fermentor experiment. For simplicity of the numerical model pyrite precipitation has been discarded from the model and only kinetic precipitation of FeS has been considered. The kinetic precipitation of FeS follows the model proposed by Pyzik and Sommer (1981).

$FeCO_3$ kinetic precipitation has been considered in the numerical model due to the observed increase of Fe(II) and C(IV) in solution during the jar-fermentor experiment. Jimenez-Lopez and Romanek (2004) have concluded that kinetic precipitation of $FeCO_3$ may occur at 25ºC, for saturation indices of $FeCO_3$ that range from 0 to 3.4×10^3. Since no kinetic rate expression has been found in the literature, the kinetic model proposed by Pyzik and Sommer (1981) for FeS has been modified to express the kinetic precipitation of $FeCO_3$.

2.4 Numerical model

Numerical models are used worldwide in order to assess the influence of microbial respiration on the geochemical evolution of groundwaters (Banwart, 1999, Watson et al., 2005, Brun and Engesgaard, 2002). The majority of these works concerns the degradation of organic contaminants such as phenol, tetrachloroethene, and benzene (Mayer et al., 2001, Watson et al., 2005, among others) in order to assess the efficiency of natural attenuation and bioremediation practices.

The present work describes a model for the oxidation of lactate and two intermediates (acetate and propionate) by microbially mediated redox reactions that are believed to occur in the jar-fermentor experiment developed by Nakajima et al. (2008).

2.4.1 Mathematical model

2.4.1.1 Partial equilibrium and extended Monod growth model

As already mentioned in section 2.1, the numerical model that has been developed to simulate microbially mediated redox reactions follows the so called partial equilibrium approach (Barry et al., 2002; Brun and Engesgaard, 2002). According to this approach, the oxidation of organic matter and reduction of inorganic EA's is divided in two half-reactions: (1) oxidation of organic matter which is treated kinetically (considered being the rate limiting process); and, (2) reduction of inorganic EA's which is let to occur under local

equilibrium. In order to simulate the sequential use of EA's, inhibition terms were introduced in the mathematical rate expressions that describe the biological activity of each microbial group considered.

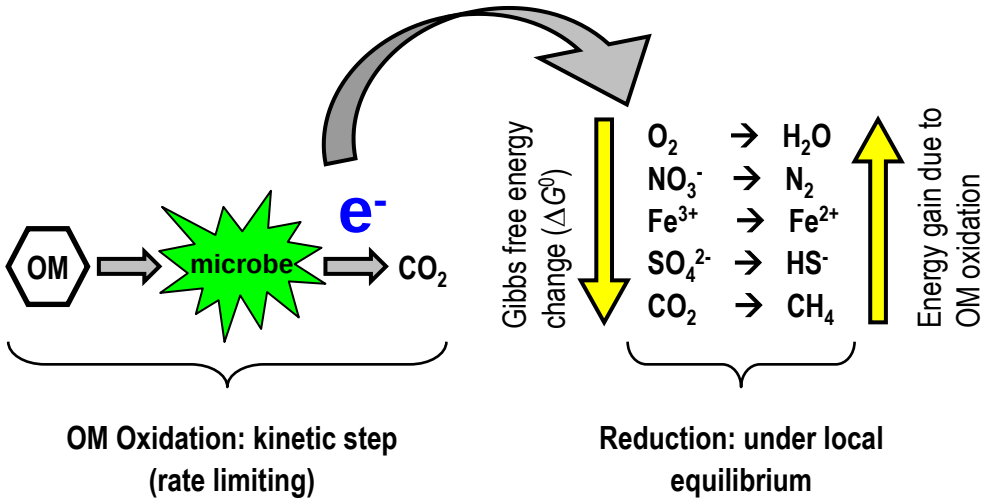

Figure 2.4 – Sketch of organic matter (OM) oxidation and EA reduction following the partial equilibrium approach. Gibbs free energy change increases from O_2 reduction to CO_2 reduction and the energy gained in these redox reactions increases at the opposite direction.

In the numerical simulation, the mathematical rate expressions that describe the biological activity of each microbial group follow the extended Monod growth model (Rittmann and VanBriesen, 1996). This model accounts for limitation terms for both the organic matter being oxidized and the EA being reduced, and an inhibition term. The formulation of this model is expressed by two mathematical rate expressions that are interdependent:

$$R^{ED} = -qm_{ED}^{Mic} \cdot [Microbes] \cdot \frac{[EA]}{K_{EA} + [EA]} \cdot \frac{[ED]}{K_{ED} + [ED]} \cdot \frac{K_{IN}}{[inhibitor] + K_{IN}}$$

(equation 2.2)

$$r_{net}^{Mic} = -Y^{Mic} \cdot R^{ED} - b^{Mic} \cdot [Microbes]$$

(equation 2.3)

Where:

R^{ED} – rate of oxidation of ED due to microbial respiration (mol of ED·L^{-1}·s^{-1}).

[ED] – concentration of electron donor in mol·L^{-1} (e.g. Lactate, Acetate, Propionate)

[EA] – concentration of electron acceptor in mol·L^{-1} (e.g. $O_{2(aq)}$, $NO_3^-{}_{(aq)}$, $SO_4^{2-}{}_{(aq)}$, $FeOOH_{(s)}$, Acetate)

qm_{ED}^{Mic} – maximum rate of oxidation of ED by microbes (mol of ED·mol of biomass^{-1}·s^{-1})

K_{EA} – half-saturation constant of EA (mol of EA·L^{-1})

K_{ED} – half-saturation constant of ED (mol of ED·L^{-1})

K_{IN} – inhibition constant (mol of inhibitor·L^{-1})

[Microbes] – concentration of biomass (mol of $C_5H_7O_2N$·L^{-1})

[inhibitor] – concentration of inhibitor (mol of inhibitor·L^{-1})

r_{net}^{Mic} – net growth rate of microbial biomass (mol of biomass·L^{-1}·s^{-1})

Y^{Mic} – specific yield coefficient of microbes (mol of biomass·mol of ED^{-1})

b^{Mic} – decay coefficient of microbes (mol of biomass·mol of ED^{-1})

Looking at equations 2.2 and 2.3, when the concentrations of a given ED and the respective EA are high, the rate of oxidation of ED (R^{ED}) is a highly negative number which makes the net growth rate of microbes (r_{net}^{Mic}) positive. In this situation microbial biomass is growing. On the other hand, if the concentration of an ED and/or EA is very low, the rate of oxidation of ED is a small negative number which makes r_{net}^{Mic} negative. Under these conditions the biomass is decreasing which simulates the decay of microbial population.

In equation 2.2, as higher the half-saturation constant (for ED or EA) as lower the rate of oxidation of a given ED which means that the microbial group is highly limited by the concentration of ED or EA. Finally, as lower the inhibition constant as lower the rate of oxidation of a given ED, meaning that the microbial group is strongly inhibited by the presence of the inhibitor species. If this inhibition term is extremely low (lower than ~10^{-10}), the term for inhibition in equation 2.2 will exert a mechanism in the mathematical expression similar to that of a switch function that has already been implemented by others (Brun and Engesgaard, 2002). When the inhibition term is high it means that the activity of a given microbial group may overlap the activity of another microbial group as already reported for SRB's and IRB's (Watson et al., 2005, among others).

In order to simulate the influence of growing and decaying biomass over the inorganic composition of the solution where the biological activity is taking place, the composition of

one mole of biomass has been considered to be $C_5H_7O_2N$. This representation of the chemical composition of biomass has been used by others (Rittmann and VanBriesen, 1996, Barry et al., 2002, Brun and Engesgaard, 2002). By assuming this chemical composition for the biomass, when a given microbial group decays, C, H, O and N will be added to solution at the proportion expressed by the stoichiometry of the molecule $C_5H_7O_2N$. On the other hand, if a given microbial group is growing these elements will be removed from solution according to the same stoichiometry.

In Table 2.2, the ED, EA and inhibitor species are summarised for each microbial group considered in the numerical simulation.

Table 2.2 – Summary of the ED's, EA's and inhibitors implemented for each microbial group.

Microbial group	ED or fermentation reactant	EA	Inhibitor
Aerobes	Lactate	O_2	-
Denitrifiers	Lactate	NO_3^-	O_2
Fermenters	Lactate		NO_3^-
IRB	Propionate	FeOOH	NO_3^-
SRB	Propionate	SO_4^{2-}	Fe(III)
Methanogens		Acetate	NO_3^-

2.4.1.2 Numerical tool and thermodynamic database

The numerical simulations have been performed with the geochemical code PHREEQC (Parkhurst and Appelo, 1999). This code solves a wide variety of low-temperature geochemical reactions, including aqueous speciation, dissolution and precipitation of pure phases and solid solutions, surface complexation, ion exchange and kinetically controlled reactions. PHREEQC was selected to develop a numerical model of the jar-fermentor experiment following the partial equilibrium approach because:

- It provides an extremely versatile tool for user-defined kinetic rate expressions, offering the possibility for the user to define the algorithms that describe each rate expression under consideration. This is possible because PHREEQC has an embedded BASIC language interpreter (Parkhurst and Appelo, 1999); and,
- It is a robust and widely benchmarked geochemical code where the mass action equations that describe the thermodynamic equilibrium reactions needed to be considered in a partial equilibrium approach are correctly simulated.

The thermodynamic database used in the present study is the NAGRA-PSI database, compiled by Hummel et al., 2002. This database contains a large set of complexation reactions as well as pure mineral equilibrium reactions for major elements and many trace elements. Additional Fe(III) carbonate complexes (Grivé, 2005) have been added to the database due to the high bicarbonate content expected as a consequence of microbial respiration.

2.4.1.3 Numerical implementation of the biological activity

Taking the biological activity of denitrifiers as an example, the following paragraphs explain how the partial equilibrium approach and extended Monod growth model have been implemented to describe the biological activity of this group. It should be mentioned that a similar procedure has been followed for the other microbial groups considered in the simulations.

As shown in Table 2.2, the ED and EA used by denitrifiers are lactate and NO_3^-, respectively. In order to impede the activity of denitrifiers against aerobic respiration, the presence of O_2 in solution is considered to inhibit the activity of denitrifiers. In the numerical simulation, regardless of the speciation of the elements that constitute the lactate molecule, the kinetic oxidation of lactate by denitrifiers can be described by the following equation:

$$Lactate \rightarrow 3C + 5H + 3O \qquad \text{(equation 2.4)}$$

In equation 2.4, one mole of lactate oxidized releases three moles of C, five moles of H and three moles of O into solution which corresponds to the chemical composition of one mole of lactate. The subsequent speciation of these elements is computed by PHREEQC according to the composition, pH and pe of the aqueous solution.

If we consider the build up of one mole of denitrifiers from the oxidation of lactate, theoretically we would get the following half reaction:

$$2C_3H_5O_3^-(aq) + NH_4^+(aq) \rightarrow C_5H_7O_2N(s) + CO_3^{2-}(aq) + H_2O(l) + 5H^+(aq) + 4e^- \qquad \text{(equation 2.5)}$$

In equation 2.4 we see that two moles of lactate are needed to produce one mole of biomass. This means that ideally the specific yield of denitrifiers would be 0.5 (1 mol of biomass per 2 mol of lactate). Nevertheless, laboratory experiments (Barry et al., 2002 and references therein), and also the numerical results attained in the present work, show that microbial growth is not that efficient, meaning that from two moles of lactate less biomass is produced in favour of more C(IV) produced. This means that respiration may be more important than the build up of new biomass per each mole of lactate used by denitrifiers.

Calibration of the numerical model that has been built to simulate the jar-fermentor experiment led to a specific yield for denitrifying bacteria of 0.05. By applying this specific yield in equation 2.5 we obtain the following rate equation for the oxidation of lactate by denitrifiers:

$$C_3H_5O_3^-(aq) + 0.05NH_4^+(aq) + 5.35H_2O(l) \rightarrow 0.05C_5H_7O_2N(s) + 2.75CO_3^{2-}(aq) + \\ + 15.55H^+(aq) + 11e^-$$

(equation 2.6)

It should be noted that the production of C(IV) is expressed in terms of CO_3^{2-} for simplicity. Nevertheless CO_3^{2-} may complexate with H^+ to form bicarbonate, depending on the pH of the solution where the microbially mediated denitrification is taking place.

As a response to the kinetic reaction expressed in equation 2.6, PHREEQC calculations lead to the reduction of dissolved NO_3^- under local equilibrium. The local equilibrium equation for the reduction of NO_3^- is:

$$2NO_3^-(aq) + 12H^+(aq) + 10e^- \leftrightarrow N_2(aq) + 6H_2O(l) \qquad \log K = 207.2676$$

(equation 2.7)

where log K is the natural logarithm of the equilibrium constant of the reaction for the reduction of NO_3^- to N_2.

Taking equations 2.2 and 2.3 to describe the biological activity of denitrifiers the following equations are obtained:

$$R_{Denit}^{Lac} = -3.5\times10^{-4}\cdot[Denit]\cdot\frac{[NO_3^-]}{10^{-6}+[NO_3^-]}\cdot\frac{[Lactate]}{10^{-4}+[Lactate]}\cdot\frac{10^{-10}}{[O_2(aq)]+10^{-10}}$$

(equation 2.8)

$$r_{net}^{Denit} = -0.05\cdot R_{Denit}^{ED} - 10^{-5}\cdot[Denit]$$

(equation 2.9)

where R_{Denit}^{Lac} is the rate of oxidation of lactate by denitrifiers, [Denit] is the concentration of denitrifying bacteria population at a given time step (mol of $C_5H_7O_2N\cdot L^{-1}$), $[NO_3^-]$ is the concentration of NO_3^- ($mol\cdot L^{-1}$), [Lactate] is the concentration of lactate (mol of $C_3H_5O_3^-\cdot L^{-1}$), and r_{net}^{Denit} is the net growth rate of denitrifying bacteria at a given time step.

As for all the other microbial groups, the values of the parameters that describe the activity of denitrifiers have been defined through calibration of the numerical model against measured data. This calibration stands on the best agreement between measured and computed values for the concentration of EA's, ED's, and the geochemical parameters pe and pH in the jar-fermentor experiment.

The inhibition constant for O_2 in equation 2.8 is very low meaning that denitrifiers will be more active when O_2 concentration is lower than 10^{-10} $mol\cdot L^{-1}$. Such a low inhibition constant leads to a sequential use of lactate by aerobes followed by denitrifiers with a short overlap lag.

2.4.2 Initial conditions

Since the partial equilibrium approach that has been applied relies on a strong linkage between kinetic microbial reactions and local equilibrium reactions triggered by microbial activity, the initial composition of the aqueous solution, mineral assemblage and headspace gas must be defined with the highest completeness possible. The reference values used to establish the initial conditions of the numerical simulation are those measured when lactate is added to the jar-fermentor (i.e. beginning of the second step of the experiment).

In the numerical simulations, and according to measured data, the initial aqueous solution is considered to be in equilibrium with calcite, and a partial pressure of 1.82×10^{-1} and 2.51×10^{-3}, for $O_2(g)$ and $CO_2(g)$, respectively. This assumption is a simplification of the real system of the jar-fermentor at the time of lactate addition. Most probably, at this time,

the system is already in disequilibrium due to the disturbance caused by bubbling which enhances the interaction between inorganic components, organic matter and microbes. Nevertheless, modelling this experiment under the partial equilibrium approach requires the definition of an initial aquatic system that represents a temporary equilibrium, controlled by the mass action law, between aqueous, gaseous and solid phases. Based on the conceptual model previously described in section 2.3 and measured data at time of lactate addition, the following assumptions have been made (Table 2.3):

1. Calcite is considered to be present, at equilibrium, with an amount of 3×10^{-3} mol·L^{-1}. This equilibrium leads to a concentration of Ca^{2+}(aq) of 9.39×10^{-4} mol·L^{-1}.
2. The partial pressure of CO_2(g) measured in the headspace gas (2.51×10^{-3}) leads to an aqueous concentration of C(IV) of 3.75×10^{-3} mol·L^{-1}.
3. The initial partial pressure of CH_4(g) measured in the headspace gas is 3.02×10^{-4} which is not thermodynamically compatible with a partial pressure of CO_2(g) of 2.51×10^{-3} and a pe of 8, as it was measured at time zero. Since the initial system is believed to have a partial pressure of CO_2(g) and a pe close to the values actually measured at time zero, the initial partial pressure of CH_4(g) has been calculated by prescribing the CO_2(g) partial pressure measured at time zero, and letting PHREEQC calculate the corresponding partial pressure for CH_4(g). The value obtained for the initial partial pressure of CH_4(g) is 6.03×10^{-142} which is extremely low, reflecting the prevailing oxidizing conditions for the initial state of the jar-fermentor experiment.
4. O_2(aq) concentration is influenced by the partial pressure of O_2(g) in the headspace gas. Measured concentration of O_2(aq) (2.12×10^{-4} mol·L^{-1}) is not in equilibrium with a partial pressure of O_2(g) of 1.82×10^{-1}, as it was measured when lactate was added. To build up the initial conditions of the numerical model, the concentration of O_2(aq) is given more importance than the partial pressure of O_2(g) measured in the headspace. Therefore, the initial partial pressure of O_2(g) was set by equilibrating the headspace gas with the measured concentration of O_2(aq), using PHREEQC. The initial partial pressure obtained for O_2(g) is 9.04×10^{-1}. After these equilibrium calculations, O_2(aq) concentration is slightly changed to 2.09×10^{-4} mol·L^{-1}.
5. In addition to O_2(g), CO_2(g) and CH_4(g) measured in the headspace gas, H_2S(g), N_2(g) and H_2(g) are let to accumulate in the headspace gas during the simulation of the experiment. The selection of these gases was set according to the main

end-products of the microbially mediated redox reactions considered in the numerical model and their initial partial pressures were set according to the output of preliminary PHREEQC geochemical calculations.

6. As mentioned in section 2.3.2, FeOOH is considered to be present at an initial concentration of 1×10^{-2} mol·L^{-1}. The concentration of this mineral during the experiment is considered to be influenced solely by kinetic processes: biotic (respiration of IRB) and abiotic (reductive dissolution of FeOOH by HS^-). According to the reaction proposed by Pyzik and Sommer (1981), S^0 precipitates as a consequence of abiotic reductive dissolution of FeOOH. S^0 is considered to be absent at time zero.
7. Due to the prevailing oxidizing conditions at time zero, FeS is considered to be absent at the beginning of the experiment but is let precipitate according to the kinetic rate expression proposed by Pyzik and Sommer (1981). This assumption, together with the microbially mediated redox reactions leads to the precipitation of FeS during the simulation which is in agreement with the observation of black precipitates as mentioned in section 2.3.2. $FeCO_3$ is also considered to be absent at the beginning of the experiment, due to the same reason as for FeS.

The preliminary geochemical equilibrium calculations performed in PHREEQC for the set up of the initial aqueous solution, gas and solid compositions led to pe (12.36) and pH (7.75) values that are different from the ones actually measured at time zero (pe = 8.31 and pH = 8.08). Nevertheless, since the real system is not in equilibrium and these are indirect geochemical parameters that depend on equilibrium calculations, it was decided to attribute a higher level of confidence to the concentrations of the aqueous, gaseous and solid species measured, and the initial value of the indirect parameters pe and pH has been defined according to the output of these preliminary PHREEQC calculations (Table 2.3).

Table 2.3 – Measured data and input data for the initial composition of the aquatic system modelled. Reasoning for setting a different initial value than the one measured is also shown.

Parameter	Measured data	Initial conditions for the simulation	Reasoning for input value
Aqueous phase (concentrations in mol/L)			
T (ºC)	30	30	Measured value
pH	8.08	7.75	Equilibrium with calcite and CO_2(g)
pe	8.31	12.35	Redox equilibrium
O(0)	2.12×10^{-4}	2.09×10^{-4}	Small numerical adjustments
N(5)	1.38×10^{-5}	1.38×10^{-5}	Measured value
N(0)	negligible	negligible	Measured value
S(VI)	6.20×10^{-4}	6.20×10^{-4}	Measured value
S(-II)	unknown	negligible	Measured value
Fe(III)	1.13×10^{-3}	1.41×10^{-3}	Redox equilibrium
Fe(II)	2.8×10^{-4}	negligible	Redox equilibrium
C(IV)	unknown	3.75×10^{-3}	Equilibrium with calcite and CO_2(g)
C(-IV)	unknown	negligible	Equilibrium with CH_4(g)
Ca	unknown	9.39×10^{-4}	Equilibrium with calcite
Cl	unknown	1.00×10^{-4}	To balance electric charge
Na	unknown	1.17×10^{-2}	To balance electric charge
Lactate	9.92×10^{-3}	9.92×10^{-3}	Measured value
Acetate	negligible	negligible	Measured value
Propionate	negligible	negligible	Measured value
Gaseous phase (concentrations in partial pressure)			
CO_2	2.51×10^{-3}	2.51×10^{-3}	Measured value
CH_4	3.02×10^{-4}	negligible	Redox equilibrium
O_2	1.82×10^{-1}	9.04×10^{-1}	Equilibrium with O_2(aq)
H_2S	unknown	negligible	Expected to accumulate due to redox reactions
N_2	unknown	negligible	Expected to accumulate due to redox reactions
H_2	unknown	negligible	Expected to accumulate due to redox reactions
Solid phase (concentrations in mol/L)			
Calcite	unknown	3×10^{-3}	Estimated from elemental data on Ca
FeOOH	unknown	1×10^{-2}	Estimated from elemental data on Fe
Smectite	unknown	6×10^{-3}	Estimated from elemental data on Na
$FeCO_3$	unknown	negligible	Expected to precipitate due to redox reactions and increase of C(IV) concentration
FeS	unknown	negligible	Expected to precipitate due to redox reactions
S(0)	unknown	negligible	Expected to precipitate due to redox reactions

2.4.3 Parameterization

The values of the parameters for the numerical rate expressions that describe the biological activity of each microbial group have been defined through calibration of the numerical model. The criteria for this calibration have been set, with a progressively decreasing weight, by finding the best agreement between measured and simulated values of:

1) aqueous concentration of inorganic EA's;
2) aqueous concentration of organic species: lactate, propionate and acetate.
3) pH;
4) pe;
5) gaseous concentration of CO_2 and CH_4.

Such calibration has led to an overall good agreement between numerical results and measured data, as will be shown in section 2.5.

According to the criteria used for calibration, the values listed in Table 2.4 (Reference case) have been attained for the parameters of the numerical model implemented. During calibration of the numerical model, the influence of each parameter on the shape of the curve that describes the evolution of each EA has been analysed.

The initial concentration of biomass for each microbial group has been found to influence the initial trend of the curve; as higher the initial concentration of biomass as earlier the consumption of the corresponding EA. On the other hand, when the initial concentration of biomass is very low, a plateau may be formed in the initial stage, meaning that the redox process is developing at a very small rate, as observed for the case of sulphate reduction (section 2.5.1.3).

A high specific yield (Y^{Bact}) tends to increase the slope of the curve of consumption of a given EA (as for the case of DO and NO_3^-, section 2.5.1.1), while a low specific yield tends to decrease this slope (e.g. sulphate reduction, section 2.5.1.3). The maximum rate of oxidation of ED (qm_{ED}^{Bact}) exerts a great influence on the time at which the optimum of a given microbial group occurs. Finally, the half-saturation constants and inhibition constants help defining the sequential use of EA's.

After calibration of the numerical model, a second model has been built by assigning the same initial concentration of biomass for all microbial groups considered (Alternative case in Table 2.4). This exercise has been done in order to assess the influence of the uncertainty related to the initial concentration of each microbial group and the non-

uniqueness of the numerical solution related to the uncertainty on the Monod parameters which has been reported by others (Schirmer et al., 1999). The initial concentration of each microbial group in an unknown of the jar-fermentor experiment, but it is a variable that can be assessed in future experiments. On the other hand, the half saturation and inhibition constants, and maximum growth rates that describe the activity of each microbial group represent variables which are much more complicated to measure and, in addition. The influence of the uncertainty related to the Monod parameters will be discussed in section 2.5.2.

By fixing an initial concentration of 1×10^{-8} mol·L^{-1} of biomass for each microbial group some difficulties have arisen when searching for the best fit between measured and simulated data. These results reveal that most probably, at time zero, the initial concentration of each microbial group in the jar-fermentor is already being influenced by the geochemical reactions taking place and therefore, the initial dimension of microbial populations is not the same for each microbial group. Further discussion of the results attained in the alternative case is presented in section 2.5.2.

Table 2.4 – Summary of the calibrated values of the parameters that describe the microbially mediated reactions.

Reference case							
parameter	**K(EA)**	**K(ED)**	**K(IN)***	**qm**	**Y**	**b**	**[Biomass]$_{initial}$**
unit	mol of EA/L	mol of ED/L	mol of Inhibitor/L	mol of ED/mol of biomass·s	mol of $C_5H_7O_2N$/mol of ED	s^{-1}	mol of $C_5H_7O_2N$/L
O_2 reduction	1.0×10^{-6}	1.0×10^{-4}	-	4.8×10^{-4}	5.0×10^{-2}	2.0×10^{-5}	8.0×10^{-6}
NO_3^- reduction	1.0×10^{-6}	1.0×10^{-4}	1.0×10^{-10} (O_2)	3.5×10^{-4}	5.0×10^{-2}	1.0×10^{-5}	3.0×10^{-6}
Lactate fermentation	-	1.0×10^{-7}	1.0×10^{-12} (NO_3^-)	3.0×10^{-2}	1.0×10^{-3}	1.0×10^{-6}	1.0×10^{-8}
FeOOH reduction	1.0×10^{-10}	1.0×10^{-10}	1.0×10^{-4} (NO_3^-)	7.0×10^{-4}	6.0×10^{-3}	2.0×10^{-6}	9.0×10^{-7}
S(VI) reduction	1.0×10^{-6}	1.0×10^{-4}	1.0×10^{-4} (Fe(III))	1.0×10^{-3}	1.2×10^{-2}	3.0×10^{-6}	9.0×10^{-7}
Methanogenesis	1.0×10^{-9}		1.0×10^{-10} (NO_3^-)	8.0×10^{-4}	6.0×10^{-3}	1.0×10^{-8}	1.0×10^{-8}
Alternative Case							
parameter	**K(EA)**	**K(ED)**	**K(IN)***	**qm**	**Y**	**b**	**[Biomass]$_{initial}$**
unit	mol of EA/L	mol of ED/L	mol of Inhibitor/L	mol of ED/mol of biomass·s	mol of $C_5H_7O_2N$/mol of ED	s^{-1}	mol of $C_5H_7O_2N$/L
O_2 reduction	1.0×10^{-6}	1.0×10^{-4}	-	3.0×10^{-3}	1.5×10^{-1}	2.0×10^{-5}	1.0×10^{-8}
NO_3^- reduction	1.0×10^{-6}	1.0×10^{-4}	1.0×10^{-10} (O_2)	3.5×10^{-4}	5.0×10^{-2}	3.0×10^{-5}	1.0×10^{-8}
Lactate fermentation		1.0×10^{-7}	1.0×10^{-4} (NO_3^-)	3.3×10^{-2}	1.15×10^{-3}	1.0×10^{-5}	1.0×10^{-8}
FeOOH reduction	1.0×10^{-10}	1.0×10^{-9}	1.0×10^{-4} (NO_3^-)	4.35×10^{-3}	6.0×10^{-3}	2.0×10^{-5}	1.0×10^{-8}
S(VI) reduction	1.0×10^{-6}	1.0×10^{-4}	1.0×10^{-2} (Fe(III))	1.5×10^{-2}	3.5×10^{-3}	3.0×10^{-5}	1.0×10^{-8}
Methanogenesis	1.0×10^{-8}		1.0×10^{-10} (NO_3^-)	3.0×10^{-3}	5.0×10^{-3}	1.0×10^{-5}	1.0×10^{-8}
* Inhibitor species is identified in parenthesis							

2.5 Discussion

2.5.1 Processes

Since most probably the initial dimension of microbial populations is different for each microbial group, the interpretation of model results and subsequent analyses of the processes influencing such results are based on the reference case where the initial dimension of biomass is different for each microbial group.

2.5.1.1 Reduction of DO and NO_3^-

In the reference model a very good agreement between measured and simulated data for DO and NO_3^- has been achieved.

In Figure 2.5a, the maximum of aerobic bacteria population coincides with the rapid consumption of dissolved oxygen, reflecting the dependence of the net growth rate of aerobic bacteria on the availability of dissolved oxygen. When dissolved oxygen is exhausted the population of aerobic bacteria quickly decays which reflects the influence of the half-saturation constant for dissolved oxygen present in the extended Monod equation that describes the rate of lactate oxidation by aerobes. Similarly, the rapid decrease of nitrate concentration (Figure 2.5b) coincides with the rapid increase of denitrifying bacteria, and when nitrate is exhausted, denitrifying bacteria population progressively decays.

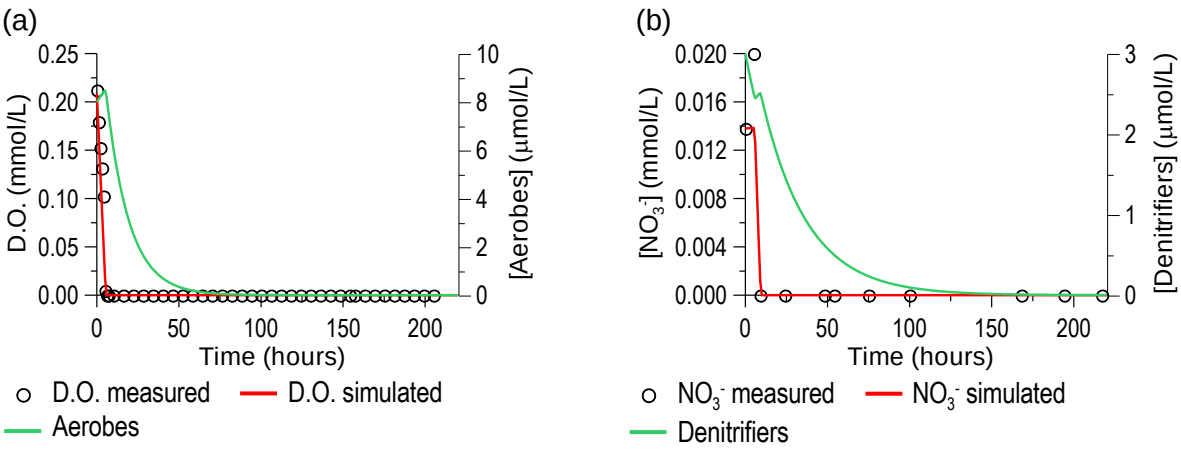

Figure 2.5 – Measured (symbols) and simulated (red line) time evolution of DO (a) and NO_3^- (b). Computed evolution of aerobes (a) and denitrifiers (b) biomass is also shown (green lines).

2.5.1.2 Lactate fermentation, evolution of acetate and propionate

Figure 2.6 shows measured and simulated results for lactate, acetate and propionate concentrations. It has been seen, in Figure 2.5, that the reduction of DO and NO_3^- (that use lactate as ED) is well reproduced by the model, and these species are reduced in 6 and 12 hours, respectively. Looking at Figure 2.6, one may see that the reduction of DO and NO_3^- has negligible influence on the concentration of lactate. In addition, the evolution of fermentative bacteria population (shown in Figure 2.6a) with a growth trend that is approximately symmetric to the trend of lactate consumption (until ~75 hours), reflects the dominating role of these bacteria on lactate concentration. Finally, when lactate is exhausted, the population of fermentative bacteria progressively decays.

As mentioned in section 2.3, lactate fermentation leads to the production of acetate and propionate. The numerical model reproduces very well the evolution of fermentation products, except for propionate which is over predicted (Figure 2.6b). Numerical results follow approximately the observed evolution of propionate, but at computed values that are ~1.6 times measured data. The reason why propionate concentration is over predicted is most probably due to model stoichiometry or other propionate-consuming processes that have not been considered in the numerical model. This subject will be further discussed in section 2.5.1.6.

According to the reaction for lactate fermentation proposed by von Gunten and Zobrist (1993), the stoichiometry of the kinetic reaction of lactate fermentation, without considering the build up of new biomass, is:

$$3C_3H_5O_3^-(aq) \rightarrow C_2H_3O_2^-(aq) + 2C_3H_5O_2^-(aq) \qquad \text{(equation 2.10)}$$

In equation 2.10, three moles of lactate are diverted into one mole of acetate and 2 moles of propionate. When build up of biomass of fermentative bacteria (with a specific yield of 0.001, Table 2.4) is considered, the following equation is attained:

$$3C_3H_5O_3^-(aq) + 0.001NH_4^+(aq) \rightarrow C_2H_3O_2^-(aq) + 2C_3H_5O_2^-(aq) + 0.001C_5H_7O_2N(s) + \\ + 0.995HCO_3^-(aq) + 0.013H_2O(l) + 0.976H^+(aq)$$

(equation 2.11)

In equation 2.11, besides the stoichiometry of lactate fermentation described by equation 2.10, the build up of fermentative bacteria biomass is also expressed. This reaction affects both pe and pH. pe is affected due to the oxidation of 0.995 moles of C(0) from lactate to 0.995 moles of C(IV) from HCO_3^-, while pH is affected due to production of 0.976 moles of H^+ per each mole of reaction 2.11. In fact it will be shown in sections 2.5.1.4 and 2.5.1.5 that, when the highest rate of lactate fermentation takes place (approximately between 40 and 75 hours, Figure 2.6A), important changes are computed (and also measured) for pe and pH.

Acetate evolution (Figure 2.6c) is initially influenced by lactate fermentation which leads to the increase of acetate concentration until 70 hours. Afterwards, when lactate is exhausted, acetate production is provided by sulphate reduction, according to the reaction proposed by von Gunten and Zobrist (1993). Finally, at approximately 175 hours acetate concentration is kept more or less stable due to balancing between sulphate reduction and consumption of acetate by methanogens.

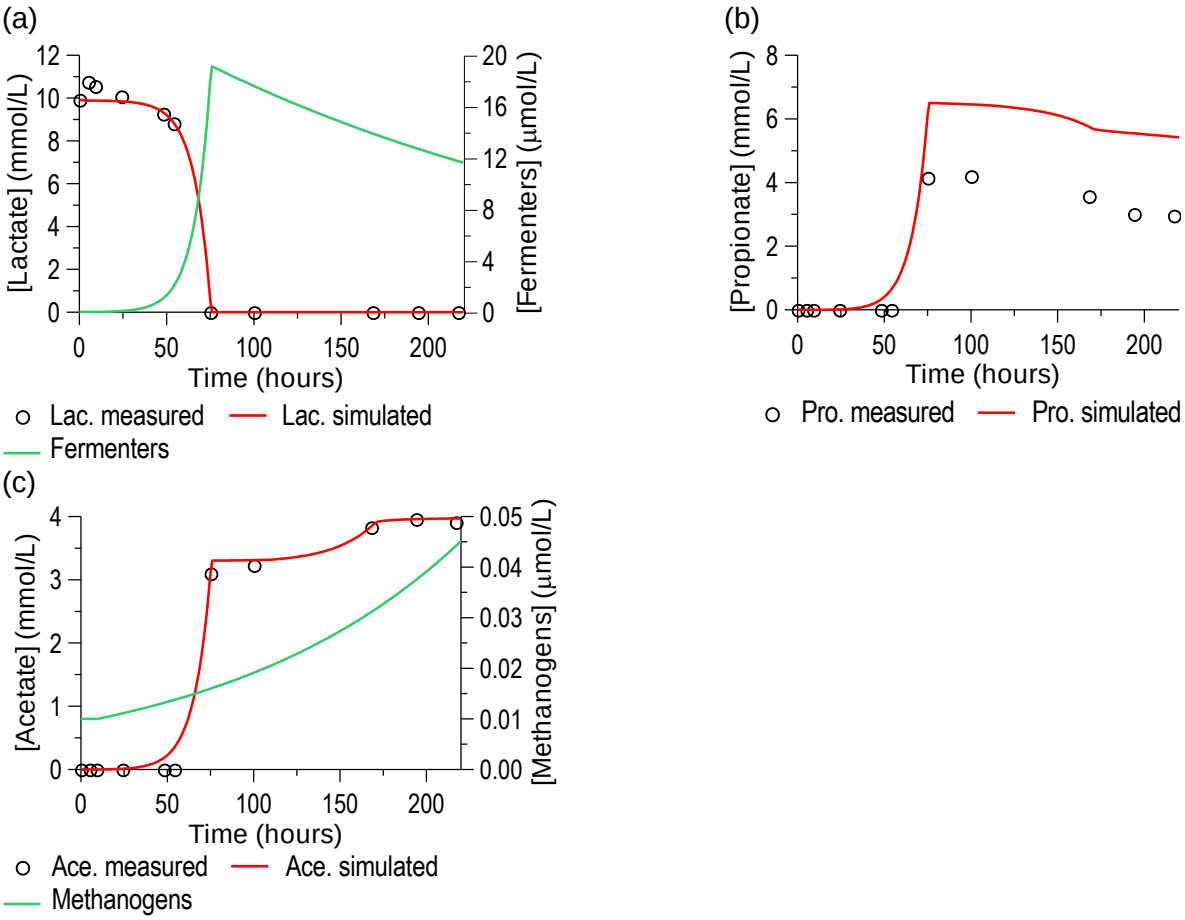

Figure 2.6 – Time evolution of measured (symbols) and simulated (red line) dissolved lactate, acetate and propionate concentrations. Computed evolution of fermentative (a) and methanogenic (c) bacteria is also shown (green line).

2.5.1.3 Reduction of Fe(III) and SO_4^{2-}, and precipitation of secondary minerals

Reductive dissolution of FeOOH is considered to occur, under kinetics, both biotically and abiotically. The first is provided by the activity of IRB's and the second is triggered by the increase of HS^- concentration. Biotic reduction of FeOOH is accompanied by oxidation of propionate while abiotic reduction of FeOOH is accompanied by oxidation of S(-II) to S(0) and subsequent precipitation of S^0 as follows (Pyzik and Sommer, 1981):

$$H_2O(l) + 2FeOOH(s) + HS^-(aq) \rightarrow S^0(s) + 2FeOH^+(aq) + 3OH^-(aq)$$

(equation 2.12)

Besides S^0, precipitation of FeS and $FeCO_3$ are also considered. FeS precipitation is supported by observations during the jar-fermentor experiment as mentioned in section 2.3.1, while precipitation of $FeCO_3$ is expected due to the increase of Fe(II) concentration and the partial pressure of CO_2 during the experiment.

The evolution of Fe(II) in solution (Figure 2.7a) reflects the combined effect of several processes. Until the first 10 hours, the FeOOH/Fe(II) system is relatively stable. From 10 to 100 hours an important increase of Fe(II) is computed (and measured). Then, from 100 to 160 hours, a relatively stable concentration of Fe(II) is computed and, during the final part of the experiment, a new increase is predicted.

The first increase in Fe(II) concentration is mainly due to the activity of IRB's, since abiotic reductive dissolution of FeOOH depends on the presence of HS^-(aq) which only becomes important after SO_4^{2-} reduction by SRB's, from approximately 150 hours (Figure 2.7b). The second increase of Fe(II) in solution, with a lower slope than the first increase, is attributed to both biotic and abiotic reductive dissolution of FeOOH, since HS^- is now available, combined with the precipitation of FeS and $FeCO_3$ which tend to decrease Fe(II)(aq) concentration (Figure 2.7c).

Between 115 and 160 hours, a small deceasing tendency followed by a plateau is simulated for the evolution of Fe(II) which is attributed to a temporary lag when precipitation of Fe(II) phases become important and reductive dissolution of FeOOH is still small to compensate the removal of Fe(II) from solution due to the precipitation of the Fe(II) secondary phases (Figure 2.7a and c).

As already mentioned, HS^- may be a species of concern with respect to the chemical integrity of a HLNW repository, since metallic canisters may be corroded by this species.

Computed HS^- evolution shows a temporal increase with a maximum of 0.37 $mmol \cdot L^{-1}$. The computed temporal increase of HS^- demonstrates that although SO_4^{2-} reduction by SRB leads to the production of HS^-, its concentration is buffered due to the precipitation of S^0 and FeS.

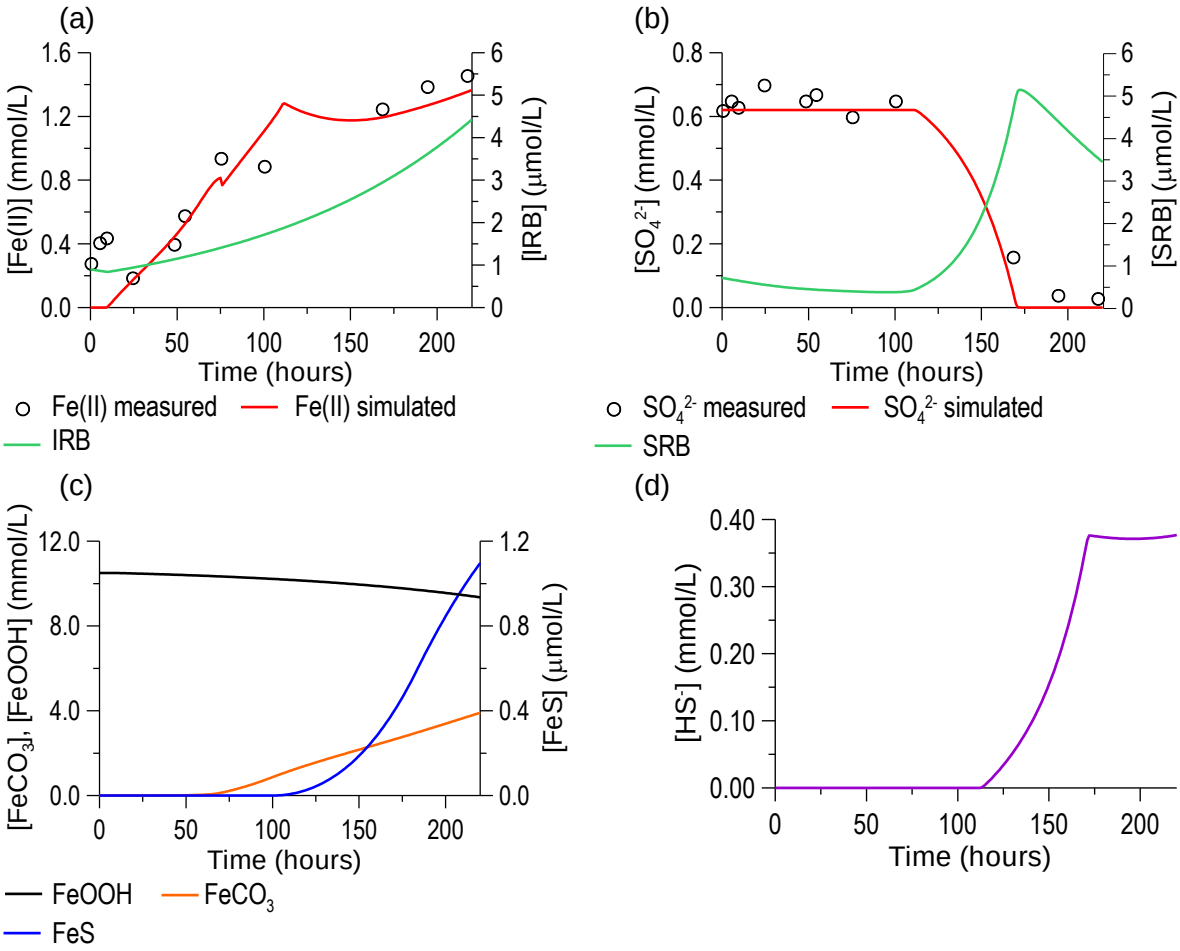

Figure 2.7 – Time evolution of measured (symbols) and simulated (red line) dissolved Fe(II) (a), and SO_4^{2-} (b) concentrations. Computed evolution of IRB's (a) and SRB's (b) is shown with green lines. Computed concentration of FeOOH(s) and the secondary mineral phases $FeCO_3$ and FeS are shown in graphic c, and computed concentration of HS^- is plotted in graphic d.

2.5.1.4 pH and the carbon system

In general, measured pH is well reproduced by the numerical model, but CO_2(g) results show some discrepancies between measured and simulated values (Figure 2.8). The general trend of CO_2(g) observed until 100 hours is relatively well reproduced by the

model, but afterwards, the observed increase of the $P(CO_2)$ is not well reproduced by the numerical model. In the next paragraphs, measured and simulated values for pH, $CO_2(g)$ and calcite (only simulated) are discussed.

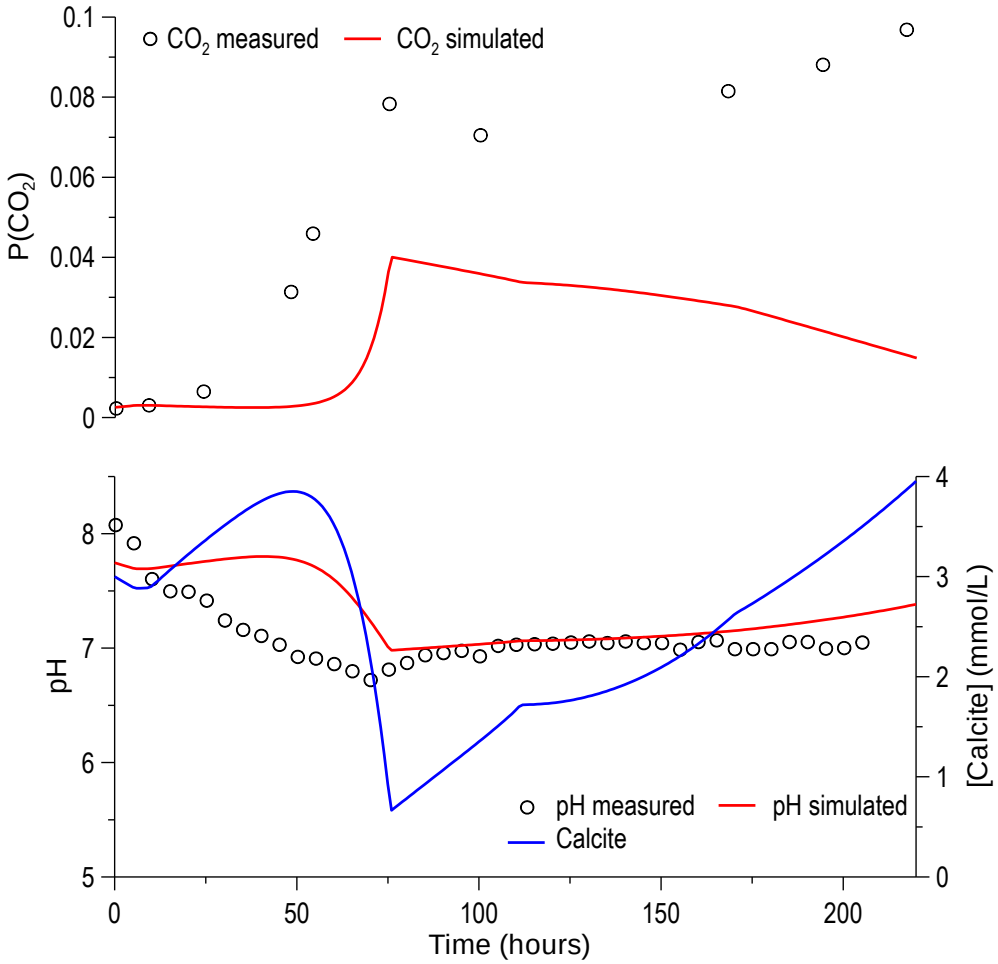

Figure 2.8 – Time evolution of measured (symbols) and simulated (red line) partial pressure of $CO_2(g)$ in the headspace and pH. Computed concentration of calcite during the experiment is also shown (blue line).

pH measured during the jar-fermentor experiment shows two trends. The first trend (from the beginning of the experiment until approximately 75 hours) shows a gradual decrease from 8.0 to 6.7 pH units. In the second trend, the pH is stabilized at a pH value around 7.0 until the end of the simulation.

Similarly to measured pH, simulated pH also shows a more or less stable circum-neutral value from approximately 75 hours until the end of the experiment. Nevertheless, at the

beginning and end of the experiment pH is overestimated with respect to measured values.

In the pH range measured during the experiment, and if pH and the carbon system would be controlled by calcite equilibrium, the following reversible reactions would be responsible for such control:

$$CO_2(g) + H_2O(l) \leftrightarrow HCO_3^-(aq) + H^+(aq) \quad \text{(equation 2.13)}$$

$$CaCO_3(s) + H^+(aq) \leftrightarrow Ca^{2+}(aq) + HCO_3^-(aq) \quad \text{(equation 2.14)}$$

Looking at equations 2.13 and 2.14, if the $P(CO_2)$ increases HCO_3^- is produced and at the same time pH decreases (due to the released H^+) which triggers calcite dissolution. Calcite dissolution, in turn, produces more HCO_3^- and buffers pH. From 75 hours until the end of the experiment, although calcite is predicted to precipitate, the simulated (and measured, at least until 100 hours) partial pressure of CO_2 decreases. This apparently contradictory relation between simulated calcite and CO_2 evolution could be explained by other carbon consuming process that hinders the increase of $P(CO_2)$, such as methanogenesis. Nevertheless, an alternative simulation has been performed without the formation of methane, but the partial pressure of CO_2 is still underestimated. Another reason for the discrepancy between measured and simulated CO_2 could be due to the fact that calcite is modelled under local equilibrium, and instead calcite could be controlled by kinetics. This hypothesis has also been tested in an alternative numerical model, by using the rate expression defined by Plummer et al. (1978) for the kinetic precipitation/dissolution of calcite. Nevertheless, very similar results have been attained compared to the simulation where calcite is treated under local equilibrium.

The differences between measured and simulated partial pressure of CO_2 are still not well understood, but could be due to one or more of the following factors (or even others that have not been identified yet): (1) overestimation of propionate production in lactate fermentation which leads to less available C(IV) in solution; (2) other propionate degrading processes could be present that would lead to more available C(IV); or (3) overestimation of abiotic methanogenesis. Abiotic methanogenesis (modelled under local equilibrium) leads to an excess of methane in the headspace gas (as will be shown in the next

section), compared to measured data, which leads to a predominance of C(-IV) against C(IV), in the final stages of the simulation.

2.5.1.5 Methanogenesis

Kinetic reduction of acetate to CH_4 is considered to be mediated by methanogens. As previously mentioned, since we are following the partial equilibrium approach, the local equilibrium reaction between C(IV) and C(-IV) (equation 2.1) has not been removed from the thermodynamic database, and therefore, abiotic methanogenesis is predicted whenever the redox potential is favourable for such reaction.

Numerical results show a considerable overestimation of $CH_4(g)$ with respect to measured values (Figure 2.9). In fact, even if the biological activity of methanogens is not included in the numerical model, computed $CH_4(g)$ is already produced abiotically (results not shown). Consideration of this microbial group has very low effect on the total CH_4 produced. On the other hand, if equation 2.1 is not included in the thermodynamic database, simulated pe is higher than the values measured during the last stage of the experiment.

The results attained in the experiment point towards the hypothesis of fully kinetic production of CH_4 from HCO_3^-, instead of the partial equilibrium approach applied here. But this consideration is not compatible with the partial equilibrium approach (where changes on the oxidation state of inorganic species are modelled under local equilibrium) that has been adopted in the present work, and for this reason the model fails to reproduce experimental data for methane and carbon dioxide.

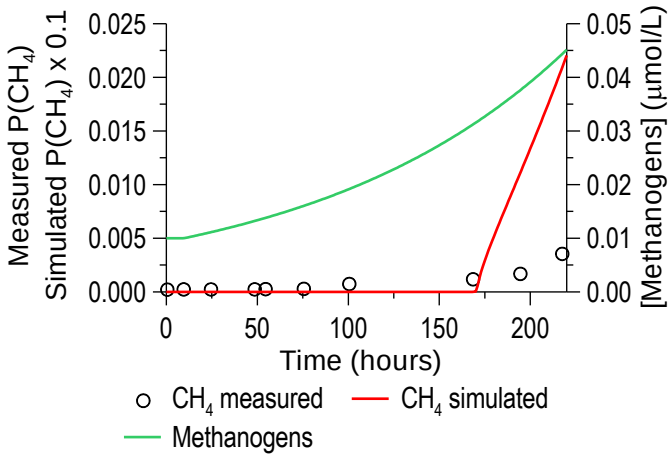

Figure 2.9 – Time evolution of measured (symbols) and simulated (red line) partial pressure of $CH_4(g)$ in the headspace. Computed concentration of methanogens is also shown (green line).

2.5.1.6 pe and the microbial redox sequence

Measured pe seems to reflect the biological activity of the microbial groups considered (Figure 2.10). The rapid decrease of measured pe until the first 15 hours reflects the reduction of O_2 and NO_3^- which is well reproduced by the model. The preceding temporal pe increase could be due to lactate fermentation, since this process is believed to follow O_2 and NO_3^- reduction, and it produces oxidized carbon without reducing any inorganic EA, as expressed by equation 2.11.

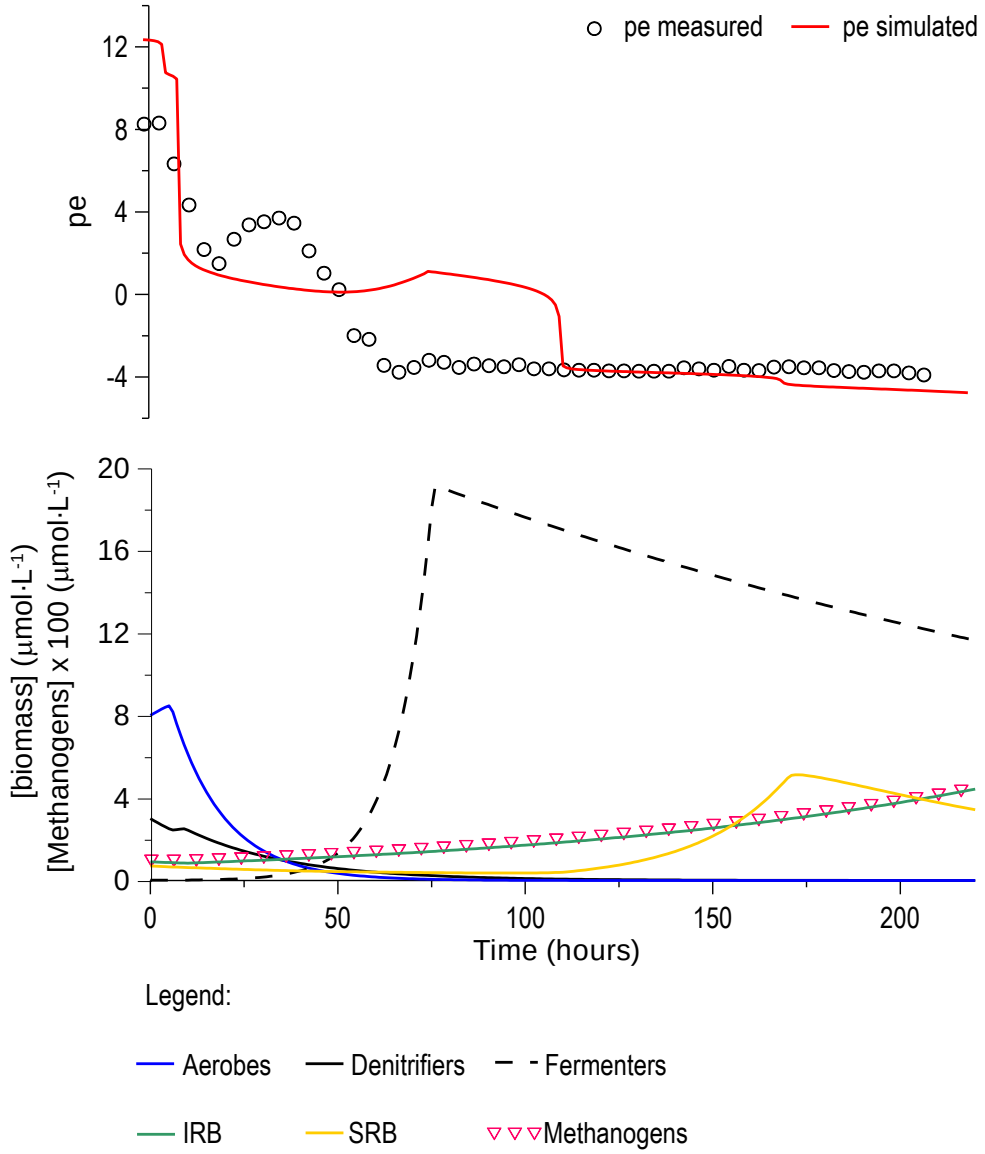

Figure 2.10 – Time evolution of measured (symbols) and simulated (red line) pe. Computed evolution of biomass of all microbial groups considered in the simulation is also shown, in the lower graphic.

In Figure 2.10, from 50 hours, fermentative bacteria biomass is much more important than all the other microbial groups. These computed results support the hypothesis for pe being controlled by the biological activity of this group when they are close to their maximum. Then, at approximately 115 hours, the rapid drop of computed pe to approximately -4 seems to reflect the relative importance of abiotic methanogenesis.

The simulated pe plateau around 2, most probably motivated by lactate fermentation, lasts longer than measured temporal pe increase (from 15 to 50 hours). Nevertheless, lactate consumption is well reproduced by the model, as observed in section 2.5.1.2.

Since measured evolution of almost all the inorganic EA's (exception made for HCO_3^- in methanogenesis) is well reproduced by the numerical model, the discrepancies observed between measured and simulated pe could be due to the stoichiometry of lactate fermentation implemented which has resulted in an overestimation of propionate (section 2.5.1.2). In fact, if we consider an alternative stoichiometry for lactate fermentation, in such a way that computed propionate does not overestimate measured propionate, computed pe matches better observed values, as shown in Figure 2.11.

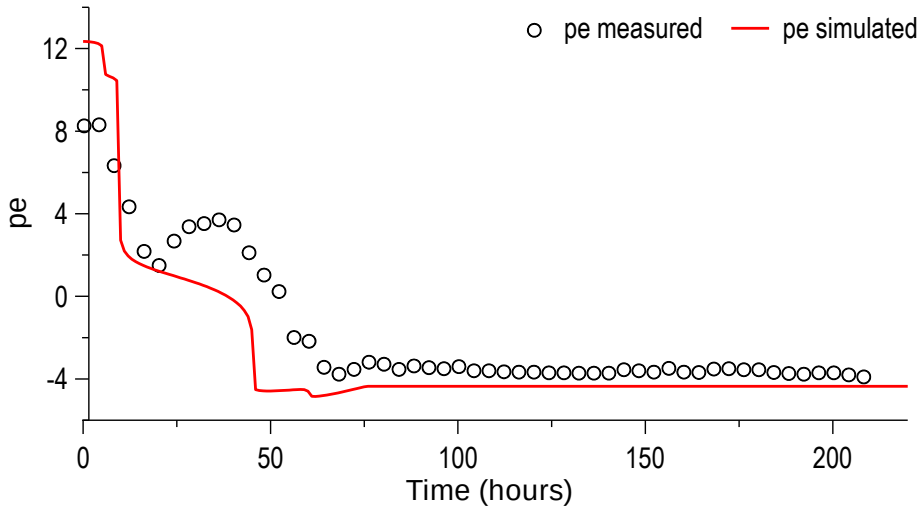

Figure 2.11 – Time evolution of measured (symbols) and simulated (red line) pe considering an alternative stoichiometry for lactate fermentation.

The alternative stoichiometry for lactate fermentation that leads to a better agreement between observed and measured pe (and also propionate, data not shown) is as follows:

3 mole of lactate → 1 mole of acetate + 1.3 moles of propionate

(equation 2.17)

In equation 2.17, the build up of new biomass of fermentative bacteria is not shown, for simplicity. In contrast to what is shown in equation 2.17, the stoichiometry used in the calibrated case that has been implemented in other works (von Gunten and Zobrist, 1993 and Schäfer et al., 1998), is:

3 mole of lactate → 1 mole of acetate + 2 moles of propionate

(equation 2.18)

With the alternative stoichiometry for lactate fermentation (equation 2.17), the small plateau computed for pe coincides with the temporal increase of measured pe (Figure 2.11). Nevertheless, this alternative stoichiometry for lactate fermentation triggers the anticipation of reduction of SO_4^{2-}. Therefore, for the objective of this study we rely on the reference case which results have been discussed in the former sections.

2.5.2 Uncertainties on Monod parameters

During parameterization of the extended Monod kinetic expressions applied for each microbial group considered in the numerical model, different combinations of the parameters have been found to lead to the same numerical solution. These results point towards non-uniqueness of the numerical solution which has also been identified by others (Schirmer et al., 1999). In this context, an alternative combination of Monod kinetic parameters has been applied by fixing an initial concentration of biomass of 1×10^{-8} $mol \cdot L^{-1}$ for all microbial groups. The values of the Monod kinetic parameters applied in this alternative case are listed in Table 2.2.

In Figure 2.12, the main results of the alternative case are shown. As for the reference case, in the alternative case, measured time evolution of pH, DO, NO_3^-, lactate, acetate

and SO_4^{2-} is very well reproduced by the numerical model. And, as observed for the reference case, propionate is overestimated in the alternative case.

Computed calcite concentration shows a more abrupt evolution than the one computed in the calibrated case. In addition, between 75 and 115 hours, the alternative case computes an exhaustion of calcite (zero moles of this mineral). These results reflect the influence of the new combination of the Monod parameters that, in general, leads to a more abrupt computed evolution of the biomass of the different microbial groups considered which, consequently, induce more abrupt curves for the EA's and ED's involved.

Fe(II) evolution does not fit so well in the alternative case (Figure 2.12e) as in the calibrated case (Figure 2.7b). This could be due to the fact that in the alternative case IRB's population is very small at the beginning of the simulation (mainly due to the imposed initial concentration of 1×10^{-8} mol·L^{-1}), and therefore computed Fe(II) is underestimated for the initial stage of the experiment.

Computed maximum of each microbial group in the alternative case also differs from the reference case. These differences are motivated by the different values of the Monod parameters. Maximum of aerobic bacteria in the alternative case is approximately the double of the maximum reached in the calibrated case, while the maximum of denitrifying bacteria in the alternative case is much smaller that in the reference case. Maxima of fermentative bacteria, IRB's and SRB's are smaller in the alternative case than in the reference case. The different partitioning of carbon between biomass and the inorganic carbon system observed in the two cases under study, has obviously an important influence on the computed results for the inorganic carbon system. Additional data must be measured in further experiments, such as calcium concentration and the initial concentration of microbial groups, in order to minimise the uncertainties associated to the experimental initial conditions and evolution, and thus, maintaining the uncertainties associated solely to the parameters describing the kinetic rates in the Monod growth model.

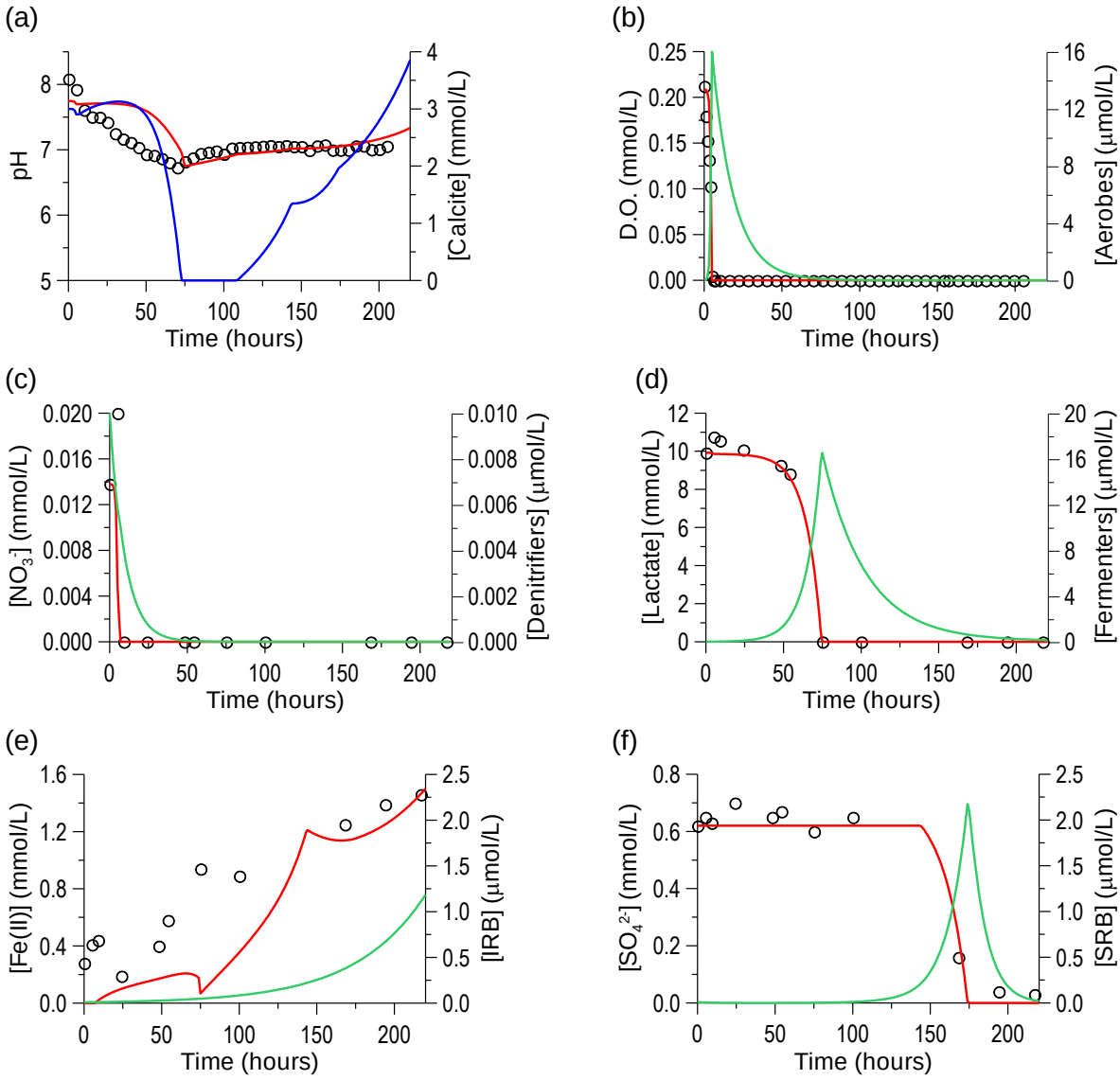

Figure 2.12 – Time evolution of measured (symbols) and simulated (red line) pH, DO, NO_3^-, lactate, acetate, propionate, Fe(II) and SO_4^{2-}. Computed evolution of calcite concentration is plotted with a blue line, and computed evolution of the biomass of each microbial group (related to each EA, and also fermenters for lactate) is plotted with green lines.

2.6 Conclusions

The results obtained have proven the weak and strong aspects of the conceptual and numerical models implemented to simulate microbial redox processes. Some discrepancies between modelled and measured data are still unsolved. Future experiments with additional data measurements and a sensitivity analysis of the Monod parameters may help solving some of these problems.

The calibration of the numerical model helped improving the understanding of the processes that influence pH and the redox potential of the jar-fermentor experiment. Undoubtedly, microbial activity exerts a great influence on pH, pe and associated composition of mineral and gas phases, within an aquatic system where organic matter is available. The results attained show that if microbes and organic matter are present in the vicinity of a deep geological repository, microbial redox reactions may provide a relatively fast evolution towards reducing conditions that are favourable to the geochemical integrity of the repository. If HS^- is produced during the sequence of microbial redox reactions, its concentration can be controlled by the precipitation of sulphur secondary phases such as S(0) and FeS which were predicted by the numerical simulation developed here. In this context, precipitation of sulphur secondary minerals may contribute to the mitigation of corrosion of the copper canisters within a deep geological repository.

By applying the partial equilibrium approach in PHREEQC a reliable estimation of the indirect parameters pH and pe has been achieved. Measured evolution of the inorganic EA's (DO, NO_3^- and SO_4^{2-}) and Fe(II) is very well reproduced by the numerical model. Simulated lactate fermentation and methanogenesis have shown some discrepancies with respect to measured data.

Fermentative bacteria seem to be the dominant microbial group during most of the experiment, and therefore, the inorganic system is highly influenced by the biological activity of this group. The temporal pe plateau around 2 seems to be controlled by the activity of fermenters, as well as the first and fastest increase of the partial pressure of CO_2 in the headspace gas which triggers calcite dissolution. The jar-fermentor experiment and the numerical simulations developed here have provided an improved understanding of aquatic systems influenced by microbial activity. In order to assess the influence of such microbial activity in the repository system new numerical simulations that account for its geochemical and hydrodynamic features should be developed.

The stoichiometry of lactate fermentation may be different (3 mol Lactate → 1 mol Acetate + 1.3 mol Propionate) from the one implemented in the reference case (3 mol Lactate → 1 mol Acetate + 2 mol Propionate), that has been implemented by others (Schäfer et al., 1998).

Methane production is overestimated with respect to measured data which seems to indicate solely kinetic processes controlling CH_4 production rather then both local equilibrium and biotic kinetic processes as implemented here.

Some uncertainties related to the Monod parameters could be solved in future experiments if additional variables are measured, such as aqueous calcium and carbonate minerals concentration, and the initial and final concentration of microbial groups.

Acknowledgements

This study was performed as a part of the “Project for Assessment Methodology Development of Chemical Effects on Geological Disposal System” funded by the Ministry of Economy, Trade and Industry, Japan. The first author is grateful to the Portuguese Ministry of Science, Technology and Education for a PhD Grant (POCI 2010, BD/16647/2004). Special thanks are given to David Parkhurst, Henning Prommer and Vincent Post for valuable comments and providing good examples of modelling approaches.

2.7 References

Ajima S., Todaka N., Molinero J. and Hallbeck L. (2008) Quantitative assessment of effective kinetic parameters for microbially mediated sulphate reduction processes in groundwaters at the Äspo site (Sweden). *Proceedings of the International Congress of the International Association of Hydrogeologists*.

Appelo C.A.J. and Postma D. (2005) *Geochemistry, groundwater and pollution*. A.A. Balkema Publishers. Amsterdam, The Netherlands, 649 pp.

Banwart S.A. (1999) Reduction of iron(III) minerals by natural organic matter in groundwater. *Geochimica et Cosmochimica Acta*, 63(19/20): 2919 – 2928.

Barry D.A., Prommer H., Miller C.T. Engesgaard P., Brun A. and Zheng C. (2002) Modelling the fate of oxidisable organic contaminants in groundwater. *Advances on Water Resources*, 25: 945-983.

Brun A. and Engesgaard P. (2002) Modelling of transport and biogeochemical processes in pollution plumes: literature review and model development. *Journal of Hydrology*, 256: 211 – 227.

Chapelle F.H. (1993) *Groundwater Microbiology and Geochemistry*. Wiley, New York.

Dromgoole E.L. and Walter L.M. (1990) Iron and manganese incorporation into calcite: Effects of growth kinetics, temperature and solution chemistry. *Chemical Geology*, 81(4): 311-336.

Duro L., Grivé M., Cera E., Gaona X., Domènech C. and Bruno J. (2006) *Determination and assessment of the concentration limits to be used in SR-Can*. SKB TR-06-32, Svensk Kärnbränslehantering AB.

Fletcher P. and Sposito G. (1989) The chemical modelling of clay/electrolyte interactions for montmorillonite. *Clay Minerals* 24: 375-391.

Grivé M. (2005) *The linkage between uranium, iron and carbon cycling. Processes at interfaces: evidences from combined solution chemical and spectroscopic studies*. PhD. Thesis, Universitat Politècnica de Catalunya, 341 pp.

Hummel W., Berner U., Curti E., Pearson F.J. and Thoenen T. (2002) *Nagra/PSI Chemical Thermodynamic Data Base 01/01*. ISBN: 1-58112-620-4. 565 p.

Jimenez-Lopez, C. and Romanek, C.S. (2004) Precipitation kinetics and carbon isotope partitioning of inorganic siderite at 25ºC and 1 atm. *Geochimica et Cosmochimica*

Acta, 68(3): 557-572.

Lovley D.R., Phillips E.J.P. and Lonergan D.J. (1991) Enzymic versus nonenzymic mechanisms for iron(III) reduction in aquatic sediments. *Environmental Science and Technology*, 25(6): 1062-1067.

Mayer K.U., Benner S.G., Frind E.O., Thornton S.F. and Lerner D.N. (2001) Reactive transport modelling of processes controlling the distribution and natural attenuation of phenolic compounds in a deep sandstone aquifer. *Journal of Contaminant Hydrology* 53: 341 – 368.

Moses C.O. and Herman J.S. (1991) Pyrite oxidation at circumneutral pH. *Geochimica et Cosmochimica Acta,* 55: 471– 482.

Nakajima S. Nagaoka T. Hirano S. Nakamura T. and Yoshida N. (2008) Microbial and geochemical processes in subsurface environments: Implication of microbially mediated redox changes during operation of nuclear waste repositories. In *Proceedings of 7th International Symposium for Subsurface Microbiology*, Shizuoka, Japan, Nov 16-21, (ISSM2008), S6-P8

Nicholson, R.V., Gillham, R.W., Reardon, E.J., 1988. Pyrite oxidation in carbonate-buffered solution: 1. Experimental kinetics. *Geochimica et Cosmochimica Acta* 52, 1077–1085.

Parkhurst D.L. and Appelo C.A.J. (1999) *User's guide to PHREEQC (version 2) – A computer program for speciation, batch-reaction, one-dimensional transport and inverse geochemical calculations*. U.S. Geological Survey Water Resources investigations report 99-4259.

Plummer L.N., Wigley T.M.L. and Parkhurst D.L. (1978) The kinetics of calcite dissolution in CO_2 – water systems at 5º to 60ºC and 0.0 to 1.0 atm CO_2. *American Journal of Science*, 278: 179-216.

Puigdomènech I. and Taxen C. (2000) *Thermodynamic data for copper. Implications for the corrosion of copper under repository conditions*. SKB Technical Report TR 00–13, Stockholm, Sweden.

Pyzik A.J. and Sommer S.E. (1981) Sedimentary iron monosulfides: Kinetics and mechanism of formation. *Geochimica et Cosmochimica Acta*, 45(5): 687-698.

Rickard D. (1997) Kinetics of pyrite formation by the H_2S oxidation of iron (II) monosulfide in aqueous solutions between 25 and 125ºC: The rate equation. *Geochimica et*

Cosmochimica Acta, 61(1): 115-134.

Rittmann B.E. and VanBriesen J.M. (1996). Microbiological processes in reactive modelling. In: Lichtner, P.C., Steefel, C.I. and Oelkers, E.H. Reactive transport in porous media. *Reviews in Mineralogy*, 34: 311 – 332.

Schäfer D., Schäfer W. and Kinzelbach W. (1998) Simulation of reactive processes related to biodegradation in aquifers: 2. Model application to a column study on organic carbon degradation. *Journal of Contaminant Hydrology*, 31: 187-209.

Schirmer M., Butler B.J., Roy J.W., Frind E.O. and Barker J.F. (1999) A relative-least-squares technique to determine unique Monod kinetic parameters of BTEX compounds using batch experiments. *Journal of Contaminant Hydrology*, 37: 69-86.

Thauer R. K. (1998) Biochemistry of Methanogenesis: a Tribute to Marjory Stephenson. *Microbiology*, 144: 2377-2406.

Todaka N., Molinero J., Murakami-Amano Y. and Iwatsuki T. (2007) Hydro-bio-geochemical modelling of batch experiments of the Mizunami underground research laboratory in Japan. *Proceedings of the International Conference on WAter POllution in natural POrous media at different scales*. Assessment of fate, impact and indicators.

Van Cappellen P. and Gaillard J-F (1996) Biogeochemical dynamics in aquatic systems. In: Lichtner, P.C., Steefel, C.I. and Oelkers, E.H. Reactive transport in porous media. *Reviews in Mineralogy*, 34: 335 – 376.

von Gunten U. and Zobrist J. (1993) Biogeochemical changes in groundwater-infiltration systems: Column studies. *Geochimica et Cosmochimica Acta*, 57: 3895-3906.

Watson I.A., Oswald S.E., Banwart S.A., Crouch R.S. and Thornton S.F. (2005) Modeling the dynamics of fermentation and respiratory processes in a groundwater plume of phenolic contaminants interpreted from laboratory-to field-scale. *Environmental Science and Technology*, 39(22): 8829-8839.

Yang C., Samper J., Molinero J. and Bonilla M. (2007) Modelling geochemical and microbial consumption of dissolved oxygen after backfilling a high level radioactive waste repository. *Journal of Contaminant Hydrology*, 93: 130-148.

Chapter 3

Quantitative assessment of radionuclide retention in glacial clays related to groundwater discharge areas

3. Quantitative assessment of radionuclide retention in glacial clays related to groundwater discharge areas[3]

Abstract

The Swedish Nuclear Fuel and Waste Management Company (SKB) has recently selected Forsmark for sitting a deep geological repository for high level nuclear waste (HLNW). At the surface, a Quaternary till overlies the granitic candidate host rock. Radionuclides potentially released from a repository may reach surface ecosystems if these are somehow related to deep groundwater discharge areas. At Forsmark, surface water bodies are partially fed by shallow aquifers which locally receive deep groundwater discharge. At the bottom of surface water bodies and overlying the Quaternary till, glacial clays are present. Reactive transport numerical simulations have been performed to evaluate the retention of radionuclides, potentially released from a repository, in the glacial clays related to groundwater discharge areas. Four radionuclides (^{235}U, ^{135}Cs, ^{226}Ra and ^{90}Sr) have been selected according to their different geochemical behaviour and potential dose relevance to surface ecosystems. Numerical results indicate that U precipitates as amorphous uraninite in the glacial clay; Sr co-precipitates with calcite and it is also adsorbed on illite. Cs is also retained by adsorption on illite. Ra is mobile, since co-precipitation with barite, the only mechanism considered to retain Ra, is not predicted by the numerical calculations.

Keywords: Glacial clay, Groundwater discharge area, Radionuclides, Reactive solute transport, PHAST

---

[3] This work has been accepted in Hydrogeology Journal, and has been developed by the following co-authors: Clara Sena[a,b], Fidel Grandia[a], David Arcos[a], Jorge Molinero[a], Lara Duro[a] and Jordi Bruno[a]

[a]Amphos XXI Consulting S.L., Spain; [b]I&D GeoBioTec, University of Aveiro, Portugal

3.1 Introduction

On June 2009, SKB has decided to select Forsmark as the site for the final repository for Sweden's HLNW. The selection of Forsmark is the result of close to 20 years of work during which SKB has conducted surveys throughout Sweden and feasibility studies in eight municipalities. These were followed by site investigations in two alternative sites: Forsmark and Oskarshamn between 2002 and 2007 (SKB, 2009). The deep geological repository is designed with a number of engineered (copper canisters, clay barriers, cement liners) and natural geological barriers to prevent and retard for long periods of time (~100,000 years) the potential migration of radionuclides to the surface (SKB, 2006). As reported by Berglund et al. (2009), flow path analysis is required in the context of safety assessment to identify discharge areas where radionuclides potentially released from a repository could reach the surface ecosystems. At Forsmark, the near-surface Quaternary sediments would constitute the last geological barrier preventing the arrival of radionuclides to the surface biosphere. For this reason, SKB has launched a comprehensive research programme for the near-surface hydro-geo-ecological study of the candidate sites. The main scientific results of such programme have been recently published in Berglund et al. (2009).

Quantitative analysis of radionuclide migration and the evaluation of the retention capacity of Quaternary sediments is part of the safety assessment of the repository. Coupled groundwater flow and reactive solute transport models provide a useful tool for such quantitative understanding of radionuclide migration through the Quaternary sediments connecting deep groundwater flow paths to surface discharge areas.

In the last years, reactive transport models have been applied to a wide variety of environmental issues some of which include characterization of landfill plumes (Brun et al., 2002), cation exchange models to describe caesium sorption at high ionic strength in subsurface sediments contaminated by HLNW (Liu et al., 2004), large-scale and long-term reactive transport simulations to validate hydrochemical and hydrogeological conceptual models (Molinero and Samper, 2006), simulation of laboratory experiments (Steefel et al., 2003) and assessment of the geochemical evolution of a deep geological repository (Arcos et al., 2008).

The work presented here focuses on the hydrogeochemical processes that influence radionuclide migration in the Quaternary sediments present at the groundwater discharge areas in one of the candidate sites (Forsmark).

Coupled groundwater flow and reactive solute transport numerical simulations have been performed to assess the retention of selected radionuclides in glacial clays present at the bottom of surface water bodies related to groundwater discharge areas. Four radionuclides (^{235}U, ^{135}Cs, ^{226}Ra and ^{90}Sr) have been selected to be studied, according to their different geochemical behaviour and potential dose relevance to surface ecosystems.

3.2 Scope

A modelling procedure to assess radionuclide retention in near-surface systems is described in the present work. This modelling procedures relies on six main steps: (1) a thorough review of site specific data that describe the hydrogeochemical behaviour of the system under study; (2) development of the conceptual model of the system based on data gathered in the first step; (3) identification and quantification of the thermodynamic parameters that describe the geochemical processes of interest; (4) implementation of the conceptual model in reactive transport numerical simulations; (5) simulation of a hypothetical repository release in the numerical model; and, (6) quantitative assessment of radionuclide retention in the modelled system based on the outputs of the numerical simulations.

Site specific data on hydraulic, hydrochemical and geochemical parameters of the glacial clays at Forsmark have been thoroughly analysed from the SKB database of the Forsmark Site Characterization Programme (SKB, 2005). The glacial clay conceptual model was then implemented in a reactive transport numerical model. By simulating a long period of coupled groundwater flow and reactive solute transport with the average concentrations of the main reactive minerals, major and minor ions, and natural isotopes of the studied radionuclides, the geochemical quasi-steady state of the glacial clays has been modelled and reproduces the present-day conditions observed at the groundwater discharge areas of Forsmark. Once the present-day hydrogeochemical conditions of the glacial clays at Forsmark have been modelled, a hypothetical repository release was simulated by injecting a deep groundwater carrying repository-derived radionuclides into the modelled domain. The simulation of repository release was performed for an additional long period of reactive solute transport. From the outputs of the numerical simulations, the radionuclide retention capacity of the glacial clays present at the bottom of surface water bodies has been quantitatively assessed.

3.3 Near-surface hydrogeology at Forsmark

The near-surface hydrogeology at Forsmark is composed of Quaternary deposits that host confined and unconfined aquifers overlying the granitic bedrock. Groundwater in the granitic bedrock flows mainly along fractures and deformation zones composed of loose granitic material and coatings of calcite, chlorite, quartz and pyrite (Drake et al., 2006).

The till deposit which is the most abundant Quaternary deposit (~75% of aerial extension, Figure 3.1) hosts unconfined porous aquifers with stratified hydraulic conductivity and porosity (Johansson et al., 2005). The thickness of the Quaternary deposits is highly variable, usually from 0 to 3 m, although in some places it can reach over 10 m (Johansson et al., 2005).

In general, the till deposit consists of sandy glacial deposits with variable amounts of boulders and clay (Albrecht, 2005). The origin of this till is associated with the glacial erosion, transport and deposition of Palaeozoic carbonate rocks located northwards from Forsmark (Tröjbom and Söderbäck, 2006), and therefore carbonate minerals are abundant in the Quaternary deposits.

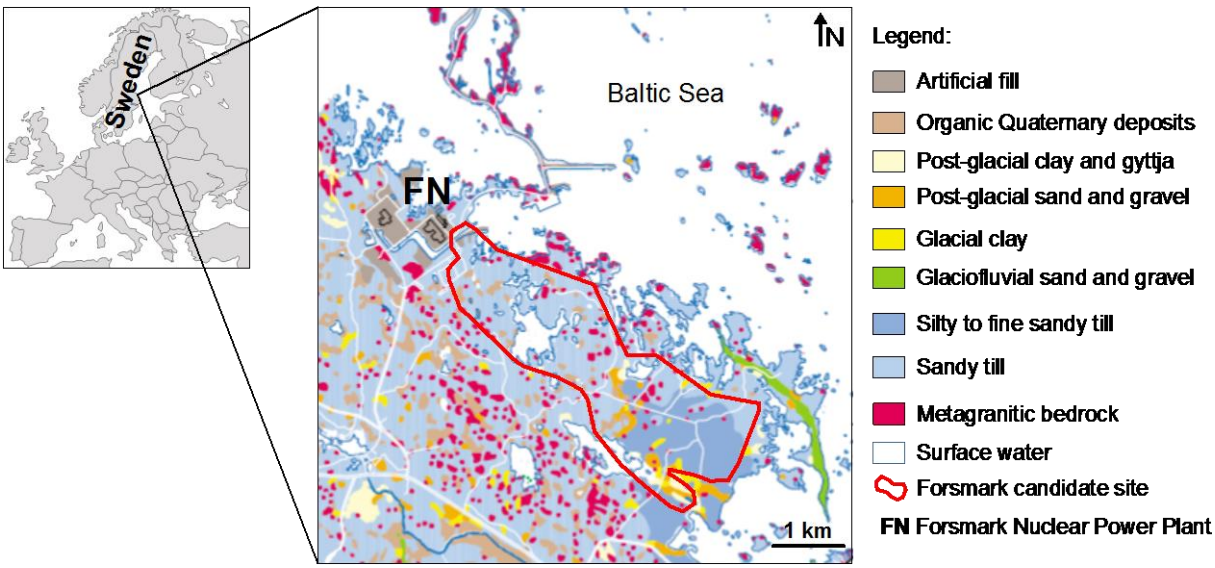

Figure 3.1 – Geological map of the Forsmark area with location of the candidate site (SKB, 2002, reproduced with permission).

At the bottom of surface water bodies such as streams, lakes or the Baltic Sea, and overlying the till deposit, glacial to post-glacial clays with organic matter-rich layers called *gyttja* are present. These are low permeability sediments basically composed of illite,

calcite, organic detritus and minor amounts of pyrite (Lokrantz and Hedenström, 2006; Vikström, 2005).

In general, groundwater flows in Quaternary deposits from elevated inland areas towards the Baltic Sea, with local discharge into the water courses that feed lakes and wetlands (Johansson et al., 2005). Hydrogeological investigations reveal that hydraulic connections between Quaternary deposits and the granitic bedrock could be in a downward direction (Bosson and Berglund, 2006). Nevertheless, local upward flow paths, between bedrock and Quaternary deposits, are also believed to occur (Laaksoharju et al., 2008).

3.4 Natural occurrence of uranium, strontium, caesium and radium at Forsmark

The concentrations of the natural isotopes of the selected radionuclides (uranium, strontium, caesium and radium) at Forsmark have been studied. By comparing the concentration of these elements (both in aqueous and solid phases) with major elements, key geochemical processes that influence radionuclide mobility in the glacial clays may be depicted. This is a fundamental step in the process of building a sound hydrogeochemical conceptual model of the problem of interest.

3.4.1 Uranium

In shallow groundwaters of Forsmark, uranium concentrations range from 1.0×10^{-4} to 1.5×10^{-1} $\mu mol \cdot L^{-1}$. This wide range indicates variable redox conditions in the near-surface systems. Lake and stream waters at Forsmark have similar uranium concentrations (4.09×10^{-3} to 1.57×10^{-2} $\mu mol \cdot L^{-1}$; Tröjbom and Söderbäck, 2006). Uranium is commonly transported forming complexes with bicarbonate, phosphate, iron and dissolved organic carbon (DOC) (Grenthe et al., 1992). However, none of these ions shows clear correlation with uranium, suggesting that multiple geochemical processes are responsible for the mobility of uranium in these waters. The presence of calcite in most of the Quaternary sediments at Forsmark leads to the predominance of circum-neutral waters with considerable amounts of dissolved carbonates which, in turn, enhance the mobility of uranium in these near-surface waters.

From elemental analysis of the solid phase of the Quaternary deposits, rough correlations between uranium and iron, manganese and phosphorous are observed, indicating that uranium could be associated with Fe-Mn oxides or phosphates.

3.4.2 Strontium

Strontium concentrations in shallow groundwaters range between 0.8 to 50 μmol·L^{-1}. Taking into account the interaction between water and the till and knowing that both Ca and Sr may be present in carbonates and exchangeable sites of clay minerals, a correlation between strontium and calcium is expected. Indeed, looking in detail at the shallow groundwaters composition in the study area, two different trends are observed when strontium concentrations are plotted against Ca (Figure 3.2).

One trend involves high salinity waters (top right border of mixing trend, Figure 3.2), and represents a mixing trend. The other trend includes dilute waters, with a Sr/Ca (molar ratio) of 10^{-4} that is consistent with congruent dissolution of a Sr-bearing calcite in the solid phase. Bruno et al. (2002) obtained an average Sr/Ca (molar ratio) of 3.5×10^{-3} in a set of groundwaters from different environments.

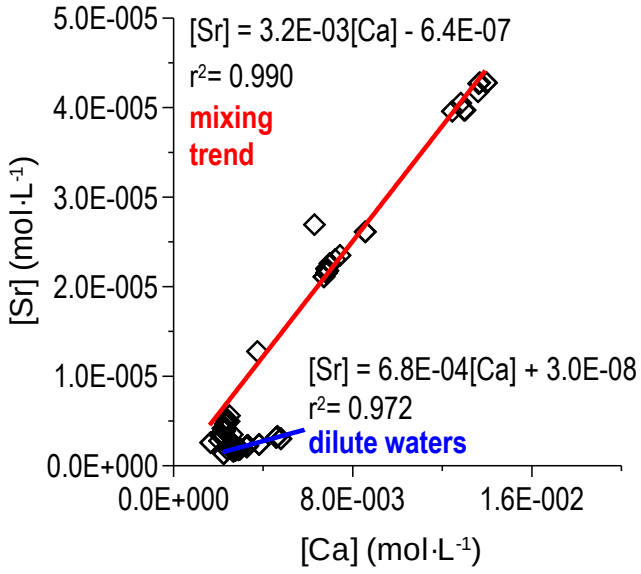

Figure 3.2 – Observed correlations between strontium and calcium in shallow groundwaters of Forsmark candidate area.

3.4.3 Caesium

Data on caesium concentrations are scarce in shallow groundwaters in the Forsmark area. Data on shallow groundwaters ranges from 5×10^{-5} to 1×10^{-3} $\mu mol\cdot L^{-1}$ which reveals relatively low concentrations of caesium in natural waters. With the available data no clear correlations with other ions have been observed. Nevertheless, caesium is expected to be involved in cation exchange in interlayered clays like illite (Bradbury and Baeyens, 2000, among others).

3.4.4 Radium

Radium concentration in natural waters is usually very low, ranging from 10^{-8} to 10^{-5} $\mu mol\cdot L^{-1}$. Among the 22 shallow groundwater samples collected in Forsmark for radium analysis (Tröjbom and Söderbäck, 2006) five were below detection limit for radium (1×10^{-8} $\mu mol\cdot L^{-1}$), and the maximum radium concentration reached was 1.09×10^{-7} $\mu mol\cdot L^{-1}$.

3.5 Reactive solute transport modelling

The numerical simulations developed in this work rely on a hypothetical scenario where a radionuclide-bearing deep groundwater flows upwards, from the repository to the surface, reaching a glacial clay sediment located at the bottom of a lake or the Baltic Sea (Figure 3.3). Glacial clays do not contact directly with the top of the granite; instead, a till deposit is always present between both geological materials (Figure 3.3). In order to evaluate the hydrogeochemical processes that take place in a glacial clay and influence radionuclide mobility, deep groundwater is assumed to flow through a preferential path of the till deposit (fracture) that contacts directly the bottom of the glacial clay layer.

It should be noted that the numerical model developed aims at depicting a realistic evolution of radionuclide mobility within the glacial clay at Forsmark and is based on site specific data whenever possible, although it considers a hypothetical scenario.

The reactive solute transport simulations have been performed with the finite-difference code PHAST v. 1.4.2 (Parkhurst et al., 2004). This code is the result of coupling a transport solver, HST3D (Kipp, 1997) and the well known geochemical code, PHREEQC (Parkhurst and Appelo, 1999). PHAST is able to simulate multi-component, reactive solute transport in three-dimensional saturated groundwater flow systems. The reactive transport equations are solved by sequential non iterative approach (SNIA) in which solute transport

and chemical reaction are decoupled for each time step. Previous static geochemical simulations were conducted to define proper and consistent initial and boundary conditions of the reactive solute transport simulations.

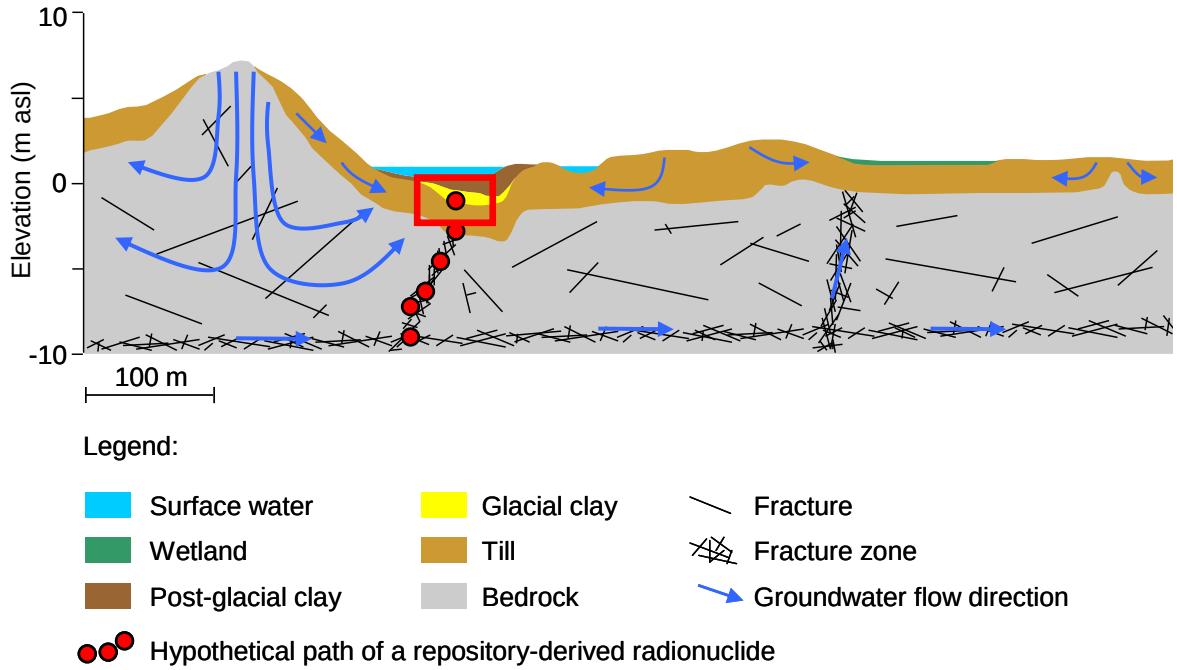

Figure 3.3 – Near-surface hydrogeological conceptual model of Forsmark candidate site (modified from Johansson et al., 2005) showing a hypothetical path of radionuclides released from a repository. The glacial clay under study is highlighted with a red rectangle.

The thermodynamic database used in the present work (Duro et al., 2006a) is an extension of the NAGRA-PSI database, compiled by Hummel et al. (2002). This database contains a large set of complexation reactions as well as pure mineral equilibrium reactions for many radionuclides and trace elements.

3.5.1 Hydrodynamic processes and parameters

According to the findings of the site characterization programme developed by SKB, glacial clays present at Forsmark are low permeability porous sediments that behave as aquitards located between the till aquifers and the surface water bodies (Johansson et al., 2005). Table 3.1 shows average values of the hydrodynamic parameters that were used in the numerical simulations of this work.

Table 3.1 – Values of the hydrodynamic parameters implemented in the numerical model for the glacial clay. (from Johansson et al., 2005).

Parameter	Value
$k_{horizontal}$ ($m \cdot s^{-1}$)	1.0×10^{-8}
$k_{vertical}$ ($m \cdot s^{-1}$)	1.0×10^{-9}
$\alpha_{longitudinal}$ (m)	0.5
$\alpha_{transverse}$ (m)	0.2
ϕ_{ε} (-)	0.2
De ($m^2 \cdot s^{-1}$)	5×10^{-10}
ρ ($kg \cdot L^{-1}$)	2.0
k – hydraulic conductivity; α – dispersivity coefficient; ϕ – porosity; De – effective diffusion coefficient; ρ – dry bulk density.	

3.5.2 Geochemical processes and parameters

The capacity of the near-surface systems to retain radionuclides depends mainly on the mineral assemblages present, which in turn, enable radionuclide sorption on, precipitation or co-precipitation with major element solid phases. Sorption and precipitation are controlled by the groundwater composition. In general, radionuclide retention is provided by (i) sorption on charged surfaces (mainly clays and oxyhydroxides); (ii) co-precipitation with sulphates, sulphides, oxyhydroxides and carbonates; (iii) redox retention processes and (iv) sorption onto organic tissues. In some cases, precipitation of pure phases (e.g., amorphous uraninite) can also be relevant despite the relatively low concentrations of these radionuclides. Since the objective of this work is the quantitative assessment of radionuclide retention in glacial clay sediments, radioactive decay was not considered in the numerical simulations.

According to Hedenström (2004), at Forsmark, the glacial clays present in the lake sediments and the Baltic Sea have considerable amounts of illite, quartz and calcite. Quartz and illite have very slow precipitation/dissolution kinetics under the pH and pe conditions that prevail in the glacial clays at Forsmark (Köhler et al., 2003). Therefore, from the observed minerals only calcite was included as a reactive solid phase in the numerical simulations, and, given that no reactivity was considered for illite, this mineral was simulated solely as a charged surface for cation exchange.

From the four radionuclides selected, caesium and strontium are considered to exchange in illite sites. In the numerical simulations, the model for cation exchange in illite is that

proposed by Bradbury and Baeyens (2000) with some modifications (see Appendix 1, and Grandia et al., 2007 for further details). The proposed model considers three types of sites: planar sites, type II sites and frayed edge sites (FES). Divalent cations (Ca^{2+}, Mg^{2+}, Sr^{2+}) only exchange in the planar sites, while monovalent cations (Na^{+}, K^{+}, NH_4^{+} and Cs^{+}) may exchange in all the types of sites. Cs^{+} is known to have high affinity for the FES (Bradbury and Baeyens, 2000, among others). Assuming a 50 wt% of illite in the glacial clays at Forsmark, with a cation exchange capacity of 0.2 $eq \cdot kg_{solid}^{-1}$, as reported by Bradbury and Baeyens (2000), a constant concentration of 0.1 $mol \cdot kg_{solid}^{-1}$ of total cation exchange sites in illite has been considered in the numerical simulations.

As mentioned above, calcite is present in the glacial clays and is likely to incorporate trace amounts of strontium. Therefore, a non-ideal calcite-strontianite solid solution (Tesoriero and Pankow, 1996) has been considered to be present in the glacial clay. From the mean $CaCO_3$ content of 26 wt% measured in the glacial clays at Forsmark (SKB 2005), and considering that only an external thin rim of the calcite grains (corresponding to 5% of total calcite) is available to react with the porewater, an initial amount of 0.8 wt% of calcite-strontianite solid solution (which corresponds to ~0.8 $mol \cdot L_{water}^{-1}$) has been prescribed in the numerical simulations. In addition, and since the studied groundwaters are rich in aqueous carbonate, Fe(III) carbonate complexes have been added to the thermodynamic database (Grivé, 2005).

Table 3.2 – Complexation reactions of aqueous Fe(III) carbonates and corresponding thermodynamic constants (from Grivé, 2005).

Reaction	Log K^0 (25ºC)
$Fe^{3+} + CO_3^{2-} + H_2O \leftrightarrow FeOHCO_3 + H^{+}$	10.76
$Fe^{3+} + 3CO_3^{2-} \leftrightarrow Fe(CO_3)_3^{3-}$	24.24

No data on pyrite content in glacial clays are available for Forsmark. Nevertheless, pyrite is known to form in lake sediments similar to the ones under study (Percival et al., 2001). In addition, elemental concentrations of sulphur in the solid phase of lake sediments at Forsmark can be up to 3.3 wt% (Hedenström, 2004). Therefore, and taking into account the predominant reducing conditions of the glacial clays at Forsmark, an initial concentration of 1.2 wt% of pyrite (which corresponds to approximately 1 $mol \cdot L_{water}^{-1}$ of pyrite) has been prescribed in the numerical model.

Siderite ($FeCO_3$) is also not mentioned in data related to the mineralogy of glacial clays at Forsmark. This mineral is redox sensitive and can precipitate in the glacial clay domain after the inflow of a reducing and Fe-rich deep groundwater. Therefore, siderite is allowed to precipitate in the simulations if oversaturation with this mineral is reached.

Uranium occurs in nature mainly as two oxidation states: U(IV) and U(VI). The former is rather immobile so that reducing waters are not able to transport much uranium (Langmuir, 1997). Amorphous uraninite, a U(IV) solid phase, could form in a glacial clay sediment if repository-derived uranium interacts with potentially reducing porewaters. On the other hand, if repository-derived uranium reaches oxidising conditions, its mobility could be enhanced and soluble U(VI) hydroxide and particularly carbonate complexes may form.

In shallow aquatic environments containing organic matter, U(VI) may be complexed by organic compounds and also reduced and immobilized as U(IV). The glacial clays at Forsmark usually contain considerable concentrations of organic matter in which humic acids are most probably present; and therefore, U(VI) humic complexes have been added to the thermodynamic database used in the reactive transport simulations. The cations considered for complexation with humic acids are calcium and uranium. The reactions and thermodynamic constants for these species are listed in Table 3.3.

Table 3.3 – Complexation reactions of organic compounds and the corresponding thermodynamic constants.

Reaction	Log K (25ºC)
$Ca^{2+} + Humate^{-} \leftrightarrow CaHumate^{+}$	4.7 [(1)]
$U^{4+} + Humate^{-} \leftrightarrow UHumate^{3+}$	7.0 [(2)]
$2U^{4+} + Humate^{-} \leftrightarrow U(Humate)_2^{2+}$	11.5 [(2)]
$UO_2^{2+} + Humate^{-} \leftrightarrow UO_2Humate^{+}$	7.64 [(3)]
$2UO_2^{2+} + 2Humate^{-} \leftrightarrow UO_2(Humate)_2$	11.54 [(3)]
[(1)] Choppin and Shanbhag (1981); [(2)] Li et al. (1980); [(3)] Shanbhag and Choppin (1981)	

The formation of solid solutions of Ba-Ca-Sr sulphates and carbonates is considered to be the solubility-limiting process for radium in natural waters (Grandia et al., 2008; and references therein). In many aqueous systems, radium is quantitatively co-precipitated with barium sulphate (barite, $BaSO_4$) due to the chemical similarity between radium and barium. In the numerical simulations, an ideal solid solution between $BaSO_4$ and $RaSO_4$ is let to form if saturation with barite is reached.

According to the processes identified to occur in the glacial clays at Forsmark that may influence radionuclide mobility, the reactive minerals considered in the numerical simulations are listed in Table 3.4. It should be noted that the saturation index of relevant pure phases that may incorporate the studied radionuclides was calculated and monitored during previous simulations. The monitored phases are becquerelite ($Ca(UO_2)_6O_4(OH)_6{:}8H_2O$), schoepite ($UO_3{\cdot}nH_2O$) and soddyite ($(UO_2)_2SiO_4{\cdot}2H_2O$) (for U); celestite ($SrSO_4$) and strontianite ($SrCO_3$) (for Sr); and radium sulphate ($RaSO_4$) (for Ra). Since saturation with these phases was not reached under the geochemical conditions modelled, these minerals were discarded for further numerical calculations.

In Table A1.2 of Appendix 1, the dissolution reactions of the minerals considered in the numerical simulations are listed.

Table 3.4 – Initial concentration of the reactive minerals considered for the reactive transport simulations. Potentially retained radionuclides and respective mechanism of retention are also shown.

Mineral	Initial concentration of reactive mineral (wt%)	Mechanism of radionuclide retention	Potentially retained radionuclides
$Ca_{1-\chi}Sr_\chi CO_3$ (χ(initial)= 1.73×10^{-5})*	0.8	Co-precipitation	Sr
Illite	50.0	Cation exchange	Sr, Cs
Amorphous uraninite ($UO_2{:}2H_2O$(am))	0.0	Precipitation	U
$Ba_{1-\chi}Ra_\chi SO_4$	0.0	Co-precipitation	Ra
Pyrite (FeS_2)	1.2	-	-
Siderite ($FeCO_3$)	0.0	-	-

*χ stands for the molar fraction of Sr and Ra in the solid solutions in which they are involved.

3.5.3 Initial and boundary conditions

The numerical model simulates the water flow and geochemical processes that occur in a glacial clay layer located underneath a surface water body that constitutes a discharge area of the till aquifer. Therefore, the flow conditions prescribed for the glacial clay depend on the flow conditions in the surrounding till aquifer. In order to evaluate the flow directions that occur in such a glacial clay layer and according to the hydrologic water balance

calculations performed for the Forsmark site (Johansson et al. 2005), a preliminary numerical model with a clay layer located at the right top corner of a till domain was built. In this previous model a shallow groundwater inflow of 14.5 $L \cdot d^{-1}$ at the left boundary, and a deep groundwater inflow of 0.25 $L \cdot d^{-1}$ was set. The numerical model of the glacial clay was then built based on the flow directions and hydraulic heads attained in the preliminary numerical model (Figure 3.4).

The modelled domain of the glacial clay is a 2D symmetric vertical cross section of a glacial clay that may be present at groundwater discharge areas of Forsmark (Figure 3.4). Based on the description of lake sediments (Johansson et al., 2005), the thickness of the glacial clay was set to 1 m. Shallow groundwater in equilibrium with the glacial clay mineralogy enters the modelled domain through the left and bottom boundaries. Deep groundwater enters the modelled domain at the bottom right corner (Figure 3.4). The water flowing in this domain flows out through the whole top boundary.

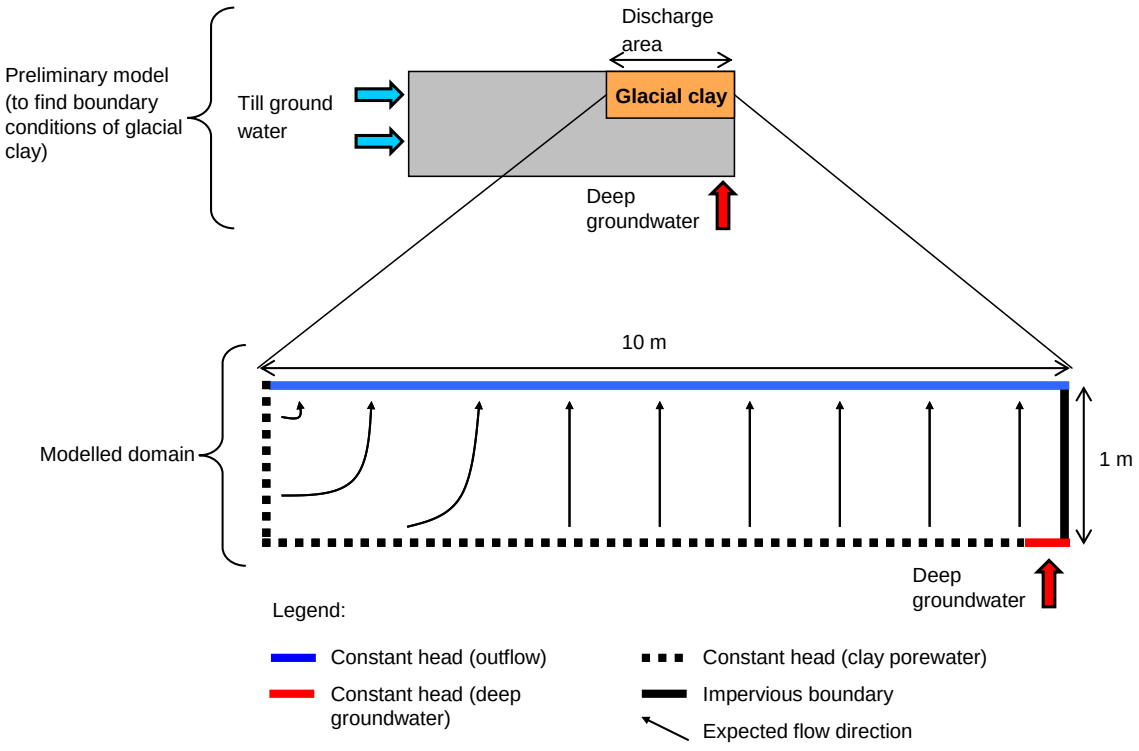

Figure 3.4 – Preliminary model developed to find the boundary conditions of the glacial clay, and modelled domain developed for the glacial clay sediment with the corresponding boundary conditions.

The reactive transport model built in this work simulates aqueous speciation and geochemical reactions between solid and aqueous phases all under local equilibrium. To compute the initial state of a reactive transport model the code used firstly equilibrates the initial porewater with the reactive minerals considered. Therefore, and in order to critically analyse the output of the initial equilibration, we have performed previous static calculations in PHREEQC (Parkhurst and Appelo, 1999) to define the initial porewater and boundary waters equilibrated with the minerals most likely to control the composition of these waters that have been identified in the previous section.

According to the main reactive minerals defined for the modelled domain, the composition of the glacial clay porewater has been obtained after equilibration of a selected sample of lake sediments porewater at Forsmark, with calcite, siderite and pyrite (Table 3.5). As this porewater is already close to the equilibrium with these minerals, the resulting composition is very similar to the sampled water. The redox state of the solution is controlled by the Fe(III)/pyrite pair.

The composition of the deep groundwater prior to repository release was set by equilibrating a selected deep groundwater sample from Forsmark with calcite and pyrite. This equilibration does not change much the original deep groundwater composition, since this water sample is close to the equilibrium with the selected phases. The composition of deep groundwater affected by repository release is modified by adding repository-derived radionuclides (RDSr, RDCs, RDU and Ra, Table 3.5). In order to distinguish repository-derived radionuclides from those of natural origin, already present in the glacial clay porewater at Forsmark, radionuclides coming from repository were labelled as RDCs, RDSr, and RDU in the model (RD stands for Repository-Derived). Radium has not been labelled since the presence of this radionuclide in the modelled domain is exclusively attributed to the release from the repository due to the extremely low concentrations observed in the natural waters at the Quaternary sediments of Forsmark.

The simulated flow conditions are constant in time, and therefore, the system is modelled under steady state for hydrodynamic processes, but not for geochemical processes. The hydrochemistry and geochemistry of the glacial clay are expected to vary due to the inflow of a deep groundwater with different composition than the clay porewater.

Table 3.5 – Initial composition of glacial clay porewater and deep groundwater (Deep GW). Concentrations of ^{RD}Cs, ^{RD}U, ^{RD}Sr and Ra in the deep GW (after repository release) represent the increment of these elements due to repository release.

Parameter	Glacial clay	Deep GW	Deep GW (after repository release)
pH	7.75	7.16	7.16
Eh (mV)	-204	-145	-145
Na_{total}	2.65×10^{-4}	6.93×10^{-2}	6.93×10^{-2}
K_{total}	5.19×10^{-5}	1.67×10^{-3}	1.67×10^{-3}
Ca_{total}	1.18×10^{-3}	1.35×10^{-2}	1.35×10^{-2}
Mg_{total}	1.16×10^{-4}	7.18×10^{-3}	7.18×10^{-3}
C(IV)	2.50×10^{-3}	2.46×10^{-3}	2.46×10^{-3}
Cl_{total}	1.53×10^{-4}	1.07×10^{-1}	1.07×10^{-1}
SO_4^{2-}	6.39×10^{-5}	3.73×10^{-3}	3.73×10^{-3}
Si_{total}	4.63×10^{-4}	7.56×10^{-5}	7.56×10^{-5}
Fe_{total}	8.34×10^{-7}	4.91×10^{-4}	4.91×10^{-4}
Sr_{total}	6.23×10^{-7}	4.13×10^{-5}	4.13×10^{-5}
U_{total}	1.98×10^{-9}	4.62×10^{-10}	4.62×10^{-10}
Cs_{total}	4.50×10^{-11}	1.62×10^{-8}	1.62×10^{-8}
NH_4^+	1.81×10^{-5}	1.95×10^{-4}	1.95×10^{-4}
Humic acid	1.00×10^{-4} (I)	-	-
^{RD}Cs	-	-	3.48×10^{-7}
^{RD}U	-	-	1.73×10^{-8}
^{RD}Sr	-	-	8.37×10^{-4}
Ra	-	-	9.15×10^{-11}

Concentrations in $mol \cdot L^{-1}$

(I) assuming that humic acid is approximately 10% of dissolved organic carbon

The simulated flow conditions are constant in time, and therefore, the system is modelled under steady state for hydrodynamic processes, but not for geochemical processes. The hydrochemistry and geochemistry of the glacial clay are expected to vary due to the inflow of a deep groundwater with different composition than the clay porewater.

The characterization programme for Forsmark candidate site has identified discharge areas related to surface water bodies where mixing between shallow groundwaters and deep groundwaters occurs. This means that the geochemical processes triggered by such mixing have been occurring for the past thousands of years (at least since the present

topography at Forsmark has formed, Berglund et al., 2009), leading to the present-day hydrogeochemical conditions.

In order to reach a geochemical quasi-steady state that represents the present-day hydrogeochemical conditions of the glacial clays at Forsmark, a long period of reactive transport (2700 years) with the natural composition of clay porewater and deep groundwater flowing through the modelled domain (according to the boundary conditions shown in Figure 3.4) has been simulated. After attaining the geochemical quasi-steady state, repository release is simulated (for additional 2700 years more) by adding RDU, RDSr, RDCs and Ra to the deep groundwater that is flowing through the modelled domain (according to the values listed in Table 3.5).

Repository release is simulated according to a very pessimistic scenario, where the ~500 m of granitic bedrock (between the repository and the lake deposits) and the engineered barriers of the repository are assumed to have a very low retention capacity over radionuclides, which is highly unlikely. In this context, radionuclide concentrations calculated for the near-field of the repository (Duro et al., 2006b), i.e., the vicinity of the canisters that contain the HLNW, are applied directly as the input concentrations in the present numerical simulations. Following this methodology, the concentration of RDSr and RDU in the deep groundwater was calculated by equilibrating the selected deep groundwater sample with their solubility limiting phases, which correspond to celestite and amorphous uraninite, respectively. The resulting aqueous concentration is 8.4×10^{2} μmol·L^{-1} of RDSr and 1.7×10^{-2} μmol·L^{-1} of RDU.

Since the solubility limiting phases for Ra and RDCs in the near-field of a HLNW repository are difficult to define, it was decided to calculate the corresponding concentrations from the radioactive release doses estimated for both radionuclides at the near-field (SKB, 2006). The reported releases are 2×10^{3} Bq·L_{water}^{-1} and 7.55×10^{2} Bq·L_{water}^{-1} for ^{135}Cs, and ^{226}Ra, respectively. By dividing these values by the respective radioactive decay constants and the Avogadro constant, the release doses can be converted into the following concentrations: 3.48×10^{-1} μmol·L_{water}^{-1} and 9.15×10^{-5} μmol·L_{water}^{-1} of RDCs and Ra, respectively.

These radionuclide concentrations are very high, considering that it is known that the engineered barriers and granitic bedrock should be able to retain much of these radionuclides. Nevertheless, since the objective of the study is to evaluate the retention capacity of the glacial clay sediments at Forsmark, such an extreme (pessimistic) scenario has been assumed.

3.5.4 Spatial and time discretisation

Spatial discretisation of the modelled domain was set 0.1 m along both axes (X and Y) for the whole domain.

As detailed in the previous section, there are two important time stages regarding the chemical condition of the system: (i) the first stage occurs at the beginning of the simulation period, when deep groundwater flows into the modelled domain and triggers major geochemical changes until a new geochemical quasi-steady state is reached, and (ii) the second stage occurs when the increased concentration of radionuclides in deep groundwater (that simulates repository release) disturbs the previous geochemical state. According to these time stages, time discretisation was refined at the beginning of the simulation period, then set progressively coarser until approximately 2700 years, and then refined again when the inflow of repository-derived radionuclides takes place. Then, time discretisation becomes coarser until the end of the simulation period.

To ensure numerical stability in the solute transport calculations, the Peclet criterion (Pe≤2) is met for the spatial discretisation of the modelled domain (ΔX =0.1 m with a longitudinal dispersivity = 0.5 m, and ΔY =0.1 m with a transverse dispersivity = 0.2 m).

The Peclet number is a dimensionless number which compares the characteristic time for dispersion and diffusion given a length scale with its characteristic time for advection, and is given by the following equation:

$$Pe = \frac{v\Delta x}{D_{xx}} = \frac{\Delta x}{\alpha_x} \qquad \text{(equation 3.1)}$$

where Pe is the Peclet number, v is water velocity (obtained by dividing Darcy's velocity over the effective porosity) in units of [LT^{-1}], Δx is the spatial discretization along the X axis, D_{xx} is the dispersion-coefficient tensor in units of [L^2T], and α_x is the dispersivity along the X axis in [L]. If the Peclet criterion is fulfilled, numerical oscillations should not occur (Unger et al., 1996).

3.6 Results

3.6.1 Transport of conservative and reactive solutes

The transport of solutes in the modelled domain is affected by geochemical processes and the groundwater flow generated from the prescribed initial and boundary conditions. The conservative solute transport has been predicted using chlorine as a tracer, given that no retention process has been implemented for this element. Computed breakthrough curves of solutes have been analysed at the top right node of the discharge boundary of the modelled domain where the fastest arrival of solutes to a hypothetical overlying surface water body is expected. According to the computed chlorine breakthrough curve the travel time of the problem is 34 years, from the deep groundwater inflow point to the discharge area of the modelled domain (Figure 3.5).

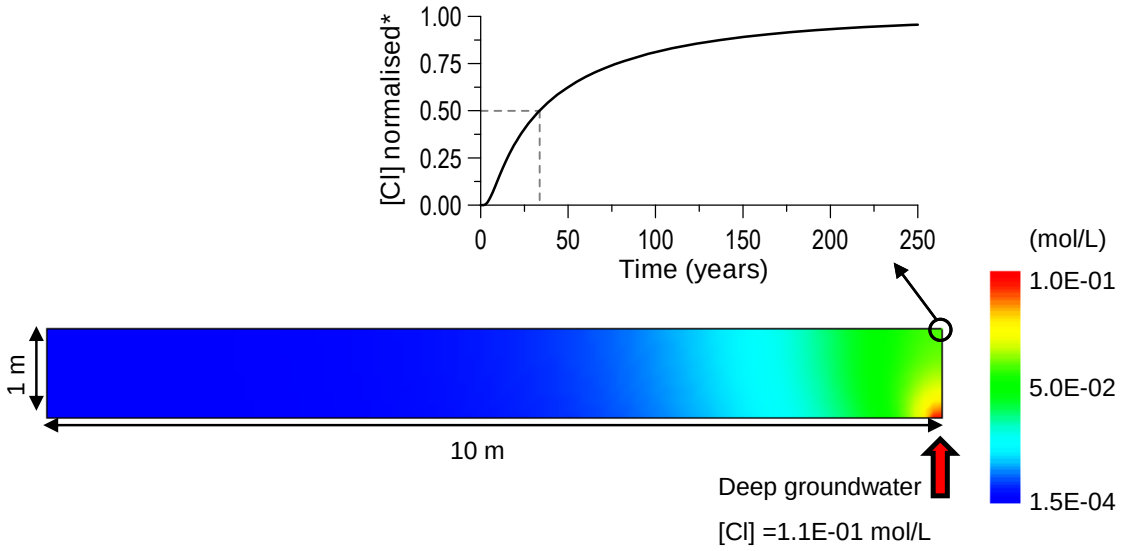

Figure 3.5 – Computed concentration of Cl(aq) in the modelled domain at the transport steady state, and computed breakthrough curve at the discharge area of the modelled domain (node X= 10 m, Y= 1 m). *[Cl] normalised stands for: $([Cl(aq)]_{predicted} - [Cl(aq)]_{initial})/([Cl(aq)]_{final} - [Cl(aq)]_{initial})$.

3.6.2 Present-day hydrogeochemical conditions

Long term simulations of groundwater flow and reactive solute transport (2700 years) with the selected minerals were done in order to reproduce the present-day hydrogeochemical conditions at Forsmark. Model results led to background concentrations of uranium, strontium, and caesium that are highly consistent with the values observed in the near-surface systems at Forsmark.

During the approach to the present-day hydrogeochemical conditions different processes that influence the behaviour of the natural isotopes of the studied radionuclides may be depicted which help us to understand the expected mobility of these radionuclides in the glacial clays at Forsmark. Figure 3.6 (a) shows that at the beginning of the simulation, a slight decrease of U(aq) is computed for the discharge area of the glacial clay. During this period no uranium pure phase is formed and therefore, the computed evolution of U(aq) is solely attributed to mixing which leads to its dilution. This slight decrease is due to the fact that U(aq) concentration in deep groundwater is approximately half an order of magnitude lower than in the glacial clay porewater (Table 3.5). Sr(aq) concentration in deep groundwater is approximately one order of magnitude higher than in the glacial clay porewater and, although the numerical simulation computes the retention of strontium in the solid phase via co-precipitation with calcite and adsorption on illite, Sr(aq) concentration increases from 0.6 $\mu mol \cdot L^{-1}$ (glacial clay porewater concentration, Table 3.5) to 20 $\mu mol \cdot L^{-1}$. The continuous, but progressively slower, increase of the Sr(aq) concentration at the discharge (Figure 3.6(b)) area reflects the decreasing capacity of illite and calcite to incorporate more strontium along time, since available exchange sites especially in illite become more and more scarce. Cs(aq) concentration in deep groundwater is approximately two and a half orders of magnitude higher than in the clay porewater. Computed Cs(aq) concentration increases during the first 250 years (Figure 3.6(c)), followed by a progressive decrease towards a quasi-steady state value of 5.7×10^{-4} $\mu mol \cdot L^{-1}$. In the first stage, cation exchange in illite is not able to buffer the increment of Cs(aq) in solution due to deep groundwater inflow, but with increasing time Cs(aq) is progressively retained in a larger area of the modelled domain and, therefore, its concentration at the discharge boundary tends to decrease.

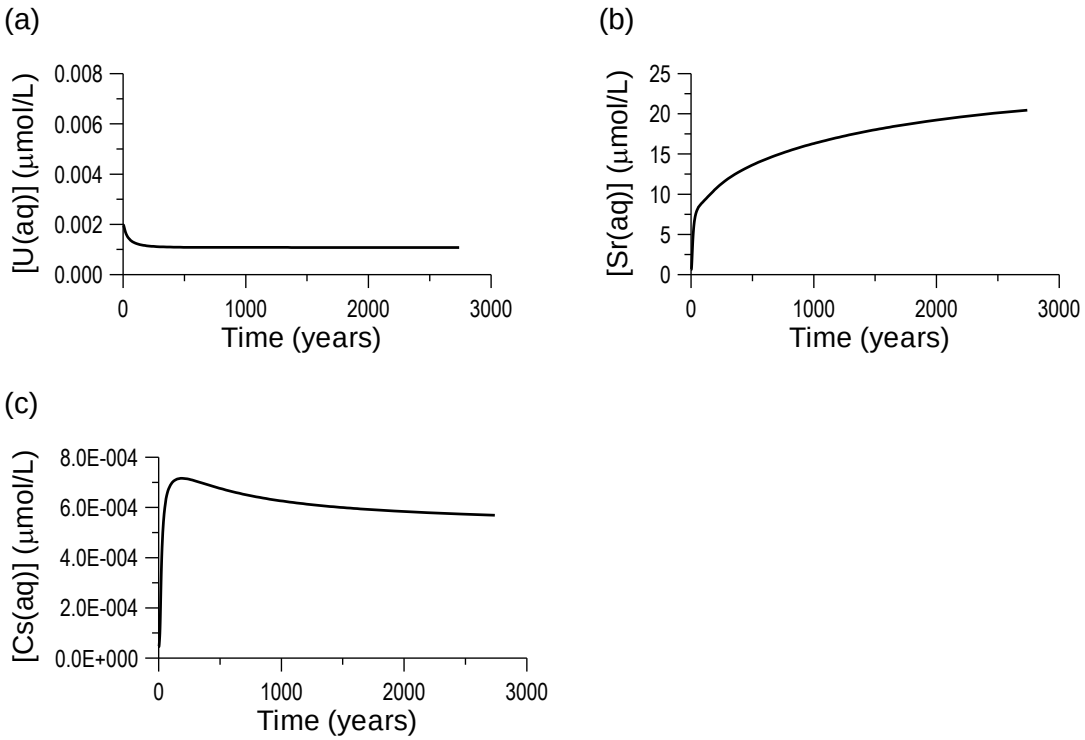

Figure 3.6. Computed evolution of the concentration of natural: a) U(aq); b) Sr(aq); and, c) Cs(aq) during the approach to the geochemical quasi-steady state that represents the present-day conditions of the glacial clays at Forsmark (observation node: X= 10 m; Y= 1 m). The concentrations at 2700 years are in the range of concentrations observed nowadays which are reported in the forth section of this work.

In Figure 3.7 it is possible to see that after the approach to the present-day hydrogeochemical conditions (2700 years of reactive transport), simulated data for strontium against calcium and for uranium against bicarbonate plot within the range of measured data.

Measured data for uranium and bicarbonate at Forsmark show a considerable wide range of values (Figure 3.7a). Simulated data plot close to the lowest content of these elements measured at Forsmark (Figure 3.7a). Simulated data for strontium against calcium (Figure 3.7b) plot along the mixing trend and the dilute waters trend previously reported in Figure 3.2. The deep groundwater is more mineralised than the glacial clay porewater and therefore, the more diluted simulated compositions correspond to the points of the modelled domain that are more distant to the deep groundwater inflow point, while the more mineralised simulated compositions, with higher strontium and calcium content, are closer to the deep groundwater inflow point (Figure 3.7c).

Data for caesium at Forsmark are scarce and therefore no graphic is shown here. Nevertheless it is possible to see that the concentration of caesium flowing out of the modelled domain after 2700 years of reactive transport (5.7×10^{-4} μmol·L^{-1} in Figure 3.6c) is within the range of data actually measured at Forsmark (5×10^{-5} to 1×10^{-3} μmol·L^{-1}). These results prove the ability of the numerical model to reproduce the hydrogeochemical conditions observed nowadays in the glacial clays at Forsmark.

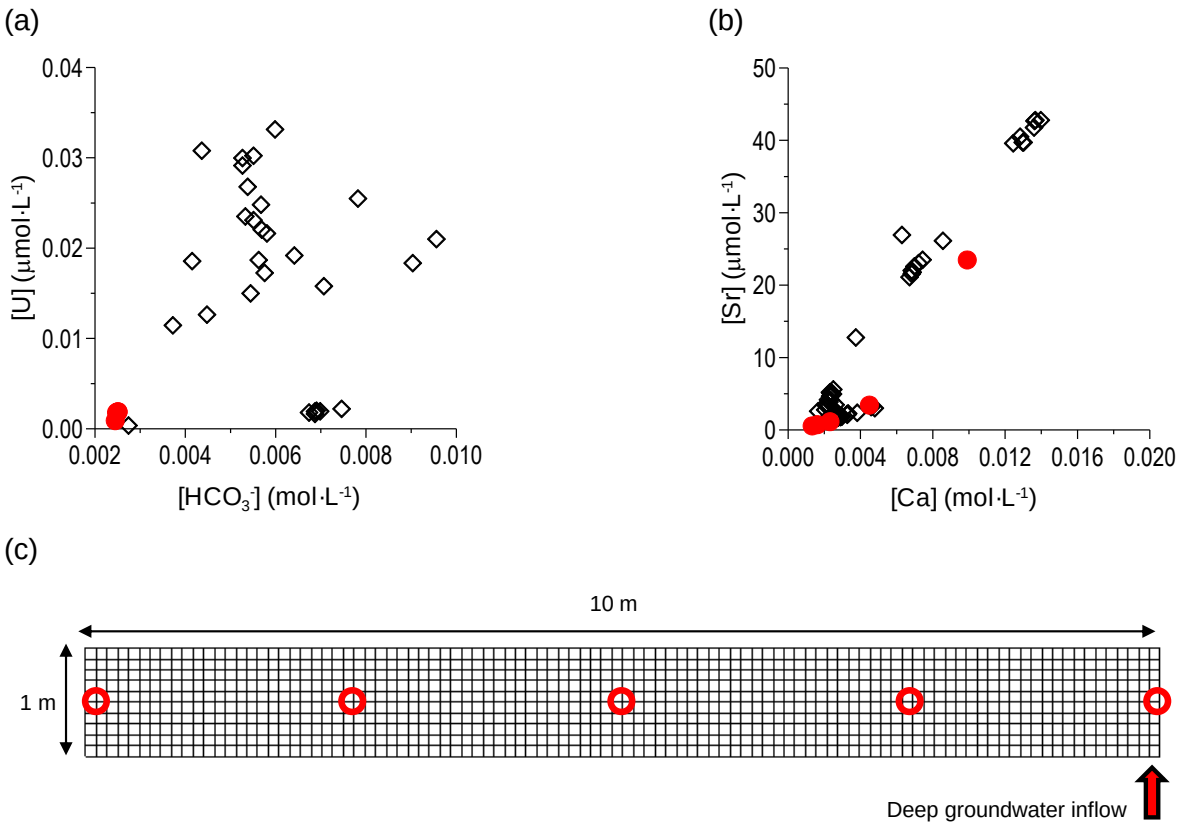

Figure 3.7 – Comparison between simulated (red symbols) composition of the porewater of the glacial clay at the present-day hydrogeochemical conditions (after 2700 years of reactive transport) and measured (black symbols) composition of the shallow groundwaters at Forsmark. a) Aqueous concentration of uranium against bicarbonate; b) Aqueous concentration of strontium against calcium; c) Location of the selected points of the modelled domain (red dots) plotted in graphics a and b.

3.6.3 Retention of repository-derived radionuclides

Once the present-day hydrogeochemical conditions have been attained, the hypothetical repository release is simulated by adding RDSr(aq), RDCs(aq), RDU(aq) and Ra(aq)

(according to the concentrations listed in Table 3.5) to the deep groundwater that enters the glacial clay deposit.

The concentration of $^{RD}U(aq)$ in the deep groundwater affected by repository release is 1.73×10^{-2} μmol·L^{-1} which is one and a half orders of magnitude higher than the natural concentration of U(aq) in deep groundwater and 30% higher than in the glacial clay porewater. 2700 years after repository release, 87% of uranium flowing out of the glacial clay to the surface water body comes from repository release (Figure 3.8).

Simulated repository release induces an increase of total U(aq) concentration in the glacial clay porewater. This increase, combined with the prevailing reducing conditions of the glacial clay, triggers the precipitation of amorphous uraninite. When amorphous uraninite precipitates, both repository-derived and natural uranium are incorporated in this mineral phase. It should be noted that, although humic acids and aqueous carbonates are present in the glacial clay porewater, favouring uranium aqueous complexation, the predominantly reducing conditions of the glacial clays provide the precipitation of amorphous uraninite which leads to the retention of ^{RD}U in the solid phase.

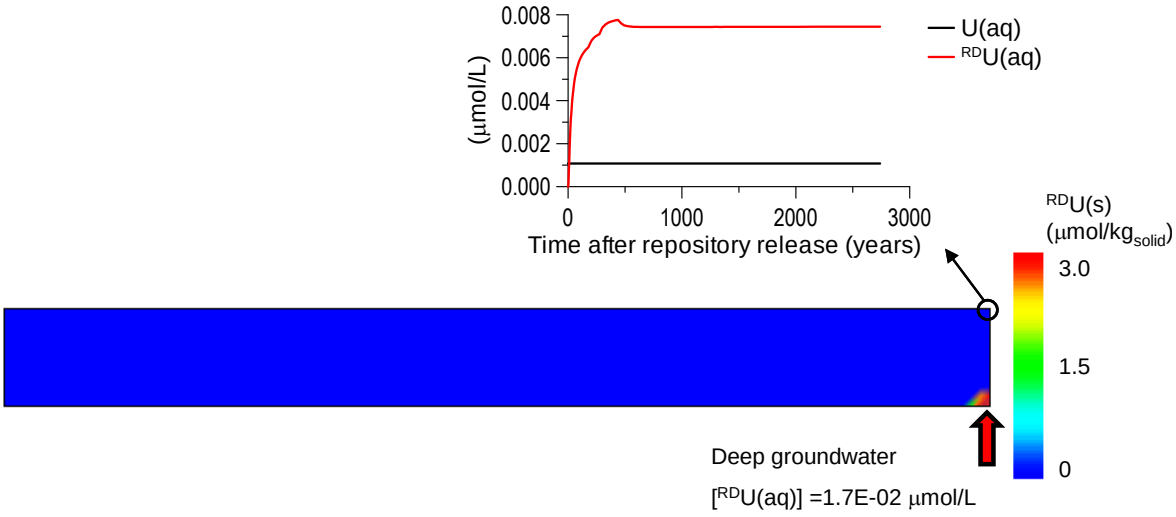

Figure 3.8 – Computed distribution of repository-derived uranium precipitated as amorphous uraninite, 2700 years after repository release (in $^{RD}U(s)$, s stands for concentration in the solid phase). Breakthrough curves for natural (black symbols) and repository-derived (red symbols) aqueous uranium are also shown.

Figure 3.9 shows the evolution of natural and repository-derived Sr(aq) at the discharge area of the glacial clay. Deep groundwater affected by repository release, has a ^{RD}Sr concentration of 840 μmol·L^{-1}, which is one and a half orders of magnitude higher than the

natural Sr(aq) concentration in deep groundwater, and three orders of magnitude higher than in the glacial clay porewater. At the end of the simulation, c. 94% of Sr(aq) flowing out of the glacial clay comes from repository release. Although strontium is retained via cation exchange in illite and co-precipitation with calcite (Figure 3.9), repository derived strontium reaches a considerably higher concentration than that of natural strontium.

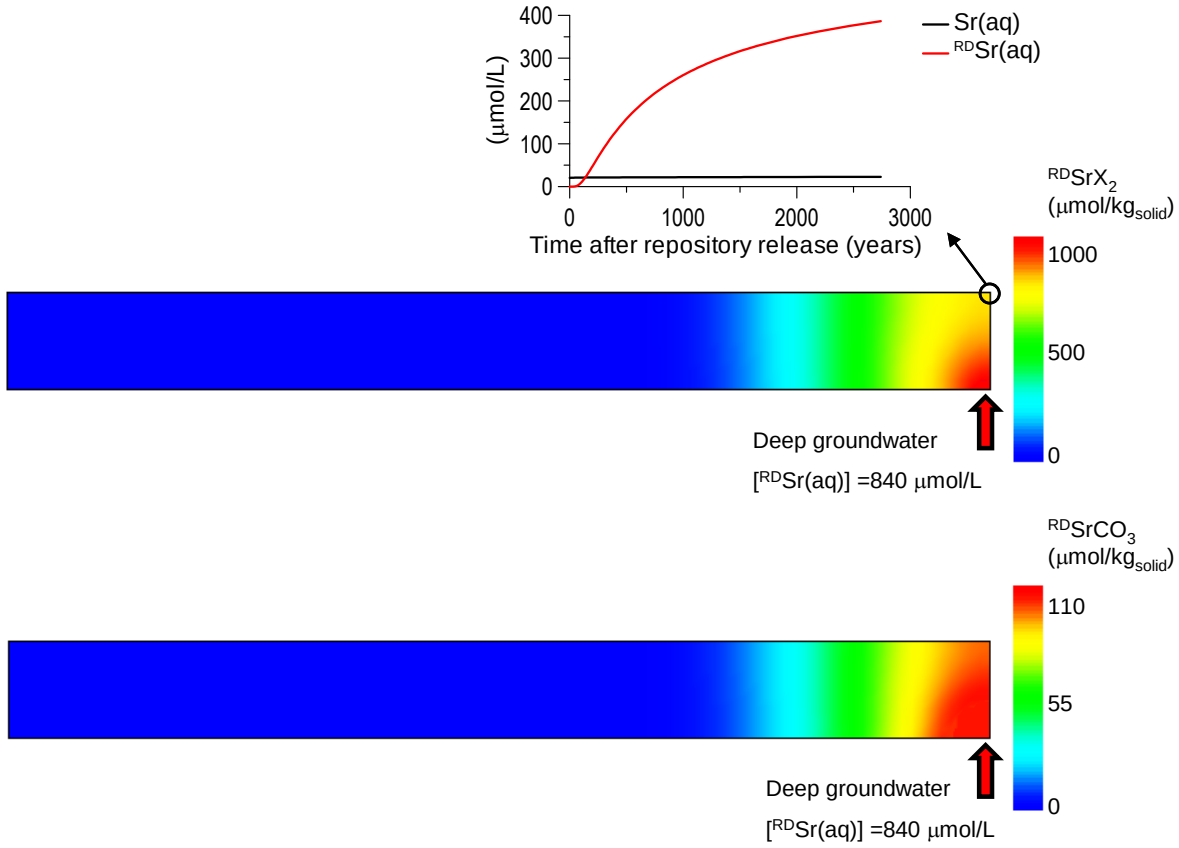

Figure 3.9 – Computed distribution of repository-derived strontium retained in the planar sites of illite ($^{RD}SrX_2$) and calcite ($SrCO_3$), 2700 years after repository release (distinct scales are used for each phase). Breakthrough curves for natural (black symbols) and repository-derived (red symbols) Sr(aq) are also shown.

The concentration of $^{RD}Cs(aq)$ in the deep groundwater affected by repository release is 3.48×10^{-1} μmol·L^{-1} which is one and a half orders of magnitude higher than before repository release and four orders of magnitude higher than in the glacial clay porewater. 2700 years after repository release only 0.3% of caesium flowing out of the clay deposit comes from repository release (Figure 3.10). The remarkable decrease of $^{RD}Cs(aq)$, from the deep groundwater inflow point to the glacial clay discharge area is due to the high

affinity of caesium for the FES of illite which readily retain caesium via cation exchange (Figure 3.10).

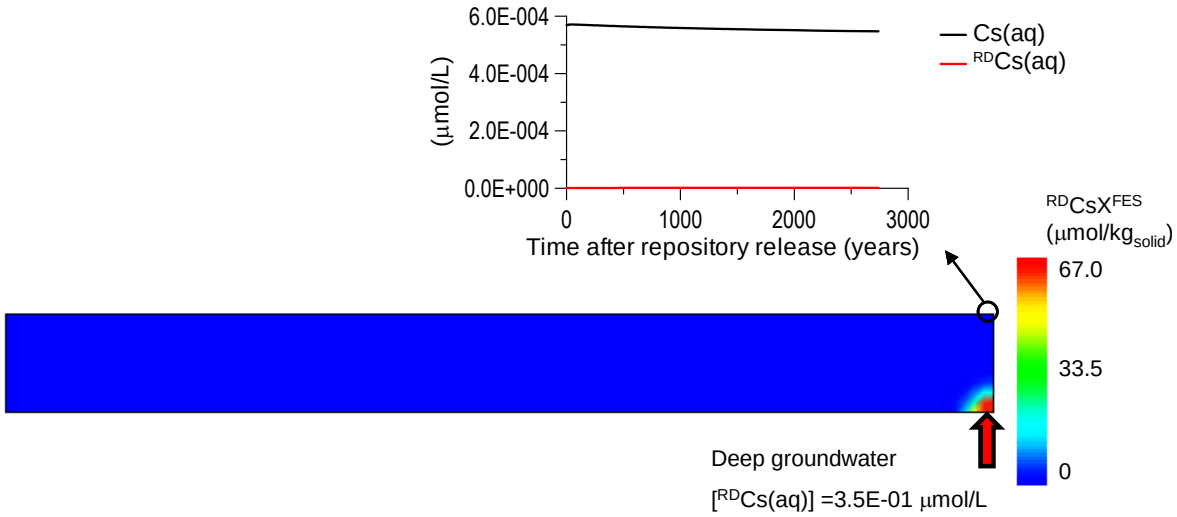

Figure 3.10 – Computed distribution of repository-derived caesium retained in the FES of illite ($^{RD}CsX^{FES}$), 2700 years after repository release. Breakthrough curves for natural (black symbols) and repository-derived (red symbols) Cs(aq) are also shown.

The numerical simulations do not predict any retention of radium in the glacial clay since saturation with barite is not attained during the simulation period. Repository-derived Ra(aq) concentration in the deep groundwater is 9.15×10^{-5} μmol·L^{-1}. The maximum Ra(aq) concentration reached at the discharge area of the glacial clay is 5.4×10^{-5} μmol·L^{-1} (Figure 3.11).

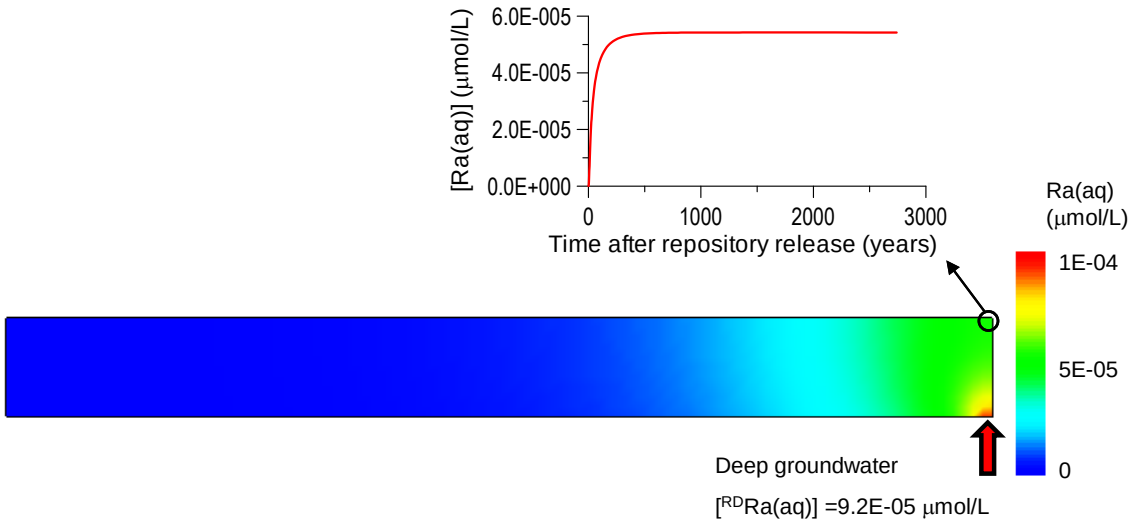

Figure 3.11 – Computed distribution of repository-derived radium retained in the aqueous phase of the glacial clay, 2700 years after repository release. The breakthrough curve for repository-derived (red symbols) Ra(aq) is also shown.

The decrease of Ra(aq) concentration from the deep groundwater inflow point to the discharge area of the glacial clay is mainly due to dilution, since the glacial clay groundwater flowing through the modelled domain carries no radium in solution.

The geochemical processes considered to occur in the glacial clays at Forsmark have been proved able to efficiently retain RDU, RDSr and RDCs. On the other hand, with the geochemical process assumed to interact with radium, no retention is computed for this radionuclide since barite saturation is not reached during the simulation time.

Retention of RDU, RDSr and RDCs in the glacial clay has been quantitatively assessed by defining a retention efficiency parameter. The retention efficiency (E) of the system under evaluation, at a given time (τ) can be quantitatively evaluated according to:

$$E^{\tau} = 100 \times \left(1 - \frac{C_R^{\tau}}{C_C^{\tau}} \right) \qquad \text{(equation 3.2)}$$

where C_R^{τ} stands for the concentration of a solute at time τ, in a given node of the modelled domain, when reactive transport processes are considered, and C_C^{τ} stands for the concentration of the same solute at time τ, in the same position, but without considering any reactive process coupled to the transport equation (i.e. assuming conservative behaviour of the solute).

According to equation 3.2, a null reactive concentration (C_R^{τ}) means that no mass of radionuclide is leaving the system at time τ, resulting in a retention efficiency of 100%. A reactive concentration (C_R^{τ}) equal to the conservative concentration (C_C^{τ}) means that no retention is occurring and that the corresponding retention efficiency is 0%. Negative efficiency means that in the reactive transport, the solid phase is releasing a previously retained species into solution, and therefore reactive concentration is higher than conservative concentration ($C_R^{\tau} > C_C^{\tau}$).

The computed evolution of retention efficiency of the glacial clay for RDU, RDSr and RDCs is plotted in Figure 3.12. From the three radionuclides predicted to be retained in the solid phase of the glacial clay, uranium is the only that is not involved in sorption processes; instead, it is retained via precipitation of a pure phase. The computed evolution of retention efficiency for RDU reflects the equilibrium with amorphous uraninite which leads the system to a stable efficiency value of 50%. Immediately after repository release, the glacial clay reaches a retention efficiency for RDSr of 100%, but thereafter, retention

efficiency for RDSr drops to 20% which reflects the progressive decreasing capacity of illite and calcite to incorporate more strontium, as previously observed. Due to the high affinity of caesium for the FES of illite, retention efficiency for RDCs is 100% during the whole simulation time.

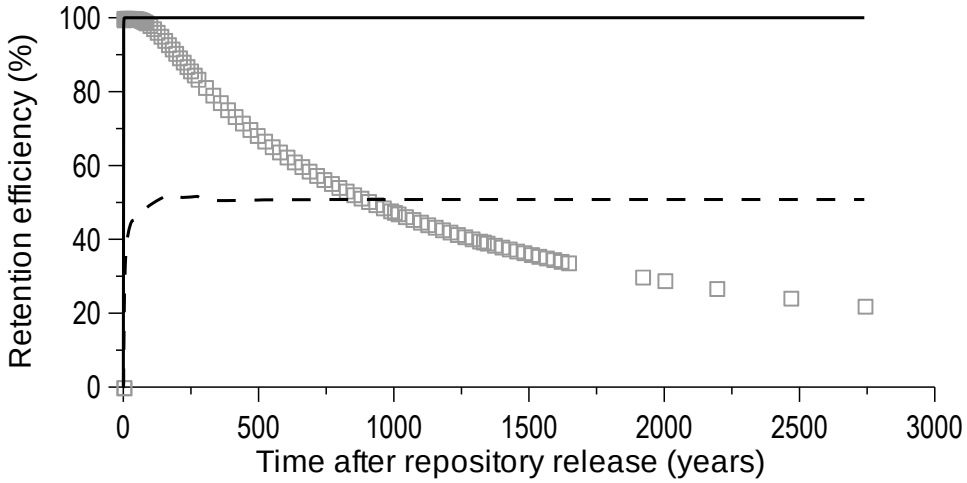

Figure 3.12 – Computed evolution of retention efficiency for RDU (dashed line), RDSr (grey squares) and RDCs (solid line), at the discharge area of the glacial clay (top right corner of modelled domain; node X= 10 m, Y= 1 m).

3.7 Conclusions

The present work has focused on the coupled hydrogeochemical processes that occur in the Quaternary glacial clays observed in the groundwater discharge areas at Forsmark, which may contribute to the retention of radionuclides potentially released from a repository. Numerical simulations of groundwater flow and reactive solute transport are able to reproduce the observed natural concentrations of uranium, strontium and caesium at the Forsmark site. These results prove the reliability of the conceptual and numerical models developed. Natural concentration of radium at Forsmark shallow groundwaters is extremely low so that its natural occurrence has been neglected in the numerical simulations.

The simulation of pessimistic scenarios of repository release has shown that the glacial clays, present in the groundwater discharge areas at Forsmark, have geochemical features that contribute to the effective retention of radionuclides. Numerical results allowed the development of a methodology for estimating radionuclide retention efficiency of the Quaternary glacial clays.

Computed results show that only uranium, strontium, and caesium are effectively retained in the solid phase of the glacial clays at Forsmark. Retention of radium is not predicted because barite precipitation, which is the only process considered to retain this radionuclide, is not reached during the simulated period and the mobilised Ra(II) concentrations are not sufficient to reach saturation with respect to pure $RaSO_4$(s) phases.

Numerical results show that when repository release is simulated, precipitation of amorphous uraninite is triggered by the increase of U(aq) concentration and therefore, both natural and repository-derived uranium are retained in the solid phase. This reaction leads to a steady retention efficiency for RDU of 50%. RDSr is retained in the solid phase via cation exchange in illite and co-precipitation with calcite. Retention efficiency for RDSr is complete (100%) immediately after repository release, but it progressively drops to 20% after about 3000 years. Caesium shows high affinity for the frayed edge sites of illite which results in 100% retention efficiency during the whole simulation period.

Acknowledgments

This work has been funded by SKB. Data and information used in this paper were generated within the SKB's Site Investigation Programme for location of a deep geological repository for the disposal of HLNW. The first author is grateful to the Portuguese Ministry of Science, Technology and Education for a PhD Grant (POCI 2010, BD/16647/2004). Special thanks are given to Sten Berglund and Tobias Lindborg for their support, encouragement and fruitful discussions during this work.

3.8 References

Albrecht J. (2005) *Forsmark site investigation: Study of Quaternary sediments in connection with investigations of bedrock lineaments.* SKB report P-05-138, Swedish Nuclear Fuel and Waste Management Co., Stockholm, Sweden

Arcos D., Grandia F., Domènech C., Fernández A.M., Villar M.V., Muurinen A., Carlsson T., Sellin P. and Hernán P. (2008) Long-term geochemical evolution of the near-field repository: Insights from reactive transport modeling and experimental evidences. *Journal of Contaminant Hydrology*, 102: 196-209.

Berglund S., Kautsky U., Lindborg T. and Selroos J.O. (2009) Integration of hydrological and ecological modelling for the assessment of a nuclear waste repository. *Hydrogeology Journal*, 17: 95–113

Bosson E. and Berglund S. (2006) *Near-surface hydrogeological model of Forsmark – Open repository and solute transport applications – Forsmark 1.2.* SKB report R-06-52, Swedish Nuclear Fuel and Waste Management Co., Stockholm, Sweden

Bradbury M.H. and Baeyens B. (2000) A generalised sorption model for the concentration dependent uptake of caesium by argillaceous rocks. *Journal of Contaminant Hydrology*, 42: 141–163.

Brun A., Engesgaard P., Christensen T.H. and Rosbjerg D. (2002) Modelling of transport and biogeochemical processes in pollution plumes: Vejen landfill, Denmark. *Journal of Hydrology*, 256: 228–247

Bruno J., Duro L. and Grivé M. (2002) The applicability and limitations of thermodynamic geochemical models to simulate trace element behaviour in natural waters. Lessons learned from natural analogue studies. *Chemical Geology*, 190(1-4): 371-393

Choppin G.R. and Shanbhag P.M. (1981) Binding of calcium with humic acid. *Journal of Inorganic Nuclear Chemistry* 43: 921-922.

Drake H., Sandström B. and Tullborg E.L. (2006) *Mineralogy and geochemistry of rocks and fracture fillings from Forsmark and Oskarshamn: Compilation of data for SR-Can*. SKB report R-06-109. Swedish Nuclear Fuel and Waste Management Co., Stockholm, Sweden

Duro L., Grivé M., Cera E., Domènech C. and Bruno J. (2006a) *Update of a thermodynamic database for radionuclides to assist solubility limits calculation for*

performance assessment. SKB report TR-06-17, Swedish Nuclear Fuel and Waste Management Co., Stockholm, Sweden

Duro L., Grivé M., Cera E., Gaona X., Domènech C. and Bruno J. (2006b) *Determination and assessment of the concentration limits to be used in SR-Can.* SKB report TR-06-32, Swedish Nuclear Fuel and Waste Management Co., Stockholm, Sweden

Grandia F., Merino J. and Bruno J. (2008) *Assessment of the radium-barium co-precipitation and its potential influence on the solubility of Ra in the near-field.* SKB TR-08-07, Swedish Nuclear Fuel and Waste Management Co., Stockholm, Sweden

Grandia F., Sena C., Arcos D., Molinero J., Duro L. and Bruno J. (2007) *Quantitative assessment of radionuclide retention in the near-surface system of Forsmark. Development of a reactive transport model using Forsmark 1.2 data.* SKB report R-07-64, Swedish Nuclear Fuel and Waste Management Co., Stockholm, Sweden

Grenthe I., Fuger J., Konings R.J.M., Lemire R.J., Muller A.J., Nguyen-Trung C. and Wanner H. (1992) *Chemical Thermodynamics of Uranium*. Elsevier, Amsterdam.

Grivé M. (2005) *The linkage between uranium, iron and carbon cycling. Processes at interfaces: evidences from combined solution chemical and spectroscopic studies*. PhD. Thesis, Universitat Politècnica de Catalunya, 341 pp.

Hedenström A. (2004) *Forsmark site investigation: Investigation of marine and lacustrine sediment in lakes. Stratigraphical and analytical data.* SKB report P-04-86, Swedish Nuclear Fuel and Waste Management Co., Stockholm, Sweden

Hummel W., Berner U., Curti E., Pearson F.J. Thoenen T. (2002) *Nagra/PSI Chemical Thermodynamic Data Base 01/01.* ISBN: 1-58112-620-4. 565 p.

Johansson P.O., Werner K., Bosson E., Berglund S., Juston J. (2005) *Description of climate, surface hydrology, and near-surface hydrogeology Preliminary site description. Forsmark area – version 1.2.* SKB R-05-06, Swedish Nuclear Fuel and Waste Management Co., Stockholm, Sweden

Kipp K.L. (1997) *Guide to the revised heat and solute transport simulator HST3D-Version 2.* U.S. Geological Survey Water-Resources Investigations Report, 97-4157, 149 p.

Köhler S.J., Dufaud F., Oelkers E.H. (2003) An experimental study of illite dissolution kinetics as a function of pH from 1.4 to 12.4 and temperature from 5 to 50°C. *Geochimica et Cosmochimica Acta*, 67-19: 3583–3594.

Laaksoharju M., Smellie J., Tullborg E.L., Gimeno M., Molinero J., Gurban I. and Hallbeck L. (2008) Hydrogeochemical evaluation and modelling performed within the Swedish site investigation programmeme. *Applied Geochemistry*, 23: 1761–1795

Langmuir D. (1997) *Aqueous environmental geochemistry.* Prentice-Hall Inc. Upper Saddle River, NJ.

Li W.C., Victor D.M. and Chakrabati C.L. (1980) Effect of pH and uranium concentration on interaction of uranium(VI) and uranium (IV) with organic ligands in aqueous solutions. *Analytical Chemistry*, 52: 520-523.

Liu C., Zachara J.M. and Smith S.C. (2004) A cation exchange model to describe Cs^+ sorption at high ionic strength in subsurface sediments at Hanford site, USA. *Journal of Contaminant Hydrology*, 68: 217-238.

Lokrantz H. and Hedenström A. (2006) *Forsmark site investigation: Description, sampling and analyses of Quaternary deposits in connection with groundwater monitoring wells, pumping wells and BAT filter tips.* SKB report P-06-92, Swedish Nuclear Fuel and Waste Management Co., Stockholm, Sweden

Molinero J., Samper J. (2006) Large-scale modelling of reactive solute transport in fractured zones of granitic bedrocks. *Journal of Contaminant Hydrology*, 82: 293-318.

Parkhurst D.L. and Appelo C.A.J. (1999) *User's guide to PHREEQC (version 2) – A computer programme for speciation, batch-reaction, one-dimensional transport and inverse geochemical calculations*. U.S. Geological Survey Water Resources investigations report 99-4259, 312 pp.

Parkhurst D.L., Kipp K.L., Engesgaard P. and Charlton S.R. (2004) *PHAST: A programme for simulating ground-water flow, solute transport, and multicomponent geochemical reactions.* U.S. Geological Survey Techniques and Methods 6-A8, 154 pp.

Percival J.B., Hunt P. and Wygergangs M. (2001) *Mineralogical investigations of Canadian till and lake- and stream-sediment reference materials: Part 1. Standardized X-ray diffraction and scanning electron microscope methods.* Geol. Surv. Can. Curr. Res. 2001-E9, 8 p.

Shanbhag P.M., Choppin G.R. (1981) Binding of uranyl by humic acid. *Journal of Inorganic Nuclear Chemistry*, 43: 3369-3372.

SKB (2002) *Forsmark – site descriptive model version 0.* SKB report R-02-32, Swedish

Nuclear Fuel and Waste Management Co., Stockholm, Sweden

SKB (2005) *Description of surface systems. Preliminary site description of Forsmark area – version 1.2.* SKB report R-05-03, Swedish Nuclear Fuel and Waste Management Co., Stockholm, Sweden

SKB (2006) *Long-term safety for KBS-3 repositories at Forsmark and Laxemar-a first evaluation.* Main report of the SR-Can project. SKB report TR-06–09, Swedish Nuclear Fuel and Waste Management Co., Stockholm, Sweden

SKB (2009) Press release: *SKB selects Forsmark for the final repository for spent nuclear fuel*. In: http://www.skb.se/Templates.

Steefel C.I., Carroll S., Zhao P. and Roberst S. (2003) Cesium migration in Hanford sediment: a multisite cation exchange model based on laboratory transport experiments. *Journal of Contaminant Hydrology*, 67: 219-246

Tesoriero A.J. and Pankow J.F. (1996) Solid solution partitioning of Sr^{2+}, Ba^{2+}, and Ca^{2+} to calcite. *Geochimica et Cosmochimica Acta*, 60-6: 1053–1064.

Tröjbom M. and Söderbäck B. (2006) *Chemical characteristics of surface systems in the Forsmark area. Visualisation and statistical evaluation of data from shallow groundwater, precipitation, and regolith.* SKB report R-06-19, Swedish Nuclear Fuel and Waste Management Co., Stockholm, Sweden

Unger A.J.A., Forsyth P.A. and Sudicky E.A. (1996) Variable spatial and temporal weighting schemes for use in multi-phase compositional problems. *Advances in Water Resources*: 19(1): 1-27

Vikström M. (2005) *Modelling of soil depth and lake sediments. An application of the GeoEditor at the Forsmark site.* SKB R-05-07, Swedish Nuclear Fuel and Waste Management Co., Stockholm, Sweden

Chapter 4

Quantitative assessment of radionuclide retention in the Quaternary sediments/granite interface of the Fennoscandian shield (Sweden)

4. Quantitative assessment of radionuclide retention in the Quaternary sediments/granite interface of the Fennoscandian shield (Sweden)[4]

Abstract

The Quaternary sediments representing the interface between the granite host rock and the Earth surface are of paramount importance when determining the potential cycling of anthropogenic and natural radionuclides in near-surface systems. This is particularly true in the case of high-level nuclear waste (HLNW) repositories placed in granite. In this work we present a modelling procedure to quantitatively determine the retention capacity of a Quaternary till in the Forsmark area, which has been recently selected to host the deep geologic storage of HLNW in Sweden. Reactive transport numerical models have been used to simulate the intrusion of a deep groundwater carrying radionuclides potentially released from a repository into a Quaternary till. Four radionuclides (^{235}U, ^{135}Cs, ^{226}Ra and ^{90}Sr) have been selected according to their different geochemical behaviour and potential dose relevance to surface ecosystems. Numerical results indicate that repository-derived (i) uranium will have a minor impact in the till, mainly due to the high natural concentration of uranium and its adsorption on ferrihydrite; (ii) caesium will be efficiently retained by cation exchange in illite; (iii) radium will be retained via co-precipitation with barite; and although (iv) strontium will be retained via co-precipitation with calcite and cation exchange in illite, the retention capacity of the Quaternary till for strontium is limited.

Keywords: Quaternary sediments/granite interface, Radionuclides, Retention efficiency, Reactive solute transport, PHAST

---

[4] This work has been submitted to Applied Geochemistry Journal, and has been developed by the following co-authors: Fidel Grandia[a], Clara Sena[a,b], David Arcos[a], Jorge Molinero[a], Lara Duro[a] and Jordi Bruno[a]

[a] Amphos XXI Consulting S.L., Spain; [b] I&D GeoBioTec, University of Aveiro, Portugal

4.1 Introduction

The concepts of deep geological disposal for HLNW are designed to retard for long periods of time (~10,000 years after closure) the migration of radionuclides to the surface (SKB, 2006). A deep geological repository for HLNW consists of a deep repository (~500 m depth) composed of engineered (metal canisters, clay barriers, cement liners) and natural (host rocks) barriers that prevent the intrusion of groundwaters and further dissolution of radionuclides from the HLNW. In performance and safety assessments of these repositories, scenarios of barrier failure and subsequent release of radionuclides to the surrounding environment are under investigation.

The Swedish Nuclear Fuel and Waste Management Company (SKB) has been studying two alternative sites (Forsmark and Laxemar) to locate a deep geological repository for HLNW and has recently selected the Forsmark area for the final emplacement. The host rock for the repository in both sites is a metagranitoid covered by glacial and post-glacial Quaternary sediments. In case of repository release, the Quaternary sediments present at the Earth's surface/granite interface, constitute the last geological barrier prior to the surface biosphere. The radionuclide solubility control of surface sediments and soils is well known from present-day analogues of possible future releases from deep repositories. The best investigated example of these analogues is the Hanford site (Washington, USA) (Zachara et al., 2002; McKinley et al., 2007; Um et al., 2007; among others).

In the last years, reactive transport numerical models have been applied to solve different environmental problems such as large-scale models of transport in fractured media (Molinero et al., 2008), geochemical evolution of engineered barriers (Arcos et al., 2008), organic contaminant biodegradation (Prommer et al., 2006), acid mine drainage (Bain et al., 2000), among many others. Numerical tools are especially useful when dealing with long-term performance assessment of deep geological repositories, mainly due to the possibility of coupling (i) groundwater flow, (ii) transport of solutes and (iii) complex geochemical processes, for long time spans. In the present work, reactive transport numerical models have been used to simulate the intrusion of a deep groundwater carrying radionuclides potentially released from a repository into a Quaternary till. The outcomes of the simulations have provided a quantitative assessment of the retention capacity of the Quaternary till at Forsmark for selected radionuclides.

4.1.1 Scope

The retention of selected radionuclides in the Quaternary sediments/granite interface of the Fennoscandian shield (Sweden) is assessed in the present work by means of reactive transport numerical simulations. The radionuclides selected are: ^{235}U as a redox-sensitive actinide; ^{135}Cs as a monovalent cation that participates in cation exchange in illite and also because it is an important contributor of radioactive doses to the surface systems (SKB, 2006); ^{90}Sr as a divalent cation that interacts with carbonate minerals and participates in cation exchange in illite; and, ^{226}Ra as the main contributor of radioactive doses to the surface systems (SKB, 2006).

Till is the most abundant outcropping Quaternary deposit at Forsmark (~75% of surface extension, SKB, 2005a) and, therefore, it was selected in the present work for the assessment of radionuclide retention in the Quaternary sediments/granite interface of the Fennoscandian shield.

The methodology applied here relies on six main steps: (1) a thorough review of site specific data that describe the hydrogeochemical behaviour of the system under study; (2) development of the conceptual model of the system based on data gathered in the first step; (3) identification and quantification of the thermodynamic parameters that describe the geochemical processes of interest; (4) implementation and verification against measured data of the conceptual model in reactive transport numerical simulations; (5) simulation of a hypothetical repository release in the numerical model; and, (6) quantitative assessment of radionuclide retention in the modelled system based on the outputs of the numerical simulations.

Site specific data that describe the hydraulic, hydrochemical and geochemical present-day conditions of the Quaternary till at Forsmark have been thoroughly analysed from the SKB database of the Forsmark Site Characterization Program (SKB, 2005a). The conceptual model of the Quaternary till was then implemented in a reactive transport numerical model in order to reproduce the present-day conditions observed at the near-surface systems at Forsmark. Once the present-day hydrogeochemical conditions of the Quaternary till at Forsmark have been modelled, a hypothetical repository release was simulated by a continuous injection, during approximately 2500 years, of a deep groundwater carrying repository-derived radionuclides into the modelled domain. Finally, from the outputs of the numerical simulations, the retention of radionuclides in the Quaternary till has been assessed.

4.2 Near-surface hydrogeology at Forsmark

The Forsmark area belongs to the Fennoscandian shield predominantly made up with metagranitoids and metavolcanics of Precambrian age, which are affected by ductile structures and a dense fracture network. More recently, the alternation of glacial and interglacial stages during the Quaternary period led to the deposition of glacial deposits that cover more than 80% of the surface (SKB, 2005b).

The near-surface hydrogeology at Forsmark is composed of Quaternary deposits, with an average thickness of 3 m that host unconfined aquifers discharging into streams, lakes or the Baltic Sea. Groundwater in the granitic bedrock flows mainly along fractures and deformation zones composed of loose granitic material and coatings of calcite, chlorite, quartz and pyrite (Drake et al., 2006).

In general, the till deposit consists of sand with variable amounts of boulders and clay (Albrecht, 2005). The origin of this till is associated with the glacial erosion, transport and deposition of Palaeozoic carbonate rocks located northwards from Forsmark (Tröjbom and Söderbäck, 2006), and therefore carbonate minerals are abundant in the Quaternary deposits. The mean calcite content in the Quaternary till is 24 wt% (SKB, 2005a). Besides calcite, quartz and illite have also been identified in the mineralogical assemblage of the Quaternary till.

Regional groundwater flows in Quaternary deposits from elevated inland areas towards the Baltic Sea, with local discharge into the water courses that feed lakes and wetlands (Johansson et al., 2005). Hydrogeological investigations reveal that hydraulic connections between Quaternary deposits and the granitic bedrock could be in a downward direction (Bosson and Berglund, 2006). Nevertheless, local upward flow paths, between bedrock and Quaternary deposits, are also believed to occur (Laaksoharju et al., 2008).

4.3 Model development

The retention capacity of the Quaternary till at Forsmark is evaluated, for selected radionuclides (uranium, caesium, strontium, and radium), using reactive transport numerical simulations. The code used for the simulations is PHAST v. 1.4.2 (Parkhurst et al., 2004). The geochemical simulations conducted to define the initial and boundary conditions of the reactive transport simulations were performed in PHREEQC v. 2.14.2 (Parkhurst and Appelo, 1999).

The database used in the simulations is an extension of the NAGRA-PSI database, originally compiled by Hummel et al. (2002), which was made in the frame of the SKB's project SKB-TDB (Duro et al., 2006a). This database contains a large set of complexation reactions as well as pure mineral equilibrium reactions for many radionuclides and trace elements.

The numerical simulations developed in this work rely on a hypothetical scenario where a radionuclide-bearing, deep groundwater flows upwards from the repository to the surface, reaching the Quaternary till (Figure 4.1). It should be noted that the numerical model developed aims at depicting a realistic evolution of the Quaternary till at Forsmark and is based on site specific data whenever possible, although it considers a hypothetical scenario.

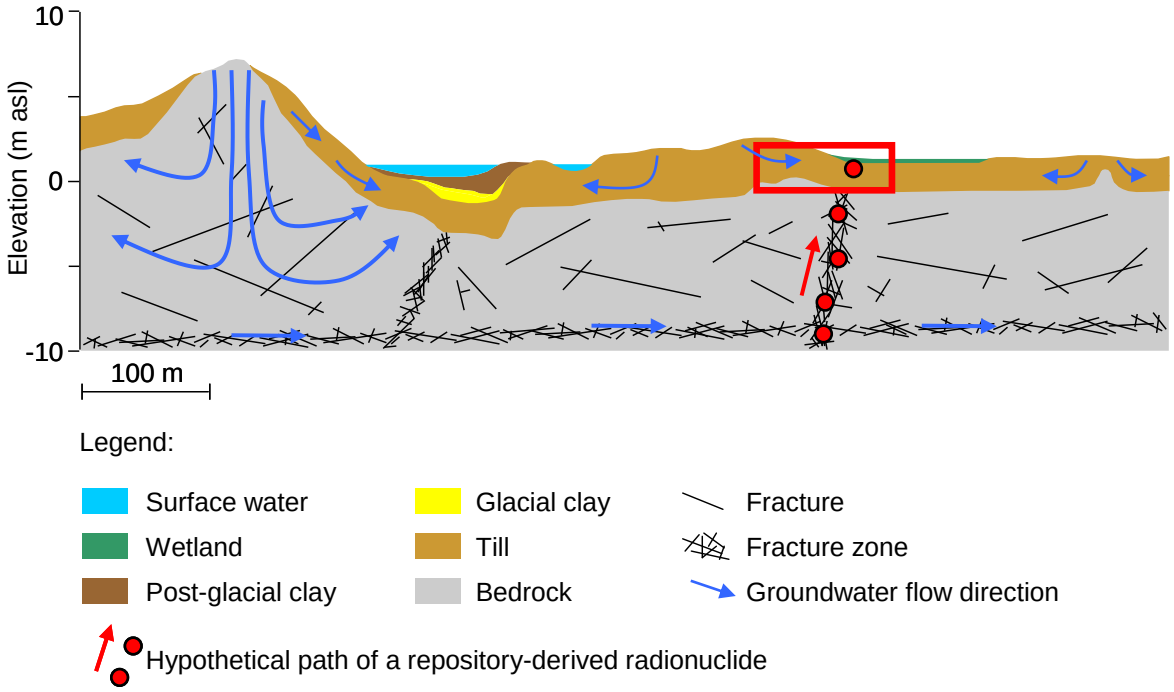

Figure 4.1 – Near-surface hydrogeological conceptual model of Forsmark candidate site (modified from Johansson et al., 2005) showing a hypothetical path of radionuclides released from a repository. The section of the Quaternary till under study is highlighted with a red rectangle.

4.3.1 Natural isotopes of the studied radionuclides at Forsmark

The concentrations of the natural isotopes of the selected radionuclides (^{235}U, ^{90}Sr, ^{135}Cs and ^{226}Ra) at Forsmark have been studied in order to identify their background

concentrations and achieve insights on the key geochemical processes that influence their mobility in the Quaternary till.

In shallow groundwaters at Forsmark, uranium concentrations range from 1.0×10^{-10} to 1.5×10^{-7} mol·L^{-1} (Tröjbom and Söderbäck, 2006). This wide range indicates variable redox conditions in the near-surface systems. Uranium is commonly transported forming complexes with bicarbonate, phosphate, iron and dissolved organic carbon (DOC) (Grenthe et al., 1992). However, none of these ions shows clear correlation with uranium at Forsmark, suggesting that multiple geochemical processes are responsible for the mobility of uranium in these waters. The presence of calcite in most of the Quaternary till at Forsmark leads to the predominance of circum-neutral waters with considerable amounts of dissolved carbonates which, in turn, enhance the mobility of uranium in these near-surface waters. From elemental analysis of the solid phase of the Quaternary deposits, rough correlations between uranium and iron, manganese and phosphorous are observed, indicating that uranium could be associated with Fe-Mn oxides or phosphates.

Strontium concentrations in shallow groundwaters range between 1.5×10^{-6} and 5×10^{-5} mol·L^{-1} (Tröjbom and Söderbäck, 2006). Two correlation trends are observed between strontium and calcium in the shallow groundwaters at Forsmark. One trend involves high salinity waters and represents a mixing trend, while the other trend includes dilute waters, with a Sr/Ca (molar ratio) of 10^{-4} that is consistent with congruent dissolution of a Sr-bearing calcite in the solid phase. Bruno et al. (2002) obtained an average Sr/Ca (molar ratio) of 3.5×10^{-3} in a set of groundwaters from different environments.

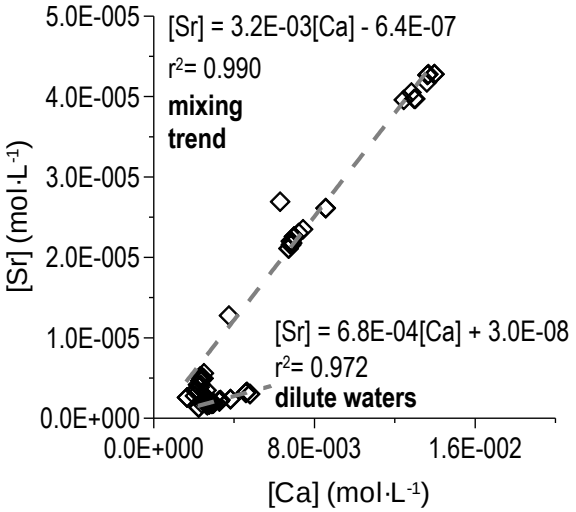

Figure 4.2 – Observed correlations between strontium and calcium in shallow groundwaters of Forsmark candidate area.

Data on caesium concentrations are scarce in shallow groundwaters in the Forsmark area. These range from 5×10^{-11} to 1×10^{-9} mol·L^{-1} (Tröjbom and Söderbäck, 2006) which reveals relatively low concentrations of caesium in natural waters. With the available data no clear correlations with other ions have been observed. Nevertheless, caesium is expected to be involved in cation exchange in interlayered clays like illite (Bradbury and Baeyens, 2000, among others).

Radium concentration in natural waters is usually very low, ranging from 10^{-14} to 10^{-11} mol·L^{-1}. Among the 22 shallow groundwater samples collected in Forsmark for radium analysis (Tröjbom and Söderbäck, 2006) five were below detection limit for radium (1×10^{-14} mol·L^{-1}), and the maximum radium concentration reached was 1.09×10^{-13} mol·L^{-1}.

4.3.2 Hydrodynamic processes and parameters

According to the findings of the site characterization programme developed by SKB, the till deposit hosts unconfined porous aquifers with stratified hydraulic conductivity and porosity (Johansson et al., 2005). In Table 4.1 the mean values of the hydrodynamic parameters of the Quaternary till implemented in the numerical model are listed.

Table 4.1 – Values of the hydrodynamic parameters implemented in the numerical model for the Quaternary till (from Johansson et al., 2005).

Parameter	Top layer	Middle layer	Bottom layer
Thickness (m)	0.8	1.4	0.8
K_h (m/s)	1.5×10^{-5}	1.5×10^{-6}	1.5×10^{-5}
K_v (m/s)	1.5×10^{-6}	1.5×10^{-7}	1.5×10^{-6}
α_L (m)	0.5	0.5	0.5
α_T (m)	0.2	0.2	0.2
ϕ (-)	0.15	0.05	0.05
D_e (m^2/s)	5×10^{-10}	5×10^{-10}	5×10^{-10}

K_h – horizontal hydraulic conductivity; K_v – vertical hydraulic conductivity; α_L – longitudinal dispersivity; α_T – transverse dispersivity; ϕ – porosity; D_e – effective diffusion coefficient.

4.3.3 Geochemical processes and parameters

The geochemical processes considered in the numerical simulations are based on the characterization of the Quaternary sediments at Forsmark, and on the present-day knowledge of the thermodynamic behaviour of the studied radionuclides. The retention capacity of the till for the selected radionuclides depends on the geochemical processes considered. Finally, since the main objective of this work is the evaluation of the retention of radionuclides in the till, radioactive decay of the selected radionuclides is not considered.

Given the strong correlation between strontium and calcium observed in the dilute shallow groundwaters at Forsmark (Figure 4.2), calcite is considered to contain trace amounts of strontianite forming a non-ideal solid solution (Tesoriero and Pankow, 1996) in the numerical simulations.

The initial molar fraction of strontium in calcite results from equilibrating the calcite-strontianite solid solution with the selected till groundwater sample. The parameters used for this solid solution are those of Tesoriero and Pankow (1996), and the resulting strontium molar fraction is 1.73×10^{-5}. From the mean 24 wt% of calcite in the Quaternary till we have considered that only 6.2 v% are available to react with the porewater. This 6.2 v% of reactive calcite correspond to the outer 0.05 mm rim of the 2 mm sized calcite grains that constitute the most of the calcite content of the Quaternary till. By multiplying the 24 wt% by 6.2v% we obtain 1.5 wt% of reactive calcite implemented in the numerical simulations. Since the studied groundwaters are rich in aqueous carbonate, Fe(III) carbonate complexes have been added to the thermodynamic database (Grivé, 2005).

Although illite has been identified as the main clay mineral in the Quaternary till at Forsmark no data on illite content has been found, and therefore a 10 wt% as been considered for the numerical simulations. Illite dissolution kinetics is very slow under the environmental conditions modelled here (Köhler et al., 2003). Therefore, dissolution of illite is not considered, and it only participates as a charged surface for cation exchange, including strontium and caesium. The model for cation exchange in illite implemented in the numerical simulations follows the model proposed by Bradbury and Baeyens (2000) (see Table A1.1 in Appendix 1). According to this model (Bradbury and Baeyens, 2000), there are three types of exchangeable sites. The most abundant sites (~80% of CEC, which is 0.2 $eq \cdot kg^{-1}$) are the “Planar sites”, which sorb divalent and monovalent cations. The second and third types of sites (“Type II” and frayed edge sites “FES”) involve solely monovalent cations. The site density is much lower (20% and 0.25% of the total sites, respectively), but the uptake of some cations like Cs^+ on the FES is particularly efficient.

Strontium is also expected to be involved in cation exchange in illite (e.g. Cole et al., 2000), and therefore strontium was added to the cation exchange model implemented in the numerical simulations (see Table A1.1 in Appendix 1).

It is very likely that other phases exist at minor concentrations, some of which can play an important role in the control of the redox conditions and radionuclide retention. Among these, ferrihydrite ($Fe(OH)_3$) is thought to be the controlling phase for the redox of the till porewater and the main uranium sorbent. The surface complexation model followed is that of Waite et al. (1994) which considers two types of adsorption sites; strong and weak binding (see Table A1.3 in Appendix 1).

According to the elemental content of Fe in the solid phase of the Quaternary till, ranging from 0.54 to 2.22 wt% (Tröjbom and Söderbäck, 2006), an initial content of 0.15 wt% of ferrihydrite has been set in the numerical simulations.

Unlike illite, ferrihydrite is a much more reactive mineral, very sensitive to changes in the redox state of the system. Intrusion of deep groundwater in the till domain may lead to dissolution of ferrihydrite, and therefore, the total amount of sites available for adsorption, in the simulations, depends on the remaining moles of ferrihydrite for each time step. Siderite ($FeCO_3$) is also redox sensitive and can precipitate in the till after the inflow of Fe-rich deep groundwater which is more reducing than till porewater. Consequently, siderite is allowed to precipitate if oversaturation is reached.

Till groundwater in Forsmark is very close to barite saturation, and the precipitation of this mineral (and radium co-precipitation) is expected due to the intrusion of deep groundwater with a relatively high sulphate concentration.

Given the relatively fast reactivity of the reactive minerals previously identified, under the geochemical conditions simulated here, all geochemical reactions are simulated under local equilibrium. Table 4.2 lists the initial concentrations of the reactive minerals considered in the numerical simulations, as well as the radionuclides potentially incorporated in these minerals.

The saturation index of relevant pure phases that may incorporate the studied radionuclides, was monitored during the simulations for the following phases: amorphous uraninite, becquerelite, schoepite and soddyite (for U); celestite and strontianite (for Sr); and radium sulphate (for Ra). None of these minerals attained oversaturation, and therefore, they were discarded from the simulations.

Table 4.2 – Initial concentration of the reactive minerals considered for the reactive transport simulations. Potentially retained radionuclides and respective mechanism of retention are also shown.

Mineral	Initial concentration of reactive mineral (wt%)	Mechanism of radionuclide retention	Potentially retained radionuclides
$Ca_{1-\chi}Sr_{\chi}CO_3$ (χ(initial)= 1.73×10^{-5})*	1.5	Co-precipitation	Sr
Illite	10.0	Cation exchange	Sr, Cs
Ferrihydrite ($Fe(OH)_3$)	0.15	Adsorption	U
$Ba_{1-\chi}Ra_{\chi}SO_4$	0.0	Co-precipitation	Ra
Siderite ($FeCO_3$)	0.0	-	-
*χ stands for the molar fraction of Sr and Ra in the solid solutions in which they are involved.			

4.3.4 Initial and boundary conditions

The numerical model represents a 2D vertical section of the Quaternary till that overlies the granitic bedrock at Forsmark. The bottom boundary of the modelled domain represents the contact between the till and the bedrock. In order to simulate the transfer of repository-derived radionuclides to the near-surface systems, a deep groundwater flowing upwards through a fracture of the granitic bedrock is assumed to transport dissolved radionuclides from the repository to the surface. The Quaternary till is assumed to be hydraulically connected to a discharge area such as a river, a lake or the Baltic Sea.

According to the water balance calculations developed for Forsmark (Johansson et al., 2005), a constant inflow rate of 14.5 L/d is assigned along the vertical left boundary. The fracture through which deep groundwater enters the till is represented by a constant inflow boundary at the bottom of the modelled domain (cell X= 20 m, Y= 0 m), with a flow rate of 0.5 L/d. The discharge area is located in the last 20 m of the top boundary, with a constant head of 3 m (Figure 4.3).

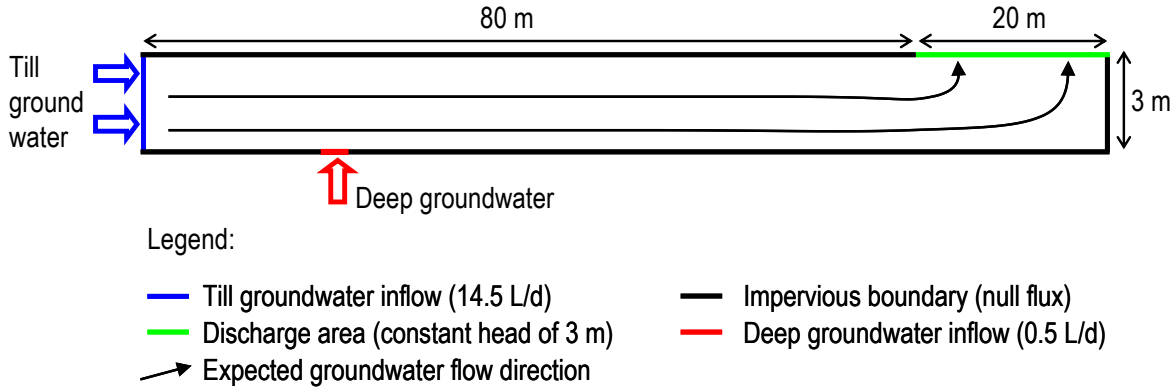

Figure 4.3 – Flow boundary conditions for the numerical model of the Quaternary till.

The reactive transport model built in this work simulates aqueous speciation and geochemical reactions between solid and aqueous phases all under local equilibrium. To compute the initial state of a reactive transport model, the code used here firstly equilibrates the initial porewater with the reactive minerals considered. Therefore, and in order to critically analyse the output of the initial equilibration, we have performed previous static calculations in PHREEQC (Parkhurst and Appelo, 1999) to define the initial porewater and boundary waters equilibrated with the minerals most likely to control the composition of these waters that have been identified in the previous section.

The chemistry of the groundwater in equilibrium with the till deposit has been obtained after equilibration of a selected groundwater sample of the till aquifer with the reactive minerals identified in the previous section which are calcite-strontianite solid solution, ferrihydrite and siderite (Table 4.2). As the groundwater sample is close to the equilibrium with these minerals, the resulting composition does not differ much from the sampled water. In Table 4.3 the water composition of the Quaternary till obtained after such preliminary equilibration is shown.

According to the minerals identified in the coatings of the granite fractures where deep groundwater flows (reported in section 4.2), the deep groundwater composition prior to repository release was set by equilibrating a selected deep groundwater sample from Forsmark with calcite and pyrite. This equilibration does not change much the original deep groundwater composition, since this water sample is close to the equilibrium with these phases.

The composition of deep groundwater affected by repository release is modified due to the addition of repository-derived radionuclides (^{90}Sr, ^{135}Cs, ^{235}U and ^{226}Ra). In order to distinguish repository-derived radionuclides from those of natural origin, radionuclides

coming from repository were labelled as RDCs, RDSr, and RDU, RD standing for Repository-Derived (Table 4.3). Radium was not labelled since its presence in the modelled domain is exclusively attributed to repository release due to the extremely low concentrations observed at Forsmark.

Table 4.3 – Initial composition of till porewater and deep groundwater (Deep GW). Concentrations of RDCs, RDU, RDSr and Ra in the deep GW (after repository release) represent the increment of these elements due to repository release.

Parameter	Till GW	Deep GW	Deep GW (after repository release)
pH	7.12	7.16	7.16
Eh (mV)	3	-145	-145
Na_{total}	1.22×10^{-3}	6.93×10^{-2}	6.93×10^{-2}
K_{total}	1.22×10^{-4}	1.67×10^{-3}	1.67×10^{-3}
Ca_{total}	2.79×10^{-3}	1.35×10^{-2}	1.35×10^{-2}
Mg_{total}	3.54×10^{-4}	7.18×10^{-3}	7.18×10^{-3}
C(4)	5.57×10^{-3}	2.46×10^{-3}	2.46×10^{-3}
Cl_{total}	1.90×10^{-3}	1.07×10^{-1}	1.07×10^{-1}
SO_4^{2-}	2.41×10^{-4}	3.73×10^{-3}	3.73×10^{-3}
Si_{total}	9.74×10^{-5}	7.56×10^{-5}	7.56×10^{-5}
Fe_{total}	1.50×10^{-5}	4.91×10^{-4}	4.91×10^{-4}
Sr_{total}	2.10×10^{-6}	4.13×10^{-5}	4.13×10^{-5}
U_{total}	2.23×10^{-8}	4.62×10^{-10}	4.62×10^{-10}
Cs_{total}	6.48×10^{-11}	1.62×10^{-8}	1.62×10^{-8}
NH_4^+	6.62×10^{-6}	1.95×10^{-4}	1.95×10^{-4}
RDCs	-	-	3.48×10^{-7}
RDU	-	-	1.73×10^{-8}
RDSr	-	-	8.37×10^{-4}
Ra	-	-	9.15×10^{-11}
Concentrations in $mol \cdot L^{-1}$			

The hydrodynamic boundary conditions are constant in time, and therefore, the system is modelled under steady state for flow, but the geochemistry of the till deposit is modelled under transient state due to the inflow of a more reducing and mineralised deep groundwater into the till domain.

The characterization program for Forsmark site has identified discharge areas where mixing between shallow groundwaters and deep groundwaters occurs (Laaksoharju et al., 2008). This means that the geochemical processes triggered by such mixing have been occurring for the past thousands of years; at least since the present topography at Forsmark has formed (Berglund et al., 2009), leading to the present-day hydrogeochemical conditions.

In order to reach a geochemical quasi-steady state that represents the present-day hydrogeochemical conditions of the Quaternary till, a long period of reactive transport (2700 years) with the natural composition of till and deep groundwaters flowing through the modelled domain has been simulated. During this long period of reactive transport simulation, mixing between both groundwaters together with the products of the geochemical reactions triggered by such mixing, leads to a new geochemical equilibrium.

After attaining the geochemical quasi-steady state, repository release is simulated by increasing the concentration of selected radionuclides in the deep groundwater that enters the till system at the bottom of the modelled domain.

Repository release is simulated according to a very pessimistic scenario, where it is assumed that the ~500 m of granitic bedrock (located between the repository and the near-surface systems) and the engineered barriers of the repository do not have a significant retention capacity over radionuclides, which is highly unlikely. Therefore, radionuclide concentrations calculated for the near-field (Duro et al., 2006b), i.e., the vicinity of the canisters that contain the spent nuclear fuel, are applied directly as the input concentrations in the present numerical simulations. Following this methodology, the concentration of RDSr and RDU in the deep groundwater was calculated by equilibrating the selected deep groundwater sample with their solubility limiting phases, which correspond to celestite and amorphous uraninite, respectively. The resulting concentrations of RDSr and RDU are 8.4×10^{-4} mol·L^{-1} and 1.7×10^{-8} mol·L^{-1}, respectively.

Since the solubility limiting phases for Ra and RDCs in the near-field of a HLNW repository are difficult to define, it was decided to calculate the corresponding concentration from the radioactive release doses estimated for both radionuclides at the near-field (SKB, 2006). The reported releases are 2×10^{3} Bq·L^{-1} for ^{135}Cs, and 7.55×10^{2} Bq·L^{-1} for ^{226}Ra. By dividing these values by the respective radioactive decay constants and the Avogadro constant, the release doses are converted into the following concentrations: 3.48×10^{-7} mol·L^{-1} of RDCs and 9.15×10^{-11} mol·L^{-1} of Ra.

These radionuclide concentrations are very high, taking into account that the engineered barriers and granitic bedrock would be able to retain much of these radionuclides. Nevertheless, since the objective of the study is to evaluate the retention capacity of the Quaternary sediments, such an extreme scenario has been assumed.

4.3.5 Spatial and time discretisation

The spatial discretization of the modelled domain was set according to the main features of the boundary conditions, which influence groundwater flow and geochemistry. Spatial discretization was refined at the position of the deep groundwater inflow and under the discharge area (outflow boundary).

As detailed in the previous section, there are two important stages regarding the chemical condition of the system: (i) the first stage occurs at the beginning of the simulation, when deep groundwater flows into the modelled domain and triggers major geochemical changes until the geochemical quasi-steady state is reached, and (ii) the second stage occurs when the increased concentration of radionuclides in the deep groundwater (that simulates repository release) disturbs the previous geochemical state. According to these stages, time discretization was refined at the beginning of each stage, and set progressively coarser towards the end of each stage.

To ensure stability in the numerical calculations, the Peclet criterion ($Pe \leq 2$) is met for the maximum ΔX (maximum ΔX =1 m, and longitudinal dispersivity = 0.5 m).

4.4 Numerical results

4.4.1 Present-day hydrogeochemical conditions

The transport of solutes in the modelled domain is affected by geochemical processes and the groundwater flow generated from the prescribed initial and boundary conditions. The conservative transport has been studied using chlorine as a tracer, given that no retention has been implemented for this element. From the chlorine breakthrough curve, observed at the discharge area, an advective travel time of 2.3 years is obtained, from the deep groundwater inflow point to the discharge area of the modelled domain.

Long-term simulations of groundwater flow and reactive solute transport (2700 years) with the selected reactive minerals were done in order to reproduce the present-day hydrogeochemical conditions at Forsmark. Model results led to background

concentrations of uranium, strontium, and caesium that are highly consistent with the values observed in the near-surface systems at Forsmark (Figure 4.4).

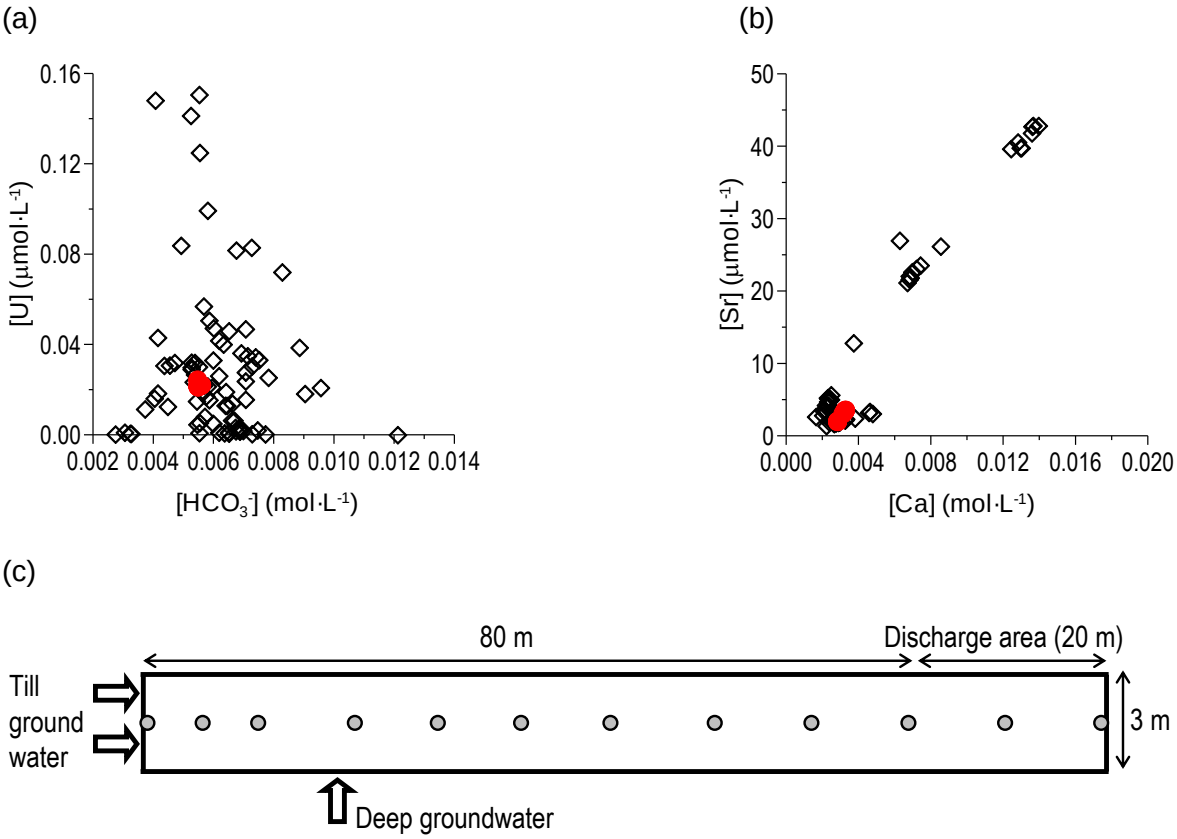

Figure 4.4 – Comparison between simulated (red symbols) composition of the porewater of the glacial clay at the present-day hydrogeochemical conditions (after 2700 years of reactive transport) and measured (black symbols) composition of the shallow groundwaters at Forsmark. a) Aqueous concentration of uranium against bicarbonate; b) Aqueous concentration of strontium against calcium; c) Location of the selected points of the modelled domain (grey dots) plotted in graphics a and b.

Measured data for uranium and bicarbonate at Forsmark show a considerable wide range of values (Figure 4.4a). Simulated data plot within the concentration range of these elements actually measured at Forsmark (Figure 4.4a). Similarly, simulated data for strontium against calcium (Figure 4.4b) plot close to the dilute waters trend previously reported in Figure 4.2. The dilute shallow groundwaters at Forsmark correspond to those shallow systems that are less influenced by deep groundwater discharge and sea water intrusion (Laaksoharju et al., 2008).

Data for caesium at Forsmark are scarce and no graphic is shown here. Nevertheless, model outputs show that the concentration of caesium (1×10^{-10} mol·L^{-1}) flowing out of the Quaternary till when the present-day hydrogeochemical conditions have been reached (after 2700 years of reactive transport) are within the range of caesium concentrations observed nowadays at Forsmark, previously reported in section 4.3.1.

4.4.2 Retention of repository-derived radionuclides

Given the good agreement between measured data for reactive solutes such as bicarbonate, calcium, uranium, and strontium, and the outputs of the reactive transport model (previously shown in Figure 4.4) that was built to simulate the present-day hydrogeochemical conditions of the Quaternary till at Forsmark, the pessimistic scenario of repository release may now be simulated by adding repository-derived radionuclides to the deep groundwater that discharges into the till aquifer.

Since the Fennoscandian shield is being subject to a regional uplift (SKB, 2005b) which triggers gradual changes of the topography and near-surface hydrology, in order to assure a relatively reliable scenario of repository release into the near-surface systems, a relatively short period (when compared to the safety assessment of a deep geological repository; ~100,000 years, SKB, 2006) of repository release has been simulated. In this context, the continuous inflow of repository-derived radionuclides into the Quaternary till has been simulated during 2700 years.

Deep groundwater affected by repository release has a RDU concentration which is ~1.5 orders of magnitude higher than before repository release, and it is 23% lower than the natural uranium concentration in the till groundwater (2.23×10^{-8} mol·L^{-1}). At the end of the simulation, only 1.8% of uranium flowing out of the till is derived from repository (Figure 4.5a). RDU is retained in the till by adsorption on the ferrihydrite (Figure 4.5b). The relatively low impact of repository release on the concentration of aqueous uranium at the discharge area is mainly due to the high concentration of natural uranium in the till groundwater.

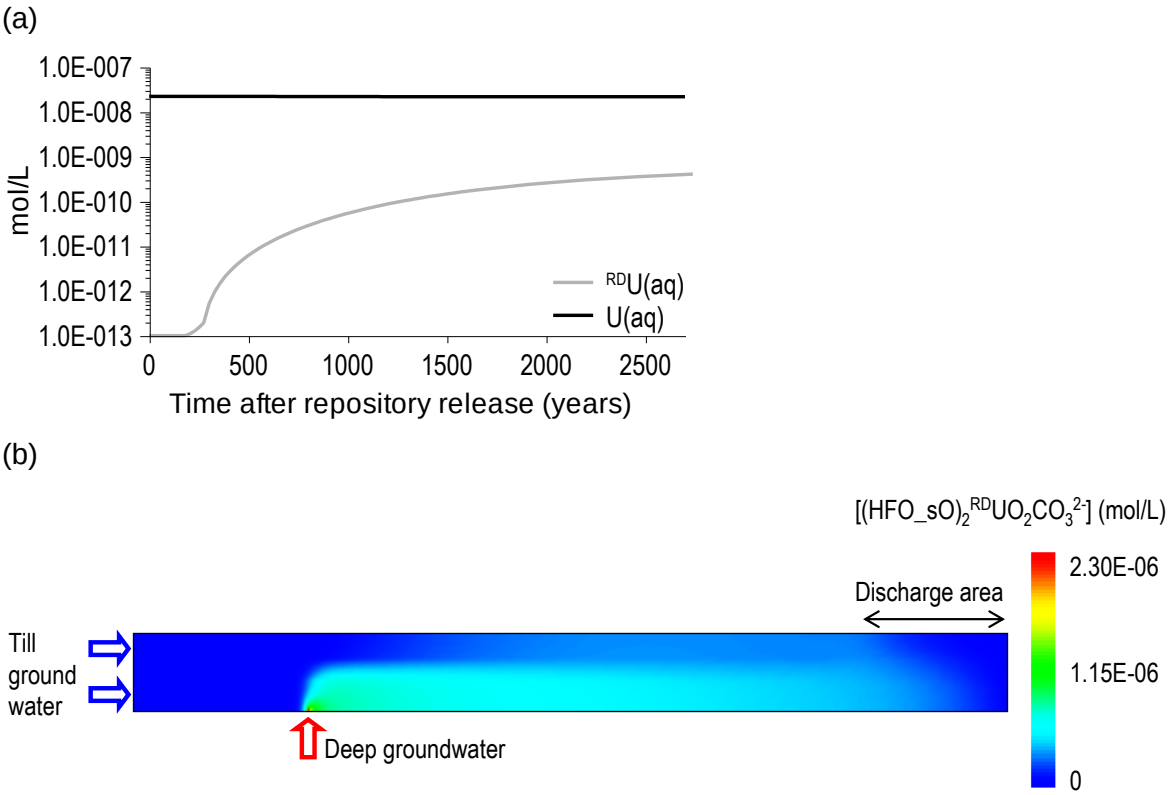

Figure 4.5 – a) Predicted evolution of the concentration of natural (U(aq)) and repository-derived (RDU(aq)) uranium after repository release, at the discharge area; b) Predicted concentration of RDU retained in the strong sites of ferrihydrite at the end of simulation period (2700 years after repository release). $(HFO\_sO)_2{}^{RD}UO_2CO_3^{2-}$ stands for the major species of repository-derived uranium sorbed onto ferrihydrite.

Approximately 1000 years after repository release, the concentration of RDSr(aq) reaches a stationary value of 2.9×10^{-5} mol·L^{-1}, which is less than 5% of the concentration of RDSr(aq) in the deep groundwater affected by repository release (Figure 4.6a). The retention of RDSr in the till domain delays its arrival to the discharge area approximately 350 years. This value is calculated by subtracting the conservative advective travel time from the reactive advective travel time. The retardation of RDSr is provided by cation exchange in illite and, to a less extent, to the precipitation of the calcite-strontianite solid solution (Figure 4.6b and c).

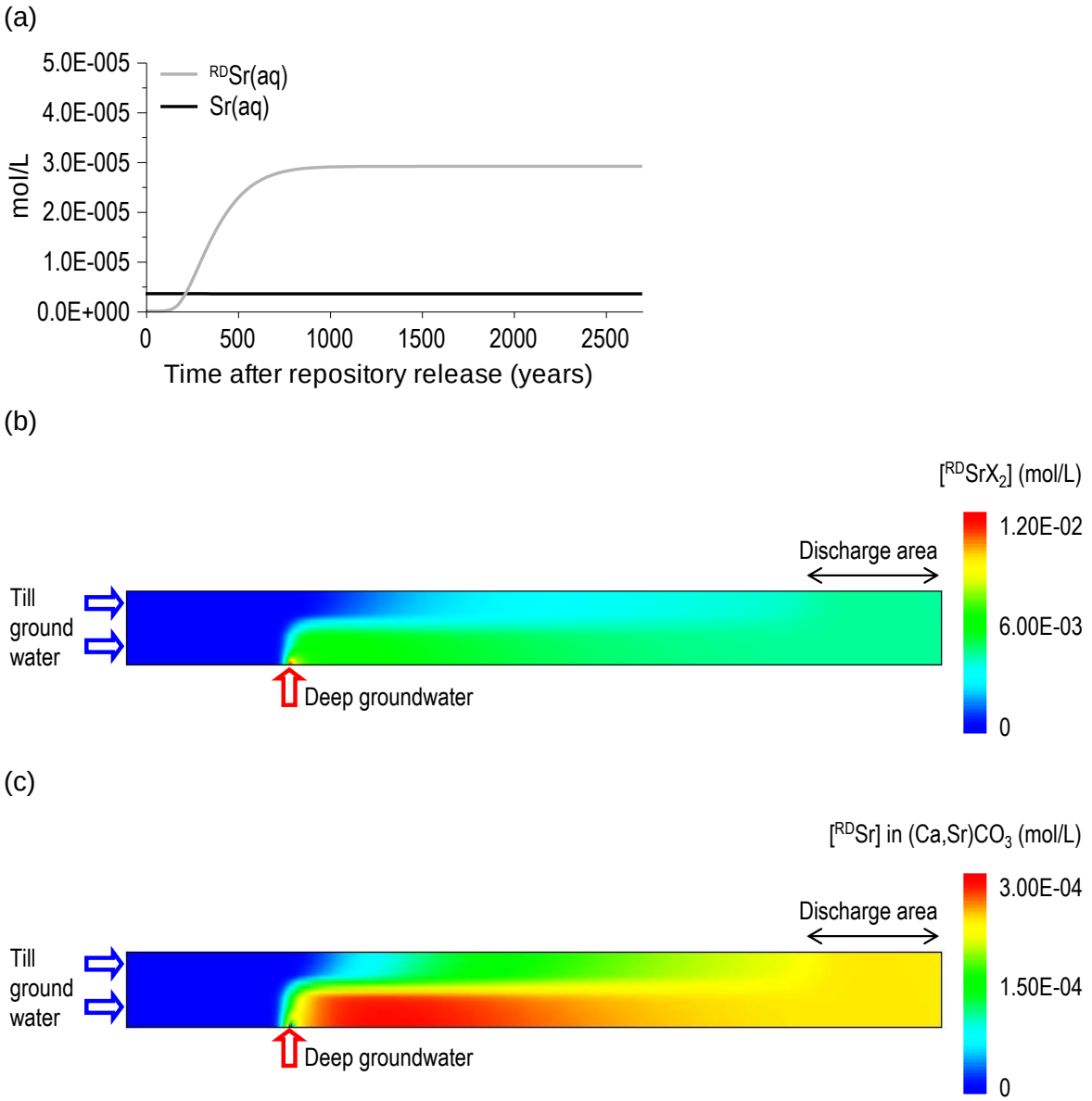

Figure 4.6 – a) Predicted evolution of natural (Sr(aq)) and repository-derived (RDSr(aq)) strontium after repository release, at the discharge area; b) RDSr retained in illite ($^{RD}SrX_2$); c) RDSr in (Ca,Sr)CO_3 solid solution, at the end of the simulation period (2700 years after repository release). RDSr is preferentially incorporated in illite (note the different scales for plots b and c).

Although deep groundwater affected by repository release transports a RDCs(aq) concentration that is 3.5 orders of magnitude higher than Cs(aq) concentration in the till porewater, at the end of the simulation only 3.5% of caesium flowing out of the till is derived from the repository (Figure 4.7a). This remarkable decrease of RDCs(aq) from the

deep groundwater inflow point to the discharge area is due to the high affinity of caesium for the FES of illite (Figure 4.7b).

(a)

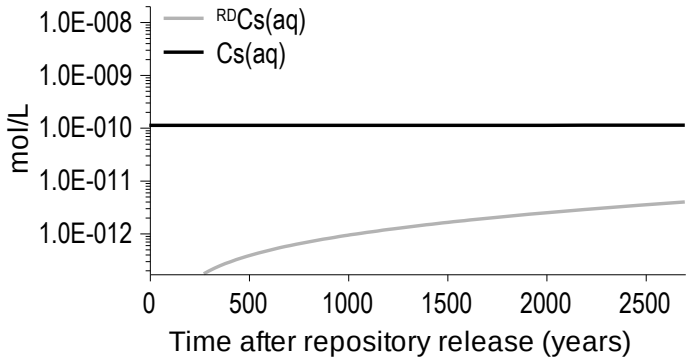

(b)

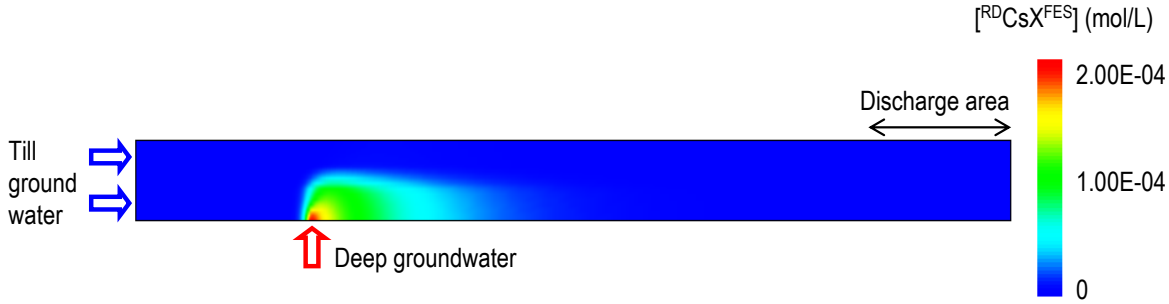

Figure 4.7 – a) Predicted evolution of natural (Cs(aq)) and repository-derived (RDCs(aq)) caesium after repository release, at the discharge area; b) Predicted concentration of RDCs retained in the FES of illite ($^{RD}CsX^{FES}$) at the end of the simulation (2700 years after repository release).

Deep groundwater affected by repository release has a radium concentration of 9.15×10^{-11} mol·L^{-1}. At the end of the simulation Ra(aq) concentration at the discharge area is 2×10^{-12} mol·L^{-1} (Figure 4.8a). Radium is retained, in the vicinity of the deep groundwater inflow point, via precipitation of (Ba,Ra)SO_4 solid solution (Figure 4.8b).

(a)

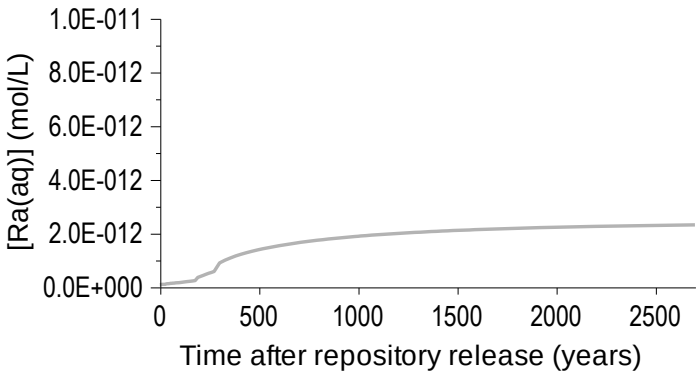

(b)

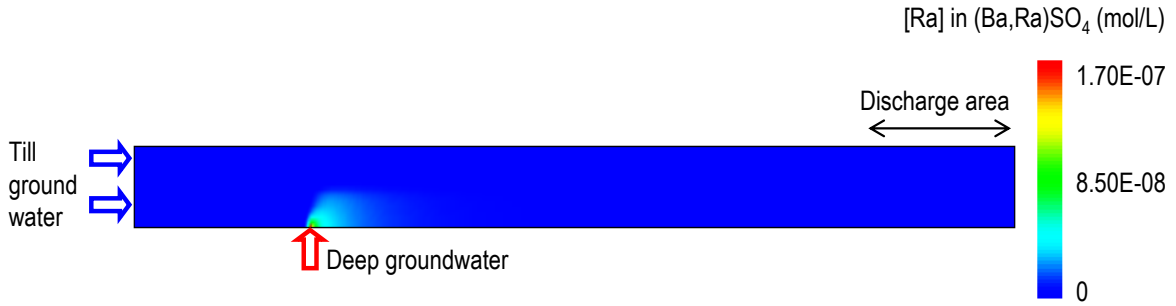

Figure 4.8 – a) Predicted evolution of repository-derived (Ra(aq)) radium after repository release, at the discharge area; b) Predicted concentration of Radium retained in (Ba,Ra)SO_4 solid solution at the end of the simulation time.

The results in the previous paragraphs show that the four repository-derived radionuclides under study are likely to be retained through different geochemical processes in the solid phase of the Quaternary till at Forsmark. The retention efficiency of the till deposit has been quantitatively evaluated by comparing the results computed in the conservative (no reactions between solid and aqueous phases) and reactive transport simulations. The retention efficiency parameter (*E*) of the system at a given time τ can be described according to equation 4.1:

$$E = 100 \times \left(1 - \frac{C_R^{\tau}}{C_C^{\tau}}\right) \qquad \text{(equation 4.1)}$$

where $C_R{}^{\tau}$ is the concentration of a given radionuclide at time τ in the reactive transport simulation, and $C_C{}^{\tau}$ is the concentration of the same radionuclide at time τ in the conservative transport simulation.

The reactive transport simulations predict that, in case of repository release, RDSr, RDCs, RDU and Radium would be retained in the till deposit (Figure 4.9). During the first 100 years the till system reaches a retention efficiency of 100% for RDSr. Thereafter, retention efficiency for RDSr drops to 0%, ~1000 years after repository release, reflecting the limited capacity of illite and the $Ca_{1-\chi}Sr_{\chi}CO_3$ solid solution to retain the added strontium. On the other hand, RDCs is efficiently retained (100%) during the whole simulation due to the high affinity of caesium for the FES of illite.

When RDU enters the till aquifer, the till is able to fully retain it (100% retention efficiency). Thereafter, retention efficiency for RDU progressively decreases. This decrease is related to the fact that ferrihydrite dissolves during the simulation, due to the inflow of deep groundwater. Since uranium is retained via adsorption on ferrihydrite, as time passes there are progressively less available sites for uranium adsorption, and, consequently, retention efficiency for RDU decreases.

Radium is the only radionuclide that is not assumed to be involved in sorption reactions, and therefore, its retention efficiency reflects the evolution of the thermodynamic equilibrium between the aqueous phase and the precipitation of $Ba_{1-\chi}Ra_{\chi}SO_4$ solid solution.

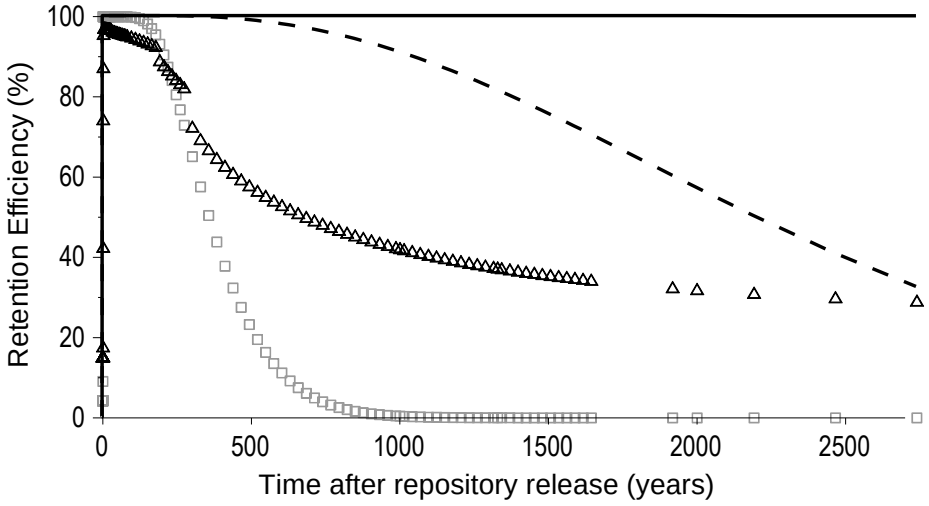

Figure 4.9 – Computed retention efficiencies for uranium (dashed line), strontium (grey squares), caesium (solid line) and radium (black triangles), derived from repository release, at the discharge area of the Quaternary till.

4.5 Conclusions

Coupled hydrogeochemical processes that are believed to occur in the Quaternary till at Forsmark have been implemented in a numerical model to assess the retention of repository-derived radionuclides. Numerical simulations of groundwater flow and reactive solute transport are able to reproduce the observed natural concentrations of uranium, strontium and caesium at the Forsmark site which proves the reliability of the conceptual and numerical models developed here. Natural concentration of radium at Forsmark shallow groundwaters is extremely low so that its natural occurrence has been neglected in the numerical simulations.

The simulation of a pessimistic scenario of a continuous repository release during 2700 years has shown that the Quaternary till has geochemical features that contribute to the effective retention of radionuclides. Numerical results show that repository-derived uranium will have a minor impact in the Quaternary till, mainly due to the high natural concentration of uranium and its adsorption on ferrihydrite; caesium will be efficiently retained by cation exchange in illite; radium will be retained via co-precipitation with barite; and, although strontium is assumed to be retained through two geochemical processes (co-precipitation with calcite and cation exchange in illite), the retention capacity of the Quaternary till for strontium is limited.

The quantitative assessment of the retention efficiency of the Quaternary till reveals that repository-derived caesium is the most effectively retained radionuclide (100% retention efficiency), while retention of repository-derived strontium and uranium becomes progressively lower. Radium retention decreases during the first years after repository release, and then approaches a steady state of 30% retention efficiency.

Acknowledgments

This work has been funded by SKB. Data and information used in this paper were generated within the SKB's Site Investigation Program for location of a deep geological repository for the disposal of HLNW. The second author is grateful to the Portuguese Ministry of Science, Technology and Education for a PhD Grant (POCI 2010, BD/16647/2004). Special thanks are given to Sten Berglund and Tobias Lindborg for their support, encouragement and fruitful discussions during this work.

4.6 References

Albrecht J. (2005) *Forsmark site investigation: Study of Quaternary sediments in connection with investigations of bedrock lineaments*. SKB report P-05-138, Swedish Nuclear Fuel and Waste Management Co., Stockholm, Sweden.

Arcos D., Grandia F., Domènech C., Fernández A.M., Villar M.V., Muurinen A., Carlsson T., Sellin P. and Hernán P. (2008) Long-term geochemical evolution of the near-field repository: Insights from reactive transport modeling and experimental evidences. *Journal of Contaminant Hydrology*, 102: 196-209.

Bain J. G., Blowes D.W., Robertson W.D. and Frind E.O. (2000) Modeling of sulphide oxidation with reactive transport at a mine drainage site. *Journal of Contaminant Hydrology*, 41: 23-47.

Berglund S., Kautsky U., Lindborg T. and Selroos J.O. (2009) Integration of hydrological and ecological modelling for the assessment of a nuclear waste repository. *Hydrogeology Journal*, 17: 95–113

Bosson E. and Berglund S. (2006) *Near-surface hydrogeological model of Forsmark – Open repository and solute transport applications – Forsmark 1.2.* SKB report R-06-52, Swedish Nuclear Fuel and Waste Management Co., Stockholm, Sweden

Bradbury M.H. and Baeyens, B. (2000) A generalised sorption model for the concentration dependent uptake of caesium by argillaceous rocks *Journal of Contaminant Hydrology*, 42: 141–163.

Bruno J., Duro L. and Grivé M. (2002) The applicability and limitations of thermodynamic geochemical models to simulate trace element behaviour in natural waters. Lessons learned from natural analogue studies. *Chemical Geology*, 190(1-4): 371-393.

Cole T., Bidoglio G., Soupioni M., O'Gorman M. and Gibson N. (2000) Diffusion mechanisms of multiple strontium species in clay. *Geochimica et Cosmochimica Acta,* 64(3): 385-396.

Drake H., Sandström B. and Tullborg, E.L. (2006) *Mineralogy and geochemistry of rocks and fracture fillings from Forsmark and Oskarshamn: Compilation of data for SR-Can*. SKB report R-06-109. Swedish Nuclear Fuel and Waste Management Co., Stockholm, Sweden

Duro L., Grivé M., Cera E., Gaona X., Domènech C. and Bruno J. (2006b) *Determination*

and assessment of the concentration limits to be used in SR-Can. SKB report TR-06-32, Swedish Nuclear Fuel and Waste Management Co., Stockholm, Sweden

Duro, L. Grivé M., Cera E., Domènech C. and Bruno J. (2006a) *Update of a thermodynamic database for radionuclides to assist solubility limits calculation for performance assessment. SKB* report TR-06-17. Swedish Nuclear Fuel and Waste Management Co., Stockholm, Sweden

Grenthe I., Fuger J., Konings R.J.M., Lemire R.J., Muller A.J., Nguyen-Trung C. and Wanner H. (1992) *Chemical Thermodynamics of Uranium*. Elsevier, Amsterdam.

Grivé M. (2005) *The linkage between uranium, iron and carbon cycling. Processes at interfaces: evidences from combined solution chemical and spectroscopic studies*. PhD. Thesis, Universitat Politècnica de Catalunya, 341 pp.

Hummel W., Berner U., Curti E., Pearson F.J. and Thoenen T. (2002) *Nagra/PSI Chemical Thermodynamic Data Base 01/01.* ISBN: 1-58112-620-4. 565 p.

Johansson P.O., Werner K., Bosson E., Berglund S. and Juston J. (2005) *Description of climate, surface hydrology, and near-surface hydrogeology. Preliminary site description. Forsmark area – version 1.2.* SKB report R-05-06. Swedish Nuclear Fuel and Waste Management Co., Stockholm, Sweden

Köhler S.J., Dufaud F. and Oelkers E.H. (2003) An experimental study of illite dissolution kinetics as a function of ph from 1.4 to 12.4 and temperature from 5 to 50°C. *Geochimica et Cosmochimica Acta*, 67-19: 3583–3594.

Laaksoharju M., Smellie J., Tullborg E.L., Gimeno M., Molinero J., Gurban I. and Hallbeck L. (2008) Hydrogeochemical evaluation and modelling performed within the Swedish site investigation programme. *Applied Geochemistry*, 23: 1761–1795.

McKinley J.P., Zachara J.M., Smith S.C. and Liu C. (2007) Cation exchange reactions controlling desorption of $^{90}Sr^{2+}$ from coarse-grained contaminated sediments at the Hanford site, Washington. *Geochimica et Cosmochimica Acta,* 71: 305–325

Molinero J., Raposo J.R., Galídez J.M., Arcos D. and Guimerà J. (2008) Coupled hydrogeological and reactive transport modeling of the Simpevarp area (Sweden). *Applied Geochemistry*, 23, 1957-1981.

Parkhurst D.L. and Appelo C.A.J. (1999) *User's guide to PHREEQC (version 2) – A computer program for speciation, batch-reaction, one-dimensional transport and inverse geochemical calculations*. U.S. Geological Survey Water Resources

investigations report 99-4259, 312 pp.

Parkhurst D.L., Kipp K.L., Engesgaard P. and Charlton S.R. (2004) *PHAST: A program for simulating ground-water flow, solute transport, and multicomponent geochemical reactions.* U.S. Geological Survey Techniques and Methods 6-A8, 154 pp.

Prommer H., Tuxen N. and Bjerg P.L. (2006) Fringe-controlled natural attenuation of phenoxy acids in a landfill plume: integration of field-scale processes by reactive transport modeling. *Environmental Science and Technology*, 40: 4732-4738.

SKB (2005a) *Description of surface systems. Preliminary site description of Forsmark area – version 1.2.* SKB report R-05-03, Swedish Nuclear Fuel and Waste Management Co., Stockholm, Sweden.

SKB (2005b) *Preliminary site description Forsmark area – version 1.2.* SKB report R-05-18. Swedish Nuclear Fuel and Waste Management Co., Stockholm, Sweden.

SKB (2006) *Long-term safety for KBS-3 repositories at Forsmark and Laxemar – a first evaluation.* Main Report of the SR-Can project. SKB report TR-06-09. Swedish Nuclear Fuel and Waste Management Co., Stockholm, Sweden.

Tesoriero A.J. and Pankow J.F. (1996) Solid solution partitioning of Sr^{2+}, Ba^{2+}, and Ca^{2+} to calcite. *Geochimica et Cosmochimica Acta,* 60-6: 1053–1064.

Tröjbom M. and Söderbäck B. (2006) *Chemical characteristics of surface systems in the Forsmark area. Visualisation and statistical evaluation of data from shallow groundwater, precipitation, and regolith.* SKB report R-06-19, Swedish Nuclear Fuel and Waste Management Co., Stockholm, Sweden.

Um W., Serne R.J., Brown C.F. and Last G.V. (2007) U(VI) adsorption on aquifer sediments at the Hanford Site. *Journal of Contaminant Hydrology*, 93: 255–269

Waite T.D., Davis J.A., Payne T.E., Waychunas G.A. and Xu N. (1994) Uranium (VI) adsorption to ferrihydrite: Application of a surface complexation model. *Geochimica et Cosmochimica Acta,* 58: 5465–5478.

Zachara J.M., Smith S.C., Liu C., McKinley J.P., Serne R.J. and Gassman P.L. (2002). Sorption of Cs+ to micaceous subsurface sediments from the Hanford site, USA. *Geochimica et Cosmochimica Acta,* Acta 66, 193– 211.

Chapter 5

Estimating effective distribution coefficients of selected radionuclides from reactive transport numerical models

5. Estimating effective distribution coefficients of selected radionuclides from reactive transport numerical models[5]

Abstract

The Swedish Nuclear Fuel and Waste Management Company (SKB) is carrying out a geoscientific characterization of Forsmark for the construction of a deep geological repository for high level nuclear waste (HLNW). Reactive transport numerical models have been used to assess the migration of selected radionuclides (U, Sr, Cs and Ra) within a Quaternary till aquifer that overlies the candidate granitic host rock. Simulation of a hypothetical inflow of a radionuclide-bearing granite groundwater into the Quaternary till has provided a quantitative assessment of the migration and retention of selected radionuclides. According to numerical results, the Quaternary till behaves as a natural reactive barrier able to retain radionuclides. Computed retention of radionuclides in the solid phase leads to a retardation of their arrival to the discharge area of the Quaternary till. Numerical results show that the distribution coefficient (Kd) of the selected radionuclides varies in time and space in the modelled domain. Computed breakthrough curves of the selected radionuclides have been analysed to obtain effective retardation factors (R). Numerical results show that for those radionuclides with a high affinity for the solid phase (e.g. Cs) and those that are solely involved in co-precipitation with mineral phases (e.g. Ra), computed breakthrough curves take very long to reach the final stabilized maximum which hinders the estimation of R and the corresponding effective Kd.

Keywords: Reactive transport models, radionuclides, distribution coefficient, effective retardation factor.

---

[5] This work has been presented at the International Groundwater Symposium of the International Association of Hydraulic Research: Flow and Transport in Heterogeneous Subsurface Formations: Theory, Modelling & Applications, in 2008.

It was developed by the following co-authors: Clara Sena[a,b], Jorge Molinero[a], Fidel Grandia[a], David Arcos[a], and Lara Duro[a]

[a] Amphos XXI Consulting S.L., Spain; [b] I&D GeoBioTec, University of Aveiro, Portugal

5.1 Introduction

The concept of deep geological repository in Sweden entails a number of engineered (copper canisters, clay barriers, and cement liners) and natural geological barriers to prevent and retard for long periods of time (~100,000 years) the migration of radionuclides to the surface (SKB, 2006). Forsmark has been recently selected by SKB for the construction of Sweden's deep geological repository for HLNW (SKB, 2009).

When dealing with the final disposal of HLNW, radionuclide migration through the engineered and natural barriers that surround the repository must be assessed. In performance assessment of deep geological repositories, the most probable failure scenarios of the repository and their environmental consequences are being analysed (e.g. SKB, 2006). In case of repository release, the surface sediments covering the repository host rock represent the last geological barrier prior to the surface ecosystems.

Reactive transport numerical models are powerful tools that couple groundwater flow, transport of solutes and geochemical reactions between solid and aqueous phases. By integrating site specific data and thermodynamic databases they can provide valuable and reliable quantitative evaluations for many environmental issues among which performance assessment of a deep geological repository is undoubtedly included (Molinero and Samper, 2006, Arcos et al, 2008, among others). Nevertheless, such reliable models demand considerable amounts of site specific data and thermodynamic parameters (needed to describe numerically the geochemical processes considered) that may not be available. In this context, Kd-based models may provide alternative tools whenever available data is not sufficient to implement the geochemical processes of interest for a given reactive transport model.

The governing equations solved by a reactive transport simulator are a set of (1) partial differential equations describing groundwater flow and solute transport for each aqueous component; (2) non-linear algebraic equations describing equilibrium chemical reactions; and, (3) ordinary differential equations describing rates of kinetic chemical reactions (Parkhurst et al., 2004). On the other hand, in a Kd-based model the simulator does not need to solve non-linear algebraic equations, since aqueous speciation and thermodynamic equilibrium are not solved by this type of models. Therefore, for a given modelled domain and same number of reactive solutes, a Kd-based numerical model should be much less time and computational demanding than a reactive transport numerical model.

In 1981, Reardon discussed the reliability of Kd-based models to describe reversible ion sorption reactions in contaminant migration, concluding that if the groundwater system is in a steady state chemical evolution a Kd-based model should be as reliable as a reactive transport model. At chemical steady state the sorbing sites at any point in the flow path are in equilibrium with the way in which groundwater is evolving chemically and therefore the Kd of a given location should be constant over time. Based on these results, Glynn (2003) performed one-dimensional (1D) reactive transport simulations to demonstrate the effects of aqueous speciation and sorption reactions on the transport of neptunium and plutonium. The author concluded that a Kd-based model would lead to remarkably different results from those attained in reactive transport simulations, pointing out the care that must be taken when choosing the type of model to be used in the performance assessment of HLNW disposal sites.

Glynn (2003) analysed the Kd obtained from the outputs of 1D reactive transport models for two redox sensitive radionuclides, neptunium and plutonium. In the present research work, a two-dimensional (2D) reactive transport model has been developed to predict the migration of four radionuclides in a Quaternary till: (1) uranium as a redox sensitive actinide that may adsorb on ferrihydrite; (2) strontium as a divalent cation that may co-precipitate with calcite ($CaCO_3$) and participates in cation exchange in illite; (3) caesium as a monovalent cation with high affinity for the frayed edge sites (FES) of illite; and, (4) radium as a divalent cation that may co-precipitate with barite ($BaSO_4$).

From the output results of the 2D reactive transport model, R and effective Kd are estimated for those radionuclides for which complete breakthrough curves have been computed. The meaning of this effective Kd is then analysed by comparing the results attained in the 2D reactive transport model with those obtained in the 2D Kd-based model.

5.2 Scope

This paper begins with a description of the reactive transport numerical model that has been built to predict the migration of selected radionuclides through a Quaternary till, by simulating a hypothetical repository release. This simulation is based on site specific data, taken from SKB's Site Descriptive Model (Johansson et al., 2005; Tröjbom et al., 2007), that describe the hydrogeology and geochemistry at Forsmark, and on a pessimistic scenario of repository release. In the following section, the results attained in the reactive transport model are analysed and discussed. From the outputs of the reactive transport numerical model, the Kd of each radionuclide in the modelled domain is analysed over

time and space. In section 5.5, R and the effective Kd of each radionuclide are calculated from the outputs of the reactive transport numerical model. The meaning of this effective Kd is analysed by comparing the results attained in the reactive transport simulations with those attained in Kd-based models. Finally, the main conclusions attained in this work are listed in section 5.6.

5.3 Reactive solute transport model

At Forsmark, the granitic candidate host rock for the deep geological repository is covered by a Quaternary till which thickness ranges from 1 to 3 m (Johansson et al., 2005). Groundwater in the granitic bedrock flows mainly along fractures and deformation zones composed of loose granitic material and coatings of calcite, chlorite, quartz and pyrite (Drake et al., 2006). The till deposit hosts unconfined porous aquifers with stratified hydraulic conductivity and porosity (Johansson et al., 2005), and is composed mainly of calcite, illite and trace amounts of Fe oxyhydroxides.

In order to assess the migration of radionuclides through the Quaternary till, a hypothetical scenario of repository release has been simulated using a reactive transport numerical model. In this hypothetical scenario a granitic groundwater carrying repository-derived radionuclides is considered to flow upwards, from the repository to the surface, reaching the Quaternary till that discharges into a surface water body, such as a lake, a stream, or the Baltic Sea (Figure 5.1).

The reactive transport simulations have been performed with the finite-difference code PHAST v. 1.4.2 (Parkhurst et al., 2004). This code is the result of coupling a transport solver, HST3D (Kipp, 1987) and the well known geochemical code, PHREEQC (Parkhurst and Appelo, 1999). PHAST is able to simulate multi-component, reactive solute transport in three-dimensional saturated groundwater flow systems. The reactive transport equations are solved by sequential non iterative approach (SNIA) in which solute transport and chemical reactions are decoupled for each time step.

The thermodynamic database used in the present work (Duro et al., 2006a) is an extension of the NAGRA-PSI database, compiled by Hummel et al. (2002). This database contains a large set of complexation reactions as well as pure mineral equilibrium reactions for many radionuclides and trace elements.

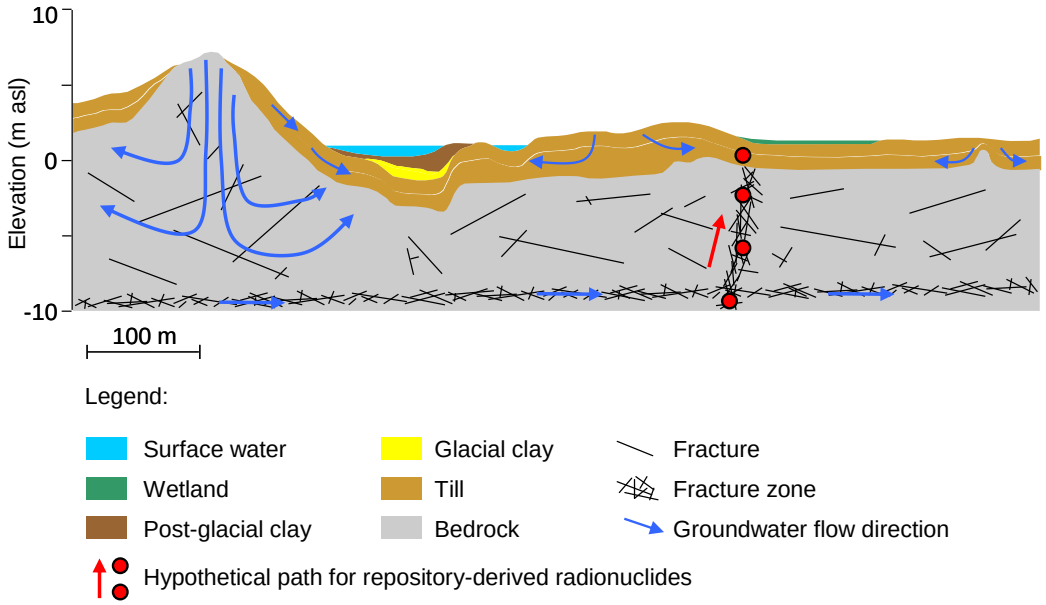

Figure 5.1 – Near-surface hydrogeological conceptual model of Forsmark candidate site (modified from Johansson et al., 2005) showing a hypothetical path of radionuclides released by a repository.

5.3.1 Hydrodynamic and geochemical processes

According to the site characterization programme developed by SKB, the Quaternary till has been divided in three layers with different hydraulic properties (Johansson et al., 2005). Table 5.1 shows average values of the hydrodynamic parameters that were used in the numerical simulations of this work.

The capacity of the Quaternary till to retain radionuclides depends mainly on the mineral assemblages present, which in turn, enable radionuclide sorption, precipitation or co-precipitation with major element solid phases. Since the objective of this work is to assess radionuclide migration in the Quaternary till, radionuclide decay was not considered in the numerical simulations.

According to the main reactive minerals present in the Quaternary till and to the geochemical behaviour of the selected radionuclides, the following geochemical processes have been implemented in the reactive transport model:

1. Adsorption of uranium on ferrihydrite ($Fe(OH)_3$).
2. Co-precipitation of strontium with calcite ($CaCO_3$).
3. Cation exchange in illite involving Ca^{2+}, Mg^{2+}, Sr^{2+}, Na^+, K^+, NH_4^+, and Cs^+.
4. Co-precipitation of radium with barite ($BaSO_4$)

Table 5.1 – Values of the hydrodynamic parameters implemented in the numerical model for the Quaternary till. Values taken from Johansson et al. (2005).

Parameter	Top layer	Middle layer	Bottom layer
Thickness (m)	0.8	1.4	0.8
$K_{horizontal}$ (m/s)	1.5×10^{-5}	1.5×10^{-6}	1.5×10^{-5}
$K_{vertical}$ (m/s)	1.5×10^{-6}	1.5×10^{-7}	1.5×10^{-6}
$\alpha_{longitudinal}$ (m)	0.5	0.5	0.5
$\alpha_{transverse}$ (m)	0.2	0.2	0.2
ϕ_c (-)	0.15	0.5	0.5
ϕ_t (-)	0.25	0.25	0.25
ρ ($kg \cdot L^{-1}$)	1.95	1.95	1.95
D_e (m^2/s)	5×10^{-10}	5×10^{-10}	5×10^{-10}

K – hydraulic conductivity; α – dispersivity coefficient; ϕ_c – kinematic porosity; ϕ_t – total porosity; D_e – effective diffusion coefficient; ρ – dry bulk density.

The surface complexation model implemented in the reactive transport model for adsorption of uranium on ferrihydrite is that of Waite et al. (1994) which considers two types of adsorption sites (see Table A1.3 in Appendix 1). Ferrihydrite is very sensitive to changes in the redox state of the system, and the inflow of a relatively reducing deep groundwater in the till domain can trigger its dissolution. Therefore, if ferrihydrite dissolves in the simulation, the total amount of adsorption sites decreases proportionally and vice-versa. An initial amount of 0.15 wt% of ferrihydrite has been set in the numerical model (Table 5.2).

Calcite present in the Quaternary till is assumed to form a non-ideal solid solution with strontium. The parameters describing the formation of this solid solution are those of Tesoriero and Pankow (1996). An initial amount of 1.5 wt% of $(Ca,Sr)CO_3$ has been assigned to the numerical model (Table 5.2). The initial strontium molar fraction (1.73×10^{-5}) has been obtained after performing a numerical equilibration of the selected till groundwater sample with the calcite-strontianite solid solution, using PHREEQC. This strontium molar fraction is consistent with data from Forsmark (SKB, 2005a; SKB, 2005b) and also with data other natural systems, as reported by Bruno et al. (2002).

In the numerical simulations, the model for cation exchange in illite is that of Bradbury and Baeyens (2000) with some modifications (see Table A1.1 in Appendix 1, and for further details the reader is referred to Grandia et al., 2007). Illite dissolution kinetics is expected to be very slow under the pH conditions modelled here (Köhler et al., 2003). Therefore, a

constant concentration of 10 wt% of illite (with a cation exchange capacity of 200 meq·kg_{solid}^{-1}) has been assumed (Table 5.2).

In many aqueous systems, radium is strongly co-precipitated with barite due to the chemical similarity between radium and barium (Grandia et al., 2008; and references therein). In the numerical simulations, an ideal solid solution between $BaSO_4$ and $RaSO_4$ has been let to form if oversaturation with this solid solution is reached (Table 5.2).

Table 5.2 – Initial concentration of the reactive minerals implemented in the reactive transport simulations.

Mineral	Initial concentration of reactive mineral (wt%)	Mechanism of radionuclide retention	Potentially retained radionuclides
$Ca_{1-\chi}Sr_{\chi}CO_3$ (χ(initial)= 1.73×10^{-5})*	1.5	Co-precipitation	Sr
Illite	10.0	Cation exchange	Sr, Cs
Ferrihydrite ($Fe(OH)_3$)	0.15	Adsorption	U
$Ba_{1-\chi}Ra_{\chi}SO_4$	0.0	Co-precipitation	Ra
Siderite ($FeCO_3$)	0.0	-	-

*χ stands for the molar fraction of Sr and Ra in the solid solutions in which they are involved.

Siderite ($FeCO_3$) is likely to form in carbonated systems similar to the Quaternary till under study; it is redox sensitive and may precipitate in the Quaternary till after the inflow of a reducing and Fe-rich deep groundwater. Therefore, siderite is allowed to precipitate in the simulations if oversaturation with this mineral is reached.

To compute the initial state of a reactive transport model, the code used here (PHAST; Parkhurst et al., 2004) firstly equilibrates the initial porewater of the modelled domain with the reactive minerals considered. Therefore, and in order to analyse the output of such initial equilibration, we have performed previous static calculations in PHREEQC (Parkhurst and Appelo, 1999) to define the composition of the initial porewater and boundary waters of the modelled domain. In this context, the initial amount of siderite set for the reactive transport simulations (Table 5.2), results from equilibrating the selected till groundwater sample with this mineral. It should be noted that since the selected till groundwater sample is close to the equilibrium with the reactive minerals considered in

the numerical model (calcite, ferrihydrite and siderite), the composition of the till groundwater used in the simulations is very similar to the one actually measured.

5.3.2 Initial and boundary conditions

The reactive transport numerical model simulates the water flow and geochemical processes that occur in the Quaternary till at Forsmark. The modelled domain is a 2D vertical cross-section of the till deposit. Following Johansson et al. (2005), the thickness is 3 m, and, based on the dimensions of the subcatchments in the Forsmark area, the horizontal length is 100 m (Figure 5.2).

According to the water balance calculations developed for Forsmark (Johansson et al., 2005), a constant inflow rate of 14.5 L/d is prescribed along the vertical left boundary. The fracture through which deep groundwater enters the till is represented by a constant inflow boundary at the bottom of the modelled domain (cell coordinates: X= 20 m, Y= 0 m), with a flow rate of 0.5 L/d. The discharge area is located in the last 20 m of the top boundary, with a constant head of 3 m (Figure 5.2).

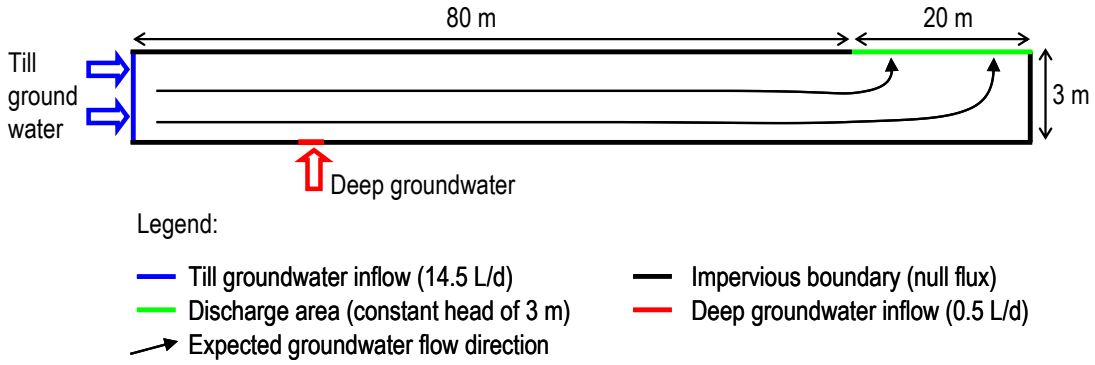

Figure 5.2 – Boundary conditions for the numerical model of the till domain.

Two groundwater compositions, representative of the till and deep granitic groundwater, were selected from SKB's database (Tröjbom and Söderbäck, 2006), and implemented in the numerical simulations (Table 5.3). The composition of deep groundwater affected by repository release is modified with respect to the deep groundwater composition prior to repository release, by adding repository-derived radionuclides (RDSr, RDCs, RDU and Ra, Table 5.3). In order to distinguish repository-derived radionuclides from their natural isotopes, already present in the till porewater and granitic groundwater, radionuclides coming from repository were labelled, in the model, as RDCs, RDSr, and RDU (RD stands for

Repository-Derived). Radium was not labelled since the presence of this radionuclide in the modelled domain is exclusively attributed to repository release due to the extremely low concentrations observed in the natural waters at the Quaternary sediments of Forsmark.

Table 5.3 – Initial composition of till porewater and deep groundwater (Deep GW). Concentrations of ^{RD}Cs, ^{RD}U, ^{RD}Sr and Ra in the Deep GW (after repository release) represent the increment of these elements due to repository release.

Parameter	Till porewater	Deep GW	Deep GW (after repository release)
pH	7.75	7.16	7.16
Eh (mV)	3	-145	-145
Na_{total}	1.22×10^{-3}	6.93×10^{-2}	6.93×10^{-2}
K_{total}	1.22×10^{-4}	1.67×10^{-3}	1.67×10^{-3}
Ca_{total}	2.79×10^{-3}	1.35×10^{-2}	1.35×10^{-2}
Mg_{total}	3.54×10^{-4}	7.18×10^{-3}	7.18×10^{-3}
C(IV)	5.57×10^{-3}	2.46×10^{-3}	2.46×10^{-3}
Cl_{total}	1.90×10^{-3}	1.07×10^{-1}	1.07×10^{-1}
SO_4^{2-}	2.41×10^{-4}	3.73×10^{-3}	3.73×10^{-3}
Si_{total}	9.74×10^{-5}	7.56×10^{-5}	7.56×10^{-5}
Fe_{total}	1.50×10^{-5}	4.91×10^{-4}	4.91×10^{-4}
Ba_{total}	7.28×10^{-7}	1.97×10^{-7}	1.97×10^{-7}
Sr_{total}	2.10×10^{-6}	4.13×10^{-5}	4.13×10^{-5}
U_{total}	2.23×10^{-8}	4.62×10^{-10}	4.62×10^{-10}
Cs_{total}	6.48×10^{-11}	1.62×10^{-8}	1.62×10^{-8}
NH_4^+	6.62×10^{-6}	1.95×10^{-4}	1.95×10^{-4}
^{RD}Cs	-	-	3.48×10^{-7}
^{RD}U	-	-	1.73×10^{-8}
^{RD}Sr	-	-	8.37×10^{-4}
Ra	-	-	9.15×10^{-11}
Concentrations in $mol \cdot L^{-1}$			

The simulated flow conditions are constant in time, and therefore, the system is modelled under steady state for hydrodynamic processes, but not for geochemical processes. The hydrogeochemistry of the Quaternary till is expected to vary due to the inflow of a more reducing and mineralised granitic groundwater.

In order to reach a geochemical quasi-steady state that represents the present-day hydrogeochemical conditions of the Quaternary till at Forsmark, a long period of reactive transport (2700 years) with the natural composition of the till porewater and deep groundwater flowing through the modelled domain (according to the boundary conditions shown in Figure 5.2) has been simulated. After attaining the geochemical quasi-steady state, repository release is simulated (for additional 8000 years) by adding RDU, RDSr, RDCs and Ra to the deep groundwater that is flowing through the modelled domain (according to the values listed in Table 5.3).

Repository release is simulated according to a very pessimistic scenario, where the ~500 m of granitic bedrock (between the repository and the Quaternary till), and the engineered barriers of the repository are assumed to have a negligible retention capacity over radionuclides, which is highly unlikely. Repository release is simulated through a continuous inflow of repository-derived radionuclides into the Quaternary till. In this context, radionuclide concentrations calculated for the near-field of the repository (Duro et al., 2006b), i.e., the vicinity of the canisters that contain the HLNW, are applied directly as the input concentrations in the numerical simulations. Following this procedure, the concentrations of repository-derived radionuclides assigned to the deep groundwater, after repository release, are shown in Table 5.3. These radionuclide concentrations are very high, considering that the engineered barriers and granitic bedrock should be able to retain much of these radionuclides. Nevertheless, since the objective of this study is to evaluate radionuclide retention in the Quaternary till, such an extreme (pessimistic) scenario has been assumed.

5.3.3 Spatial and time discretisation

The spatial discretisation of the modelled domain was set according to the main features of the boundary conditions which influence groundwater flow and geochemistry. Accordingly, spatial discretisation was refined at the position of the deep groundwater inflow and under the discharge area (outflow boundary).

As detailed in the previous section, there are two important stages regarding the chemical condition of the system: (i) the first stage occurs at the beginning of the simulation, when radionuclide-free deep groundwater flows into the modelled domain and triggers major geochemical changes until the geochemical quasi-steady state is reached (at 2700 years), and (ii) the second stage occurs when the increased concentration of radionuclides in the deep groundwater (that simulates repository release) disturbs the previous geochemical

state. According to these stages, time discretisation was refined at the beginning of each stage, and set progressively coarser towards the end of each stage.

To ensure stability in the numerical calculations, the Peclet criterion (Pe≤2) is met for the maximum ΔX (maximum ΔX =1 m, and longitudinal dispersivity = 0.5 m).

5.4 Results from the reactive solute transport model

5.4.1 Transport of a conservative solute

The transport of solutes in the modelled domain is affected by the geochemical processes and groundwater flow generated from the prescribed initial and boundary conditions. The conservative transport has been studied using chlorine as a tracer, given that no retention has been assigned to this element. From the chlorine breakthrough curve computed at the discharge area, an advective travel time of 2.3 years is obtained, from the deep groundwater inflow point to the discharge area of the modelled domain.

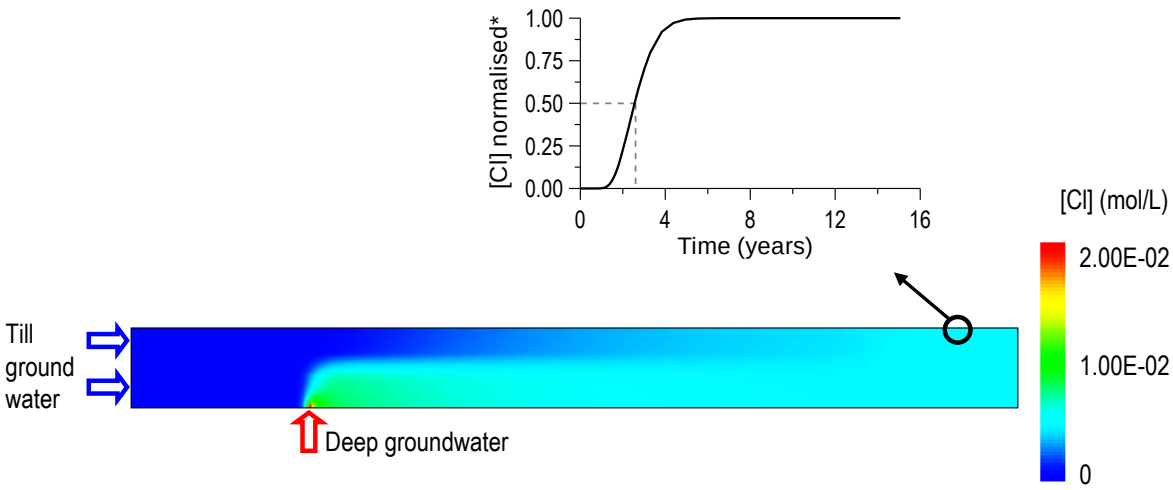

Figure 5.3 – Computed concentration of Cl(aq) in the modelled domain at the transport steady state, and computed breakthrough curve at the discharge area of the modelled domain (node X= 80 m, Y= 3 m). *[Cl] normalised stands for: $([Cl(aq)]_{predicted} - [Cl(aq)]_{initial})/([Cl(aq)]_{final} - [Cl(aq)]_{initial})$.

5.4.2 Distribution coefficient (Kd) of radionuclides and their natural isotopes

While chlorine behaves conservatively other elements (also known as reactive solutes), including the studied radionuclides and their natural isotopes, are expected to react with the minerals present in the solid matrix of the Quaternary till which leads to their partitioning between aqueous and solid phases. Partitioning of a given reactive solute in the modelled domain can be expressed by a Kd value that is calculated from the numerical results.

The concentration of a given reactive solute in the solid phase and in the aqueous phase is computed by PHAST for every time writing step and every node of the modelled domain. From this output, the Kd of a given reactive solute can be calculated. If the concentration of a given reactive solute retained in the solid phase (also known as sorbate) is expressed in $mol \cdot kg^{-1}_{rock}$, and the concentration of this reactive solute in the aqueous phase is expressed in $mol \cdot L^{-1}_{water}$, then the Kd, expressed in $L \cdot kg^{-1}$, is calculated from the following equation (Appelo and Postma, 2005):

$$Kd = \frac{[sorbate]_{(mol/kg\_of\_rock)}}{[solute]_{(mol/L\_of\_water)}} \qquad \text{(equation 5.1)}$$

Applying equation 5.1 to calculate the Kd of each radionuclide and respective natural isotope has provided charting their Kd in the modelled domain, for selected time steps. The output concentration of a sorbate in PHAST is given in units of $mol \cdot L^{-1}_{water}$. To convert these units into $mol \cdot kg^{-1}_{rock}$, the following equation has been applied:

$$[sorbate]_{(mol/kg\_of\_rock)} = [sorbate]_{(mol/L\_of\_water)} \cdot \frac{\phi_t}{\rho_b} \qquad \text{(equation 5.2)}$$

where ϕ_t is the total porosity (dimensionless) and ρ_b is the dry bulk density of the rock, expressed in $kg \cdot L^{-1}$ (data used in this work are listed in Table 5.1).

Strontium, uranium and caesium are naturally present in trace amounts in the two waters selected for the numerical simulations (Table 5.3), and therefore, they are considered to be present in the modelled domain before and after repository release. Since natural

radium is below detection limit in most of the water samples at Forsmark, the presence of this radionuclide in the modelled domain is exclusively related to repository release.

As previously mentioned, repository-derived radionuclides have been labelled as RDU, RDSr and RDCs to distinguish them from their natural isotopes in the modelled domain. This labelling procedure has been done by duplicating the thermodynamic database of each natural isotope for the corresponding labelled radionuclide, and by defining new ideal solid solutions that incorporate both the repository-derived radionuclide and its natural isotope, so that no artificial isotopic fractionation is introduced in the simulations. Therefore, from the moment when repository release is simulated, the Kd of each natural isotope (U, Sr, Cs) is equal to that of the corresponding repository-derived radionuclide (RDU, RDSr, RDCs, respectively).

During the approach to the geochemical quasi-steady state, the inflow of radionuclide-free deep groundwater into the Quaternary till triggers major geochemical changes which, in turn, lead to a readjustment of the partitioning of reactive solutes between solid and aqueous phases. Consequently, the Kd calculated from the outputs of the reactive transport simulations changes over time and space. Nevertheless, after the approach to the geochemical quasi-steady state (2700 years of reactive transport), the Kd of the selected radionuclides is relatively stable in time, but it is not homogeneous in space (Figure 5.4, Figure 5.5, Figure 5.6, and Figure 5.7).

Uranium is initially present in the modelled domain, in the till porewater and adsorbed on the surface of ferrihydrite. Partitioning of uranium between aqueous and solid phases in the Quaternary till leads to an initially homogeneous Kd(U) of 114 $L \cdot kg^{-1}$ (results not shown). During the first 5 years of reactive transport simulation a dilution of U(aq) occurs because the deep groundwater has a lower uranium concentration than that of the till porewater (Table 5.3). This dilution causes the initial increment of the Kd(U) in the modelled domain (darker green area in the top image of Figure 5.4). Thereafter, the Kd(U) progressively decreases, and the resulting till domain becomes heterogeneous with a Kd(U) that ranges from 114 $L \cdot kg^{-1}$, close to the till groundwater inflow area (left border of the modelled domain), to 90 $L \cdot kg^{-1}$ in the vicinity of the deep groundwater inflow point.

From the moment when repository release is simulated, the Kd of both natural and repository derived uranium is the same, since no isotopic fractionation is considered in the simulations.

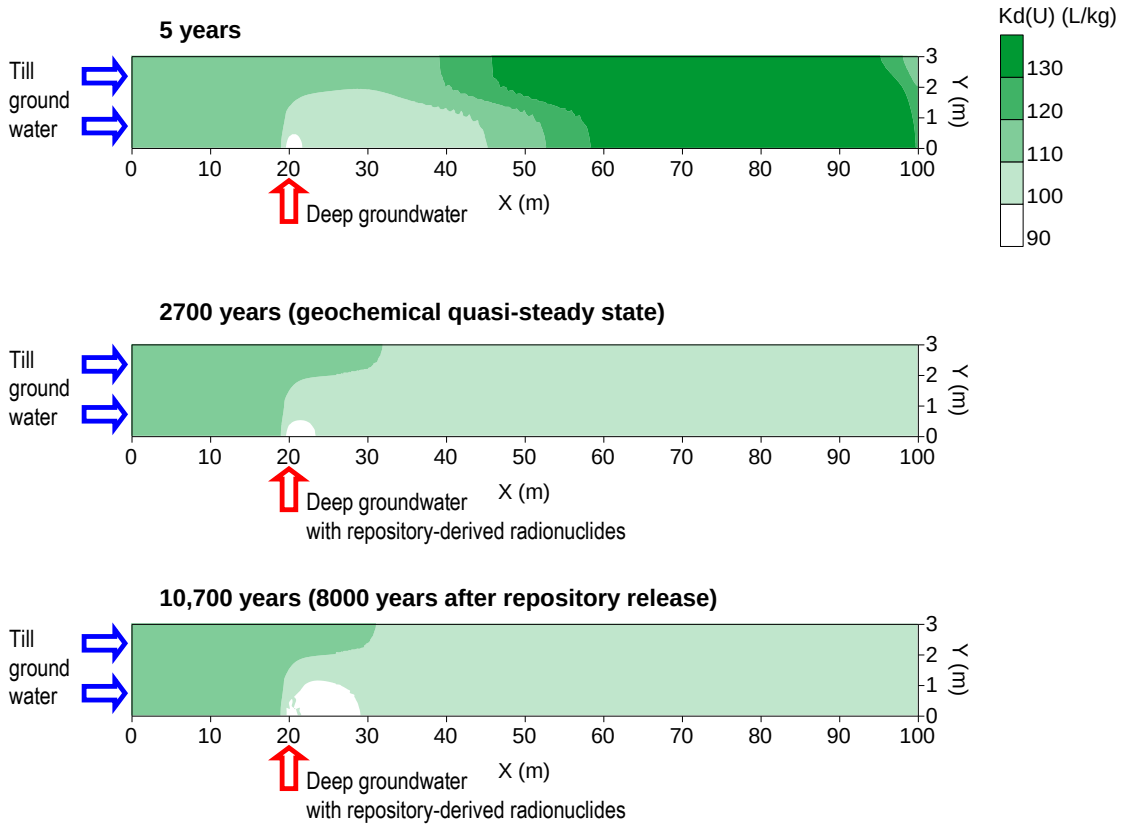

Figure 5.4 – Predicted evolution of Kd(U) along the simulation time. In the beginning of the simulation period the Kd varies with time. From 2700 years until the end of the simulation (10,700 years), relatively small geochemical changes occur, and hence Kd does not vary much.

Before the inflow of deep groundwater, strontium is present in the till porewater, in the $(Ca,Sr)CO_3$ solid solution and adsorbed on illite, leading to a homogeneous Kd(Sr) of 20 $L \cdot kg^{-1}$ (results not shown). The inflow of the deep groundwater in the till deposit leads to a decrease of the Kd(Sr) over time and space (Figure 5.5). After the establishment of the geochemical quasi-steady state, the Kd(Sr) varies little over time, but it is heterogeneous in space, ranging from 20 $L \cdot kg^{-1}$ in the area unaffected by the deep groundwater intrusion (darker blue area of the modelled domain), to 12 $L \cdot kg^{-1}$ in the vicinity of the deep groundwater inflow point (Figure 5.5).

Deep groundwater has a higher strontium concentration than the till porewater. Mixing between both waters in the modelled domain leads to an enrichment of strontium in illite and in the $(Ca,Sr)CO_3$ solid solution. The local equilibrium calculations developed for each time step lead to a retention of the added strontium in the solid phase that is lower than the increment of strontium in the aqueous phase, and therefore the Kd(Sr) decreases over

time in the area affected by the deep groundwater. From the moment when repository release is simulated, the Kd(Sr) (and also the Kd(RDSr)) varies little, since the geochemical quasi-steady state has been attained (Figure 5.5).

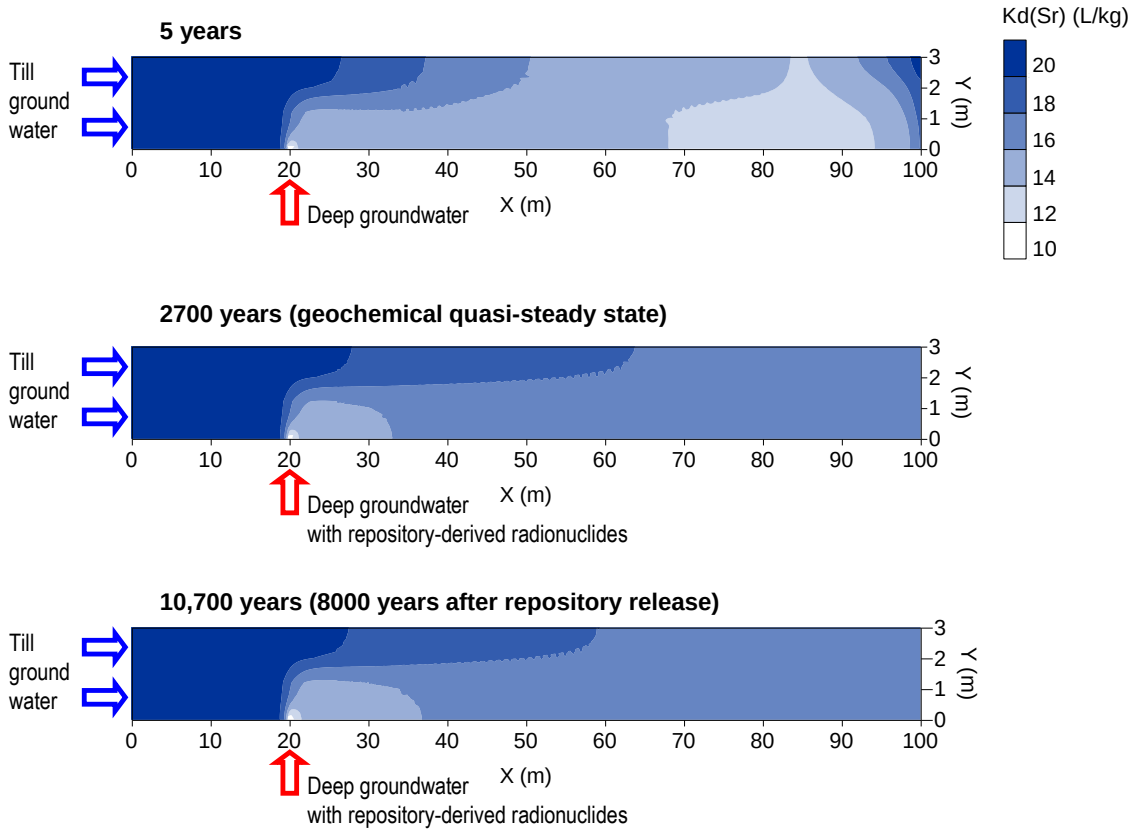

Figure 5.5 – Predicted evolution of Kd(Sr) along the simulation time. In the beginning of the simulation period the Kd varies with time. From 2700 years until the end of the simulation (10,700 years), relatively small geochemical changes occur, and hence Kd does not vary much.

Before the inflow of deep groundwater, caesium is present in the till porewater and adsorbed on illite, leading to an initially homogeneous Kd of 7950 $L \cdot kg^{-1}$ (data not shown). As already observed for uranium and strontium, the inflow of deep groundwater in the till deposit also leads to a decrease of the Kd of caesium in the area affected by the deep groundwater (Figure 5.6).

Deep groundwater has a much higher caesium concentration than the till porewater, and its intrusion leads to a remarkable enrichment of caesium in the FES of illite. Although this retention is relatively efficient, the amount of caesium retained in the solid phase, computed under local equilibrium for each time step, is lower than the increment of

caesium in the aqueous phase, and therefore the Kd(Cs) decreases along the simulation time.

From the moment when repository release is simulated both natural and repository-derived caesium are retained in the solid phase, resulting in a heterogeneous distribution of Kd in the mixing area of the modelled domain (lower image in Figure 5.6).

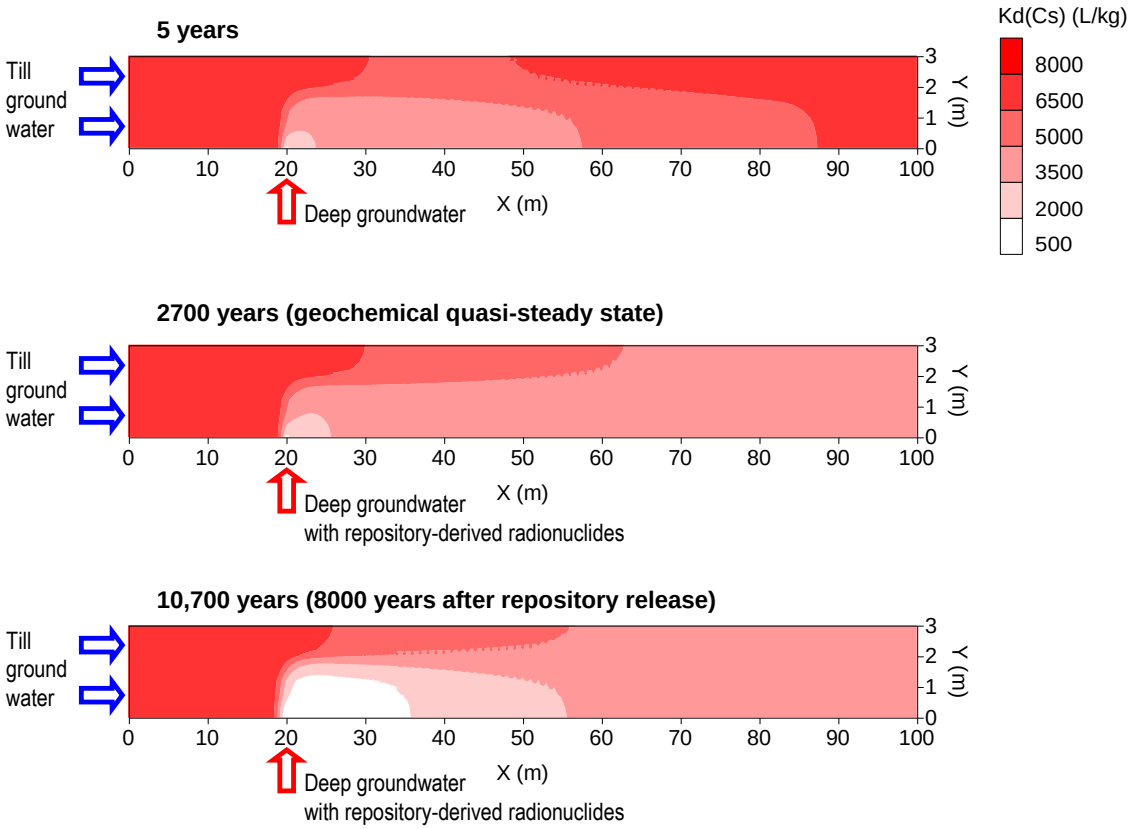

Figure 5.6 – Predicted evolution of Kd(Cs) along the simulation time. In the beginning of the simulation period the Kd varies with time. From 2700 years until the end of the simulation (10,700 years), relatively small geochemical changes occur, and hence Kd does not vary much.

The water sample selected for the till porewater is very close to equilibrium with barite. From the moment when the radionuclide-free deep groundwater, which has a higher sulphate concentration, enters the till domain, part of the mixing area reaches oversaturation with respect to barite and this mineral starts to precipitate in the vicinity of the deep groundwater inflow point. After repository release, the inflow of deep groundwater, carrying repository-derived radium, triggers the co-precipitation of radium with barite, retaining radium in the solid phase. Co-precipitation of radium with barite leads

to the partitioning of radium between aqueous and solid phases which is expressed by the distribution of the Kd(Ra) from 0 (where no barite has precipitated) to 7000 $L \cdot kg^{-1}$ (Figure 5.7).

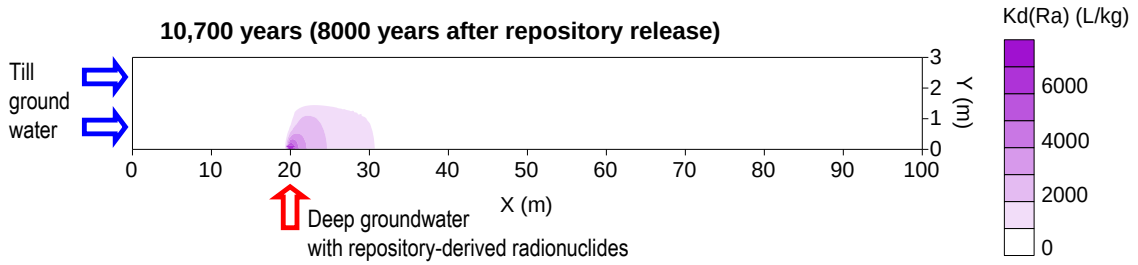

Figure 5.7 – Predicted distribution of Kd(Ra) at the end of the simulation time, 8000 years after repository release.

The previous paragraphs have shown that, before the simulation of repository release, the Kd of the natural isotopes of the selected radionuclides varies, in the modelled domain, over time and space. These variations are related to:

1. Mixing of the till groundwater and deep groundwater. The two waters have different concentrations of solutes, and different redox potential and pH. The mixing leads to concentration and dilution of solutes in the till system, depending on the relative concentration of solutes in both waters.
2. Local thermodynamic equilibrium. Changes in the aqueous concentration of reactive solutes imply changes in the composition of the solid phases that involve these reactive solutes.

After the establishment of the geochemical quasi-steady state, the Kd of the different radionuclides and their natural isotopes has small variations over time, but it is heterogeneous in space. Under this geochemical quasi-steady state, repository-derived radionuclides enter the Quaternary till and are partitioned along the mixing area between solid and aqueous phases, until finally be flushed out at the discharge area of the modelled domain.

5.4.3 Retention and breakthrough curves of repository-derived radionuclides

The reactive transport simulations predict that RDU, RDSr, RDCs, and Ra can be retained in the Quaternary till. In order to improve our understanding on the migration and retention of radionuclides in the Quaternary till, reactive and conservative transport simulations have been compared. In the reactive transport simulations, migration of repository-derived radionuclides is affected by their interaction with the reactive minerals in the modelled domain, while in the conservative transport simulations all reactive solutes, including repository-derived radionuclides, are simulated as conservative solutes, meaning that their interaction with the reactive minerals is neglected. The comparison between both simulations relies on the analysis of the breakthrough curves computed in each simulation (conservative and reactive transport) at the discharge area of the modelled domain (Figure 5.8).

When reactive transport is simulated, RDU is predicted to be retained in the Quaternary till by adsorption on ferrihydrite. In this case, the arrival of RDU to the discharge area is delayed approximately 2190 years with respect to its arrival when no interaction with the solid phase is considered (Figure 5.8a). The delay lag is calculated by subtracting the advective travel time computed in the reactive transport model to that computed in the conservative transport model.

In the reactive transport simulation, approximately 1000 years after repository release, the concentration of RDSr(aq), at the discharge area of the modelled domain, reaches a stationary value of 3.0×10^{-5} mol·L^{-1} (Figure 5.8b). The retention of RDSr in the Quaternary till delays its arrival to the discharge area approximately 350 years. The computed retention of RDSr is provided by cation exchange in illite and, to a less extent, to its co-precipitation with calcite.

The breakthrough curve computed for RDCs in the reactive transport simulation (Figure 5.8c) shows a remarkably slow tendency towards a stable maximum value. This slow increase of the concentration of RDCs(aq) at the discharge area of the Quaternary till is due to the high affinity of caesium for the FES of illite which readily retain RDCs in the solid phase of the modelled domain.

Deep groundwater affected by repository release has a radium concentration of 9.15×10^{-11} mol·L^{-1}. At the end of the reactive transport simulation, Ra(aq) concentration computed for the discharge area is 2.43×10^{-12} mol·L^{-1}, which is 74% of the maximum Ra(aq) concentration computed in the conservative transport simulation (Figure 5.8d). The

numerical results predict that radium is retained, via co-precipitation with barite, in the vicinity of the deep groundwater inflow point (Figure 5.7).

From the four radionuclides studied, radium is the only radionuclide that is solely influenced by the precipitation of a mineral phase (i.e. it is not involved in sorption reactions). Co-precipitation of radium with barite leads to an asymptotic breakthrough curve which is typical for those solutes solely influenced by the thermodynamic equilibrium with a mineral phase. This behaviour leads to a very slow increase of Ra(aq) at the final stage of the reactive transport simulation (Figure 5.8d).

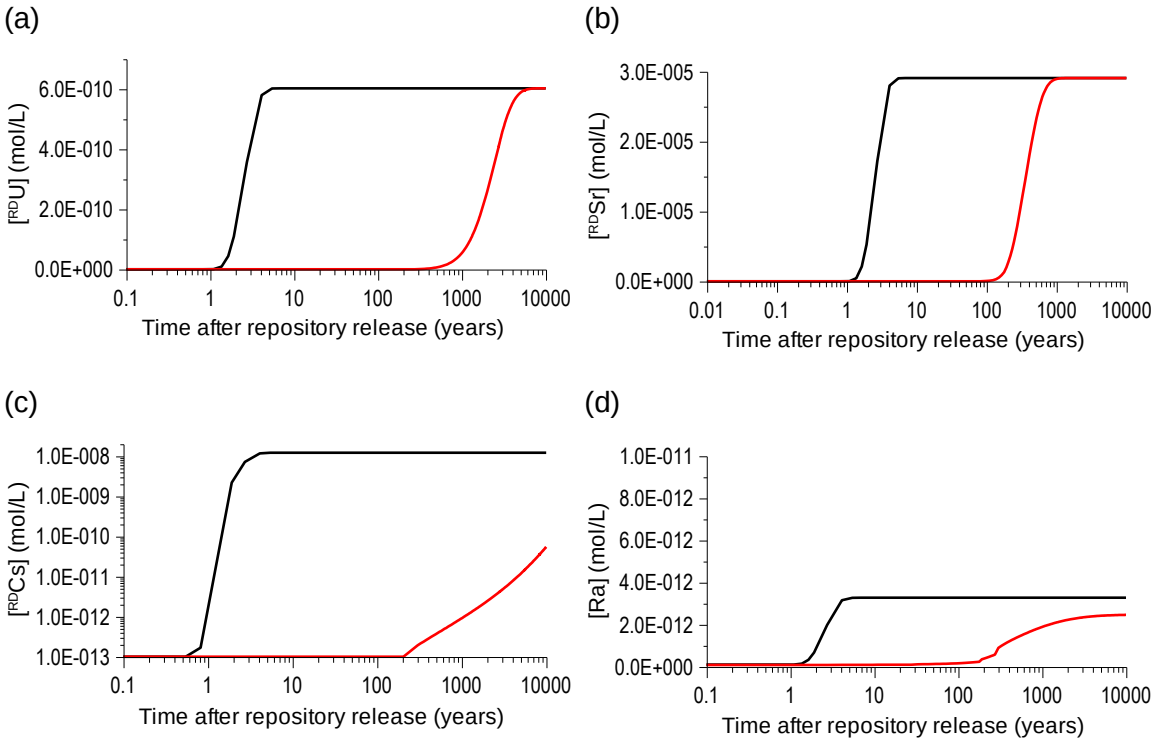

Figure 5.8 – Computed breakthrough curves at the discharge area of the modelled domain (node X= 80 m; Y= 3 m, see Figure 5.3) for repository-derived radionuclides, considering the geochemical reactions that affect radionuclide mobility (reactive transport, red line) and without considering any geochemical reaction (conservative transport, black line).

5.5 Retardation factor (R) of repository-derived radionuclides

The retardation factor (R) of a given reactive solute can be estimated from the numerical results according to two alternative procedures. If the computed breakthrough curve of a reactive solute (including the selected radionuclides) is complete, than R can be calculated from the following equation:

$$R = \frac{T^{R}_{1/2}}{T^{C}_{1/2}} \qquad \text{(equation 5.3)}$$

where $T^{R}_{1/2}$ is the advective travel time of the reactive solute in the reactive transport simulation, and $T^{C}_{1/2}$ is the advective travel time of the same solute in the conservative transport simulation. Equation 5.3 can be applied to estimate R for RDU and RDSr, for which complete breakthrough curves have been computed. By applying equation 5.3 we obtain an effective retardation factor of 956 for RDU and 156 for RDSr.

If the breakthrough curve of a reactive solute is not complete (i.e., the maximum stabilized concentration has not been reached, as for the case of RDCs and Ra), equation 5.3 cannot be used to calculate R. In this case, and assuming a fully water saturated porous media (such as the Quaternary till modelled here), and that the geochemical reactions between reactive solutes and the solid matrix occur as a singular and instantaneous process (such as the local thermodynamic equilibrium reactions simulated here), R can be calculated from the following equation that relates R with Kd_e:

$$R = 1 + Kd_e \cdot \frac{\rho_b}{\phi_e} \qquad \text{(equation 5.4)}$$

where Kd_e is the effective distribution coefficient [$L^{-3}M$], ρ_b is the dry bulk density of the sediment [$M\ L^{-3}$], and ϕ_ε is the effective porosity (-).

In case of incomplete breakthrough curves (RDCs and Ra in this work), equation 5.4 should provide the approach to calculate the corresponding R. Nevertheless, when applying equation 5.4 to calculate R one must have a single value for Kd_e and ϕ_ε which is not the case presented here; both these parameters are heterogeneous, as shown in section 5.4.2 and Table 5.1, respectively.

In order to find an effective porosity for the studied Quaternary till a conservative transport model was built using FEFLOW (Diersch, 2005). This model was calibrated using the values of the hydraulic parameters shown in Table 5.1, and adjusting a single effective porosity for the whole modelled domain that leads to the same conservative advective travel time as the one attained in the conservative transport model built in PHAST (Figure 5.3). The effective porosity attained from this calibration is 0.0789, which is approximately

the average of the kinematic porosities shown in Table 5.1 weighted by the thickness of the respective layers.

In Figure 5.9 a very good agreement between the breakthrough curve computed in PHAST and the calibrated conservative transport model computed in FEFLOW is observed.

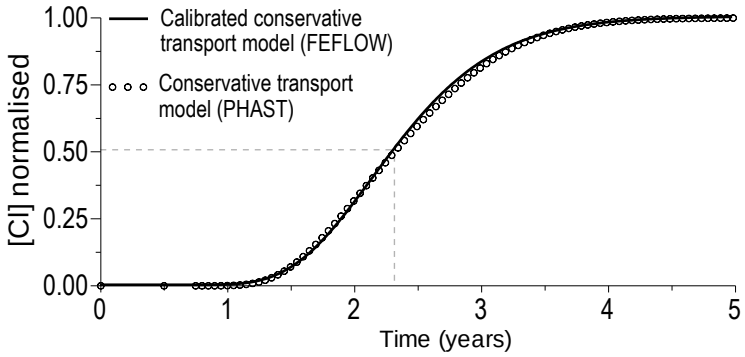

Figure 5.9 – Predicted breakthrough curves for a conservative solute in PHAST and the calibrated conservative transport model built in FEFLOW. Monitoring point X= 80 m, Y= 3 m (discharge area).

The effective porosity determined for the Quaternary till (in the simulation performed using FEFLOW) is able to reproduce the advective travel time computed when the kinematic porosity is stratified (PHAST simulation). This effective porosity is equivalent to the weighted average of the layered kinematic porosities that characterize the till deposit (Table 5.1). Now, the Kd_e for ^{RD}U and ^{RD}Sr (for which we have calculated R) must be found, and its mathematical meaning will be assessed, in order to provide a quantitative tool to calculate the effective Kd for ^{RD}Cs and Ra. Re-writing equation 5.3 to obtain the Kd_e, the following equation is obtained:

$$Kd_e = (R-1)\frac{\phi_e}{\rho_b} \qquad \text{(equation 5.5)}$$

and introducing the values listed below:

$R(^{RD}U) = 956$

$R(^{RD}Sr) = 156$

$\phi_\varepsilon = 0.0789$

ρ_b = 1.95 kg·L^{-1}

a Kd_e of 38.6 L·kg^{-1} for uranium and 6.27 L·kg^{-1} for strontium are obtained.

These values are clearly out of the range of the Kd values previously calculated for the modelled domain, shown in Figure 5.4 and Figure 5.5, respectively. This apparent discrepancy is due to the fact that the Kd obtained for the modelled domain, was calculated applying equation 5.2 which uses the total porosity (0.25) instead of the effective porosity (0.0789). These results reflect that as for porosity, where:

1. the kinematic porosity is related to the interconnected porous that contribute to the transport of solutes; and,
2. the total porosity accounts for all isolated and interconnected voids,

for Kd, it seems that a Kd related to the bulk of the sediment (total Kd), and a Kd only available for the transport of solutes (kinematic Kd) should exist.

If the effective porosity is applied in equation 5.2, to calculate the Kd in the modelled domain, the spatial distribution of kinematic Kd for the four radionuclides selected is obtained (Figure 5.10). The effective Kd previously calculated for RDSr (6.27 L·kg^{-1}) falls in the range of kinematic Kd's calculated for the modelled domain (3 to 7 L·kg^{-1}, in Figure 5.10), while the effective Kd previously calculated for RDU (38.6 L·kg^{-1}) is slightly higher than the maximum kinematic Kd (36 L·kg^{-1}, in Figure 5.10).

These results show that opposite to what was found for porosity, where the effective porosity is the weighted average of the kinematic porosities, it seems that the effective Kd may not be related to the range of kinematic Kd's by any statistic parameter. With these results we still cannot find a reliable way to calculate R for those radionuclides for which incomplete breakthrough curves have been computed. This would lead us to the ultimate option of computing longer time periods of reactive transport to achieve the complete breakthrough curves for RDCs and Ra. Since this is not the purpose of the present work, the breakthrough curves computed in the reactive transport model with those computed in Kd-based models for RDSr and RDU (for which we have complete breakthrough curves) will be compared, and the validity of R and respective Kd_e, calculated from the outputs of the reactive transport simulations, will be assessed.

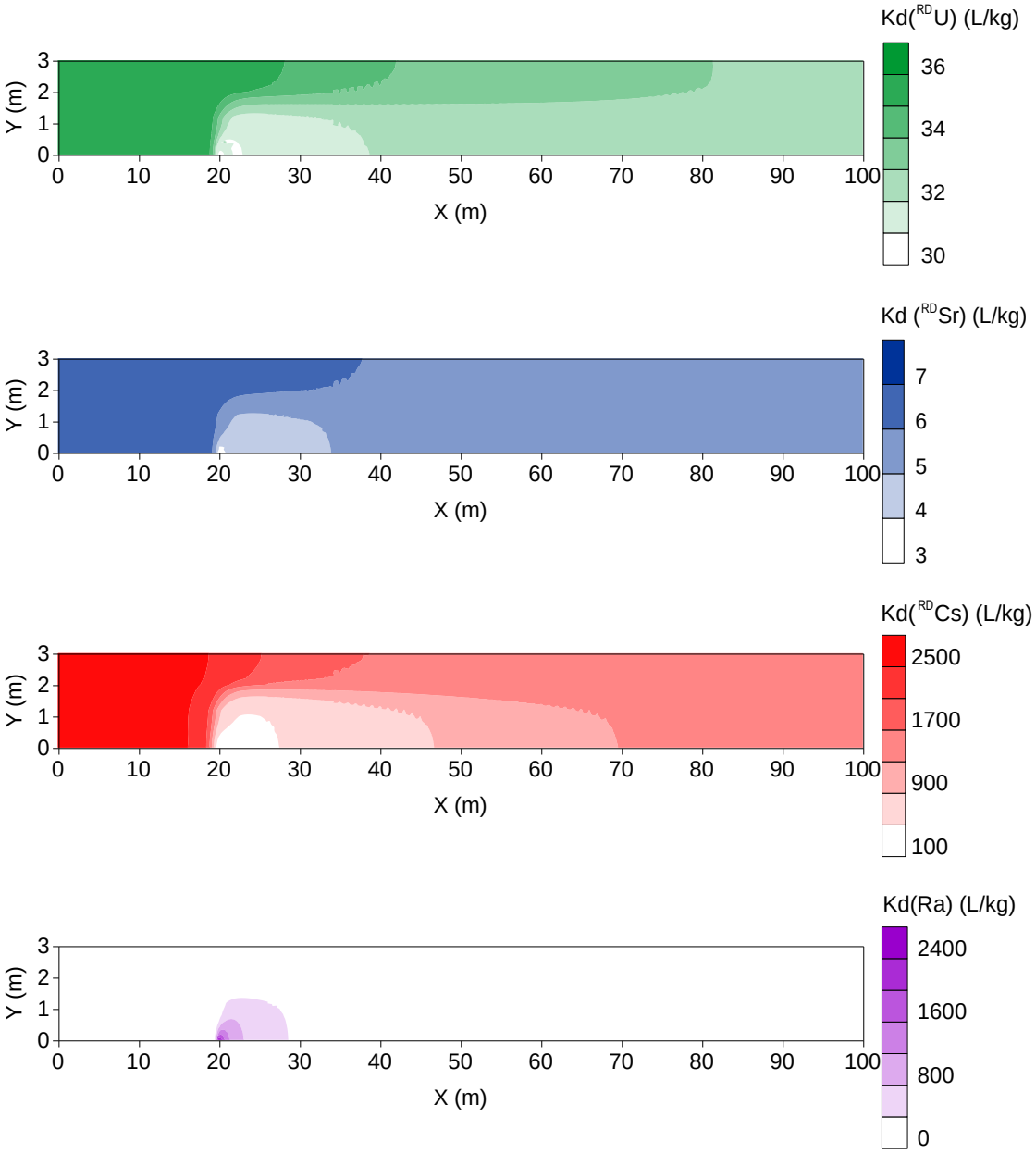

Figure 5.10 – Computed distribution of kinematic Kd for the selected radionuclides 8000 years after repository release. Kinematic Kd is calculated for each node of the modelled domain by applying equation 5.2, using the effective porosity (0.0789) instead of the total porosity (0.25).

The breakthrough curves computed for RDSr in the reactive transport model (using PHAST) and in the Kd-based model (using FEFLOW) agree relatively well (Figure 5.11). Nevertheless, one may see that depending on the solution method selected for the reactive transport model, an increased numerical dispersion appears if the solution method is backwards-in-time and upstream-in-space. Only when the solution method of

the reactive transport model is centred-in-time and centred-in-space, both models lead to the same numerical results. These results prove that the Kd_e and corresponding R, previously calculated for ^{RD}Sr, from the outputs of the reactive transport model, are reproducible in a Kd-based model. Therefore, when the system is in a geochemical quasi-steady state, as the one previously built prior to the simulation of repository release, a Kd-based model can be as reliable as a reactive transport model.

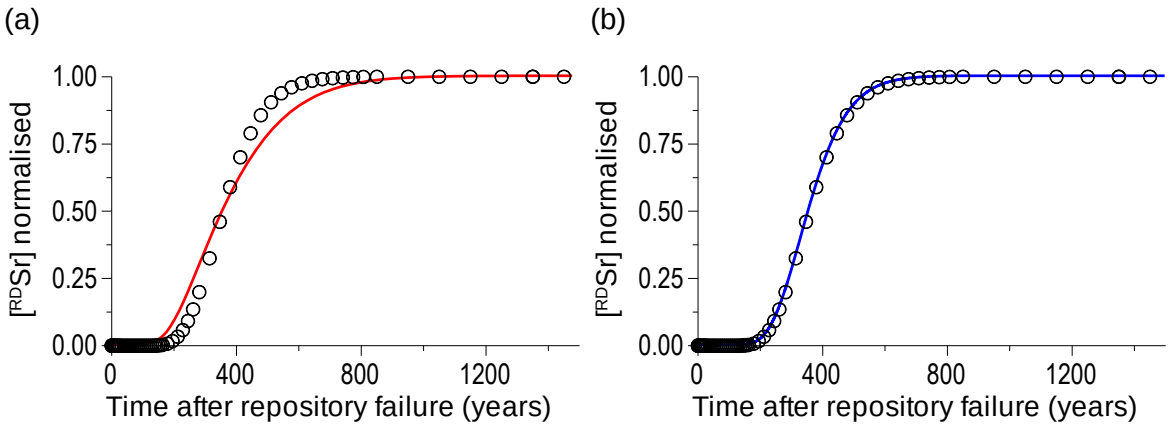

Figure 5.11 – Computed breakthrough curves for ^{RD}Sr normalised. Legend: symbols: Kd-based model computed in FEFLOW; red line: reactive transport model (computed in PHAST) solved backwards-in-time and upstream-in-space; blue line: reactive transport model (computed in PHAST) solved centred-in-time and centred-in-space.

As already seen for the case of ^{RD}Sr, the breakthrough curves computed for ^{RD}U in the reactive transport model (using PHAST) and in the Kd-based model (using FEFLOW) are relatively similar. In addition, by comparing the graph in Figure 5.11a with that in Figure 5.12a, it is possible to see that the dispersion computed for ^{RD}U is higher than in the case of ^{RD}Sr. This is most likely due to the cumulative effect of dispersion with time. As longer the simulation time, as more visible the effect of dispersion on the breakthrough curves of reactive solutes.

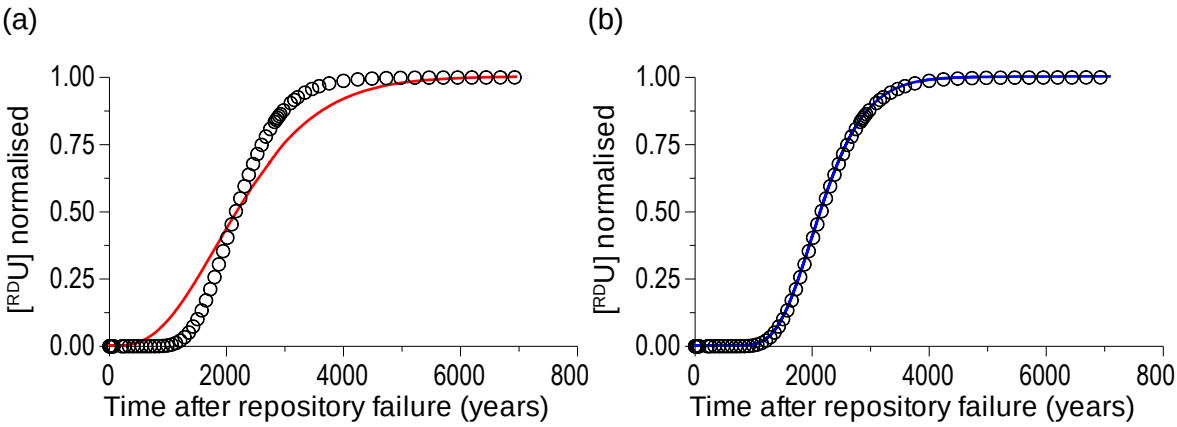

Figure 5.12 – Computed breakthrough curves for RDU normalised. Legend: symbols: Kd-based model computed in FEFLOW; red line: reactive transport model (computed in PHAST) solved backwards-in-time and upstream-in-space; blue line: reactive transport model (computed in PHAST) solved centred-in-time and centred-in-space.

5.6 Conclusions

HLNW is partially composed of long-lived radionuclides, such as U^{235}, Ra^{233}, Cs^{137}, and therefore, the assessment of the migration of these radionuclides in the systems surrounding a deep geological repository often relies on numerical transport models that provide powerful quantitative tools to cope with the long-term scenarios needed to face.

In this work, a reactive transport model that simulates a hypothetical pessimistic scenario of a continuous repository release, during 8000 years, has been built. The migration and retention of RDU, RDSr, RDCs and Ra through a Quaternary till that covers the candidate host rock at Forsmark (Sweden) have been assessed. The outputs of the reactive transport model show that the four radionuclides can be retained in the solid phase of the Quaternary till due to different geochemical processes: RDU is adsorbed on ferrihydrite; RDSr is retained via co-precipitation with calcite and cation exchange on illite; RDCs is also retained via cation exchange on illite; and, radium is retained via co-precipitation with barite. Retention of the radionuclides in the solid phase provides a retardation of their arrival to the discharge area of the Quaternary till.

The retardation factor of the radionuclides studied has been calculated, from the outputs of the reactive transport model, only for those radionuclides for which complete breakthrough curves have been computed (strontium and uranium). The estimation of the retardation factor for caesium and radium was not possible, since complete breakthrough curves have not been achieved. The high affinity of caesium for the FES of illite, and the

fact that radium is solely involved in co-precipitation reactions, delay the achievement of a complete breakthrough curve, and therefore, hinder the estimation of the corresponding retardation factor.

The validity of the retardation factor calculated for uranium and strontium, from the outputs of the reactive transport model, has been assessed by developing Kd-based models that accounted for the retardation factor so obtained.

In order to build the Kd-based models, the naturally stratified kinematic porosity had to be upscaled to an effective porosity which corresponds to the weighted average of the kinematic porosities. As for porosity, it has been proven that for Kd there is a total Kd and a kinematic Kd. The retardation factor of a reactive solute is related to an effective Kd which, in turn, is closer to the range of kinematic Kd's than to the range of total Kd's. In other words, it is the kinematic Kd the one responsible for the retardation of the transport of reactive solutes. In the present work, it has been proven that the kinematic Kd is usually lower than the total Kd. These results have a deep impact on the laboratory methods that are used to obtain a Kd value to be implemented in Kd-based models for performance assessment exercises.

As Reardon (1981) had concluded, we have demonstrated that when a given system reaches a geochemical quasi-steady state, a Kd-based model is able to provide numerical results as reliable as those attained in an equivalent reactive transport model. It should be noted, however, that the solution method selected for the reactive transport model may introduce additional numerical dispersion that is not computed in a Kd-based model. Finally, care must be taken when choosing the type of model to evaluate long-term contamination scenarios, since most likely these will undergo geochemical changes that are better coped in reactive transport numerical models than in Kd-based numerical models.

Acknowledgments

This work has been funded by SKB. Data and information used in this work were generated within the SKB's Site Investigation Program for location of a deep geological repository for the disposal of HLNW. The first author is grateful to the Portuguese Ministry of Science, Technology and Education for a PhD Grant (POCI 2010, BD/16647/2004). Special thanks are given to Sten Berglund and Tobias Lindborg for their support, encouragement and fruitful discussions during this work.

5.7 References

Appelo C.A.J. and Postma D. (2005) *Geochemistry, groundwater and pollution*. A.A. Balkema Publishers. The Netherlands, 649 pp.

Arcos D., Grandia F., Domènech C., Fernández A.M., Villar M.V., Muurinen A., Carlsson T., Sellin P. and Hernán P. (2008) Long-term geochemical evolution of the near field repository: insights from reactive transport modelling and experimental evidences. *Journal of Contaminant Hydrology*, 102: 196-209.

Bradbury M.H. and Baeyens, B. (2000) A generalised sorption model for the concentration dependent uptake of caesium by argillaceous rocks *Journal of Contaminant Hydrology*, 42: 141–163.

Bruno J., Duro L. and Grivé M. (2002) The applicability and limitations of thermodynamic geochemical models to simulate trace element behaviour in natural waters. Lessons learned from natural analogue studies. *Chemical Geology*, 190(1-4): 371-393.

Diersch H.J.G. (2005) *WASY software FEFLOW, Finite element subsurface flow and transport simulation system, user's manual*, Berlin, Germany.

Duro L., Grivé M., Cera E., Domènech C. and Bruno J. (2006a) *Update of a thermodynamic database for radionuclides to assist solubility limits calculation for performance assessment.* SKB report TR-06-17, Swedish Nuclear Fuel and Waste Management Co., Stockholm, Sweden

Duro L., Grivé M., Cera E., Gaona X., Domènech C., Bruno J. (2006b) *Determination and assessment of the concentration limits to be used in SR-Can*. SKB report TR-06-32, Swedish Nuclear Fuel and Waste Management Co., Stockholm, Sweden

Glynn P.D. (2003) Modeling Np and Pu transport with surface a complexation model and spatially variant sorption capacities: implications for reactive transport modelling and performance assessments of nuclear waste disposal sites. *Computers and Geosciences*, 29, 331-349.

Grandia F., Merino J. and Bruno J. (2008) *Assessment of the radium-barium co-precipitation and its potential influence on the solubility of Ra in the near-field*. SKB TR-08-07, Swedish Nuclear Fuel and Waste Management Co., Stockholm, Sweden

Grandia F., Sena C., Arcos D., Molinero J., Duro L. and Bruno J. (2007) *Quantitative assessment of radionuclide retention in the near-surface system at Forsmark.*

Development of a reactive transport model using Forsmark 1.2 data. SKB R-07-64, Svensk Kärnbränslehantering AB.

Johansson P.O., Werner K., Bosson E., Berglund S. and Juston J. (2005) *Description of climate, surface hydrology, and near-surface hydrogeology Preliminary site description. Forsmark area – version 1.2*. SKB R-05-06, Swedish Nuclear Fuel and Waste Management Co., Stockholm, Sweden

Kipp K.L. (1987) *HST3D – A computer code for simulation of heat and solute transport in three-dimensional ground-water flow systems.* U.S. Geological Survey Water-Resources Investigations Report 86-4095, 517 p.

Köhler S.J. Dufaud F. and Oelkers E.H. (2003) An experimental study of illite dissolution kinetics as a function of ph from 1.4 to 12.4 and temperature from 5 to 50°C. *Geochimica et Cosmochimica Acta*, 67-19: 3583–3594.

Molinero J. and Samper J. (2006) Large-scale modelling of reactive solute transport in fractured zones of granitic bedrocks. *Journal of Contaminant Hydrol*ogy, 82: 293-318.

Parkhurst D.L. and Appelo C.A.J. (1999) *User's guide to PHREEQC (version 2) – A computer program for speciation, batch-reaction, one-dimensional transport and inverse geochemical calculations*. U.S. Geological Survey Water Resources investigations report 99-4259, 312 pp.

Parkhurst D.L., Kipp K.L., Engesgaard P. and Charlton S.R. (2004) *PHAST: A program for simulating ground-water flow, solute transport, and multicomponent geochemical reactions*. U.S. Geological Survey Techniques and Methods 6-A8, 154 pp.

Reardon E.J. (1981) Kd's – can they be used to describe reversible ion sorption reactions in contaminant migration? *Ground Water*, 19(3): 279-286.

SKB (2005a) *Description of surface systems. Preliminary site description of Forsmark area – version 1.2.* SKB report R-05-03, Swedish Nuclear Fuel and Waste Management Co., Stockholm, Sweden.

SKB (2005b) *Preliminary site description Forsmark area – version 1.2.* SKB report R-05-18. Swedish Nuclear Fuel and Waste Management Co., Stockholm, Sweden.

SKB (2006) *Long-term safety for KBS-3 repositories at Forsmark and Laxemar-a first evaluation. Main report of the SR-Can project*. SKB report TR-06–09, Swedish Nuclear Fuel and Waste Management Co., Stockholm, Sweden

SKB (2009) Press release: *SKB selects Forsmark for the final repository for spent nuclear fuel*. In: http://www.skb.se/Templates.

Tesoriero A.J. and Pankow J.F. (1996) Solid solution partitioning of Sr^{2+}, Ba^{2+}, and Ca^{2+} to calcite. *Geochimica et Cosmochimica Acta,* 60-6: 1053–1064.

Tröjbom M. and Söderbäck B. (2006) *Chemical characteristics of surface systems in the Forsmark area. Visualisation and statistical evaluation of data from shallow groundwater, precipitation, and regolith.* SKB report R-06-19, Swedish Nuclear Fuel and Waste Management Co., Stockholm, Sweden.

Tröjbom M., Söderbäck B. and Johansson P.O. (2007) *Hydrochemistry in surface water and shallow groundwater. Site descriptive modelling (SDM) – Site Forsmark*. SKB report R-07-55, Swedish Nuclear Fuel and Waste Management Co., Stockholm, Sweden

Waite T. D. Davis J.A. Payne T.E. Waychunas G.A. and Xu N. (1994) Uranium (VI) adsorption to ferrihydrite: Application of a surface complexation model. *Geochimica et Cosmochimica Acta*, 58: 5465–5478.

Chapter 6

Summary, conclusions and discussion

6. Summary, conclusions and discussion

6.1 Summary and Conclusions

The main geochemical processes that influence the migration of radionuclides in near-surface systems have been studied in the present work.

Hydrogeochemical numerical models have been developed to simulate both laboratory and field scale multicomponent problems. These simulations provided the assessment and quantification of the processes that are likely to influence the behaviour of radionuclides in near-surface systems. The numerical models developed here are based on two hydrogeochemical codes: PHREEQC (Parkhurst and Appelo, 1999) and PHAST (Parkhurst et al., 2004). The first code is widely used for at least a decade, in the context of different environmental and scientific issues, while the second code is not so widespread but it results from coupling the first code with a transport code (HST3D, Kipp, 1987). Therefore, the code PHAST is useful when dealing with complex geochemical systems coupled with the transport of solutes such as the ones studies here, and also when the problem cannot be reduced to 1D. Finally, in Chapter 5 a third code has been used (FEFLOW, Diersch, 2005) to compare Kd-based transport models with the reactive transport models previously developed using PHAST (Parkhurst et al., 2004).

A descriptive numerical model has been developed in Chapter 2 of this thesis to simulate a jar-fermentor experiment where evidences of microbially driven redox reactions have been observed.

Microbially driven redox reactions are interpreted as the oxidation of organic carbon by microbes, and subsequent reduction of inorganic species that are available in the surrounding aquatic system. The linkage between microbial activity and the redox sensitive species has been conceptualized through the partial equilibrium approach (Barry et al., 2002; Brun and Engesgaard, 2002) which assumes that the rate limiting step is the oxidation of organic matter, and that the subsequent reduction of inorganic species occurs under local equilibrium. In the present work, this approach has been successfully applied to the reduction of dissolved oxygen, nitrate, sulphate, ferric iron, and fermentation of lactate, mediated by aerobes, denitrifiers, sulphate reducing bacteria, iron reducing bacteria, and fermenters, respectively, but not to microbially driven methanogenesis.

Besides the partial equilibrium approach, the Monod growth model was also applied in Chapter 2, to simulate microbial respiration and growth, taking into account, half-

saturation constants for the organic and inorganic substrates, and also inhibition terms that describe the sequential use of terminal electron acceptors (O(II), N(V), Fe(III), S(VI), acetate and C(VI)). Coupling of the partial equilibrium approach with the Monod growth model seems to provide a solid theoretical basis, able to accurately describe microbially driven redox reactions. In addition, by considering that when microbial biomass grows, the elements carbon, hydrogen, oxygen and nitrogen are removed from solution according to the stoichiometry of a simplified biomass molecule ($C_5H_7O_2N$) and vice-versa, a robust mass balance between biomass and the different phases (solid, aqueous and gaseous) of the inorganic aquatic system of the jar-fermentor has been achieved.

The numerical results achieved in Chapter 2 prove that, if microbes and organic matter are available at repository depth, dissolved oxygen, one of the most damaging species for a metallic over pack, may be consumed relatively fast, while HS^- (which may also corrode the metallic over pack) may be produced by sulphate reducing bacteria. Nevertheless, sulphur secondary phases may precipitate and limit the concentration of HS^-.

Uncertainties on the Monod parameters provide the possibility for different combinations of these parameters which lead to similar numerical solutions. Nevertheless, these different combinations of the Monod parameters lead to different partitioning of carbon between biomass and the different phases of the inorganic carbon system (aqueous, solid, and gaseous). Should more variables be analysed in future experiments, such as the concentration of Ca^{2+}, the amount of carbonate minerals, and the initial and final concentration of the different microbial groups, some uncertainties on the Monod parameters could be constrained.

Two predictive numerical models have been developed in Chapters 3 and 4, to assess the retention capacity of the near-surface systems at Forsmark (Sweden) under a pessimistic scenario of repository release and subsequent arrival of radionuclides to the near-surface Quaternary sediments (glacial clay and calcite-rich till). Comparison between the outputs of the numerical models developed for the glacial clay and the calcite-rich till with measured concentrations of reactive solutes such as bicarbonate, calcium, strontium and uranium, has proven the reliability of the conceptual model built for these systems. Under this premise, a hypothetical repository release has been simulated through a continuous injection of repository-derived radionuclides into both Quaternary sediments. The outputs of this hypothetical repository release into the Quaternary sediments have provided a quantitative assessment of the capacity of the glacial clay and the calcite-rich till to retain the four radionuclides selected: ^{235}U, ^{90}Sr, ^{135}Cs and ^{226}Ra.

Taking into account the knowledge attained from the data gathered until now, and under the assumptions made for each near-surface system, it is possible to conclude that the four radionuclides studied are likely to be efficiently retained in the till and glacial clay for at least several hundreds of years. Exception is made for radium in the glacial clay where it seems that it could be mobile.

Finally, it has been seen in Chapter 5 that the Kd of reactive solutes may vary over time and space. Nevertheless, when the geochemical quasi-steady state is approached in the numerical model, effective Kd's may be calculated from the outputs of such numerical model. The validity of these effective Kd's has been assessed in Kd-based transport models developed in FEFLOW (Diersch, 2005). In order to build these Kd-based models, the naturally stratified kinematic porosity had to be upscaled to an effective porosity which corresponds to the weighted average of the kinematic porosities. As for porosity, it has been proven that also for Kd there is a total Kd and a kinematic Kd.

The retardation factor of a reactive solute is related to an effective Kd which in turn is closer to the range of kinematic Kd's than to the range of total Kd's. These results have a deep impact on the laboratory methods that are used to obtain a Kd value to be implemented in Kd-based models within performance assessment exercises.

The laboratory methods performed to calculate the Kd of a given radionuclide are often based on batch experiments. The Kd calculated from such experiments corresponds to the total Kd, and this total Kd is higher than the kinematic Kd that would be obtained from a column experiment. Total Kd would then lead to the estimation of a longer advective travel time of a given radionuclide compared with the travel time obtained if the kinematic Kd would be used. By considering a longer travel time than the one that could actually be observed, the safety assessment based on total Kd's would lead to less conservative predictions. Therefore, in the context of safety assessment, it is recommended to study the kinematic Kd's instead of the total Kd's.

6.2 Discussion

The work presented has contributed to improve our understanding on the (bio)geochemical and hydrodynamic processes that influence radionuclide mobility in near-surface systems. The numerical implementation of the conceptual models built for each case has been accurately developed. Despite the successful results attained in each numerical model, some unsolved problems still exist, some of which provide ideas for future works, others can be viewed as weak points of this thesis, and others reflect the

need for further development in computational power or more efficient numerical models, and additional thermodynamic data.

In the next paragraphs the main unsolved questions that prevail after the development of the research work described in Chapters 2 to 5 are discussed.

6.2.1 Chapter 2: lactate fermentation and the inorganic carbon system

In Chapter 2, propionate evolution is still not well understood and consequently not well simulated. The stoichiometry of lactate fermentation implemented here has been reported by others (von Gunten and Zobrist, 1993, among others). Nevertheless, the most probable cause for overestimation of propionate seems to be an apparently unsuitable stoichiometry of lactate fermentation for the jar-fermentor experiment modelled here. These results point to the hypothesis that lactate fermentation could vary depending on the environment in which it takes place.

Methane production is far overestimated, while for carbon dioxide the opposite is true. The most probable reason for the overestimation of methane could be due to the fact that, as for the other types of microbial respiration considered in the numerical model, microbial methanogenesis is simulated following the partial equilibrium approach. Under this premise, the local equilibrium reaction that describes the reduction of C(IV) to C(-IV) has been maintained in the thermodynamic database. By doing so, the numerical model computes an excess of methane production. An alternative to this assumption would be that methane could be solely produced through kinetics. Nevertheless, under this alternative assumption, the change in the oxidation state of carbon, from C(IV) to C(-IV), could not be coupled to the redox potential since this equilibrium reaction would have had to be discarded from the thermodynamic database. These uncertainties point to the following questions:

Is the thermodynamic constant of the reaction that describes the reduction of HCO_3^- to CH_4:

$$HCO_3^-(aq) + 9H^+(aq) + 8e^- \leftrightarrow CH_4(aq) + 3H_2O(l) \quad \log k = 27.8493$$

(equation 6.1)

, used in the numerical model, suitable in systems where microbial methanogenesis takes place? Should a different thermodynamic constant be used when microbial methanogenesis prevails? What would be the applicability of such constant to other systems?

The uncertainties related to methane production have inevitable consequences on the accuracy of modelled carbon dioxide production. Therefore, the simulated evolution of carbon dioxide also shows a poor agreement with measured data.

The precipitation/dissolution of carbonate minerals should also influence the carbon system. Under the assumptions made for conceptual model that describes the behaviour of the carbon system, the numerical model developed in Chapter 2 fails to reproduce methane and carbon dioxide production. As previously mentioned, future experiments with additional measured data could help to improve our understanding on the evolution of the carbon system in environments where microbial activity plays an important role.

6.2.2 Chapter 3: geochemical behaviour of radium in the glacial clay

In Chapter 3, from the four radionuclides considered in the numerical model, radium is predicted to be mobile, i.e., it is not retained in the solid phase. In this numerical model, radium was let to co-precipitate with barite if oversaturation with this phase is reached. Nevertheless, since barite oversaturation was not computed for the glacial clay modelled in Chapter 3, radium was not predicted to be retained in the solid phase of the glacial clay. Should other phases be considered to react with radium, such as barium carbonate ($BaCO_3$), which has been reported as a feasible process by others (Andrews et al., 1989), radium could have been predicted to be retained in the glacial clays at Forsmark.

6.2.3 Chapters 3 and 4: coupling of wider and more complex geological settings

Looking at the work presented in Chapters 3 and 4, one could ask: Why were the glacial clay and till systems, which are by nature hydraulically connected, modelled separately? Could they have been integrated in a single and more complex numerical model? Most probably yes. In fact, during the construction of the reactive transport numerical models, we have tried to couple both sediments in a single numerical model. Nevertheless, some difficulties have arisen related to both the conceptualization and the numerical implementation of the hydrodynamic and geochemical processes responsible for the differentiation between both sediments. Therefore, for the time being, both sediments have been modelled separately.

Following the reasoning of the previous paragraph, one could ask if the whole system, from the deep geological repository, passing through the ~500 m of granite, to the near-

surface systems, could have been simulated in a single reactive transport model, and therefore more accurate predictions could have been made. I might say that human actions tend to augment the range of possible things and these depend on the time at which a question to be solved is posed and the schedule that one has to face to give the answer. I would say it is possible, and theoretically, such a complex hydrogeochemical model is nearing its accomplishment.

In addition to the geochemical processes that have been implemented in the numerical simulations developed in Chapters 3 and 4, other geochemical processes could influence radionuclide migration in the glacial clay and till sediments. Nevertheless, uncertainties on (1) site specific data, (2) the mechanisms inherent to the geochemical processes, and (3) the lack of thermodynamic and kinetic parameters hinder the implementation of additional geochemical processes.

The additional geochemical processes relevant for the glacial clay and till sediments that could be implemented in future works are:

- Microbial activity. The work developed in Chapter 2 has proven the role of microbial activity on the redox state of aquatic systems, and therefore, the mobility of redox sensitive radionuclides such as uranium may be remarkably modified in the presence of microbial activity.
- Sorption on organic tissues. The glacial clays at Forsmark may have organic matter-rich layers (Tröjbom and Söderbäck, 2006) where sorption of radionuclides on solid organic matter could be a relevant process for the cycling of radionuclides in near-surface systems (Hou et al., 2003).
- Colloid-borne radionuclide transport. Colloid-borne radionuclide transport may be a relevant process on the migration of radionuclides (van de Weerd and Leijnse, 1997). Nevertheless, the uncertainties related to the mechanisms that underlie the radionuclide attachment to colloid particles and subsequent colloid mobility hinder the simulation of the interaction between radionuclides and colloids.

6.2.4 Chapters 3 and 4: reliability of the numerical predictions

The final question I would pose to the work presented here is how reliable are the predictive models developed for the near-surface systems at Forsmark. We have performed long periods of reactive transport to reproduce the hydrogeochemical conditions observed nowadays at Forsmark, the outputs of which have shown a relatively good agreement with observed data; namely, the molar ratio between bicarbonate and

uranium, and the molar ratio between calcium and strontium in the aqueous phase, computed in the numerical models developed in Chapters 3 and 4, fall within the range of data actually measured at Forsmark. Therefore, if the topography and hydrology of the Forsmark area will not change much for the next ~2500 years, the numerical predictions made here can be viewed as relatively reliable under the pessimistic scenario that has been assumed.

6.2.5 Chapter 5: uncertainties on the parameterization of solute transport

In Chapter 5, the reliability of Kd-based models compared to reactive transport models has been assessed. This work has proven that only when the system is under geochemical quasi-steady state conditions, Kd-based models can provide as reliable estimates as reactive transport models. Nevertheless, uncertainties on the Kd value to be applied in Kd-based models must be assessed through proper sensitivity analyses. On the other hand, in reactive transport models, uncertainties related to the values of effective diffusion coefficients, longitudinal and transverse dispersivities also apportion additional uncertainties to the results of reactive transport models. In this context, future sensitivity analyses on the magnitude of these parameters should be performed to assess the influence of these parameters on the predictions for radionuclide mobility in near-surface systems.

6.3 References

Andrews J.N., Ford D.J., Hussain N., Trivedi D., Youngman M.J. (1989) Natural radioelement solution by circulating ground waters in the Stripa granite. *Geochimica et Cosmochimica Acta* 53, 1791–1802.

Barry D.A., Prommer H., Miller C.T. Engesgaard P., Brun A. and Zheng C. (2002) Modelling the fate of oxidisable organic contaminants in groundwater. *Advances on Water Resources*, 25: 945-983.

Brun A. and Engesgaard P. (2002) Modelling of transport and biogeochemical processes in pollution plumes: literature review and model development. *Journal of Hydrology*, 256: 211 – 227.

Diersch H.J.G. (2005) *WASY software FEFLOW, Finite element subsurface flow and transport simulation system, user's manual*, Berlin, Germany.

Hou X.L., Fogh C.L., Kucera J., Andersson K.G., Dahlgaard H. and Nielsen S.P. (2003) Iodine-129 and Caesium-137 in Chernobyl contaminated soil and their chemical fractionation. *The Science of the Total Environment*, 308(1-3): 97-109.

Kipp K.L. (1987) *HST3D – A computer code for simulation of heat and solute transport in three-dimensional ground-water flow systems.* U.S. Geological Survey Water-Resources Investigations Report 86-4095, 517 p.

Parkhurst D.L. and Appelo C.A.J. (1999) *User's guide to PHREEQC (version 2) – A computer program for speciation, batch-reaction, one-dimensional transport and inverse geochemical calculations*. U.S. Geological Survey Water Resources investigations report 99-4259.

Parkhurst D.L., Kipp K.L., Engesgaard P. and Charlton S.R. (2004) *PHAST: A program for simulating ground-water flow, solute transport, and multicomponent geochemical reactions*. U.S. Geological Survey Techniques and Methods 6-A8, 154 pp.

Tröjbom M. and Söderbäck B. (2006) *Chemical characteristics of surface systems in the Forsmark area. Visualisation and statistical evaluation of data from shallow groundwater, precipitation, and regolith.* SKB report R-06-19, Swedish Nuclear Fuel and Waste Management Co., Stockholm, Sweden.

van de Weerd H. and Leijnse A. (1997) Assessment of the effect of kinetics on colloid facilitated radionuclide transport in porous media. *Journal of Contaminant Hydrology*, 26(1-4): 245-256.

von Gunten U. and Zobrist J. (1993) Biogeochemical changes in groundwater-infiltration systems: Column studies. *Geochimica et Cosmochimica Acta*, 57, 3895-3906.

Appendix 1

Appendix 1

In Table A1.1, the cation exchange model applied in the numerical simulations developed in Chapters 3 to 5 is shown.

Table A1.1 - Cation exchange reactions and thermodynamic constants in the illite interlayer.

Reaction	Log K (25ºC)	Reference
Total exchange capacity (CEC) = 200 meq/kg		
Planar sites (0.8 × CEC)		
$X^- + Na^+ \leftrightarrow NaX$	0.0	(1)
$X^- + K^+ \leftrightarrow KX$	1.1	(1)
$X^- + Cs^+ \leftrightarrow CsX$	1.6	(1)
$2X^- + Sr^{2+} \leftrightarrow SrX_2$	1.5	(2)
$2X^- + Ca^{2+} \leftrightarrow CaX_2$	1.3	(3)
$2X^- + Mg^{2+} \leftrightarrow MgX_2$	1.5	(3)
Type II sites (0.2 × CEC)		
$X^{II-} + Na^+ \leftrightarrow NaX^{II}$	0.0	(1)
$X^{II-} + K^+ \leftrightarrow KX^{II}$	2.1	(1)
$X^{II-} + Cs^+ \leftrightarrow CsX^{II}$	3.6	(1)
Frayed edge sites (FES) (0.0025 × CEC)		
$X^{FES-} + Na^+ \leftrightarrow NaX^{FES}$	0.0	(1)
$X^{FES-} + K^+ \leftrightarrow KX^{FES}$	2.4	(1)
$X^{FES-} + Cs^+ \leftrightarrow CsX^{FES}$	7	(1)
$X^{FES-} + NH_4^+ \leftrightarrow NH_4X^{FES}$	3.5	(1)

(1) /Bradbury and Baeyens 2000/. (2) /Cole et al. 2000/. (3) /Tournassat et al. 2007/.

In Table A1.2, the dissolution reactions of the minerals considered in the numerical simulations developed in Chapters 3 to 5, with the corresponding thermodynamic constants, are listed. All reactions are simulated under local thermodynamic equilibrium.

Table A1.2 – Dissolution/precipitation reactions of the reactive solid phases considered in the numerical simulations developed in Chapters 3 to 5. Thermodynamic equilibrium constants and corresponding references are also listed.

Reaction	Log K (25ºC)	Reference
Calcite: $CaCO_3 + H^+ \leftrightarrow Ca^{2+} + HCO_3^-$ (I)	+1.85	(1)
Strontianite: $SrCO_3 + H^+ \leftrightarrow Sr^{2+} + HCO_3^-$ (I)	+1.05	(1)
Barite: $BaSO_4 \leftrightarrow Ba^{2+} + SO_4^{2-}$ (II)	-9.97	(2)
$RaSO_{4(cr)} \leftrightarrow Ra^{2+} + SO_4^{2-}$ (II)	-10.26	(3)
Siderite:$FeCO_3 + H^+ \leftrightarrow Fe^{2+} + HCO_3^-$	-0.47	(4)
Gypsum:$CaSO_4 \cdot 2H_2O \leftrightarrow Ca^{2+} + SO_4^{2-} + 2H_2O$	-4.85	(4)
Quartz: $SiO_2 + H_2O \leftrightarrow Si(OH)_4$	-3.75	(5)
Pyrite: $FeS_2 + 2H^+ + 2e^- \leftrightarrow Fe^{2+} + 2HS^-$	-18.5	(6)
Hydroxilapatite: $Ca_5(OH)(PO_4)_3$ +4H+ $\leftrightarrow H_2O + 3HPO_4^{2-} + 5Ca^{2+}$	-3.07	(7)
$UO_2 \cdot 2H_2O_{(am)} + 4H+ \leftrightarrow U^{4+} + 4H_2O$	+1.50	(8)
Ferrihydrite: $Fe(OH)_{3\,(am)} + 3H^+ \leftrightarrow Fe^{3+} + 3H_2O$	+5.00	(9)
Uranophane: $Ca(UO_2)_2(SiO_3OH)_2 \cdot 5H_2O + 6H+ \leftrightarrow Ca^{2+} + 2UO_2^{2+} + 2Si(OH)_4 + 5H_2O$	+9.42	(10)
Becquerelite: $Ca(UO_2)_6O_4(OH)_6:8H_2O + 14H+ \leftrightarrow Ca^{2+} + 6UO_2^{2+} + 18H_2O$	+29.00	(11)
Soddyite: $(UO_2)_2SiO_4 \cdot 2H_2O + 4H+ \leftrightarrow 2UO_2^{2+} + Si(OH)_4 + 2H_2O$	+5.00	(12)
Schoepite: $UO_3 \cdot 2H_2O + 2H+ \leftrightarrow UO_2^{2+} + 3H_2O$	+5.96	(13)

(I) Minerals involved in the $Ca_{1-X}Sr_XCO_3$ solid solutions.

(II) Minerals involved in the $Ba_{1-X}Ra_XSO_4$ solid solutions.

(1) Plummer and Busenberg, 1982; (2) Blount, 1997; (3) Langmuir and Riese, 1985; (4) Nordstrom et al., 1990 ; (5) Cox et al., 1989 ; (6) Robbie and Waldbaum 1968 ; (7) Johnson et al., 2000; (8) Guillamont et al., 2003; (9) Hummel et al., 2002 (10) Nguyen et al., 1992; (11) Casas et al., 1997; (12) Pérez et al., 1997; (13) Bruno and Sandino, 1989.

The surface complexation model for ferrihydrite, implemented in the numerical model developed in Chapter 4, is that of Waite et al. (1994). This model considers two types of adsorption sites (of strong and weak binding, respectively). The adsorbable species and corresponding constants are listed in Table A1.3. The total concentration of sites is 0.875 mol per mol of ferrihydrite (Waite et al., 1994). Most of these sites are of low affinity (weak binding) and only 0.0018 mol per mol of ferrihydrite correspond to high-affinity (strong binding) sites.

Table A1.3 – Complexation reactions on ferrihydrite surface and corresponding thermodynamic constants (from Waite et al., 1994).

Reaction	Log K (25ºC)
Strong sites (1.8×10^{-3} $mol_{site} \cdot mol_{Fe(OH)3}^{-1}$)	
$\equiv HFO^{s}OH + H^{+} \leftrightarrow \equiv HFO^{s}OH^{2+}$	6.51
$\equiv HFO^{s}OH \leftrightarrow \equiv HFO^{s}O^{-} + H^{+}$	-9.13
$\equiv HFO^{s}OH + UO_2^{2+} \leftrightarrow \equiv (HFO^{s}O)_2UO_2 + 2H^{+}$	-2.57
$\equiv HFO^{s}OH + UO_2^{2+} + CO_3^{2-} \leftrightarrow \equiv (HFO^{s}O)_2UO_2CO_3^{2-} + 2H^{+}$	3.67
$\equiv HFO^{s}OH + CO_3^{2-} + 2H^{+} \leftrightarrow \equiv HFO^{s}CO_3H + H_2O$	19.50
$\equiv HFO^{s}OH + CO_3^{2-} + H^{+} \leftrightarrow \equiv HFO^{s}CO^{3-} + H_2O$	11.51
Weak sites (0.875 $mol_{site} \cdot mol_{Fe(OH)3}^{-1}$)	
$\equiv HFO^{w}OH + H^{+} \leftrightarrow \equiv HFO^{w}OH^{2+}$	6.51
$\equiv HFO^{w}OH \leftrightarrow \equiv HFO^{w}O^{-} + H^{+}$	-9.13
$\equiv HFO^{w}OH + UO_2^{2+} \leftrightarrow \equiv (HFO^{w}O)_2UO^{2} + 2H^{+}$	-6.28
$\equiv HFO^{w}OH + UO_2^{2+} + CO_3^{2-} \leftrightarrow \equiv (HFO^{w}O)_2UO_2CO_3^{2-} + 2H^{+}$	-0.42
$\equiv HFO^{w}OH + CO_3^{2-} + 2H^{+} \leftrightarrow \equiv HFO^{w}CO_3H + H_2O$	19.50
$\equiv HFO^{w}OH + CO_3^{2-} + H^{+} \leftrightarrow \equiv HFO^{w}CO^{3-} + H_2O$	11.51

A1. References

Blount C.W. (1997) Barite solubilities and thermodynamic quantities up to 300ºC and 1400 bars. *American Mineralogist*, 62: 942-957.

Bradbury M.H. and Baeyens, B. (2000) A generalised sorption model for the concentration dependent uptake of caesium by argillaceous rocks *Journal of Contaminant Hydrology*, 42: 141–163.

Bruno J. and Sandino A. (1989) The solubility of amorphous and crystalline schoepite in neutral to alkaline aqueous solutions. *Materials Research Society Symposium Proceedings* 127, 871-878.

Casas I., Bruno J., Cera E., Finch R.J. and Ewing R.C. (1997) Characterization and dissolution behaviour of a Becquerelite from Shinkolobwe, Zaire. *Geochimica et Cosmochimica Acta*, 61: 3879-3884.

Cole T., Bidoglio G., Soupioni M., O'Gorman M. and Gibson N. (2000) Diffusion mechanisms of multiple strontium species in clay. *Geochimica et Cosmochimica Acta,* 64(3): 385-396.

Cox J.D., Wagman D.D., Medvedev V.A. (1989) *CODATA Key Values for Thermodynamics*, Hemisphere Publishing Corp., New York.

Guillaumont R., Fanghänel J., Neck V., Fuger J., Palmer D.A., Grenthe I. and Rand M.H. (2003) *Chemical Thermodynamics 5. Update on the Chemical Thermodynamics of Uranium, Neptunium, Plutonium, Americium and Technetium.* NEA OECD, Elsevier.

Hummel W., Berner U., Curti E., Pearson F.J., and Thoenen T. (2002) *Nagra/PSI Chemical Thermodynamic Data Base 01/01.* ISBN: 1-58112-620-4. 565 pp

Johnson J., Anderson G. and Parkhurst D. (2000) *Database from "thermo.com.V8.R6.230". Prepared by at Lawrence Livermore National Laboratory* (revision 1.11). LLNL report.

Langmuir D. and Riese A.C. (1985). The thermodynamic properties of radium. *Geochimica et Cosmochimica Acta*, 49: 1593-1601.

Nguyen N.S., Silva R.J., Weed H.C., Andrews Jr J.E. (1992) Standard Gibbs free energies of formation at the temperature 303.15K of four Uranyl silicates: soddyite, uranophane, sodium boltwoodite and sodium weeksite. *Journal of Chemical Thermodynamics*, 24, 1, 359-376.

Nordstrom D.K., Plummer L.N., Langmuir D., Busenberg E., May H.M., Jones B.F., Parkhurst D.L. (1990) Revised chemical equilibrium data for major water-mineral reactions and their limitations. In R.L. Bassett and D. Melchior, (eds.), Chemical modelling in aqueous systems II: Washington D.C., *American Chemical Society Symposium Series 416*, Chapter 31: 398-413.

Pérez I., Casas I., Torrero M.E., Cera E., Duro L. and Bruno J. (1997) Dissolution studies of soddyite as long-term analogue of oxidative alteration of spent nuclear fuel matrix. *Materials Research Society Symposium Proceedings*, 465: 565-572.

Plummer L.N. and Busenberg E. (1982) The solubilities of calcite, aragonite and vaterite in CO_2-H_2O solutions between 0ºC and 90ºC, and an evaluation of the aqueous model for the system $CaCO_3$-CO_2-H_2O. *Geochimica et Cosmochimica Acta* 46(6): 1011-1040.

Robie R.A. and Waldbaum D.R. (1968) Thermodynamic properties of minerals and related substances at 298.15ºK (25ºC) and one atmosphere (1.013bars) pressure and at high temperatures, *U.S. Geological Survey Bulletin*, 1259.

Tournassat C., Gailhanou H., Crouzet C., Braibant G., Gautier A., Lassin A., Blanc P., Gaucher E.C. (2007) Two cation exchange models for direct and inverse modelling of solution major cation composition in equilibrium with illite surfaces. *Geochimica et Cosmochimica Acta*, 71:1098–1114.

Waite T.D., Davis J.A., Payne T.E., Waychunas G.A., Xu N. (1994) Uranium (VI) adsorption to ferrihydrite: Application of a surface complexation model. *Geochimica et Cosmochimica Acta*, 58: 5465–5478.